MICROBIAL RESPONSES TO MARINE OIL SPILLS: IMPACTS OF SALINITY, DISPERSANT APPLICATION AND OIL PROPERTIES

by

©Yiqi Cao, B.Eng, B.Sc.(Ag), M.Eng.

A Thesis submitted to the School of Graduate Studies

in partial fulfillment of the requirements for the

Degree of Doctor of Philosophy

Faculty of Engineering & Applied Science

Memorial University

Oct 2022

St. John's Newfoundland and Labrador Canada

ABSTRACT

Marine oil spills can cause catastrophic impacts on ecosystems and human life. Natural attenuation by indigenous oil-degrading bacteria is one of the vital weathering processes that can result in oil mitigation. Various environmental factors, oil spill response options, and types of spilled oils would affect microbial physiologies for oil biotransformation. This thesis aims to uncover the effects of salinity, dispersant application, and oil property on microbial responses to oil biodegradation.

To reveal the salinity effects on oil biodegradation, a halotolerant oil-degrading bacterium, *Exiguobacterium* sp. N4-1P, was tested as a model. The microbial eco-physiological strategy for salinity-mediated crude oil biodegradation was proposed for the first time. The impacts of dispersant application on oil biodegradation under diverse salinities were also evaluated, which showed that dispersant addition could override the oil biodegradation barriers at hyper-salinities primarily through enriching cell abundance.

Increased production of unconventional heavy crude oils has led to increased marine transportation and spill risks. The effects of dispersants on the natural attenuation of the dilbit (diluted bitumen) within microbial communities over time were comprehensively evaluated using a metagenomic/metatranscriptomic approach. We found that dispersant has short-term inhibiting effects, but over the long term, its effects are insignificant. In addition, magnetic nanoparticles decorated bacteria (MNPB) were developed for responding to a

simulated heavy crude oil attachment. A strategy named “access-dispersion-recovery” was proposed, and it led to enhanced mitigation of heavy crude oil pollution.

The responses of an *Alcanivorax* species isolated from the North Atlantic Ocean for degrading alkanes and plastics were also studied. Experimental results indicated that the well-recognized obligate alkane-degrader *Alcanivorax* tied to ocean hydrocarbon cycles could also strongly degrade plastics. The existing biogeochemical processes involved in hydrocarbon biodegradation may aid in the ecosystem’s resilience to the impact of the new anthropogenic plastic-based carbon.

The outputs of the thesis could advance the understanding of sophisticated marine crude oil biodegradation processes, generate potentially promising remediating tools for oil spill responses, provide new insights into marine hydrocarbon degradation, and benefit decision-making for adopting oil spill responding options.

ACKNOWLEDGEMENT

Firstly, I would like to express my sincere gratitude to my supervisor, Dr. Baiyu (Helen) Zhang. I am indebted for her encouragement, advice, and support in my research and life. Dr. Zhang always taught me to have the courage to explore the unknown world and weigh my abilities. I also greatly appreciate my co-supervisor, Dr. Bing Chen, and supervisory committee member, Dr. Charles W. Greer, for their guidance and support. They have inspired me through rigorous scholarship, patience, and an optimistic attitude. They consistently provided invaluable advice and encouragement whenever I ran into any predicament.

Secondly, I gratefully acknowledge the Natural Sciences and Engineering Research Council of Canada (NSERC), Fisheries and Oceans Canada (DFO), Canada Foundation for Innovation (CFI), and Canada Research Chair (CRC) program for their funding support during my research. Special thanks also go to our Northern Region Persistent Organic Pollution Control (NRPOP) lab, Memorial University, National Research Council (NRC), and Compute Canada for providing me with the research environment and technical support.

Thirdly, I thank Lidan Tao for her selfless help. My further gratitude goes to my colleagues Dr. Zhiwen Zhu, Dr. Qinhong Cai, Dr. Xing Song, Dr. Bo Liu, Dr. Xiujuan Chen, Dr. Hongjing Wu, Dr. Weiyun Lin, Dr. Xudong Ye, Dr. Xixi Li, Qiao Kang, Jingjing Ling, Ming Yang, Yuanmei Zhang, Miao Yu, Hoda Tafvizi, Jiabin Liu, Masoumeh Rostami, and

other NRPOP lab members, for their friendship and assistance. Also, special appreciation goes to Dr. Julien Tremblay, Dr. Lars Schreiber, Nathalie Fortin, Christine Maynard, Miria Elias, and Sylvie Sanschagrin from NRC for providing advice and guidance with genomic sample treatments and data analyses.

Finally, I must express my profound gratitude to my family members, my wife Guihua Dong, my father Guozhu Cao, my mother Yonghong She, and my siblings and relatives for providing unfailing support and selfless love throughout my Ph.D. program.

TABLE OF CONTENTS

LIST OF TABLES

LIST OF FIGURES

LIST OF ABBREVIATIONS AND SYMBOLS

16S rRNA	16S ribosomal RNA
AlkB	Alkane 1-monooxygenase
ANI	Average nucleotide identity
ANS	Alaska North Slope
ANOVA	Analysis of variance
ATE	Average treatment effect
BLAST	Basic local alignment search tool
BFT	Baffled flask test
BM	Basic medium
cDNA	Complementary DNA
C15	*n*-pentadecane
CATE	Conditional average treatment effect
CPM	Counts per million
CSH	Cell surface hydrophobicity
dPCR	Digital polymerase chain reaction
DAG	Directed acyclic graph
DCM	Dichloromethane
Do	Dilbit only

DoD9500	Dilbit plus dispersant
DOR	Dispersant:oil ratio, vol/vol
DOSS	Dioctyl sodium sulfosuccinate
EDS	Energy dispersive X-ray spectroscopy
FAME	Fatty acid methyl esters
FTIR	Fourier transform infrared
GC-MS	Gas chromatography - mass spectrometry
HMW	High molecular weight
KEGG	Kyoto encyclopedia of genes and genomes
LOD	Limit of detection
LMW	Low molecular weight
MAG	Metagenome-assembled genomes
MATH	Microbial adhesion to the hydrocarbon
MEGA	Molecular evolutionary genetics analysis
MG	Metagenomics
MNP	Magnetic nanoparticles
MNPB	Magnetic nanoparticles decorated bacteria
MSM	Mineral salt medium
MT	Metatranscriptomics

nMDS	Non-metric multidimensional scaling
NCBI	National center for biotechnology information
OD	Optical density
ODM	Oil degradation medium
OTU	Operational taxonomic unit
ppt	Parts per thousand
ppm	Parts per million
PAH	Polycyclic aromatic hydrocarbon
PB	Pure bacteria
PCoA	Principal coordinates analysis
PHB	Polyhydroxybutyrate
PhaZ	PHB depolymerase
PLFA	Phospholipid-derived fatty acid
PY	Pyruvate
SCM	Structural causal model
SEM	Scanning electron microscopy
TEM	Transmission electron microscopy
WGS	Whole-genome sequencing
XRD	X-ray diffraction spectroscopy

CHAPTER 1 INTRODUCTION

1.1 Background

Marine oil spills, occurring naturally through geophysical processes (i.e., natural seeps) and anthropogenically due to offshore oil exploitation, refining, or transportation, can cause catastrophic impacts on human life and ecosystems (Beyer et al., 2016; King et al., 2015a). Annually, the amounts of oils released into the sea globally due to natural seeps and human activities are between 0.47 and 8.3 million tonnes of oils (McGenity et al., 2021). The 2010 *Deepwater Horizon* spill discharged nearly 3.19 million barrels of crude oil into the Gulf of Mexico, making it one of the most significant marine disasters in history (Martin et al., 2020).

Following an oil spill, a set of weathering processes, including evaporation, dissolution, photooxidation, and biodegradation, take place and affect the physicochemical properties of the oils spread at sea (Figure 1.1). In these processes, volatile compounds and lighter-weight aromatics can be quickly evaporated (Stout et al., 2016), while high molecular weight (HMW) polar compounds are readily dissolved into the seawater (Stanford et al., 2007). In contrast, photooxidation will increase the oxygen content in oil components to generate water-soluble carbons (Vaughan et al., 2016). Ultimately, biodegradation will take place and transform oils into biomass and carbon dioxide (CO_2) (Cao et al., 2021a), resulting in the mitigation of spilled oils.

To tackle marine oil spills, multi-faceted and multidisciplinary response options have been developed, including the deployment of booms and skimmers to physically contain released oils, in situ burning, the application of chemical dispersants to increase oil dilution in seawater and minimize oil delivery to shorelines, and microbially mediated natural attenuation for oil biotransformation (Li et al., 2016c). However, booms and skimmers are of relatively low efficiency and cannot be easily adopted in high-wave energy marine environments (Dhaka & Chattopadhyay, 2021). The application of chemical dispersants does not remove spilled oils but enhances their dispersity and solubility in seawater (Merlin et al., 2021). Microbially mediated natural attenuation is a natural weathering process that does not rely on externally actionable conditions. The indigenous oil-degrading bacteria will respond quickly to utilize energy and carbon sources from the degradation of petroleum hydrocarbons, leading to biodegradation through an environmentally-friendly pathway (Péquin et al., 2022).

The efficiency of microbially mediated natural attenuation highly depends on microbial responses to spilled oils. Multiple oil-degrading bacteria can proliferate and degrade petroleum hydrocarbons (Dubinsky et al., 2013). Some species are specialized obligate hydrocarbon utilizers, while others can utilize non-hydrocarbon substrates, such as components from chemical dispersants and other marine carbons (Kimes et al., 2014). Besides, some oil-degrading bacteria have a broad environmental adaptivity, while others

can only survive under specific conditions (Hazen et al., 2016). Since oil-degrading bacteria have different carbon biases and environmental adaptivity, varied environmental parameters, response options (e.g., applying chemical dispersants), and types of spilled oils in the marine environment would affect microbial physiologies and behaviors for oil biodegradation. Understanding sophisticated microbial responses to different oil spills are of great importance and may contribute to predicting the capacity and efficiency of microbially mediated natural attenuation of marine oil spills.

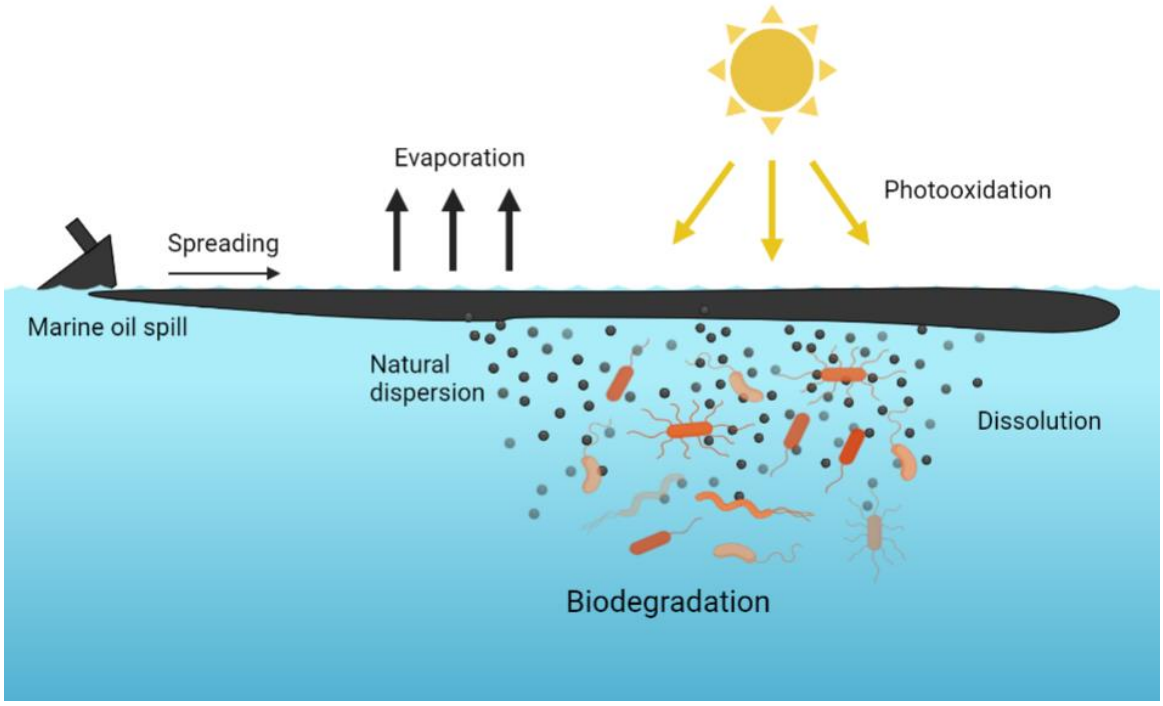

Figure 1.1 Schematic graph of weathering processes of marine oil spills.

1.2 Oil Spills and Biodegradation under Diverse Saline Environments

Marine oil spills can occur in diverse saline environments, including regions with continuously variable salinity (Turner et al., 2019) and permanently low and high saline environments (Timmis et al., 2010).

Coastal regions always exhibit a rather noticeable variation in salinities (McGenity & Gramain, 2010). Various ecosystems, including estuaries, supratidal zones, and lagoons in the coastal regions, are also susceptible to oil spills. The estuaries are regions where freshwater enters the seawater (salinity range from 0.5 to 35 ppt). Oil transportation and spill events are always reported in estuaries, like in Changjiang Estuary, China (Chen, 2021) and Humber Estuary, UK (Eke et al., 2021). The supratidal zones are above the routine intertidal zones and are only inundated during spring tides. Due to evaporation, the salinity of the supratidal zones can reach up to 160 ppt (Geng et al., 2016). Significant oil spill events were reported to contaminate the supratidal zones, such as the *Exxon Valdez* oil spill (Taylor & Reimer, 2008) and those that occurred during the Gulf War (Fowler et al., 1993). Recent studies also demonstrated in the upper parts of seashores (Abou Khalil et al., 2021) and sandy beaches (Abou-Khalil et al., 2022), biodegradation of oil is noticeably slow when salinity increases from 30 ppt to 160 ppt.

The coastal lagoons are shallow inland water bodies separated from the ocean by a barrier and are connected to the sea by restricted inlets which remain intermittently open

(Ferrarin et al., 2014). They are identified as transitional water systems and exhibit substantial temporal and spatial variations in salinity with an average of 0.5 to 35 ppt (Boutron et al., 2021). Specific coastal lagoons, such as Laguna Madre in the Gulf of Mexico (Salcedo et al., 2017), are also considered hypersaline environments with a salinity of more than 50 ppt when they have limited connectivity with the sea and have a high evaporation rate (Quammen & Onuf, 1993). Observations of spilled oils can also distribute over the coastal lagoons, such as the *Deepwater Horizon* oil spill (Radović et al., 2020) and the *Wakashio* oil spill off Mauritius (Rajendran et al., 2021).

Sea ice brine channels also have variable salinities. The brine channels are formed when freshwater freezes firstly to exclude salts, leaving brine (i.e., salty water) trapped in the ice channels (Mundy & Meiners, 2021). Nearly 10 to 30% of the ice volume is filled with brine. In warmer seasons, more than 50% of sea ice melts, leading to a change in salinity. Further, global warming will also affect the salinity of brine channels (Lannuzel et al., 2020). The Arctic Ocean is more potentially subject to oil spills due to increased oil exploration and transportation (Meier et al., 2014).

Apart from that, there are permanently low and high saline environments worldwide. The Baltic Sea (3 - 9 ppt) (Kostianoy et al., 2006) and Gulf of Finland (2 - 3 ppt) (Chapman et al., 2007) are the well-known permanently low saline regions that are susceptible to oil spill events. Besides, oil spills in consistently high saline environments, such as salt lakes,

deep-sea brine pools, and oil reservoirs, have also been reported. Salt lakes, like the Dead Sea, have an average salinity of 342 ppt (Sokol et al., 2014). Deep-sea brine pools found in the Red Sea and the Mediterranean Sea are enriched by natural seeps and have salinity 3 - 10 folds higher than normal seawater due to the dissolution of salt during seafloor activities (Duarte et al., 2020; Schmidt et al., 2015). Oil reservoirs harboring oil and gas sources are usually hypersaline and exposed to oil biodegradation (Ke et al., 2019).

Oil-degrading bacteria capable of surviving under various salinities in the marine environment are essential for the biodegradation of spilled oils. Typically, salinity affects microbial behavior due to the alternation of cell cytoplasmic membrane composition, especially the solute contents regulating water fluxes. As shown in Figure 1.2, increased salinity induces water efflux and dehydration. In contrast, a decrease in salinity causes high solute contents to induce water influx, resulting in cell swelling or even lysis (Wood, 2015). The halotolerant (i.e., salt-tolerant) bacteria can adapt to a broad range of salinities from the absence to relatively hypersaline stress (Roberts, 2005b). Therefore, they play a vital role in microbially mediated natural attenuation. Some halotolerant oil-degrading bacteria belonging to *Halomonas* (Wang et al., 2007), *Marinobacter* (Gao et al., 2013), *Alcanivorax* (Fathepure, 2014), *Bacillus* (Huang et al., 2019), *Lipomyces* (Shetaia et al., 2016), *Pseudomonas* (Varjani & Upasani, 2019), *Ochrobactrum* (Varjani et al., 2015) and *Acinetobacter* (Dahal et al., 2017), *Exiguobacterium* (Sakdapetsiri et al., 2021), are also

identified. Although many studies highlighted the importance of salinity on biodegradation efficiency (Jurelevicius et al., 2013; Mille et al., 1991; Riis et al., 2003), how halotolerant oil-degrading bacteria perform during salt-mediated crude oil biodegradation has not yet been well studied. It is essential to know their physiological responses to oil biodegradation under diverse salinities in order to advance our understanding of sophisticated microbially mediated natural attenuation process.

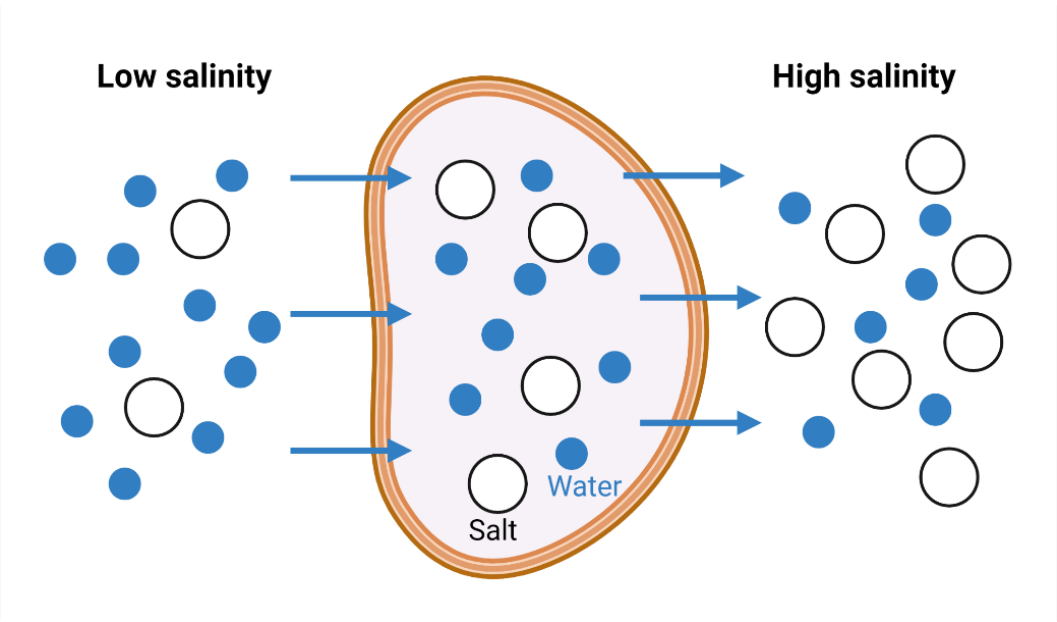

Figure 1.2 Schematic graph of the salinity effects on water flux in cells.

1.3 Effects of Chemical Dispersant on Oil Biodegradation

Chemical dispersants are mixtures of emulsifiers/surfactants and solvents. They are widely applied to tackle catastrophic marine oil spills in the open sea. During the *Deepwater Horizon* oil spill, nearly 7 million liters of chemical dispersants (mostly Corexit 9500A) were applied (Campo et al., 2013). Compared with the naturally dispersed oils that occurred through wave energy, the application of chemical dispersants can significantly enhance the break-up of oil slicks into tiny oil droplets (Figure 1.3). The oil concentration in the seawater could be increased to thousands of ppm in the first few hours of dispersant application and rapidly diluted to a few ppm (Lewis & Prince, 2018). Dispersant application can thus increase oil dilution in seawater, minimizing oil delivery to shorelines and eco-fragile regions (King et al., 2015b), and is a well-recognized response option for marine oil spills.

Since chemical dispersants can transfer floating oil slicks into the water column by lowering the oil-water interfacial tension and emulsifying oils into tiny droplets, they can increase oil bioavailability to oil-degrading bacteria, change the compositions of microbial communities, and ultimately affect the degradation of spilled oils. However, to date, controversial results of the effects of dispersant application on oil biodegradation have been reported. The enhanced oil bioavailability, as a result of dispersant application, can stimulate biodegradation (Prince et al., 2013; Tremblay et al., 2017), while an increased oil

concentration in the water column may cause short-term inhibitory effects toward biodegradation (Kleindienst et al., 2015a; Rahsepar et al., 2016). Besides, compounds present in dispersant formulations can also act as carbon and energy sources and may be preferred by some microorganisms, which compete with oil biodegradation (Kleindienst et al., 2015b). These could be explained by the variations in types of spilled oils and seawaters and the different conditions employed for investigations. Evaluation of the real effects of dispersant application on oil biodegradation is desired.

In addition, although most chemical dispersants are formulated to be highly effective at salinities of 20 - 40 ppt (Lewis & Prince, 2018), they are also recognized as preferred oil spill treating agents in specific regions, including low (e.g., Gulf of Finland) (Kostianoy et al., 2006) and high (e.g., Arctic brine channels) saline environments, where other oil spill responses could hardly be adopted due to the existence of sea ice. Despite the extensive investigations on the role of dispersants in oil biodegradation, salinity remains a missing piece in the complicated dispersed oil biodegradation puzzle.

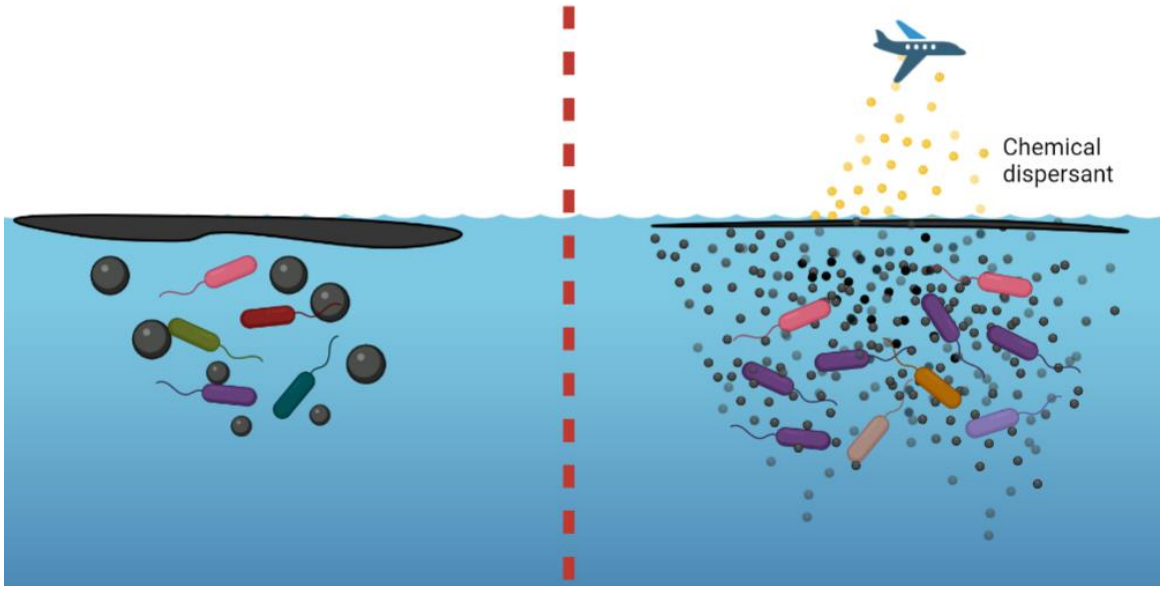

Figure 1.3 Schematic graph of biodegradation of naturally dispersed oils and chemically dispersed oils in the marine environment.

1.4 Effects of Oil Property on Biodegradation

There are many types of crude oils produced worldwide. Typically, the crude oils are divided into light and heavy crude oils. Light crude oil is liquid petroleum with a low density and flows freely at room temperature (Figure 1.4). Compared with the physical properties of light crude oils, heavy crude oils have higher density and viscosity. Heavy crude oils have API (American Petroleum Institute) gravity of less than 20° and viscosity of more than 10,000 centipoises (Ilyin et al., 2016). Besides, heavy crude oils are closely related to natural bitumen obtained from oil sands, categorized as extra-heavy oil with API gravity less than 10° (Azinfar et al., 2018). The high density and viscosity of heavy crude oils may increase their ability to stick to surrounding environments, limiting their bioavailability to oil-degrading bacteria.

Different oil components presented in heavy crude oils have various biodegradabilities. The organic crude oil components are typically divided into four parts: saturates (including linear, branched, and cyclic saturated hydrocarbons), aromatics, resins, and asphaltenes (SARA) (Figure 1.4) (Yuan et al., 2018). The light crude oils are mainly composed of saturates (typically more than 50%) and low molecular weight (LMW) aromatics (nearly 20 - 40%), and less than 20% of resins and asphaltenes (Ashoori et al., 2017). In contrast, heavy crude oils mainly comprise HMW aromatics, resins, and asphaltenes (Rakhmatullin et al., 2020). The saturates, especially LMW n-alkanes with

short and medium chains, are more easily biodegraded. In contrast, the HMW aromatics, resins, and asphaltenes are much less biodegradable or completely recalcitrant (Nduagu & Gates, 2015).

Although the application of chemical dispersants is a well-recognized oil spill response option, some studies have shown that the effectiveness of dispersants is highly dependent on the composition of oil (Noirungsee et al., 2020). The LMW aliphatic hydrocarbons and aromatics are the most dispersible components, whereas HMW aliphatic hydrocarbons, resins, and asphaltenes cannot be effectively dispersed (Fingas et al., 2003). Increasingly global energy demands draw our sights into the production and usage of unconventional heavy crude oils (Davoodi et al., 2020). There are large oil sand deposits (e.g., Athabasca, Cold Lake, and Peace River regions) for bitumen recovery in Canada. For transportation in pipelines, bitumen is diluted with lower-density hydrocarbons to form the unconventional heavy crude oil dilbit (diluted bitumen) (Schreiber et al., 2021). The increase in marine dilbit transportation increases the risk of a potential spill. However, the feasibility of applying chemical dispersants for tackling marine dilbit spills has not been clarified.

Apart from that, due to the specific physical and chemical properties of heavy crude oils, traditional bioremediation practices show extremely low effectiveness in mitigating heavy crude oil pollution (Davoodi et al., 2020). For instance, previous studies showed that only 19 – 29% of resins and 10 – 18% of asphaltenes could be removed after 45 days of

biodegradation (Wang et al., 2018b). New toolboxes are needed to extend the feasibility of heavy crude oil bio-mitigation.

Taking a deeper look, although many studies investigated how oil property affects oil biodegradation, few studies have evaluated the responses of oil-degrading bacteria to degrade specific hydrocarbon components. Besides, the ocean is the ultimate pool of other organic contaminants, especially the widespread plastic waste due to improper disposal (Samalens et al., 2022). The seawater was reported to have high contents of plastic-based carbon (e.g., the North Pacific Gyre surface waters were reported to have plastics to be 83% carbon by mass) (Stubbins et al., 2021). Some important oil-degrading bacteria, such as the well-known obligate alkane-degrader *Alcanivorax* (Zadjelovic et al., 2020), also demonstrated the capacity to degrade plastics. It is desired to make detailed comparisons of the responses of essential bacteria to specific hydrocarbons and plastics so that the resilience of marine ecosystems can be elucidated.

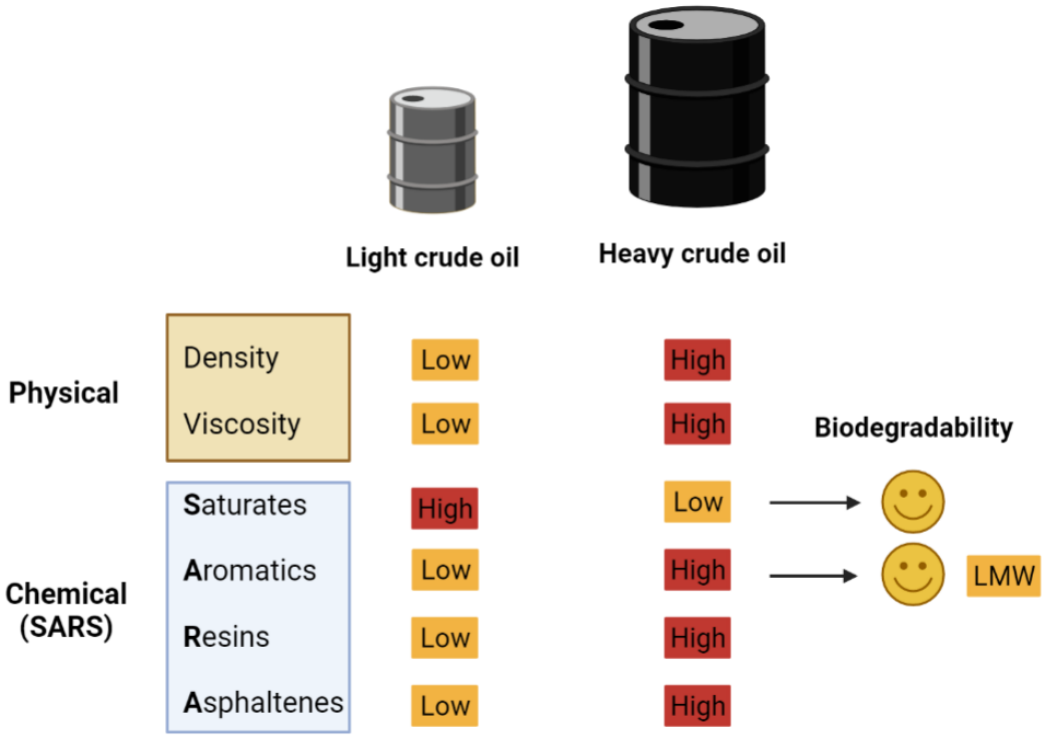

Figure 1.4 The physical and chemical properties of light and heavy crude oils.

1.5 Objectives and Structure of the Thesis

Prior to harnessing the power of microbial biodegradation for mitigating oil pollution in the marine environment, the responses of specific model species and microbial communities to marine oil spills should be clearly understood. This thesis aims to address the identified challenges and advance understanding of microbial responses to marine oil spills. This thesis is prepared in a manuscript style. It focuses on unraveling the impacts of (1) salinity (Chapters 2 and 3), (2) dispersant application (Chapters 3 and 4), and oil properties (Chapters 4, 5, and 6) on the biodegradation of spilled petroleum hydrocarbons in the marine environment. The main contents of this thesis are schematically summarized in Figure 1.5.

Chapter 2 identified salinity effects on crude oil biodegradation using a model halotolerant oil-degrading bacterium *Exiguobacterium* sp. N4-1P. Through detailed characterization of microbial growth behavior, cell surface hydrophobicity (CSH), the performance of oil biodegradation, and the productivity of bio-emulsifiers under diverse salinities, the microbial eco-physiological mechanisms towards salinity-mediated crude oil biodegradation were illustrated.

Chapter 3 evaluated the effects of chemical dispersant application on oil biodegradation under diverse salinities using this model halotolerant bacterium. It entails the characterization of dispersant effectiveness, microbial abundance, biosurfactant

productivity, and oil biodegradation under a broad salinity range. Further, a structural causal model (SCM) was applied to estimate the strength of the parameters for oil biodegradation.

Chapter 4 examined microbial community responses towards naturally and chemically dispersed dilbit over time using microcosm studies. Effects of microcosm scale, dispersant addition, and time period on microbial community assembly were evaluated based on 16S rRNA gene amplicon sequencing. Further, the oil biodegradation and microbial functions and activities are unraveled from substance removal and metagenomics/metatranscriptomics perspectives. This chapter also comprehensively evaluated the application of chemical dispersants for responding to a marine dilbit spill.

Chapter 5 developed a new tool for enhanced bio-mitigation of heavy crude oil pollution. The magnetic nanoparticles decorated bacteria (MNPB) were synthesized first. A novel strategy, named access-dispersion-recovery, was proposed and identified with a solid capacity for removing heavy crude oil in a simulated scenario. This chapter also evaluated the feasibility of applying MNPB in the real environment.

Chapter 6 isolated a new *Alcanivorax* species from the North Atlantic region and investigated its adaptations and abilities to assimilate individual alkane and polyhydroxybutyrate plastics (PHB, one of the emerging bioplastics that may capture the future plastic market). Whole-genome sequencing was employed to identify this species. The growth profiling, cell membrane composition, enzyme activity, and expression of

specific genes were further evaluated to reveal the physiological responses. The marine ecosystem's resilience to the impact of plastics was raised.

Chapter 7 concluded and summarized the findings made in this thesis work. Significant research contributions were highlighted, and recommendations for future research activities were provided.

1.6 Outputs of this Thesis

The key findings of this thesis work include: (1) the identification of microbial eco-physiological strategies for salinity-mediated crude oil biodegradation; (2) the evaluation of dispersant effects on crude oil biodegradation under diverse salinities; (3) the discovery of chemical dispersant effects on microbial community responses towards the spill of an unconventional heavy crude oil, i.e., dilbit (diluted bitumen); (4) the development of magnetic nanoparticles decorated bacteria (MNPB) for responding to heavy crude oil pollution; and (5) an in-depth characterization of a newly isolated *Alcanivorax* species from North Atlantic for degradation of alkanes and plastics. Studies carried out in thesis work provide new insights into the complicated microbially mediated biodegradation of spilled petroleum hydrocarbons and benefit decision-making for adopting oil spill responding options.

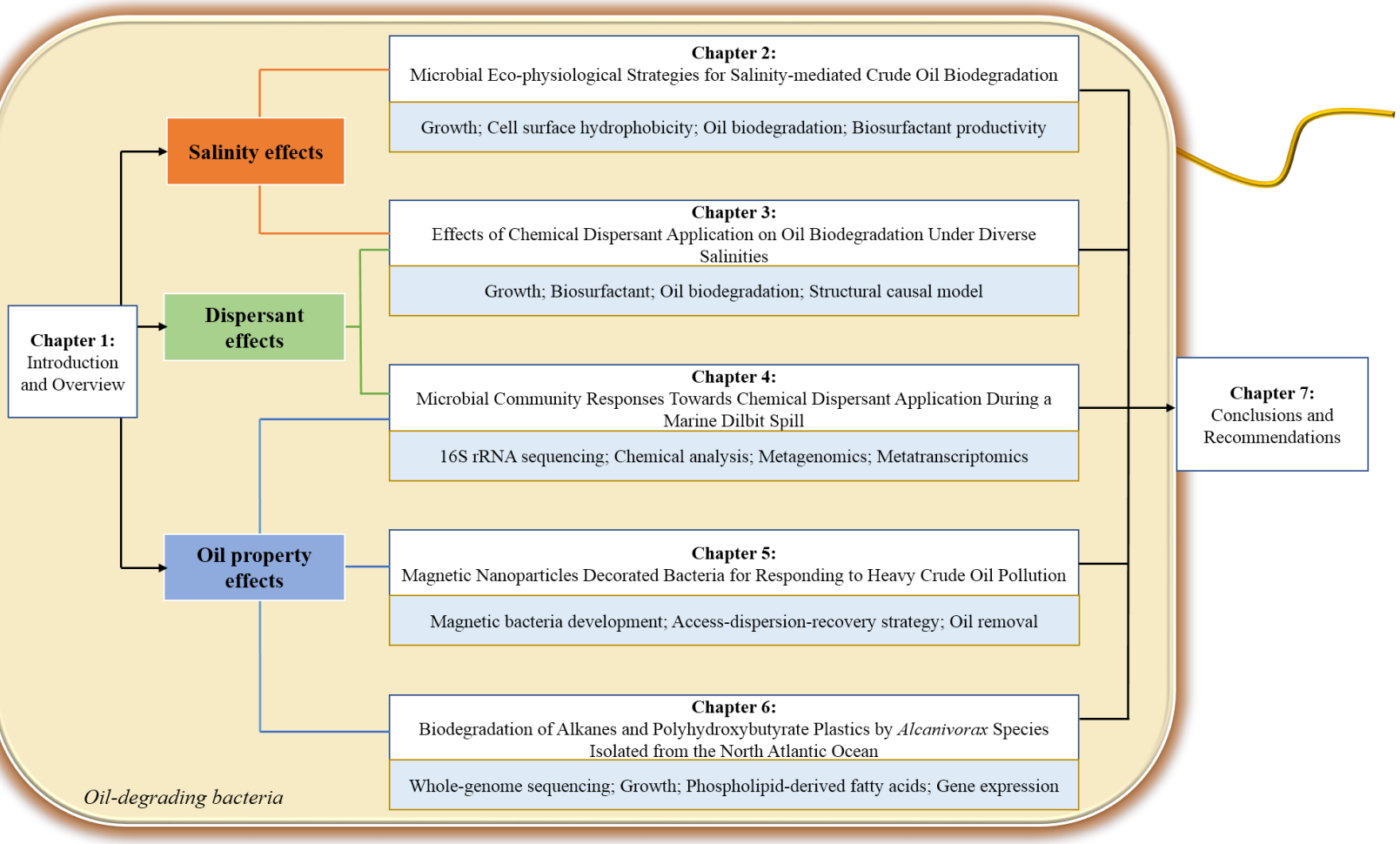

Figure 1.5 The structure of the thesis.

CHAPTER 2 MICROBIAL ECO-PHYSIOLOGICAL STRATEGIES FOR SALINITY-MEDIATED CRUDE OIL BIODEGRADATION[1]

[1] This chapter is generated based on and expanded from the following paper:

Cao, Y., Zhang, B., Zhu, Z., Song, X., Cai, Q., Chen, B., Dong, G., & Ye, X. (2020). Microbial eco-physiological strategies for salinity-mediated crude oil biodegradation. *Science of the Total Environment*, 727, 138723. DOI: 10.1016/j.scitotenv.2020.138723

Roles: Cao designed and conducted the study under the guidance of Dr. Baiyu Zhang and Dr. Bing Chen and acted as the first author of the manuscript. Zhu did the formal analysis, Song did the methods, and others did the review and editing. Most contents of this paper were written by Cao and further polished by the other co-authors.

2.1 Introduction

Biodegradation by indigenous oil-degrading bacteria is one of the key weathering processes that dominate the fate of spilled oil (Prince, 2015). However, continuously variable salinity always occurs in marine systems, especially in coastal regions (McGenity & Gramain, 2010). Bacteria without the ability to fit the diverse salinities thus could hardly survive and function well (Li et al., 2016c; Park & Park, 2018b).

Halotolerant bacteria can adapt to a broad range of salinities from the absence to relatively hypersaline stress (Margesin & Schinner, 2001), by accumulating a variety of small molecules in the cytoplasm to counteract the external salt stress (Roberts, 2005a). Identification and characterization of the halotolerant bacteria with strong oil biodegrading ability is essential to the microbially mediated natural attenuation process.

The versatile genus *Exiguobacterium* is widely recognized as a highly diversified group of pigmented gram-positive extremophiles with robust plasticity and adaptation capacity (Kasana & Pandey, 2018). They are widespread in harsh habitats and are mainly divided into two major phylogenetic clades, including strains isolated from cold and alkaline marine (or hot springs) environments. (Vishnivetskaya et al., 2009). In addition to dynamic thermal/alkaline adaptation, some *Exiguobacterium* strains are also halotolerant (Patel et al., 2018; Remonsellez et al., 2018), indicating their potential as model organisms

in the ecosystem (White III et al., 2019). Recently, a novel bio-emulsifier producing *Exiguobacterium* sp. strain N4-1P was isolated from petroleum hydrocarbon-contaminated coastal regions in Northern Atlantic Canada (Cai et al., 2017c). Gene annotations demonstrated that this strain harbors several cold-adapted proteins, external stress response proteins, mono- or dioxygenases, and dehydrogenases (Cai et al., 2017b), confirming its capacity to fit in the diverse salinities for crude oil biodegradation.

In this study, *Exiguobacterium* sp. strain N4-1P was selected as a representative species, and Alaska North Slope (ANS) crude oil (0.5%, vol/vol) was used to simulate an oil spill. Through evaluating microbial growth behavior, cell surface hydrophobicity (CSH), the performance of oil biodegradation, and the productivity of bio-emulsifiers under diverse salinities, we illustrated the microbial eco-physiological mechanisms for salinity-mediated crude oil biodegradation. The research outputs are expected to advance our understanding of the performance of indispensable halotolerant oil-degrading bacteria when facing spilled oil under an extensive range of salinities.

2.2 Materials and Methods

2.2.1 Strain and medium

Strain: *Exiguobacterium* sp. strain N4-1P used in this study was previously isolated from shoreline sediment samples in the vicinity of a refinery company in Northern Atlantic

Canada (Cai et al., 2014). Three types of media, seed medium, basic medium, and oil degradation medium, were applied for microbial enrichment, phenotypic properties characterization, and oil degradation experiments, respectively, with components stated below:

Seed medium: Marine Broth 2216 (Difco #279110) was used to prepare the seed medium following the manufacturer's guidelines. Sterile 100 mL seed medium was introduced into a 250 mL Erlenmeyer flask, inoculated by *Exiguobacterium* sp. strain N4-1P, and continuously shaken at 150 rpm at 30 °C for 24 h to achieve microbial enrichment. The obtained seed culture was further used for phenotypic properties characterization and oil degradation experiments at an inoculation amount of 1% (vol/vol).

Basic medium (BM): Basic medium was prepared as follows: one liter distilled water containing $(NH_4)_2SO_4$, 10 g; $FeSO_4 \cdot 7H_2O$, 0.00028 g; KH_2PO_4, 3.4 g; $K_2HPO_4 \cdot 3H_2O$, 4.4 g; $MgSO_4 \cdot 7H_2O$, 1.02 g; yeast extract, 0.5 g and trace element ($ZnSO_4$, 0.29 g; $CaCl_2$, 0.24 g; $CuSO_4$, 0.25 g; $MnSO_4$, 0.17 g) (Cai et al., 2017c).

Oil degradation medium (ODM): BM supplemented with sterilized ANS crude oil was used as ODM. ANS concentration (0.5%, vol/vol) used in this study was based on previous studies of microbial degradation of crude oils (Overholt et al., 2016).

2.2.2 Pigment and biofilm formation capacity tests

The pigments and biofilm formation capacity were measured using the methods developed by Remonsellez et al. (2018).

Pigment measurement: After cultivation in seed medium overnight, pellets were collected at 6,000 g for 10 min and washed with sterile distilled water three times. The pellets were then suspended in 5 mL absolute methanol, subjected to a vigorous vortex for 2 min, followed by a resting period of 10 min, and centrifuged at 6,000 g for 10 min. The absorption spectrum of the pigment extract (i.e., colored supernatant) was measured within wavelengths of 270 - 660 nm in a UV-VIS spectrophotometer (Thermo Fisher, GENESYS 10S).

Biofilm formation capacity test: Biofilm formation ability was measured following the crystal violet staining method using 24 well polystyrene plates. Briefly, overnight cultures of the *Exiguobacterium* strain grown in seed medium with different NaCl concentrations were diluted to an OD600 of 0.05 with fresh BM with their respective salt concentrations. Then, 1 mL of diluted bacterial culture was incubated in 24 well polystyrene plates for 50 h at 30°C. The bacterial cultures were then removed from the wells, and the wells were stained with 1 mL of 0.1% crystal violet, rinsed, and thoroughly dried. Then, the crystal violet was solubilized by adding 1.2 mL of ethanol - acetone (80:20). One mL of the

solubilized samples was used to determine the OD570 using a UV-VIS spectrophotometer. The OD570 values were normalized using the cell density (OD600) to represent the biofilm formation capacity (OD570/OD600).

2.2.3 Setting of salinity and biodegradation

Different NaCl concentrations were used to reproduce diverse salinities to well represent real marine environmental systems from freshwater to hypersaline environments. Pre-lab testing was conducted and demonstrated that *Exiguobacterium* sp. strain N4-1P could not grow when the salinity was higher than 120 g/L NaCl. Hence, NaCl concentrations of 0, 5, 15, 35, 50, 70, 90, and 120 g/L were used to represent diverse salinities of BM and ODM. Microbial growth behavior was monitored, and corresponding salinities were selected for biodegradation experiments using ODM to ensure *Exiguobacterium* sp. strain N4-1P could grow well in these salinities.

Each experimental run was conducted using a 250 mL Erlenmeyer flask filled with 100 mL BM or ODM with each selected salinity and continuously shaken at 150 rpm under 30 °C. The seed microbial inoculation size was 1% (vol/vol). For each salinity level, a flask with the same settings but without adding bacteria was prepared and operated as the control run.

2.2.4 Measurements of microbial growth and cell surface hydrophobicity (CSH)

Cell growth in BM and ODM: In BM, cell density was determined by directly measuring the cell density at OD600. In ODM, cells were firstly harvested by centrifuging the entire broth at 6,000 rpm for 10 min, followed by washing three times using BM with corresponding salinities and diluting it to the same volume (100 mL) for cell density measurement at OD600. The growth curves were generated accordingly.

CSH in BM and ODM: Cells harvested on the 7^{th} day in both BM and ODM were used for CSH analysis. Cells were harvested by centrifuging the entire broth at 6,000 rpm for 10 min, followed by washing three times using distilled water. CSH was measured using the microbial adhesion to hydrocarbon (MATH) test (Cai et al., 2019). Briefly, cells were diluted to an OD600 value of around 0.8. One milliliter of kerosene was added to 5 mL of each cell suspension in a test tube, followed by vigorous agitation for 2 min with a Vortex mixer. The mixture was let stand for 20 min at room temperature. The OD600 of the water phase was measured, and the percentage of the cells partitioned to the hydrocarbon phase represented CSH (%).

2.2.5 Extraction and analysis of oil in ODM

Oil extraction: On day 7 and day 30, the remaining oil in each flask was extracted by adding 10 mL of dichloromethane (DCM). The extraction was repeated at least three times to dissolve the organic hydrocarbon phase fully. Residual water was then removed using

0.5 g of sodium sulfate. The organic phase (30 - 40 mL) was then concentrated to 10 mL by rotary evaporation, which was ready for gas chromatography - mass spectrometry (GC-MS) analysis to obtain oil compositions and the associated concentrations in each sample. C30 17β(H) 21β(H) - hopane was used as the internal standard (Song et al., 2016).

GC-MS analysis: The GC-MS analytical method used for oil components analysis has been previously developed and adopted (Song et al., 2018). The Agilent 7890A equipped with a DB-5MS column fused silica capillary column was used to differentiate hydrocarbon contents. Helium was applied as the carrier gas at a flow rate of 1.0 mL min^{-1}, and the GC oven temperature was set at 50 °C for 2 min, then ramped at 6 °C min^{-1} to 300°C for 20 min. MS detection was conducted in the electron ionization mode at 70 eV and an ion source temperature of 300 °C. To characterize ANS crude oil biodegradation efficiency, each oil component was normalized to conserved internal biomarker 17α(H),21β(H) - hopane (30ab hopane, detected and quantified with m/z of 191) due to its high stability (Venosa et al., 1997). The peak areas of n-alkanes and polycyclic aromatic hydrocarbons (PAHs) with relatively high abundance (more than 0.02%) were analyzed, and total n-alkanes and total PAHs were defined as the sum peak areas of n-alkanes and PAHs, respectively (Nguyen et al., 2018). The crude oil biodegradability by using *Exiguobacterium* sp. N4-1P was determined in parallel by comparing the runs with the

bacterial inoculation and the corresponding control run without bacteria addition.

Biodegradation means the breakdown of organic matter by microorganisms; biotransformation is the biochemical modification of one chemical compound or a mixture of chemical compounds; oxidation is the loss of electrons during a reaction; mineralization is the ultimate or complete biodegradation, which means the degradation of a compound to its mineral components (i.e., carbon dioxide and water). Here, the GC-MS analysis only showed the oxidation or biotransformation results.

2.2.6 Determination of bio-emulsifier productivity in ODM

The bioavailability of crude oil highly depends on the productivity of bio-emulsifiers, which was measured following the cold-acetone precipitation method (Cai et al., 2017c). Cell-free media were prepared first. On day 7, each ODM broth was centrifuged at 6,000 rpm for 5 min, and the supernatant was filtered through the 0.22 μm polyethersulfone membrane to remove the precipitate thoroughly. The cell-free medium was then used for bio-emulsifiers measurement. Each cell-free medium (15 mL) was mixed with cold-acetone (1:3, v/v) and stored at 4 °C for three days to fully precipitate the crude bio-emulsifiers. Finally, the supernatant was removed by centrifugation, and the precipitation was fully dried and then weight quantified. To avoid the effects of disparate salt participation, BM with different selected salinities but without bacterial incubation were used as controls. The

weight difference between runs with bacterial incubation and the control represented crude bio-emulsifier productivity.

2.2.7 Statistical analysis

All experiments were conducted in triplicate for quality control. The error bar represented each standard deviation from the means of the independent experiment. Statistical difference was evaluated using the One-way ANOVA analysis ($n = 3$) with $P < 0.05$ as significant.

2.3 Results and Discussion

2.3.1 Salinity-mediated microbial growth between hydrophobic and aqueous phases

The phenotypic property of *Exiguobacterium* sp. N4-1P in BM was characterized first. The colonies are regular, circular, and orange-pigmented. The spectrophotometric scanning of methanol-extracted pigment showed shoulder peaks with the absorbance maxima at 430, 453, and 482 nm (Figure 2.1), which is a typical pattern (400 - 500 nm) of carotenoid (Remonsellez et al., 2018). Moreover, genomic data (accession no. CP022236 to CP022241 in GeneBank) demonstrated enzymes related to carotenoid biosynthesis pathways, supporting the existence of carotenoids, which are widely distributed in extremophiles to help improve salt tolerance (Patel et al., 2018).

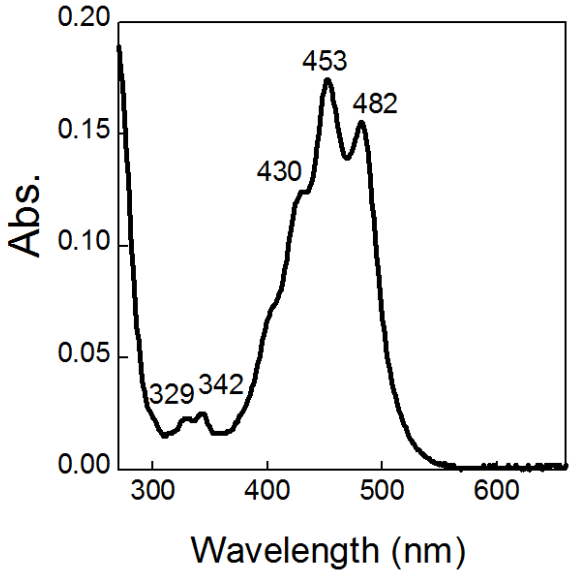

Figure 2.1 Spectrum of extracted pigments of *Exiguobacterium* sp. N4-1P.

To understand how salinity affects the cell growth behavior, we applied a NaCl range of 0 - 120 (i.e., 0, 5, 15, 35, 50, 70, 90, 120) g/L in BM and measured the growth curve accordingly. Under the salinity of 0 - 50 g/L NaCl, *Exiguobacterium* sp. N4-1P exhibited similar growth behavior with high growth rates (Figure 2.2). It reached a stationary phase with the highest OD600 value (around 0.2) within almost 20 h. Under the salinity of 70, 90, and 120 g/L NaCl, however, the stationary phase was delayed with decreased OD600 values of 0.16, 0.06, and 0.02, respectively. It was well known that microbial growth was inhibited under increased salinities due to limited microbial salt tolerance ability (Díaz et al., 2002; Mukherji et al., 2004). Hence, the suitable salt stress for *Exiguobacterium* sp. N4-1P was within 0 - 50 g/L NaCl concentrations, similar to the halotolerant strain *Exiguobacterium* sp. SH31 isolated from Salar de Huasco, Chilean Altiplano (Remonsellez et al., 2018).

Interestingly, in ODM, the growth behavior of *Exiguobacterium* sp. N4-1P was entirely changed. It achieved the maximum growth rate under the salinity of 50 g/L NaCl, followed by the salinity of 70, 35, 15, 5, and 0 g/L. Under the salinity of 90 and 120 g/L NaCl, *Exiguobacterium* sp. N4-1P exhibited strongly inhibited growth behavior, similar to the growth in BM. In addition, *Exiguobacterium* sp. N4-1P required a longer time (i.e., almost 4 - 5 days) to reach the stationary phase at salinities below 50 g/L NaCl. Compared with the growth curve in BM under the same salinities (Figure 2.2), cellular growing states

played another critical role in microbial growth, particularly in an oil-based growth medium.

We hypothesized that microbes might accumulate in either oil or aqueous phase and regulate their growth accordingly. Those cells residing in the aqueous phase with yeast extract as a carbon source tended to have a higher growth rate. CSH was then tested in both BM and ODM under these salinities to verify this. The CSH test determines the microbial ability to attach to hydrophobic components and reflects the growth state between hydrophobic and aqueous phases (Cai et al., 2019). As expected, CSH decreased along with the increased salinity in both BM and ODM, indicating *Exiguobacterium* sp. N4-1P preferred to grow in the aqueous phase when salinity was increased. Data for the salinity of 120 g/L NaCl was omitted due to limited cell amounts for determination. It was reported that many halophiles would adapt to high saline conditions by producing hydrophilic cell surfaces (Hart & Vreeland, 1988). Under such conditions, cells displayed a stronger affinity for water molecules to prevent desiccation, with preferred growth in the aqueous phase. On the contrary, strains maintained a hydrophobic cell surface to defend against water under low salinity conditions. Thus, under a low salinity, cells preferred to grow in the hydrophobic phase with the utilization of hydrocarbons, whose metabolic activity was much lower than the simple source yeast extract in the aqueous phase.

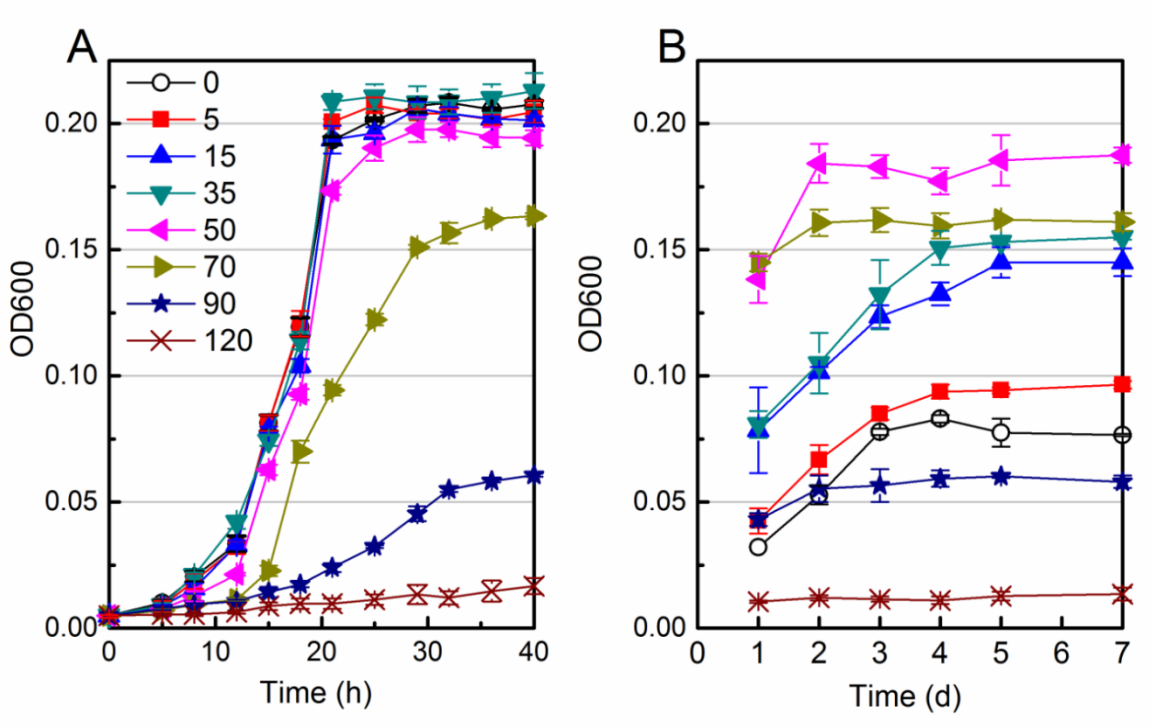

Figure 2.2 Growth behavior of *Exiguobacterium* sp. N4-1P in (A) BM and (B) ODM under the salinity of 0, 5, 15, 35, 50, 70, 90, 120 g/L NaCl, respectively.

Moreover, CSH was significantly enhanced under NaCl concentration of 35 or 50 g/L in ODM compared with that in BM, but barely changed under the other salinities (Figure 2.3). In the BM, *Exiguobacterium* sp. N4-1P exhibited an extremely high CSH, with over 90% of cells easily attached to the hydrophobic phase at a NaCl concentration lower than 15 g/L. Under high salt stress (i.e., more than 70 g/L NaCl), however, *Exiguobacterium* sp. N4-1P needed to survive by producing a hydrophilic cell surface to avoid desiccation. When exposed to spilled oils, oil-degrading bacteria could modify their cell membrane, which acts as a sensitive and selective barrier between the cell and its surrounding environment to assist the cells in attaching to the hydrophobic hydrocarbons (Li et al., 2015).

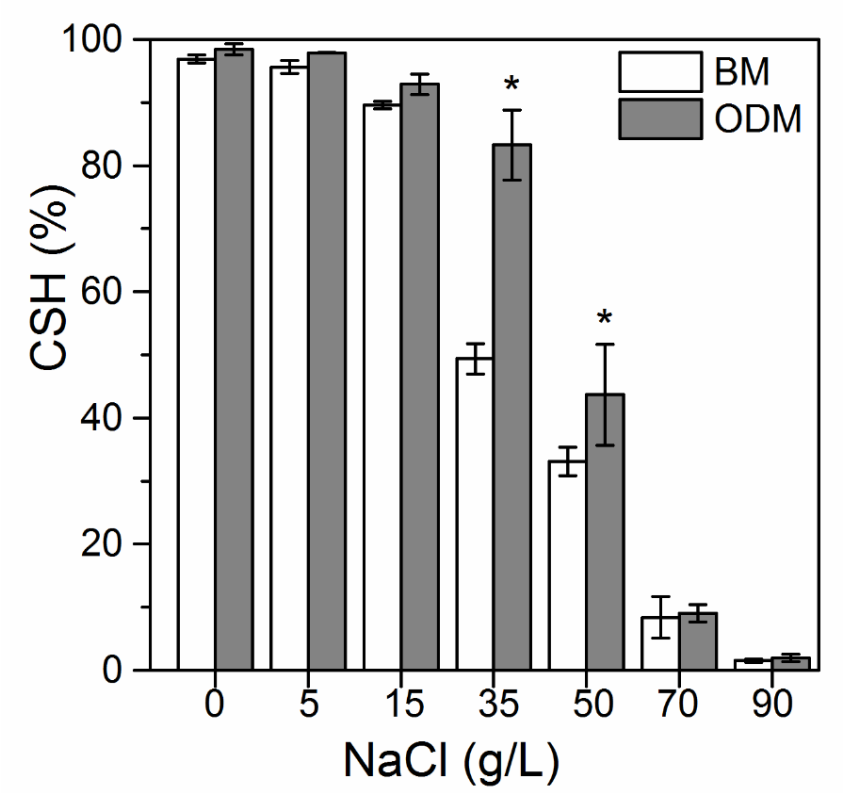

Figure 2.3 CSH of *Exiguobacterium* sp. N4-1P growing in the BM and ODM under different salinities. "*" indicates significantly different.

2.3.2 Crude oil biodegradation under various salinities

A biodegradation assay was then conducted using ODM with a salinity range of 0 - 70 (i.e., 0, 5, 15, 35, 50, 70) g/L NaCl since higher salinity strongly inhibited the growth of *Exiguobacterium* sp. N4-1P (Figure 2.2). Percentages of oil components biodegraded were calculated by comparing them with sterilized controls. After seven days, degradation of ANS crude oil was undetectable (i.e., essentially 0% degraded) due to the relatively slow hydrocarbon biotransformation process. We then extended the biodegradation duration to 30 days to track the oil biodegradation well. As expected, a noticeable change in hydrocarbon components was detected when comparing the biodegradation runs with and without bacterial addition. For each ANS oil sample, n-alkanes with the number of carbon atoms less than 11 were entirely lost in both the control runs and the ones with bacterial treatment (Figure 2.4) since these short-chain n-alkanes are more volatile and easily biodegraded during natural weathering (Gros et al., 2014). Generally, *Exiguobacterium* sp. N4-1P could degrade both alkanes and PAHs, and like most oil-degrading bacteria, it exhibited a preference for n-alkanes over aromatic hydrocarbons during biodegradation (Varjani, 2017).

Exiguobacterium sp. N4-1P could biodegrade all n-alkane components to a certain degree in a salinity range of 0 - 70 g/L. The highest oil biodegrading efficiency was

achieved under 15 g/L NaCl concentration, with 40% total n-alkanes and 24% PAHs degraded within 30 days (Figure 2.4). In contrast, when NaCl stress reached the maximum level (70 g/L), the degradation efficiency for total n-alkanes and PAHs was only 26% and 7%, respectively (Figure 2.4). Oil biodegradation by microbial biofilm is more favorable than by planktonic bacteria (Zhu et al., 2019). To illustrate why salinity could mediate crude oil degradation, the ability of biofilm formation by *Exiguobacterium* sp. N4-1P was measured in BM with different salinities. In this study, biofilm-producing ability peaked at a salinity of 15 g/L and then gradually dropped (Figure 2.5). At a salinity of 70 g/L NaCl, biofilm productivity by *Exiguobacterium* sp. N4-1P was higher than that at a salinity of 50 g/L NaCl. It is believed that when facing extreme conditions, extremophile bacteria would generate increased extracellular polymeric substances (EPS) as a protective diffusion barrier to resist adverse conditions (Hall-Stoodley et al., 2004; Le Magrex-Debar et al., 2000). The findings indicated that within a certain salinity range (i.e., 0 - 50 g/L NaCl), *Exiguobacterium* sp. N4-1P had its maximum ability for biofilm formation under the salinity of 15 g/L NaCl for enhanced biodegradation of crude oil. In contrast, with a high NaCl concentration (e.g., 70 g/L), biofilm was produced mainly for resistance to the hypersaline environment.

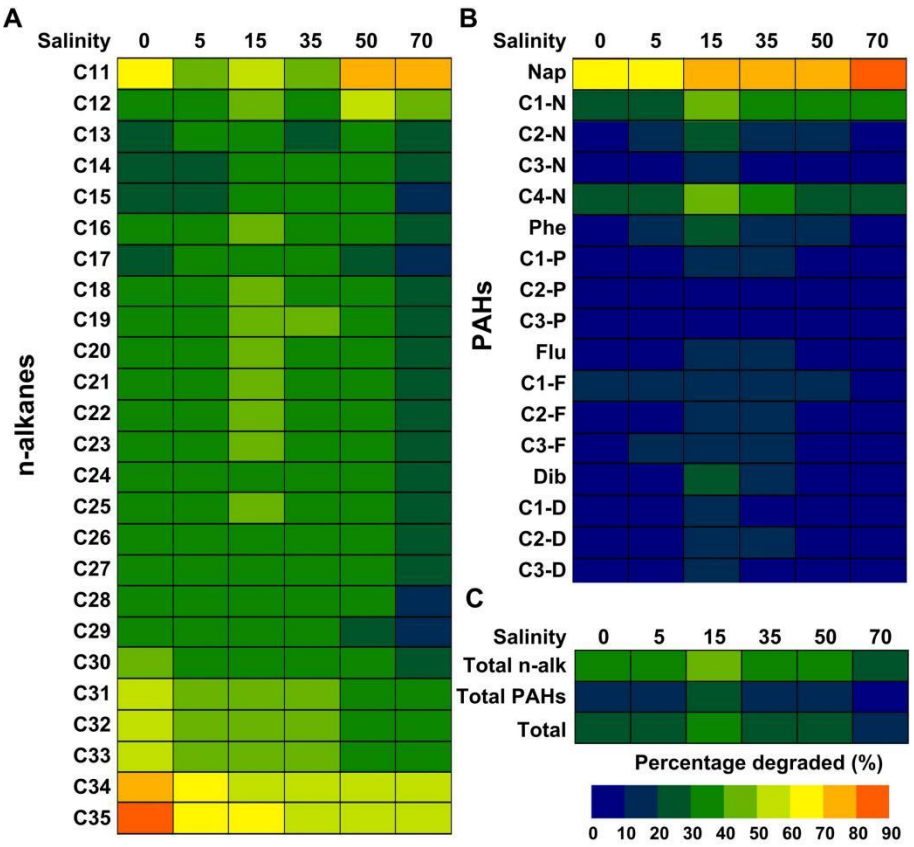

Figure 2.4 Biodegradation efficiency of ANS crude oil hydrocarbon components (A) n-alkanes; (B) PAHs; (C) total n-alkanes and PAHs after 30 days of incubation under the salinity of 0, 5, 15, 35, 50, 70 g/L NaCl, respectively.

In this figure, C11 - C35: n-alkanes with corresponding number of carbon atoms; Nap, naphthalene; C1-N, C2-N, C3-N, and C4-N: alkylated homologs of naphthalene; Phe: phenanthrene; C1-P, C2-P, and C3-P: alkylated homologs of phenanthrene; Flu: fluorene; C1-F, C2-F, and C3-F: alkylated homologs of fluorene; Dib: dibenzothiophene; C1-D, C2-D, and C3-D: alkylated homologs of dibenzothiophene.

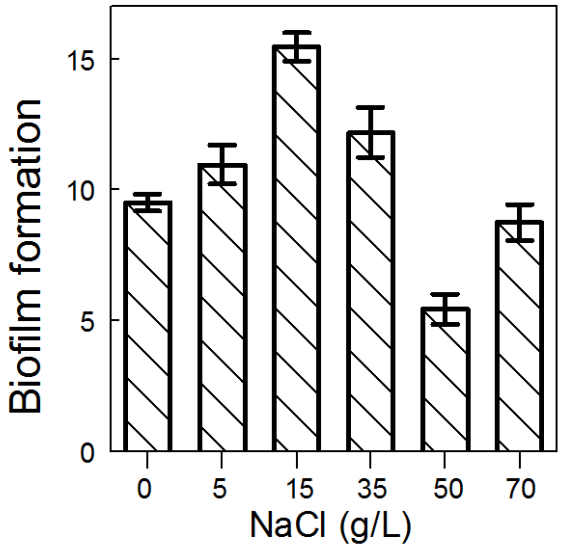

Figure 2.5 Biofilm formation capacity (OD570/OD600) of *Exiguobacterium* sp. N4-1P under the salinity of 0, 5, 15, 35, 50, 70 g/L NaCl in BM.

For n-alkanes, biodegradation of short-chain (i.e., C11 - C17) and middle chain (i.e., C18 - C29) components comparably followed the tendency of total alkane degradation, with the highest degradation efficiency of almost 40% achieved at the salinity of 15 g/L (Figure 2.6). Differently, biodegradation efficiency for long-chain n-alkanes (i.e., C30 - C35) was higher and peaked at the salinity of 0 g/L NaCl with an extent of 54% (Figure 2.6). Although n-alkanes have different proportions in crude oil, the high removal percentage of these long-chain alkanes indicated that *Exiguobacterium* sp. N4-1P harbors crucial enzymes belonging to the flavin-binding family (Wang & Shao, 2012). The genome of *Exiguobacterium* sp. N4-1P (NCBI accession no. CP022236) further demonstrated the existence of four genes coding flavin-dependent oxidoreductase, which may be involved in the biodegradation of long-chain alkanes. Some other oil-degrading bacteria were also reported with higher degradation efficiencies for long-chain alkanes, such as *Bacillus* (Adam, 2016), *Acinetobacter*, *Marinobacter*, *Parvibaculum*, and *Geobacillus* (Shao & Wang, 2013). Moreover, the degradation efficiency of long-chain alkanes increased along with decreased salinity (Figure 2.6). It could be due to a higher CSH in a low salinity leading to an increased cell accumulation capacity in the hydrophobic phase and resulting in microbes' easier access to these compounds with enhanced biodegradation (Rojo, 2009).

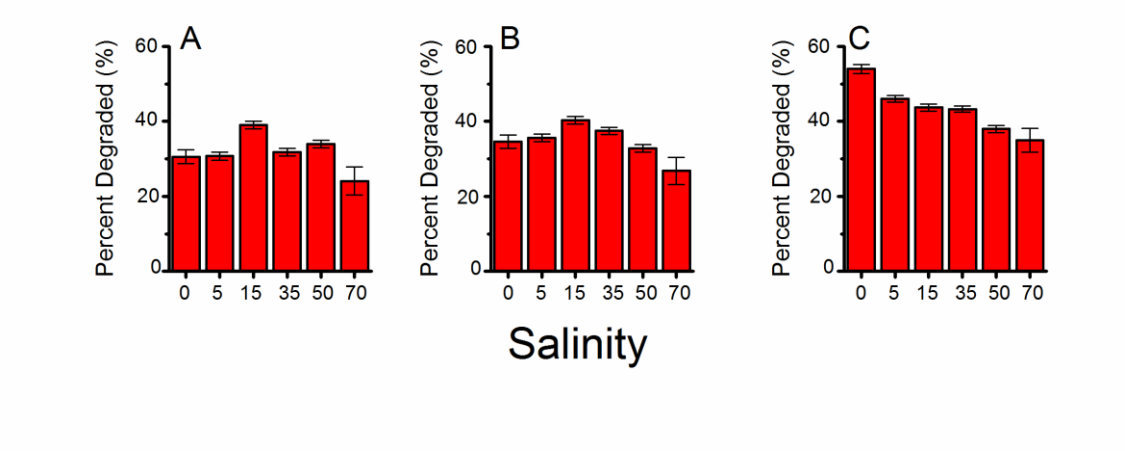

Figure 2.6 Biodegradation efficiency of (A) short-chain n-alkanes; (B) middle-chain n-alkanes; (C) long-chain n-alkanes under different salinities.

For aromatic hydrocarbons, LMW PAHs (i.e., naphthalene and its alkylated homologs) were more susceptible to being treated (Figure 2.4) due to their relatively higher biodegradability (González-Gaya et al., 2019; Xue et al., 2015). Under the salinity of 15 g/L NaCl, degradation of naphthalene and its alkylated homologs reached the highest efficiency of 31%, with 15% in the salinity of 70 g/L NaCl (Figure 2.7). The degradation of C4-N was better than C3-N, which indicates that demethylation could be a possible reaction in the biodegradation of C4-N (Huang et al., 2004). Interestingly, the degradation efficiency of naphthalene was enhanced with increased salinity, and it achieved the highest level of 80% under the salinity of 70 g/L NaCl. LMW PAHs show certain solubility in water (e.g., naphthalene of 30 mg/L), and their uptake by microorganisms occurs mostly within the aqueous phase (Haritash & Kaushik, 2009). In addition, the decreased CSH led to a higher cell mass accumulated in the aqueous phase, which could further enhance naphthalene biodegradation.

For other multiple rings PAHs and their alkylated homologs, although they were with high hydrophobicity like long-chain n-alkanes, the biodegradation efficiency was low and even undetectable (Figure 2.4) due to their stable chemical structures and relatively recalcitrant biodegradability (Wang et al., 1994). Almost no degradation of these PAHs and their alkylated homologs were detected under the salinity of 70 g/L (Figure 2.7) since cells

with low CSH could hardly access them. Phenanthrene, dibenzothiophene, and their alkylated homologs showed a similar degradation tendency, with the highest degradation efficiency achieved under the salinity of 15 g/L NaCl. In contrast, the associated highest degradation efficiency for fluorene and its alkylated homologs was achieved under the salinity of 35 g/L (Figure 2.7). It is necessary to illustrate these complicated PAH biodegradation processes under diverse salinities by comparing the biodegradation performance when grown on a sole PAH and combined PAHs in future studies.

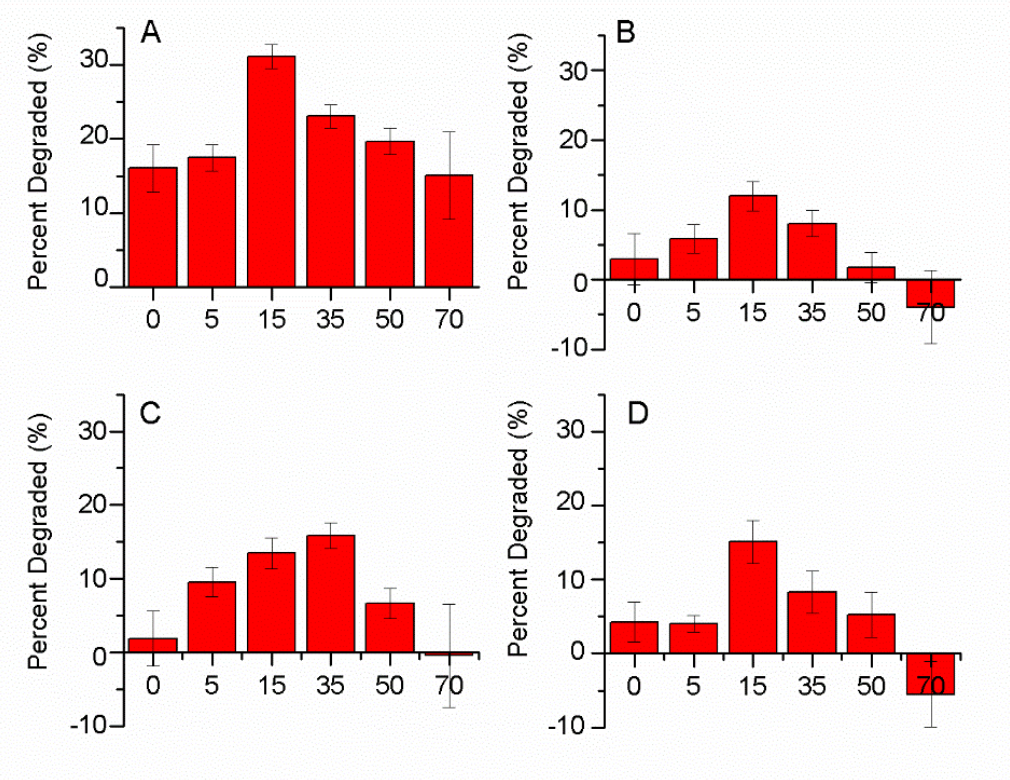

Figure 2.7 Biodegradation efficiency of (A) naphthalene and its alkylated homologs; (B) phenanthrene and its alkylated homologs; (C) fluorene and its alkylated homologs; (D) dibenzothiophene and its alkylated homologs under different salinities.

2.3.3 Impact of salinity on bio-emulsifier productivity for oil bioavailability

Biodegradation efficiency is highly dependent on the bioavailability of hydrocarbons (Bianco et al., 2020). To improve the bioavailability of hydrocarbons, oil-degrading bacteria produce amphipathic surface-active biosurfactants to trap hydrocarbons into their hydrophobic core to form soluble micelles (Kumar et al., 2006; Perfumo et al., 2010). Bio-emulsifiers are HMW biosurfactants. In addition to stabilizing oil-water emulsions to facilitate oil motility (Zheng et al., 2011), they bind tightly to oil droplets to prevent drop coalescence (Thavasi & Banat, 2010).

It was reported that bio-emulsifiers produced by *Exiguobacterium* sp. N4-1P could form stable oil-in-water emulsions (Cai et al., 2017c). In our study, although degradation of ANS crude oil was undetectable within 7 days of incubation, the formation of oil droplets was clearly observed as *Exiguobacterium* sp. N4-1P would firstly produce bio-emulsifiers to sufficiently emulsify two immiscible liquids to enhance the bioavailability of hydrocarbons. The bio-emulsifier productivity was then measured with the salinity range of 0 - 70 g/L NaCl in ODM, and our results showed that under the salinity of 15 g/L NaCl, *Exiguobacterium* sp. N4-1P produced the maximum bio-emulsifiers (Figure 2.8) with the highest degradation efficiency for both n-alkanes and PAHs. However, cell densities were diverse under different salinities. To test the bio-emulsifier producing ability, the amount

of bio-emulsifier in a sample was standardized by dividing the OD600 value, representing bio-emulsifier production per turbidity unit. As shown in Figure 2.8, cells with the lowest NaCl stress exhibited the highest bio-emulsifier productivity, and the productivity established a linear relationship with the salinity stress ($R^2 = 0.947$). It could be concluded that under a relatively low salinity, improved CSH induced cells to grow in the oil phase with the stimulation of bio-emulsifiers productivity.

Biodegradation initiates when mass transfer across the cell membranes occurs (Si-Zhong et al., 2009). Previous studies demonstrated that hydrocarbons could be mobilized intracellularly through directly aqueous transportation or cell surface-adsorbed hemispherical micelles (i.e., hemi-micelles) (Brown, 2007; Lanzon & Brown, 2013). In our study, sufficiently bio-emulsifier productivity enhanced the transportation of hydrocarbons, especially these extra hydrophobic compounds like long-chain alkanes with a decreased salinity. Under an increased salinity, however, the depressed bio-emulsifier productivity limited the hemi-micelles transportation, resulting in decreased degradation efficiency.

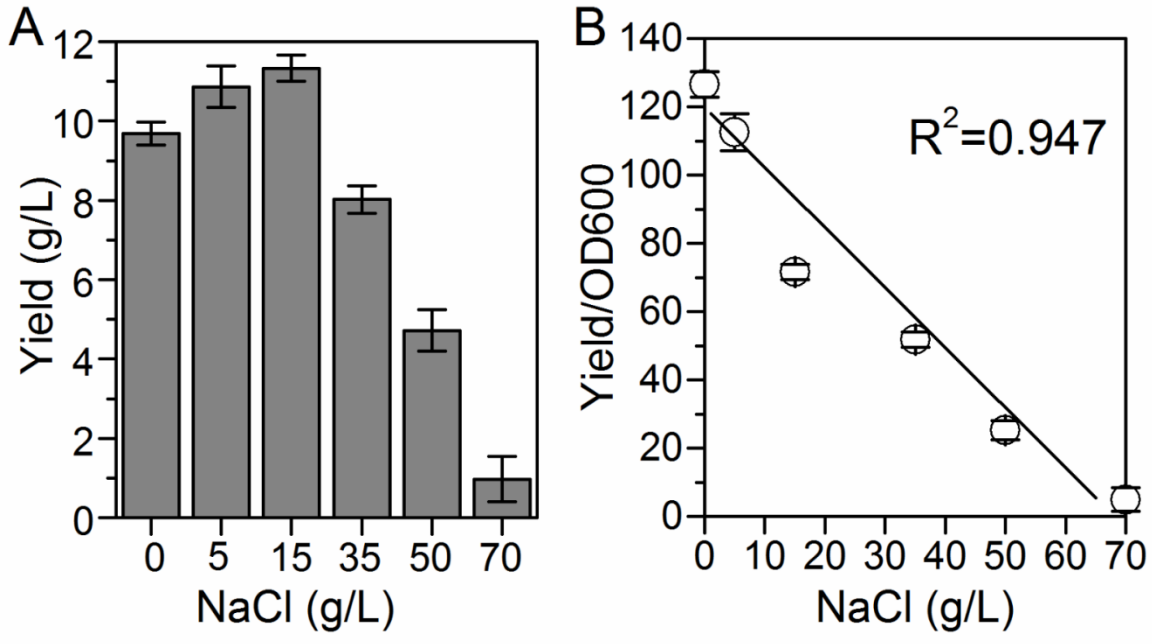

Figure 2.8 (A) Total bio-emulsifier productivity and (B) bio-emulsifier productivity per OD600 unit after 7 days of incubation.

2.3.4 Mechanism of microbial eco-physiological activities

Based on the findings in this study, we proposed a schematic diagram to illustrate the microbial eco-physiological mechanism of the salinity-mediated crude oil biodegradation by *Exiguobacterium* sp. N4-1P (Figure 2.9). Microbial cells balanced their extracellular and intracellular osmotic levels by regulating CSH for water transportation. Under low salinities (i.e., 0 - 35 g/L), the high CSH would drive cells to attach to the hydrophobic oil phase with the stimulation of producing sufficiently bio-emulsifiers, which accelerated the formation of micelles to increase hydrocarbon bioavailability. The transportation pathway might occur mainly through hemi-micelles with the enhanced degradation of the most hydrophobic compounds (i.e., long-chain n-alkanes). On the other hand, high salinities (i.e., 50 - 70 g/L) induced water to permeate intracellularly to balance the osmotic level, leading to enhanced growth in the aqueous phase with decreased bio-emulsifier productivity. The biodegradation of relative water-soluble components like naphthalene was promoted as intracellular transportation was mainly through the direct aqueous pathway.

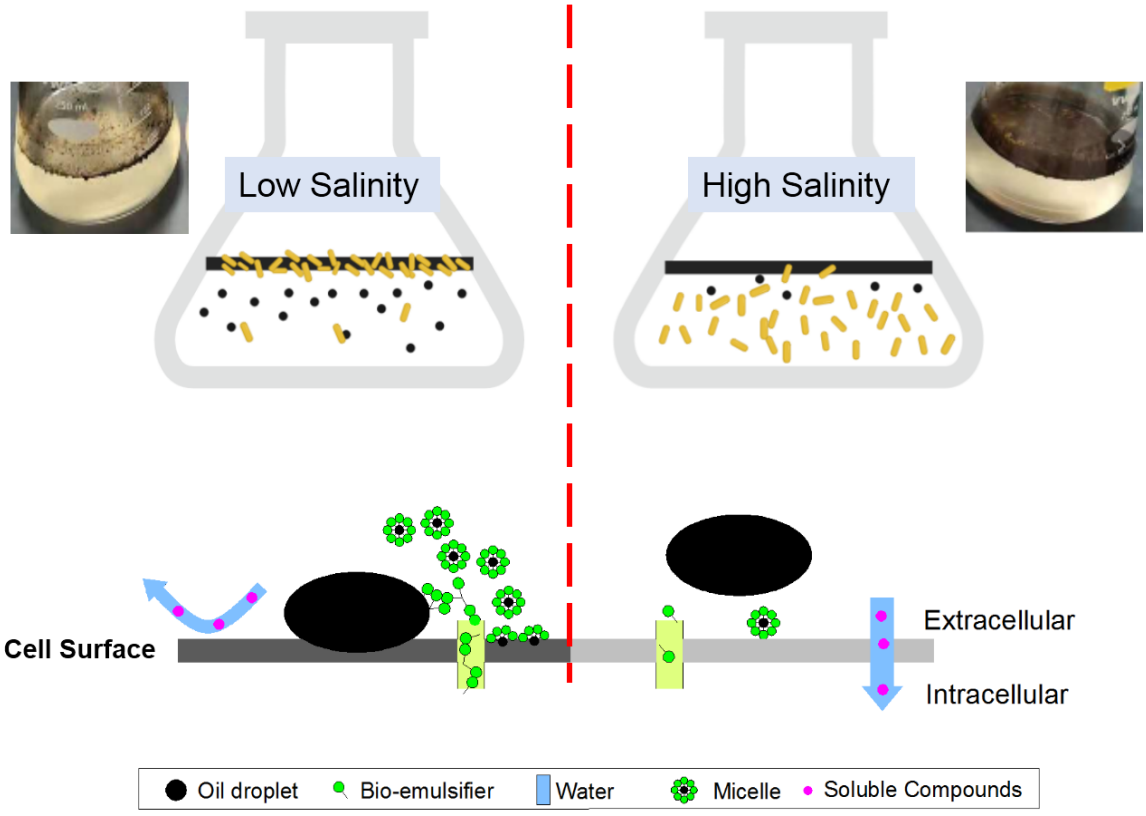

Figure 2.9 Schematic diagram describing the microbial eco-physiological mechanism when facing crude oil under low and high salinities.

2.4 Summary

In this study, microbial eco-physiological strategies for salinity-mediated crude oil biodegradation were investigated. A halotolerant bio-emulsifier producer, *Exiguobacterium* sp. N4-1P, was examined in detail as a model strain. Our results indicated that various salinity levels are correlated to a shift in microbial growth behavior, CSH, biofilm formation ability, and bio-emulsifier productivity that affect crude oil biodegradation. Increased salinity results in decreased CSH and migration of microbial growth from the oil phase to the aqueous phase, leading to limited bio-emulsifier production and depressed degradation of insoluble long-chain n-alkanes while enhancing the degradation of relatively soluble naphthalene. The findings from this study illustrated the important microbial eco-physiological mechanism for spilled oil biodegradation under diverse salinities and advanced the understanding of sophisticated marine crude oil biodegradation processes.

CHAPTER 3 EFFECTS OF CHEMICAL DISPERSANT APPLICATION ON OIL BIODEGRADATION UNDER DIVERSE SALINITIES[2]

[2] This chapter is generated based on and expanded from the following paper:

Cao, Y., Kang, Q., Zhang, B., Zhu, Z., Dong, G., Cai, Q., Lee, K., & Chen, B. (2022). Machine learning-aided causal inference for unraveling chemical dispersant and salinity effects on crude oil biodegradation. *Bioresource Technology*, 345, 126468. DOI: 10.1016/j.biortech.2021.126468

Roles: Cao designed and conducted the study under the guidance of Dr. Baiyu Zhang and Dr. Bing Chen and acted as the first author of the manuscript. Kang did the model analysis, Zhu did the formal analysis, and others did the review and editing. Most contents of this paper were written by Cao and further polished by the other co-authors.

3.1 Introduction

Marine oil spills can cause devastating impacts on human life and ecosystems. The application of chemical dispersants is a well-recognized oil spill response option. By emulsifying spilled oils into tiny droplets, chemical dispersants can promote oil dissolution into water columns to reduce oil slick delivery to ecologically fragile regions and enhance oil bioavailability to microorganisms (Pi et al., 2017; Tremblay et al., 2017).

Despite the extensive investigations on the role of dispersants in oil biodegradation, salinity remains a missing piece in the complicated dispersed oil biodegradation puzzle. Salinities could exhibit a rather pronounced variation in the aquatic environment, especially in coastal regions and Arctic ice brine channels where oil spills can potentially occur (Turner et al., 2019). Besides, in permanently low saline environments like the Baltic Sea (3 - 9 ppt) and Gulf of Finland (2 - 3 ppt) (Kostianoy et al., 2006), where other oil spill responses could rarely be adopted due to the existence of sea ice, the usage of dispersant is a preferred treatment to oil spills (Chapman et al., 2007). Comparatively, hypersaline environments (usually higher than 30 - 35 ppt) have received limited attention (Abou Khalil et al., 2020). Potential oil exploration and production in hypersaline water bodies like brine pools and salt ponds recently (Tansel et al., 2014; Zermeno-Motante et al., 2016) necessitate the study of the effects of dispersant application at hyper salinities.

Most chemical dispersants are formulated to be highly effective for marine environments with salinity between 20 - 40 ppt (Lewis & Prince, 2018). The effectiveness of a dispersant is a function of surfactants that are available at the oil-water interface for interfacial tension reduction (Cai et al., 2021). Decreased salinity leads to the increased solubility of dispersant, whereas hyper salinities may cause salting-out effects. Neither of these cases favors the dispersant availability at the oil-water interface (Chandrasekar et al., 2006). To identify the salinity effects on oil biodegradation, the *Exiguobacterium* species could be selected as a blueprint model due to its plasticity in global environments, including extreme conditions (White III et al., 2019). Under the salinities of 0 - 35 g/L NaCl, the bacteria showed increased secretion of biosurfactants to enhance the bioavailability of crude oils for biodegradation, while suppressed biosurfactant productivity occurred under hypersaline environments (i.e., 50 - 70 g/L NaCl). Dispersant addition may affect the whole pictures of oil biodegradation under these salinities, and several questions are then raised. What are the effects of dispersant addition on cell abundance and biosurfactant productivity under different salinities? Does dispersant addition or salinity change directly affect oil biodegradation or indirectly through improving cell abundance or biosurfactant productivity? From a global perspective, what are the effects of dispersant addition on crude oil biodegradation under different salinities?

The aforementioned questions are causal and can be generally viewed as what will happen to an outcome when some changes occur to treatment under a series of conditions. With only observational data available and the existence of many confounders, these questions can hardly be answered by traditional statistical methods such as correlation analysis, which are incapable of ruling out pseudo correlations and may increase the chance of biased evaluations (Imbens & Rubin, 2015; Pearl & Mackenzie, 2018). From this point of view, analytical tools capable of investigating causal relationships from data itself are in great need.

Benefit from the rich discussions on causal inference in the statistics and artificial intelligence fields recently, some effective causal inference methods have emerged and thrived, enabling their applications to causal reasoning from observational data, which can hardly be done by previous methods with no semantics to introduce prior knowledge (Butcher et al., 2021; Glymour et al., 2019; Prosperi et al., 2020). Among the most discussed causal inference methods, the Structural Causal Model (SCM), one of the well-established counterfactual-based causal inference tools (i.e., a method through thinking about alternative possibilities for past or future events), utilizes prior knowledge as part of inputs and ensures the causal relationships in the model projecting real-world links (Ospina-Forero et al., 2020; Rohrer, 2018). Compared with its predecessors - Bayesian

Network (Carriger et al., 2016) and Structural Equation Model (Schmidt et al., 2018), SCM has overcome the following limitations of the other two: (1) The prior knowledge used in SCM is a data generating process with causal directions rather than a probability distribution, which is bidirectional. Thus, the relationships in SCM can more accurately represent real-world causal links; (2) Intervention (i.e., purposely change of the factor in the real world to observe the response of the result) is a supported action in SCM in the form of the do-calculus (i.e., an axiomatic system for replacing probability formulas containing the do operator with ordinary conditional probabilities). More importantly, such interventions are reduceable through a series of logic calculations in the SCM methodology, enabling SCM to perform causal reasoning from observational data. When compared with SCM's most unignorable competitor Rubin Causal Model (Markus, 2021; Rubin, 1974), SCM is believed to be more versatile and lucid by many researchers due to its more generalized definition of causal effects. Recently, the SCM has been used for investigating the causal relationships between bioavailability of pollutants and environmental factors (Liu et al., 2017), lignocellulose derived by-products impact on lytic-polysaccharide monooxygenase activity (Rezić et al., 2021), as well as potential causality between COVID-19 severity and environmental factors (Kang et al., 2021). These indicate the capability of SCM for the quantitative estimation of the causal links among the impacting

factors and oil biodegradation to facilitate answering the above questions.

Therefore, this study experimentally investigated microbial abundance, biosurfactant productivity, and oil biodegradation (with/without dispersant added) under different salinities using the model species *Exiguobacterium* sp. N4-1P. The SCM was then applied to quantitatively estimate the mentioned causal links among salinity, dispersant, cell abundance, biosurfactant productivity, and oil biodegradation. The results of this study will contribute to decision-making before dispersant application, and the employed logic will shed light on adopting advanced causal inference tools to unravel the complicated biodegradation processes of contaminants.

3.2 Materials and Methods

3.2.1 Strain and culture conditions

Exiguobacterium sp. strain N4-1P was previously isolated from shoreline sediment samples in the vicinity of a refinery company in Northern Atlantic Canada. Bacteria were grown in mineral salt medium (MSM) composed of $(NH_4)_2SO_4$, 5 g; KH_2PO_4, 3.4 g; $K_2HPO_4 \cdot 3H_2O$, 4.4 g; $MgSO_4 \cdot 7H_2O$, 1.02 g; $FeSO_4 \cdot 7H_2O$, 0.00028 g and trace element ($ZnSO_4$, 0.29 g; $CaCl_2$, 0.24 g; $CuSO_4$, 0.25 g; $MnSO_4$, 0.17 g) per litter (Cao et al., 2020c). The MSM was different from the BM in Chapter 2 by removing the yeast extract. The crude oils were then the sole carbon source in the medium. Considering both the salinity adapting

capacity of *Exiguobacterium* sp. N4-1P and the representativeness of global aquatic systems, different NaCl concentrations of 0 - 70 g/L (i.e., 0, 5, 15, 35, 50, 70 g/L) were selected and added in MSM to represent diverse salinities. The cultures were shaken in 250 mL Erlenmeyer flasks containing 50 mL MSM for sufficient aeration at 150 rpm at room temperature. Each flask was covered with a gas permeable lid to avoid anoxic incubation. The bacterial inoculation size was 1% (v/v) using the overnight microbial enrichments as stated previously (Cao et al., 2020c).

The crude oil Alaska North Slope (ANS) and chemical dispersant Corexit 9500A were used throughout this study. Three carbon source treatments were tested: (i) ANS (0.1%, vol/vol), (ii) chemical dispersant Corexit 9500A (0.004%, vol/vol) and (iii) a Corexit-oil mixture. The dispersant: oil ratio (DOR, vol/vol) was selected based on dispersion effectiveness results under diverse salinities. Six parallel flasks were performed for the (i) and (iii) treatments, with three parallels for microbial growth and biosurfactant productivity tests and the other three for biodegradation measurement. Three more parallels were set for the (ii) treatment for microbial growth and biosurfactant productivity tests. The (ii) treatment was set for three replicates because they were not used for the oil biodegradation analysis. A Flask with the same conditions but without adding bacteria was used as the control run at each salinity level to calculate the oil degradation ratio and avoid the potential

errors caused by evaporation.

3.2.2 Dispersion effectiveness under diverse salinities

Baffle flask test (BFT) (Venosa et al., 2002; Zhu et al., 2020b) was used to test the dispersant effectiveness of DOR at 1:25 and 1:50. Briefly, 100 μL oil was added to 120 mL media with different salinities, followed by addition of 4 μL and 2 μL Corexit 9500A, reaching a DOR of 1:25 and 1:50, respectively. The baffled flask was placed on an orbital shaker to have the components inside mixed at 200 rpm for 10 min. The resulting mixture was kept stationary for 10 min in each run. Oil dispersed in the water phase was collected and extracted using DCM. Oil dispersion effectiveness was calculated based on absorption data obtained from a UV-VIS spectrophotometer (Thermo Fisher, GENESYS 10S) at wavelengths of 340, 370, and 400 nm. DCM was used as the blank for spectrophotometer analysis. The area under the absorbance vs. wavelength curve was calculated using the trapezoidal rule.

3.2.3 Measurement of cell abundance and biosurfactant productivity

Microbial abundance and biosurfactant productivity were measured using broth samples in the same flask after 20 days of incubation. Cells were harvested by centrifuging the entire broth at 6,000 rpm for 10 min, followed by washing two times with a phosphate-buffered saline (PBS) buffer and diluting it to a final volume of 5 mL for cell abundance

measurement at OD600 (Cao et al., 2020c). The cells would not grow in the oil-free inoculations since the external carbons were adequately removed by washing.

The cell-free medium was then used for biosurfactant productivity measurement. The biosurfactant was first precipitated using the cold-acetone method (Cai et al., 2017c). Briefly, each cell-free medium (10 mL) was mixed with cold acetone (40 mL) and stored at 4 °C for three days. The crude biosurfactants were then collected through centrifugation at 6,000 for 10 min. Since *Exiguobacterium* sp. N4-1P majorly produced the lipopeptide-based biosurfactants (Cai et al., 2021), the productivity was estimated by measuring the total protein contents with the Pierce BCA Protein Assay Kit (Thermo Scientific).

3.2.4 Determination of remaining oil components using GC-MS

The oil components in each sample were determined using a previously developed method (Cao et al., 2020c; Song et al., 2018). On day 20, the whole medium in each flask treated with oil or oil plus dispersant was extracted three times using a total of 10 mL dichloromethane (DCM). The residual water was removed by centrifugation at 6,000 g for 10 min. The organic (lower) phase (1 mL) was then transferred to a GC vial. The stable chemical C30 17β(H) 21β(H) - hopane was used as the internal standard. The GC-MS (Agilent model 7890A) with a DB-5MS column fused with a silica capillary column was used for oil component analysis. Helium was applied as the carrier gas at a flow rate of 1.0

mL/min. The GC oven temperature was set at 50 °C for 2 min, then ramped at 6 °C/min to 300 °C for 20 min. MS detection was conducted in the electron ionization (EI) mode. Each oil component was identified from the mass spectra, and the peak area was normalized to conserved internal biomarker 17α(H),21β(H) - hopane (30ab hopane, detected and quantified with m/z of 191). The biodegradation ratio was calculated as the ratio of the target oil component in the selected run to the control without bacteria added. The top 15 oil components with the highest biodegradation ratio were selected for the total oil biodegradation ratio assessment.

To visualize the group differences (i.e., biodegradation efficiency of each oil component under different treatments), the PCoA (Bray Curtis dissimilarity matrix) method implemented in the R package "vegan" was applied. The distance among different treatments represents the similarity of oil biodegradation, i.e., the longer distance indicates the higher dissimilarity.

3.2.5 SCM aided estimation of causal effects

Intervention is an essential concept that enables SCM to estimate causal effects in the data generation process by setting the value of X (i.e., treatment variables) to x (i.e., individual value in the corresponding variables), which allows users to calculate the corresponding variable Y. From a probability perspective, the intervention action can be

expressed in the form of probability distribution: P(y|do(x)), i.e., the conditional distribution of Y when the observation variable X is set to x. Mathematically, the primary goal of SCM is to estimate P(y|do(x)). However, in most SCM-applicable cases, such interventions are not directly accessible. To tackle this counterfactual challenge, SCM is equipped with a series of proven graphic-based operations. By applying such procedures and criteria to a given causal diagram of a problem, users can identify which variables in the diagram are sufficient to calculate the desired causal effect. The identified variables are thus called sufficient sets. If a causal effect can be estimated, all the variables in the sufficient set would be observable. In other words, the sufficient set will not contain any unobserved or unmeasurable variables and will further allow the users to estimate P(y|do(x)) with the existing observational dataset. Given a sufficient set S, the causal effect can be expressed as:

$$P(Y|do(X = x)) = \sum_{s} P(Y = y|X = x, S = s)P(S = s)$$

Where do(·) mean the intervention action, X and Y indicate the treatment and the outcome variables, respectively, and S indicates the sufficient set variables. In contrast, x, y, and s indicate the individual (value) in the corresponding variables (Judea, 2010).

In SCM, a causal diagram is usually in the form of a directed acyclic graph (DAG), which can reflect the causal relationships among different variables with directions. Each

DAG node represents a variable in the causal settings, and an arrow indicates a causal link with a direction. Such a graph allows users to introduce prior knowledge about the data-generating process explicitly. To construct the DAG for this study, nine pairs of causal relationships between treatments (causes) and outcomes (consequences) within the oil biodegradation system were taken into account, including (1) salinity and cell abundance; (2) salinity and biosurfactant productivity; (3) salinity and overall biodegradation ratio; (4) dispersant addition and cell abundance; (5) dispersant change and biosurfactant productivity; (6) dispersant change and oil biodegradation; (7) cell abundance and biosurfactant productivity; (8) cell abundance and biosurfactant productivity; and (9) biosurfactant productivity and overall biodegradation ratio.

The causal effects of each treatment can be quantitatively evaluated in two different metrics: average treatment effect (ATE) and conditional average treatment effect (CATE).

ATE can be expressed using the following equation:

$$\mathrm{ATE} = \frac{1}{\mathrm{N}}\sum\left(\mathrm{y}_1(\mathrm{i}) - \mathrm{y}_0(\mathrm{i})\right)$$

Where y_0 (i) is the outcome value when the individual i is not treated, and on the contrary, y_1 (i) is the outcome when the individual i is treated, N is the total amount of individuals. When the variable's value is continuous instead of binary, y_1 indicates that the individual is treated with one more unit than y_0. The CATE is the ATE value calculated

under different conditions. Specifically, for links (1) (2) (3), the dispersant addition is the condition; and for links (4) (5) (6), increment of per salinity (i.e., 1 g/L NaCl) is the condition. In general, the treatment effect indicates the quantitative change of an outcome when treatment is adjusted by a single unit, while all the other conditions remain the same.

With the treatment and outcome selected and the target causal effect expressed with the variables in the appropriate sufficient set, the final step is to pick an estimator (e.g., linear and non-linear regressors) to calculate the causal effects. In this study, the DMLOrthoForest (Microsoft Research, 2020) algorithm was chosen as the estimator inside the SCM due to its ability to handle continuous treatment variables and provide reliable estimates. The DMLOrthoForest was adapted from the Double/Debiased Machine Learning method (Chernozhukov et al., 2017) and the Orthogonal Random Forest algorithm (Foster & Syrgkanis, 2019). A linear estimator has also been applied as a complement to the machine learning-based estimator.

The causal inference workflow in this study was achieved based on the DoWhy package (Sharma & Kiciman, 2020), a Python software specialized in providing causal inference interfaces. The DMLOrthoForest algorithm used in the case study can be found in EconML (https://github.com/microsoft/EconML), a package with machine learning causal estimators.

All the analyzed and processed data in the study, as well as the scripts used, can be found along with the results of the case study in the GitHub repository: https://github.com/kangqiao-ctrl/dispersant_salinity_causal

3.2.6 Statistical analysis

All experiments were conducted in triplicate for quality control. The error bar represented each standard deviation from the means of the independent experiment. Statistical difference was evaluated using the One-way ANOVA analysis ($n = 3$) with $P < 0.05$ as significant.

3.3 Results and Discussion

3.3.1 Oil dispersion effectiveness under different salinities

Oil dispersion effectiveness was first evaluated using MSM with different salinities. When the DOR was 1:50, the dispersion effectiveness varied under different salinities. The dispersion effectiveness was extremely low when salinity was higher than 35 g/L NaCl and could drop to only 3% when salinity was at 70 g/L NaCl. Differently, when DOR was 1:25, it showed similarly high dispersion effectiveness (nearly 80%) under these salinities (Figure 3.1). It indicated that when using Corexit 9500A, a DOR of 1:25 could be adopted for tackling a spill of ANS crude oils under diverse salinities. Hence, the following biodegradation experiments were conducted using the DOR of 1:25.

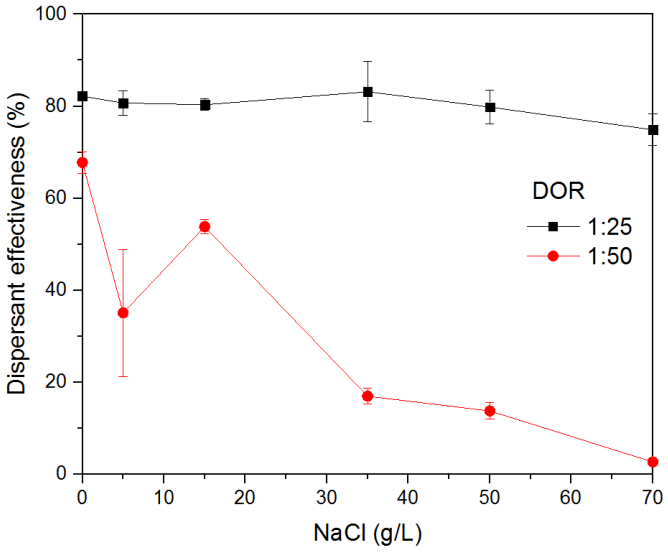

Figure 3.1 Impacts of the DOR on oil dispersion effectiveness under different salinities.

3.3.2 Cell abundance and biosurfactant productivity under different salinities

The cell abundance and biosurfactant productivity were evaluated after 20 days of incubation under the salinity ranges of 0 - 70 (i.e., 0, 5, 15, 35, 50, 70) g/L NaCl. When using oil as the only carbon source, the cell density reached the highest level (nearly 0.19 of OD600) at the salinities of 5 and 15 g/L NaCl (Fig. 1A). Lower or higher salinities decreased cell abundance, and the lowest OD600 value was only 0.05 under the salinity of 70 g/L NaCl due to the highest osmotic pressure (Cao et al., 2020c). Dispersant addition increased microbial cell abundance at all these salinities (Figure 3.2). The highest level was achieved at the salinity of 15 g/L NaCl with an OD600 value of 0.37. There was another tendency that when salinity was higher than 35 g/L, dispersant addition had the highest increment of cell abundance. At the salinity of 70 g/L NaCl, the cell abundance reached up to 0.30 when dispersant was added (Figure 3.2).

In addition to enhancing the oil bioavailability, chemical dispersants may also be degraded by microorganisms to increase cell abundance (Kleindienst et al., 2015a). The stimulation of cell growth by Corexit 9500A, the most commonly used dispersant worldwide, which is primarily composed of degradable light petroleum distillates, glycols, and dioctyl sulfosuccinate, has been widely reported (Schreiber et al., 2019). Interestingly, the cell abundance results showed that microbes behaved differently when using this

dispersant as the sole carbon source. Under low salinities (i.e., 0 and 5 g/L NaCl), the OD600 value was only 0.01 and 0.02, respectively (Figure 3.2). These dispersant components could cause detrimental effects on microbial cells in the absence of crude oil (Rughöft et al., 2021). It was reported that Corexit 9500A was more soluble and may cause higher toxicity under low salinities (DeLorenzo et al., 2016; Kuhl et al., 2013). In contrast, in the dispersant-only treatments, cell abundance was significantly improved when salinities were higher than 15 g/L NaCl and could even reach the levels in oil plus dispersant treatments when salinity was higher than 35 g/L.

In crude oil-only samples, falling biosurfactant productivity levels were reported at salinities higher than 5 g/L NaCl (Figure 3.2). The relatively lower productivity under the salinity of 0 g/L NaCl than 5 g/L NaCl may be due to low cell abundance (Cao et al., 2020c). Biosurfactant productivity tends to level out in oil samples, regardless of dispersant addition, at low and medium salinities (0 - 35 g/L NaCl) (Figure 3.2). On the contrary, stimulated biosurfactant productivity was observed under hyper salinities with the dispersant addition. The productivity was increased from 0.09 to 0.19 g/L and from 0.08 to 0.20 g/L under the salinity of 50 and 70 g/L, respectively (Figure 3.2).

Biosurfactant productivity was also detected in the dispersant-only treatments (nearly 0.15 g/L), indicating degradation of dispersant components also required the microbial

secretion of biosurfactants (Zhu et al., 2021) (Figure 3.2). However, salinity did not show significant effects on biosurfactant productivity in these runs. Under the low salinity level (i.e., 0 and 5 g/L NaCl), the productivity level is similar to the runs with the addition of oil-only and oil plus dispersant, even though with a low cell abundance (Figure 3.2). It may be because the toxicity of dispersants under low salinity induced the microbial secretion of extracellular polymeric substances, including biosurfactants, to protect themselves from the toxic pressure under low salinities (Kuhl et al., 2013; Satpute et al., 2010).

A schematic diagram was used to visualize the associated scenarios under low, medium, and high salinities (Figure 3.2) based on the experimental data. Generally, increasing salinity is harmful to cell abundance and biosurfactant productivity in the oil microcosms. The addition of dispersant to oil could enrich cell abundance, especially under high salinity, which may be due to the degradation of dispersed oil and dispersant components.

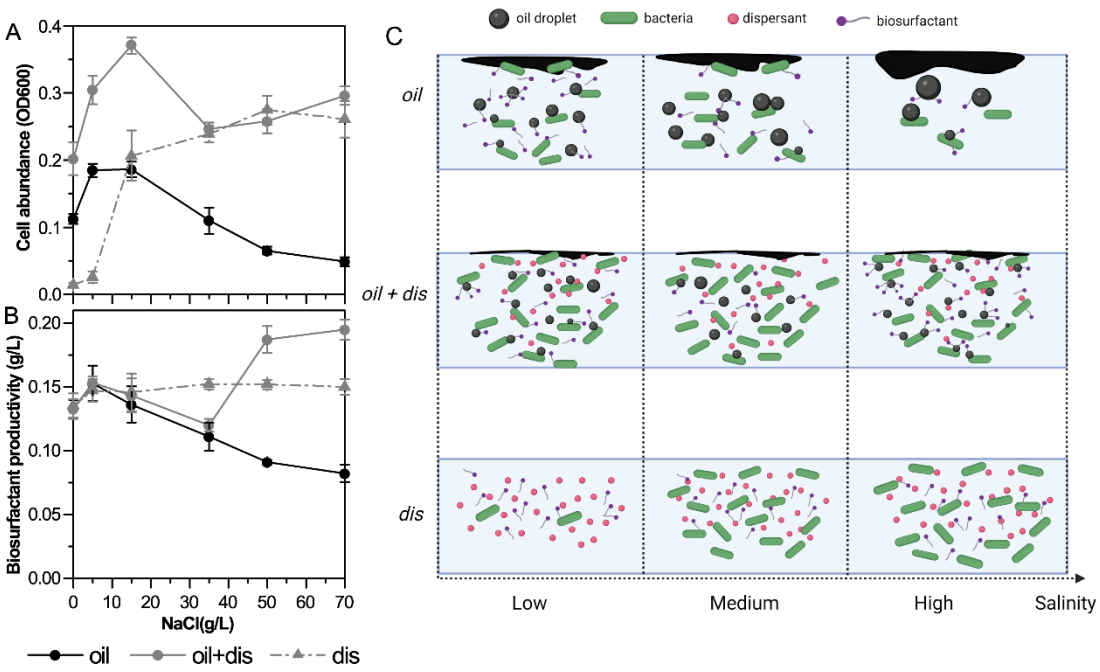

Figure 3.2 Effects of dispersant addition on (A) cell abundance and (B) biosurfactant productivity under different salinities; and (C) a schematic diagram for visualization.

3.3.3 Microbial biodegradation of crude oil and chemically dispersed oil

GC-MS detectable n-alkanes, aromatics, and their alkylated homologs were characterized to illustrate the oil biodegradation mechanism. The degradation ratio of each component was calculated by comparing it to control runs without bacterial inoculation. The results showed that *Exiguobacterium* sp. N4-1A preferred to degrade short-chain alkanes (i.e., C9 - C15) and LMW aromatics (e.g., alkylated decalins, naphthalene, and its alkylated homologs) (Figure 3.3). The result is different from the previous study (Figure 2.4), which showed that this species could also efficiently degrade long-chain alkanes. It may be because that supplement yeast extract in the medium could enhance the microbial biodegradation of long-chain alkanes (Liu et al., 2019).

Salinity also affected their biodegradation. Under the salinity of 5 - 15 g/L NaCl, *Exiguobacterium* sp. N4-1P performed the highest biodegradation capacity. Long-chain *n*-alkanes and HMW aromatics are relatively resistant to biodegradation due to their relatively stable chemical structures (González-Gaya et al., 2019). In general, the degradation ratios of HMW n-alkanes and aromatics at lower salinities (0 - 15 g/L NaCl) were higher than that of higher salinities (35 - 70 g/L NaCl) (Figure 3.3). Differently, degradation rates of LMW aromatics (i.e., naphthalene, alkylated decalins, and naphthalenes) were relatively high within the salinity of 5 - 50 g/L NaCl and the depression of oil degradation was

observed under the salinity of 0 and 70 g/L NaCl (Figure 3.3). These LMW components are relatively soluble, and microbes would like to grow in the hydrophobic phase under the salinity of 0 g/L NaCl, leading to their depressed degradation (Cao et al., 2020c). In contrast, the decreased biodegradation under high salinity (70 g/L NaCl) may primarily be due to the high osmotic pressures that suppress microbial growth.

The addition of the chemical dispersant can override the degradation barriers of LMW alkylated aromatics under both low and high salinities (Figure 3.3). The impact of dispersant addition on oil biodegradation under respective salinity was then assessed by comparing oil plus dispersant to oil-only treatments, using the difference in the value for the biodegradation ratio of each component. It showed that for these primarily degradable LMW components, the addition of dispersant mostly benefited their biodegradation under high salinities (50 and 70 g/L NaCl) but had negative effects under the middle salinities (15 and 35 g/L NaCl) (Figure 3.4). For HMW components, it is obvious that dispersant addition had relatively minor effects (most less than 0.08) on their biodegradation than LMW components. It means that dispersant addition could cause only the change of a specific component's removal ratio of less than 0.08. Obviously, dispersant addition can improve the degradation ratio of some HMW aromatics under high salinities, especially 50 g/L NaCl, but depress the degradation of HMW alkanes under salinities of 0 and 15 g/L NaCl.

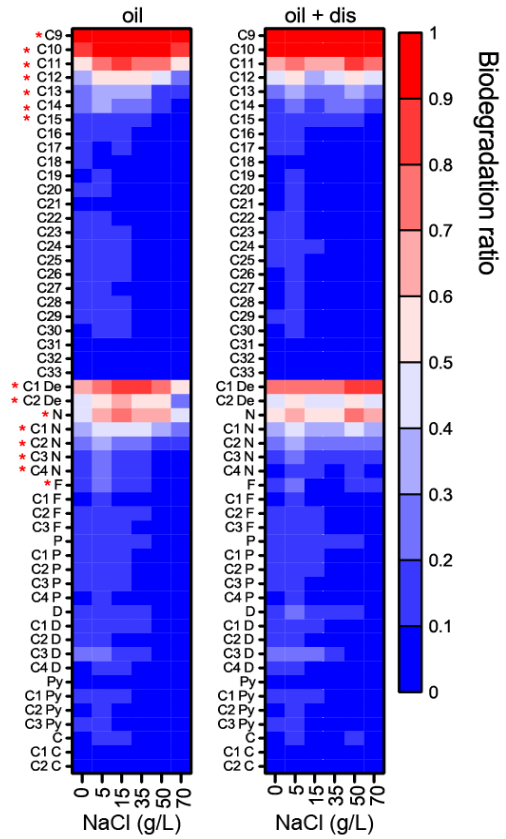

Figure 3.3 Biodegradation efficiency of GC-MS detectable components under different salinities in the oil (left) and oil plus dispersant (oil + dis, right) treatments.

In this figure, C9 - C33: n-alkanes with corresponding carbon atoms; C1 De and C2 De: alkylated decalins; N, C1 N, C2 N, C3 N, and C4 N: naphthalene and its alkylated homologs; F, C1 F, C2 F, and C3 F: fluorene and its alkylated homologs; P, C1 P, C2 P, C3 P, and C4 P: phenanthrene and its alkylated homologs; D, C1 D, C2 D, C3 D, and C4 D: dibenzothiophene and its alkylated homologs; Py, C1 Py, C2 Py, and C3 Py: pyrene and its alkylated homologs; C, C1 C, C2 C: chrysene and its alkylated homologs.

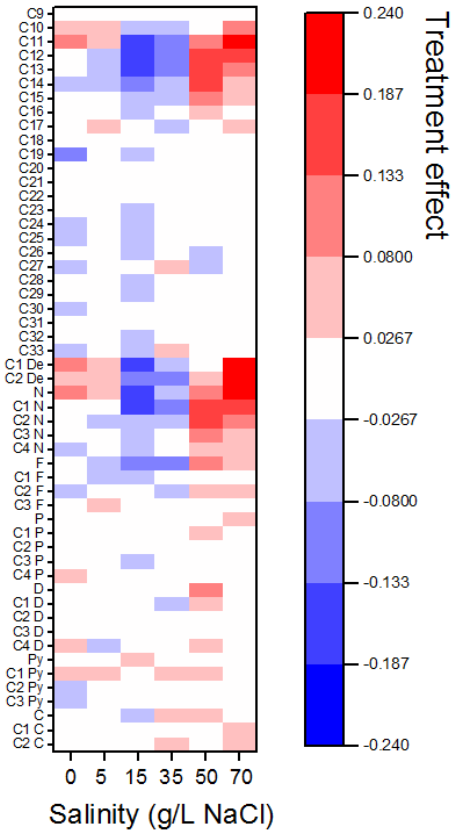

Figure 3.4 Heatmap showing the individual treatment effects regarding biodegradation of each oil component caused by dispersant addition.

The cluster analysis (Pearson correlation) was further applied to evaluate the dispersant effects on the biodegradation of each oil component (Figure 3.5). It showed that the salinity of 70 g/L was clustered to the 0 g/L NaCl, and 15 g/L was clustered to the 35 g/L NaCl. Besides, dispersant effects on the high and low salinities differed from the medium salinities. Further, dispersant effects on the biodegradation ratio of C10 - C15, alkylated decalins, naphthalene and its alkylated homologs, and fluorene clustered together.

Biodegradation ratios of GC-MS detectable oil components were clustered using Principal Coordinates Analysis (PCoA) (Abou Khalil et al., 2021) to illustrate the dispersant and salinity effects on oil biodegradation. The three points per condition are from the triplicate samples. It shows that oil biodegradation scenarios under salinities of 15 and 35 g/L NaCl were quite similar to those under the oil-only conditions (Figure 3.6). The addition of dispersant tended to level out the biodegradation efficiencies and provided them a tendency to merge with the biodegradation efficiencies under medium salinity conditions with oil-only treatment. The results indicate that dispersant addition can assist oil biodegradation under low and high salinities. In contrast, oil biodegradation behaviors segregated away from the group when adding dispersant under medium salinities. They shifted to those under the lower saline conditions (0 and 5 g/L NaCl) with oil-only treatments. The phenomenon suggests that the dispersant's effect is related to the decrease

in salinity.

The sum degradation ratio of the top 15 degradable components (i.e., C9 - C15, C1 and C2 alkylated decalins, naphthalene, and C1 - C4 alkylated naphthalene, and fluorene) was used to represent the total oil biodegradation ratio. The results showed that dispersant addition had no significant impact on the total oil biodegradation ratio under the low salinities, while depressed effects were observed under the medium salinities, and stimulated effects were evident under the high salinities (Figure 3.7).

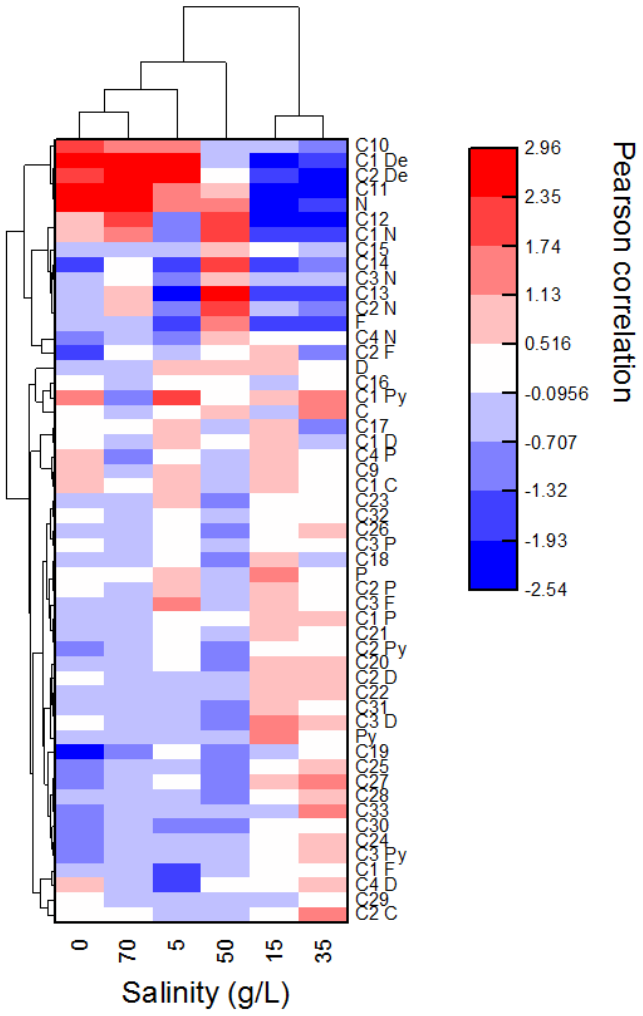

Figure 3.5 Cluster analysis (Pearson correlation) of dispersant treatment effects regarding the biodegradation ratio of each oil component under different salinities.

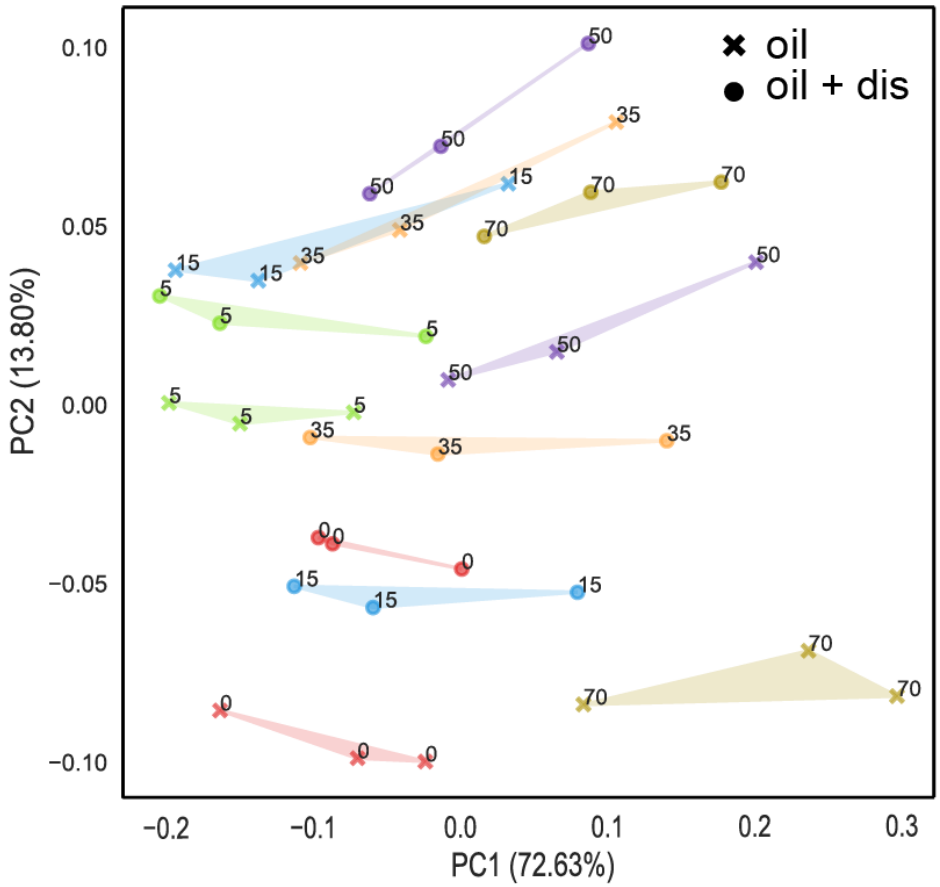

Figure 3.6 PCoA analysis of GC-MS detectable biodegradation ratio of oil components under different salinities.

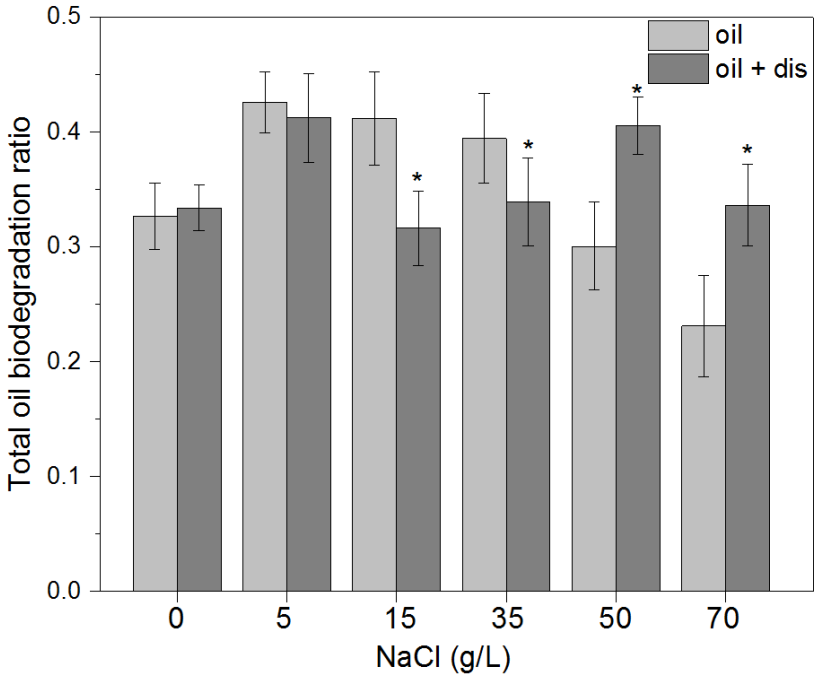

Figure 3.7 Total oil biodegradation ratio under different salinities in the oil-only and oil plus dispersant treatments. "*" indicates significantly different.

3.3.4 Causal inference results and interpretation

3.3.4.1 A weighted DAG revealing the causal relationships

We firstly built nine causal links to reveal the causal effects among each parameter. (Figure 3.8). By assigning the normalized ATE values to the edges in the DAG, the diagram became weighted and could clearly reflect the strength of the complicated relationships among the variables (Figure 3.8). Specifically, for the causal relationships with salinity involved, the ATE represents the change in the outcome brought by one unit increase of salinity (l g/L NaCl). For the dispersant-addition involved causal relations, the ATE represents the outcome change compared with those with no dispersant-addition. For the cell abundance and biosurfactant productivity, the ATE values are normalized to represent the increment from their lowest level to the highest level in both oil only and oil plus dispersant treatments, as shown in Figure 3.2. The weighted DAG showed that per unit increase of salinity led to a drop of 0.002 OD600 (i.e., cell abundance), 0.001 g/L biosurfactant productivity, and 0.004 (4‰) of total oil biodegradation ratio. The addition of dispersant could enhance the cell abundance, biosurfactant productivity, and total oil biodegradation ratio at 0.477 OD600, 0.3 g/L, and 0.034 (34‰), respectively. Besides, the increase in normalized cell abundance can cause positive effects on biosurfactant productivity (0.813 g/L) and the overall oil biodegradation ratio (0.525). The growth of

normalized biosurfactant productivity can meanwhile enlarge the overall oil biodegradation ratio (0.544).

Taking all these ATE values together, the positive effects of dispersant addition on the oil biodegradation ratio under various salinities were observed. For the halotolerant oil-degrading bacteria, the inhibiting effects of salinity increment on oil biodegradation are minimal under a broad salinity range. Most importantly, the contributions of dispersant, cell abundance, and biosurfactant productivity to oil biodegradation were unraveled. The addition of dispersant had only 0.034 (34‰) direct contribution to the total oil biodegradation ratio whilst majorly increasing the cell abundance and biosurfactant productivity resulting in oil biodegradation enhancement (Figure 3.8). The results indicated that the positive impact of dispersant addition on biodegradation was achieved indirectly by boosting cell abundance and biosurfactant productivity. Such findings would further help prove the overall positive effects of dispersant application, which could promote cell growth and biosurfactant production rather than serving as a competing food source of crude oils (Kleindienst et al., 2015b).

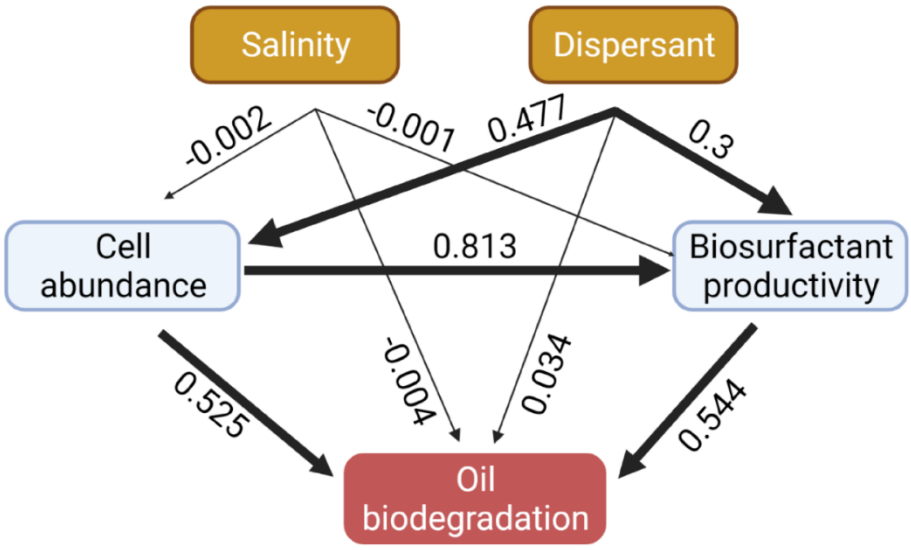

Figure 3.8 A weighted DAG showing ATE among different treatments.

3.3.4.2 Quantitative causal effects of CATE

Compared to ATE, a generic metric which is more suitable to reflect overall tendencies, the CATE enables interpretation of the causal relationships from another perspective: condition-specific estimations of causal effects. In this study, CATE was estimated under two conditions: (1) with or without the addition of dispersants and (2) different salinity levels. The results showed that dispersant addition had negative effects on oil biodegradation ratio under low salinities but positive effects under high salinities. The impact of dispersant addition on oil biodegradation increased along with the salinity rise (Figure 3.9), indicating that dispersant addition could alleviate the negative effects on oil biodegradation caused by salinity increase. Besides, dispersant addition had positive effects on cell abundance improvement at all these salinities (Figure 3.9). When no oil was introduced, the dispersant itself had limited enrichment of cell abundance under low salinities (Figure 3.2). It indicated that the degradation of dispersant components might account for the high proportion of cell abundance in an oil plus dispersant system under low saline conditions. Therefore, the negative effects of dispersant application on oil biodegradation under low saline conditions might be mainly because the oil biodegradation capacity under the low salinities was originally high, and dispersant components may be primarily degraded competing with the degradation of oil components.

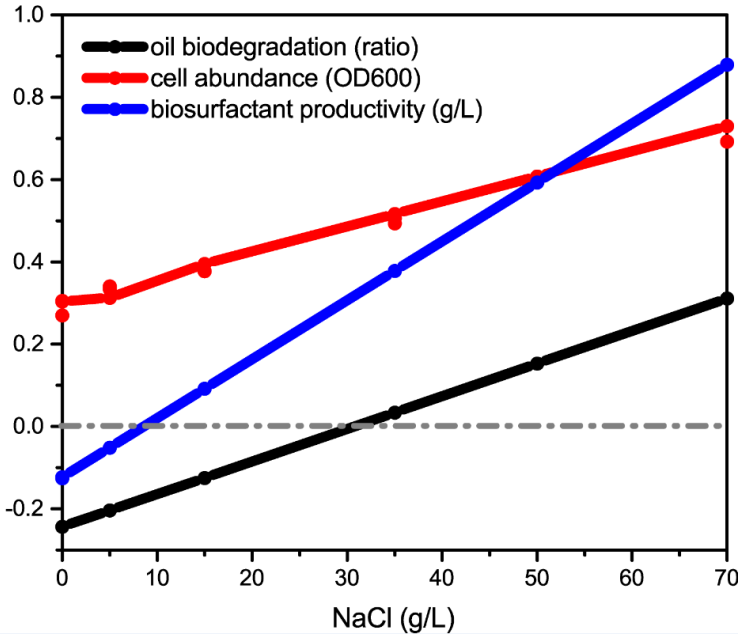

Figure 3.9 CATE of dispersant addition affecting overall oil biodegradation ratio, cell abundance (OD600), and biosurfactant productivity (g/L) under different salinities.

For the salinity effects on the global oil dispersion operations, dispersant addition can eliminate the negative effects (8‰) caused by the per-unit increase of salinity and lead to slightly positive effects (2‰) on oil biodegradation (Figure 3.10). An increase in salinity had positive effects on cell abundance and biosurfactant productivity, indicating salinity increment is overall beneficial for dispersant usage. Meanwhile, the different values of CATE estimates suggest the fluctuant effects of dispersant usage on oil biodegradation under different salinities, providing scientific support for guideline development of dispersant application under different saline conditions.

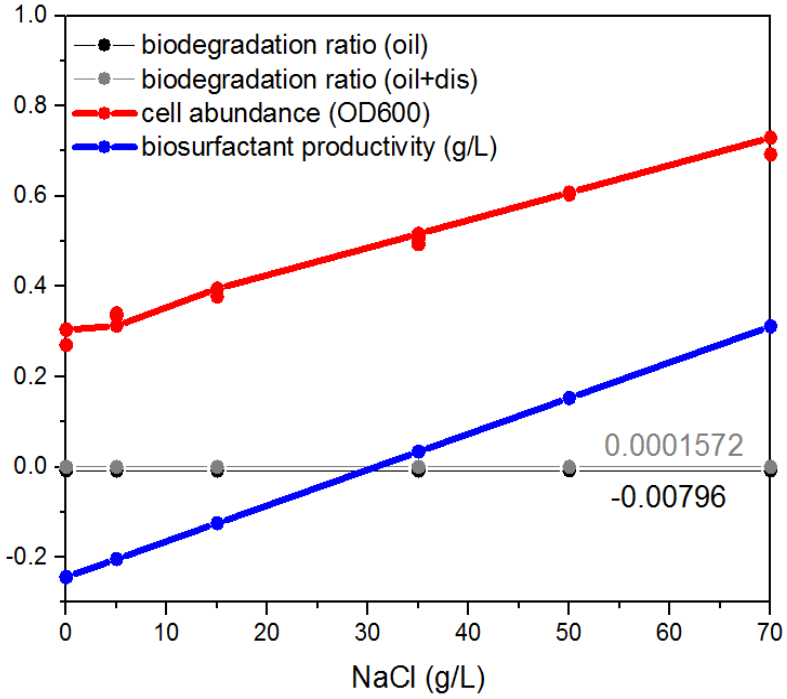

Figure 3.10 CATE of increase of per salinity on biodegradation ratio (oil), biodegradation ratio (oil plus dispersant), cell abundance (OD600), and biosurfactant productivity (g/L).

3.3.5 Evaluation of dispersant application under diverse saline environments

Effects of individual salinity or dispersant application on oil biodegradation have been previously reported. An increase in salinity could cause inhibiting effects on oil biodegradation within microbial communities (Abou Khalil et al., 2021). In contrast, dispersant application had controversial effects on oil biodegradation. Dispersant application can enhance oil bioavailability to stimulate biodegradation (Tremblay et al., 2017), while the increased oil concentration, especially these xenobiotics in the water column, could cause inhibitory effects (Kleindienst et al., 2015b). Besides, the dispersant components could be primarily utilized to enrich cell abundance, for competing for oil biodegradation, or for enhancing oil biodegradation (Rahsepar et al., 2016). In addition, microbes would secrete biosurfactants for increasing oil bioavailability and meanwhile enriching cell amounts to degrade oils further.

Although previous studies have explored the individual effects of salinity or dispersant on oil biodegradation, there is a lack of evaluation regarding the comprehensive impacts of salinity and dispersant addition on oil biodegradation. There were multiple causal links among salinity, dispersant application, cell abundance, biosurfactant productivity, and oil biodegradation in the aquatic systems. The related processes were extraordinarily sophisticated and could hardly be answered by traditionally popular indexes (e.g.,

coefficients in regression models or feature importance in tree-based machine learning models that indicate variable contributions).

To unravel the relationships among these aforementioned parameters, this study proposed nine causal links in a DAG diagram and employed the SCM, a diagram-based causal inference method with the capacity of conducting quasi-experiments, to quantitatively estimate the strength of the causal links with the aid of machine learning. By integrating experimental work with causal inference analysis, it was revealed that dispersant addition could override the biodegradation barriers under hyper salinities primarily through enriching cell abundance. Hence, dispersant application could be a promising oil spill response option in hypersaline (50 - 70 g/L NaCl) environments. Under other salinities, especially the low salinities (0 - 5 g/L NaCl), dispersant application may not be advantageous.

3.4 Summary

In this study, the application of the chemical dispersant Corexit 9500A could overcome the biodegradation barriers under high salinities and lead to the formation of GC-MS detectable components through oil biodegradation similar to the lower salinities. Nine causal links were elaborated in a weighted DAG, which shows that dispersant addition can enhance the degradation of crude oils mainly through enriching cell abundance. These results suggest the beneficial usage of dispersants under hypersaline aquatic systems. The employed logic will shed light on adopting advanced causal inference tools to unravel the complicated contaminants' biodegradation process and elicit further discussion and research on environmental causal inference.

CHAPTER 4 MICROBIAL COMMUNITY RESPONSES TOWARDS CHEMICAL DISPERSANT APPLICATION DURING A MARINE DILBIT SPILL[3]

[3] This chapter is generated based on and expanded from the following paper:

Cao, Y., Zhang, B., Greer, C., Lee, K., Cai, Q., Song, X., Tremblay, J., Zhu, Z., Dong, G., & Chen, B. (2022). Metagenomic and metatranscriptomic responses of chemical dispersant application during a marine dilbit spill. *Applied and Environmental Microbiology*, 88(5). DOI: 10.1128/aem.02151-21

Roles: Cao designed and conducted the study under the guidance of Dr. Baiyu Zhang and Dr. Charles W. Greer and acted as the first author of the manuscript. Cai, Song, and Trembley did the methods. Other co-authors did the review and editing. Most contents of this paper were written by Cao and further polished by the other co-authors.

4.1 Introduction

The global energy demand boosts the daily unrefined petroleum use worldwide up to nearly 100 million barrels per day. Meanwhile, the production of unconventional oils, such as bitumen, has also increased (Nduagu & Gates, 2015; Sleep et al., 2018). For transportation in pipelines, bitumen blends are diluted with lower-density hydrocarbons to form dilbit (diluted bitumen) oils. The increase in marine dilbit transportation increases the risk of a potential oil spill, causing harmful impacts on marine ecosystems and coastal environments (Johannessen et al., 2020). As an important marine oil spill treating agent, the chemical dispersant can transfer floating oil slicks into the water column by lowering the oil-water interfacial tension and emulsifying oils into tiny droplets, which increases their bioavailability for degradation.

Natural attenuation field trails, although reflecting the real marine environment with the real wave and current impact, are expensive, logistically and legislatively complicated. Therefore, laboratory microcosm studies have been widely adopted to identify dispersant effects on the natural attenuation of spilled oils under well-controlled and comparable conditions. Recent advancements in metagenomic and metatranscriptomic analyses, together with the oil composition characterization, have been applied as emerging tools to reveal the whole picture of microbial functions and activities and oil biodegradation process,

elucidate the effects of dispersant application on oil biodegradation, and predict their transport in marine environments. To date, controversial results on the biodegradation of chemically dispersed oil have been reported. They could be explained according to the types of spilled oils and seawaters and the microcosm conditions. The enhanced oil bioavailability, as a result of dispersant application, can stimulate biodegradation (Prince et al., 2013; Tremblay et al., 2017), while the increased oil concentration in the water column may cause short-term inhibitory effects toward biodegradation (Kleindienst et al., 2015a; Rahsepar et al., 2016). Besides, compounds present in dispersant formulations can also act as carbon and energy sources and may be preferred by some microorganisms and hence compete with oil biodegradation (Kleindienst et al., 2015b). However, previously adopted microcosms for oil spill investigations can be improved by decreasing the used oil concentrations and enlarging the microcosm scale.

High oil concentrations (more than 100 ppm) in small-scale microcosms (a few hundred milliliters) have been widely applied (Kleindienst et al., 2015b; Prince et al., 2013; Tremblay et al., 2019; Tremblay et al., 2017). In the field, however, dispersed oils will be rapidly diluted in the open oceans due to high wave energies and diffuse apart and drop to a concentration much below 100 ppm within a few hours of dispersant application (Lee et al., 2013). The exponentially increased oil concentrations applied to closed systems will

limit biodegradation due to the depletion of nutrients (Lee et al., 2013; Prince & Butler, 2014). The small-scale microcosms, therefore, were supplemented with external nutrients (i.e., nitrogen and phosphate) to facilitate oil biodegradation (Gofstein et al., 2020; Ortmann et al., 2019; Schreiber et al., 2019; Tremblay et al., 2019; Tremblay et al., 2017). However, the increased nutrients were reported to eliminate some essential degraders like *Cycloclasticus* while accelerating the growth of others, such as *Alcanivorax* (Singh et al., 2014), which will affect the actual evaluation of microbial community dynamics for oil biodegradation.

In addition, a small-scale system can hardly include a sufficient inoculum of hydrocarbonoclastic bacteria (Lewis & Prince, 2018) and fails to have an in-situ reflection of microbial communities in marine environments (Kujawinski et al., 2020; Schreiber et al., 2019). Further, microbial populations in a small-scale microcosm are more susceptible to stochastic effects over time, especially for species at the low diversity bottleneck, causing a biased subsequent microbial recovery trajectory (Pagaling et al., 2017; Zhou & Ning, 2017). Although it is challenging to design and interpret microcosms for monitoring in-situ conditions, increasing the microcosm scale may help provide more reproducible community results. Such a hypothesis has been studied in previous nutrient-cycle microcosm studies (Pagaling et al., 2017) but not for oil spill investigations. Taking all

these together, an in-depth understanding of the scale-up effect on oil biodegradation is of great importance to understanding the response of microbes to dispersed oils and their ultimate fate in a natural marine environment (i.e., low dilbit concentration and no additional nutrients).

In this study, two-scale microcosm systems (i.e., small - 250 mL and large - 1500 mL) without nutrient addition using a low dilbit concentration (30 ppm) were set to track microbial community dynamics during a hypothetical marine dilbit (i.e., Cold Lake Blend, CLB) spill with and without a chemical dispersant (i.e., Corexit 9500A). Through 16S rRNA gene amplicon sequencing, we examined the impact of microcosm scale on community dynamics over time. To further explore microbial functions and activities, shotgun metagenomic and metatranscriptomic sequencing with combined contig-based and binning-centric analysis was applied to the large-scale microcosms.

4.2 Materials and Methods

4.2.1 Microcosm setup

All biotic and abiotic microcosms were performed under identical settings with continuous mixing at 150 rpm at room temperature (~22 °C). A total of 80 L of seawater (~10 m depth, 31.24 ppt) was collected from the Ocean Science Centre at Memorial University (47.6248°N, 52.6627°W) in the spring of 2019. This seawater was well mixed

and used immediately for the preparation of all the microcosms throughout this study to ensure they were homogenous. All flasks were acid-washed and autoclaved prior to use, and all microcosms were conducted in triplicate. The biotic microcosms were set up with freshly collected seawater, while the abiotic microcosms were set up using pre-sterilized seawater using an autoclave. For small-scale microcosms, each 500 mL flask was filled with 250 mL seawater. For large-scale microcosms, each 4000 mL flask was filled with 1500 mL seawater. The dilbit (Cold Lake Blend, CLB) and chemical dispersant (Corexit 9500A) were obtained from Fisheries and Oceans Canada, Dartmouth NS. The dilbit was fully dispersed at room temperature and added directly using a pipette (GILSON MICROMAN E) to achieve a final dilbit concentration of 30 ppm (i.e., 7.5 mg in small-scale microcosms and 45 mg in large-scale microcosms). To select the dispersant dose, the dispersion effectiveness was tested beforehand at dispersant:oil ratios (DOR, v/v) of 1:10, 1:20, 1:50, and 1:100, respectively, using the Baffled Flask Test. A DOR of 1:10 was selected because it led to the best performance. The dispersant was then directly pipetted onto the oil slick (i.e., 0.82 µL in small-scale microcosms and 4.92 µL in large-scale microcosms). The experimental design for the microcosm studies is presented in Figure 4.1.

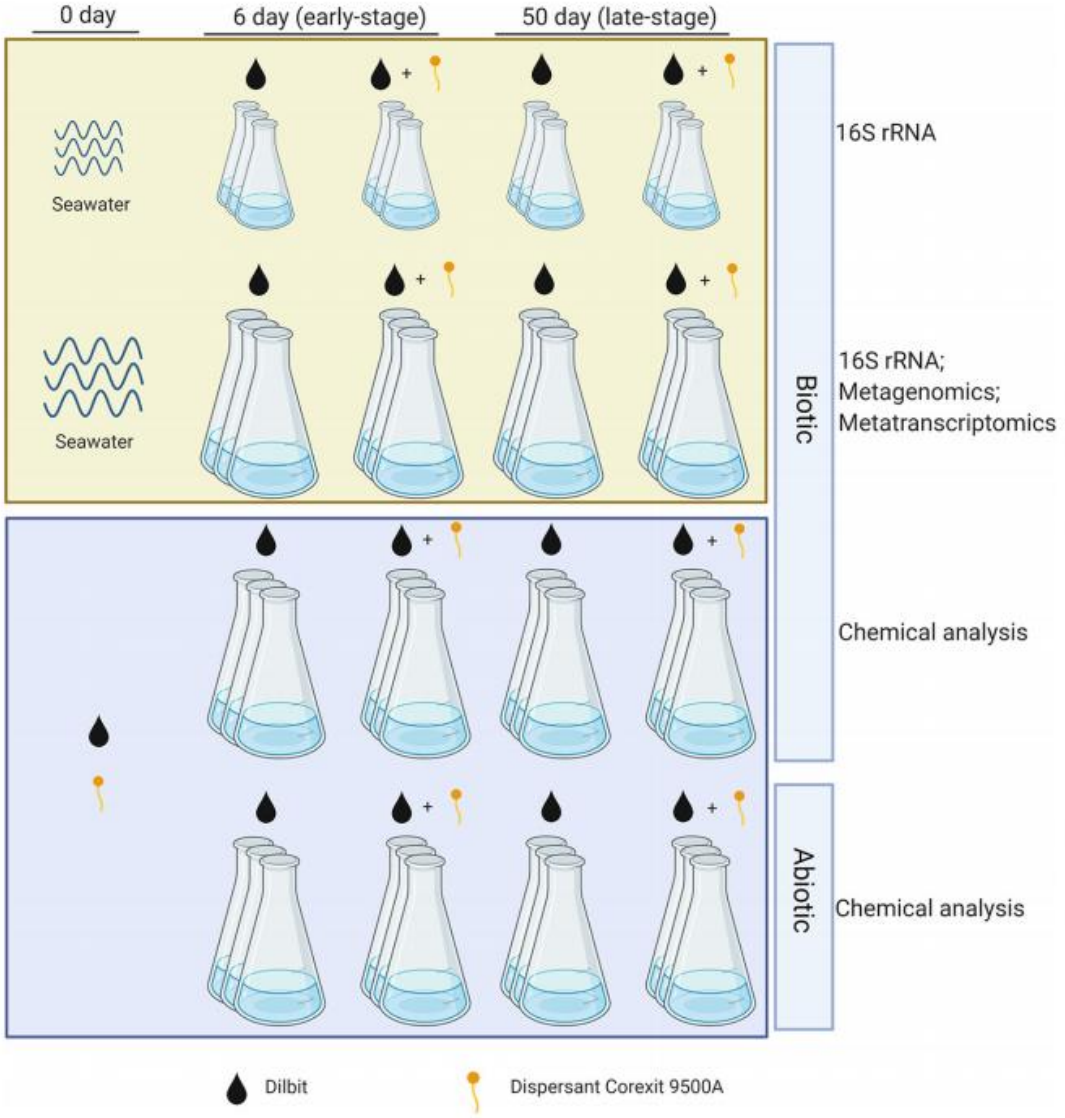

Figure 4.1 Overview of the microcosm setup.

4.2.2 Chemical analysis

Determination of n-alkanes and aromatics of dilbit and dispersant components was performed by sacrificing the complete microcosm contents (including the flask wall) after 6 and 50 days of incubation. Liquid-liquid extraction was performed for extraction (Song et al., 2018). Approximately 30 mL of dichloromethane was added three times into each large-scale flask to extract the hydrocarbons. The three organic solvent fractions were combined, and residual water was removed using anhydrous sodium sulfate. The solvent fraction was concentrated to 1 mL. An Agilent 7890A GC-MS equipped with a DB-5MS column was applied for oil analysis according to procedures developed in our previous study (Cao et al., 2020b). Helium was applied as a carrier gas at a flow rate of 1.0 mL $min^{-1,}$ and the GC oven temperature was set at 50 °C for 2 min, then ramped up at a rate of 6 °C min^{-1} to 300 °C for 20 min. MS detection was conducted in the electron ionization mode at 70 eV, and the ion source temperature was set at 300 °C. Individual compounds were identified from their mass spectra. All hydrocarbon data was normalized in reference to the conserved internal biomarker 17α(H), 21β(H) - hopane.

4.2.3 Sample preparation for DNA and RNA sequencing

Experimental procedures for sample preparation and DNA and RNA sequencing followed the same protocol as described previously (Schreiber et al., 2019). At each time

point, 6 and 50 days, microcosms for genomics analysis were harvested by filtering the entire contents of each flask through 0.22 μm polyethersulfone membranes. The initial seawater (250 mL for small-scale and 1500 mL for large-scale microcosms) at T = 0 was directly filtered. Microbes were collected on the membranes, which were transferred into 50 mL Falcon tubes and immediately flashed frozen by submersion in liquid nitrogen and stored at -80 °C. The DNA and RNA were extracted simultaneously from the filters following the Qiagen RNeasy Power Water kits. The extracted DNA samples were treated with RNase If (New England Biolabs) to remove RNA for downstream 16S rRNA gene amplicon (for both small and large scales microcosms) and shotgun metagenomic sequencing (only for large-scale microcosms). The RNA samples were treated with the Turbo DNA-free kit to remove all the remaining DNA. The rRNA-depleted RNA was then subjected to reverse transcription to produce complementary DNA (cDNA) for shotgun metatranscriptomic sequencing for large-scale microcosms.

4.2.4 16S rRNA gene amplicon sequencing for both small and large scales microcosms

The V4 and V5 hyper-variable region of the 16S rRNA gene amplified with 515F-Y (5′-GTGYCAGCMGCCGCGGTAA-3′) and 926R (5′-CCGYCAATTYMTTTRAG TTT-3′) was used to detect both archaea and eubacteria. The 16S rRNA gene libraries for sequencing were prepared according to Illumina's "16S Metagenomic Sequencing Library

Preparation" guide (Part # 15044223 Rev. B). Amplification of the DNA was performed in 25 μL containing 0.5 - 15 ng of DNA template, 0.4 μM each primer, and 0.5 mg/ml Bovine Serum Albumin and Kapa HiFi HS RM polymerase (Roche). PCR amplification reaction conditions involved an initial denaturation at 96 °C for 3 min, followed by 25 cycles of 30 s at 95 °C, 30 s at 55 °C, and 30 s at 72 °C, and final elongation for 5 min at 72 °C. PCR products were evaluated by gel electrophoresis and purified with the Macherey-Nagel NucleoMag NGS Clean-up and Size Select kit (D-MARK Biosciences). Equal amounts of each purified PCR product were pooled and sequenced using the Illumina Miseq platform.

Sequencing data were analyzed using Amplicon Tagger (Tremblay & Yergeau, 2019). The raw reads were quality-checked, assembled, and clustered at 97% (VSEARCH) to form the final clusters and OTUs (Rognes et al., 2016). Clusters having abundances lower than 25 were discarded. The OTUs were assigned to a taxonomic lineage with the RDP classifier software using an in-house training set containing the complete Silva release 128 databases. With taxonomic lineages in hand, an OTU table limited to bacterial and archaeal microorganisms was generated. A consensus rarefied OTU table was generated as described. Taxonomic summaries were generated using QIIME v1.9.1. Community richness and diversity were estimated with ten times rarefaction analysis to 10765 sequences to improve data robustness. Alpha diversity (i.e., community richness and diversity metrics) and beta

diversity (i.e., Bray Curtis dissimilarity matrix) were computed using the R package "vegan". Statistical significance of diversity and richness differences was assessed using Student's t-test.

4.2.5 Shotgun metagenomic and metatranscriptomic analysis for large-scale microcosms

Metagenomic and metatranscriptomic libraries were sequenced on an Illumina HiSeq4000 system with a rapid mode 2 × 100 bp configuration. A total of 15 samples were submitted for metagenomic sequencing, and 9 samples (i.e., the initial seawater at T=0 and microcosms after 6 days of incubation with sufficient RNA) were used for metatranscriptomic sequencing. The resulting data (9.8 Gb for metagenome and 55.9 Gb for metatranscriptome) were processed through bioinformatic pipelines described previously (Tremblay et al., 2017). Shotgun metagenomic sequencing reads were quality controlled (QC) (Trimmomatic v0.39) and co-assembled using Megahit v1.2.9 (Li et al., 2016b). The taxonomy of each contig was determined using CAT v5.0.3. Genes were *ab initio* predicted on each assembled contig using Prodigal v2.6.2 (Hyatt et al., 2010) and annotated following the JGI's guidelines, including the assignment of KEGG orthologs. The QC-passed reads were mapped against contigs to assess the quality of assembly and to obtain contig abundance profiles. Alignment files in bam format were sorted by reading

coordinates using samtools v1.9 (Li & Durbin, 2009), and only properly aligned read pairs were kept for downstream steps. Each bam file (containing properly aligned paired-reads only) was analyzed for coverage of contigs and predicted genes using bedtools v2.17.0 (Kuppusamy et al., 2016) using a bed file having each gene coordinate on each contig. Only paired reads both overlapping their contig or gene were considered for gene and contig abundance computation. These latter matrices were normalized to obtain CPM (Counts Per Million) using edgeR v3.10.2 (Robinson et al., 2010). Shotgun metagenomic data were further processed to generate MAGs using MetaBAT v2.12.1 (Kang et al., 2019). Genes annotated with KEGG entries associated with dilbit accessing and degradation were chosen for a focused analysis. For the microbial chemotaxis and secretion systems, genes in Bacterial Chemotaxis (ko02030) and Bacterial Secretion System (ko03070) were integrated. For the degradation of alkanes, genes in Fatty Acid Degradation (ko00071) that are responsible for the degradation of alkanes were analyzed. For the degradation of aromatics, genes in modules (M00538, M00537, M00419, M00547, M00548, M00551, M00568, M00569, M00539, M00543, M00544, M00418, M00541, M00540, M00534, M00624, M00623, M00636, M00545) in Degradation of Aromatic Compounds (ko01220) were summarized.

Shotgun metatranscriptomic sequencing data were controlled for quality

(Trimmomatic) and aligned on metagenomic co-assembled contigs generated as described above to obtain a gene expression matrix of each sample readily comparable with the gene abundance matrix obtained with metagenomic data. The gene expression matrix was normalized with edgeR to generate normalized CPM counts. All raw sequence reads, including 16S rRNA gene amplicon sequencing, metagenome, and metatranscriptome, have been submitted to NCBI's SRA and are available under the BioProject PRJNA704368.

4.3 Results and Discussion

4.3.1 Effects of increasing microcosms scale on microbial community dynamics evaluation over time

We performed two sets (i.e., small and large-scale) of microcosms using the fresh seawater sampled from the same place at the same time with incubation for 6 days (early-stage) and 50 days (late-stage), respectively. The DNA was harvested from the initial seawater and each microcosm for 16S rRNA gene amplicon sequencing. Four samples (one small-scale seawater sample and three early-stage small-scale microcosms amended with dilbit only) produced invalid results due to their low extractable DNA concentrations (Figure 4.2). The amplicon data from a total of 26 samples were processed to generate Operational Taxonomic Units (OTUs) for community profiling.

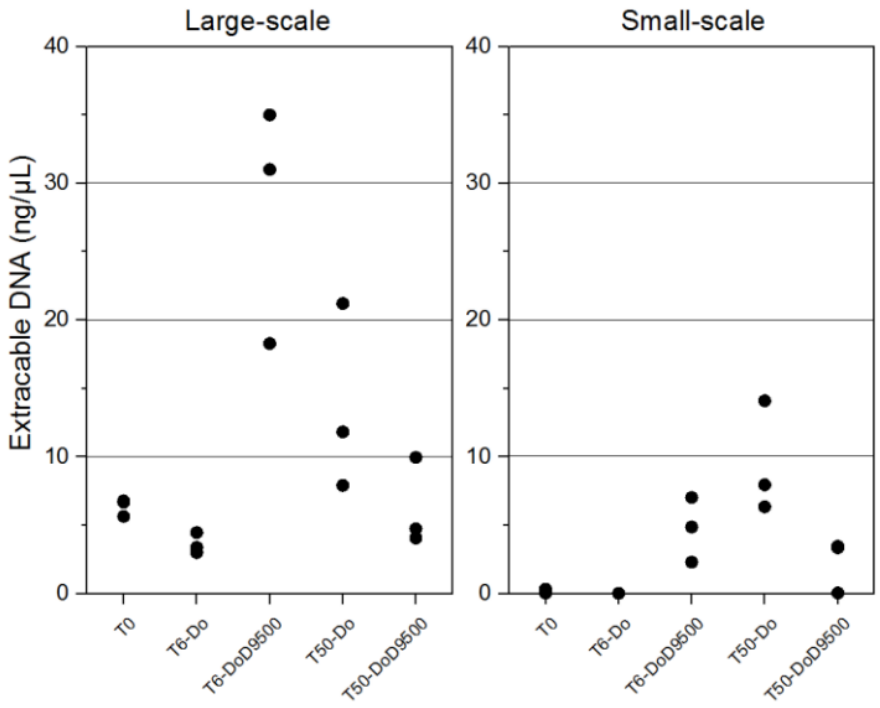

Figure 4.2 DNA concentration extracted from initial seawater and each microcosm.

The DNA was adjusted to a final volume of 100 µL.

In this figure, T0: the microbial community of the initial seawater; T6-Do and T6-DoD9500: microbial communities in the early stage (6 days) with dilbit-only and dilbit plus dispersant, respectively; T50-Do and T50-DoD9500: microbial communities in the late stage (50 days) with dilbit-only and dilbit plus dispersant, respectively. Small-scale: 250 mL; Large-scale: 1500 mL microcosms.

The microbial richness (i.e., based on Chao 1 and Observed Species indexes) and diversity (i.e., based on Shannon and Simpson indexes) metrics of the initial seawater samples for the large volume (1500 mL) were higher than those of the small volume (250 mL) (Figure 4.3). The different microbial richness and diversity results of the same raw seawater could be explained by the limited DNA extracted from the small-scale communities (Figure 4.2). Some species with extremely low abundance may be under the detection limit due to unsuccessful PCR amplification for sequencing. This indicates that large-scale microcosms could better represent *in situ* microbial communities of the marine environment due to the increased biomass for deep sequencing. The rarefaction curve also showed that the large volume provided a better estimate of the alpha diversity and reduced stochasticity between replicates of each treatment (Figure 4.4). In the early-stage large-scale microcosms, microbial richness and diversity of microcosms amended with dilbit plus dispersant were significantly lower than those amended with dilbit-only (Figure 4.3). In the late-stage large-scale microcosms, microbial communities were equally rich and diverse regardless of dispersant addition (Figure 4.3). In contrast, in the late-stage small-scale microcosms, dispersant addition apparently still had a negative effect on microbial richness but not on microbial diversity. Overall, this indicates that dispersant addition plays a significant role in shaping the early-stage communities regardless of the microcosm scale.

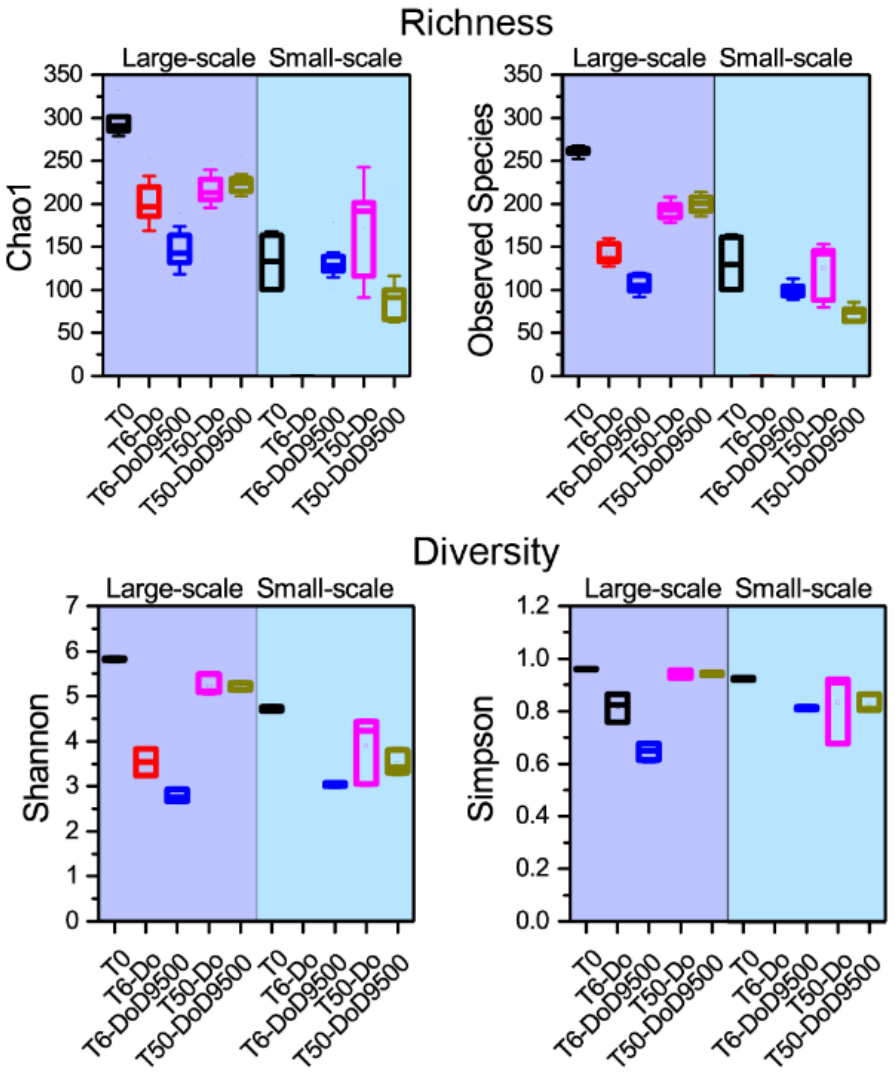

Figure 4.3 Alpha diversity analysis for microbial richness (Chao1 and Observed Species indexes) and diversity (Shannon and Simpson indexes).

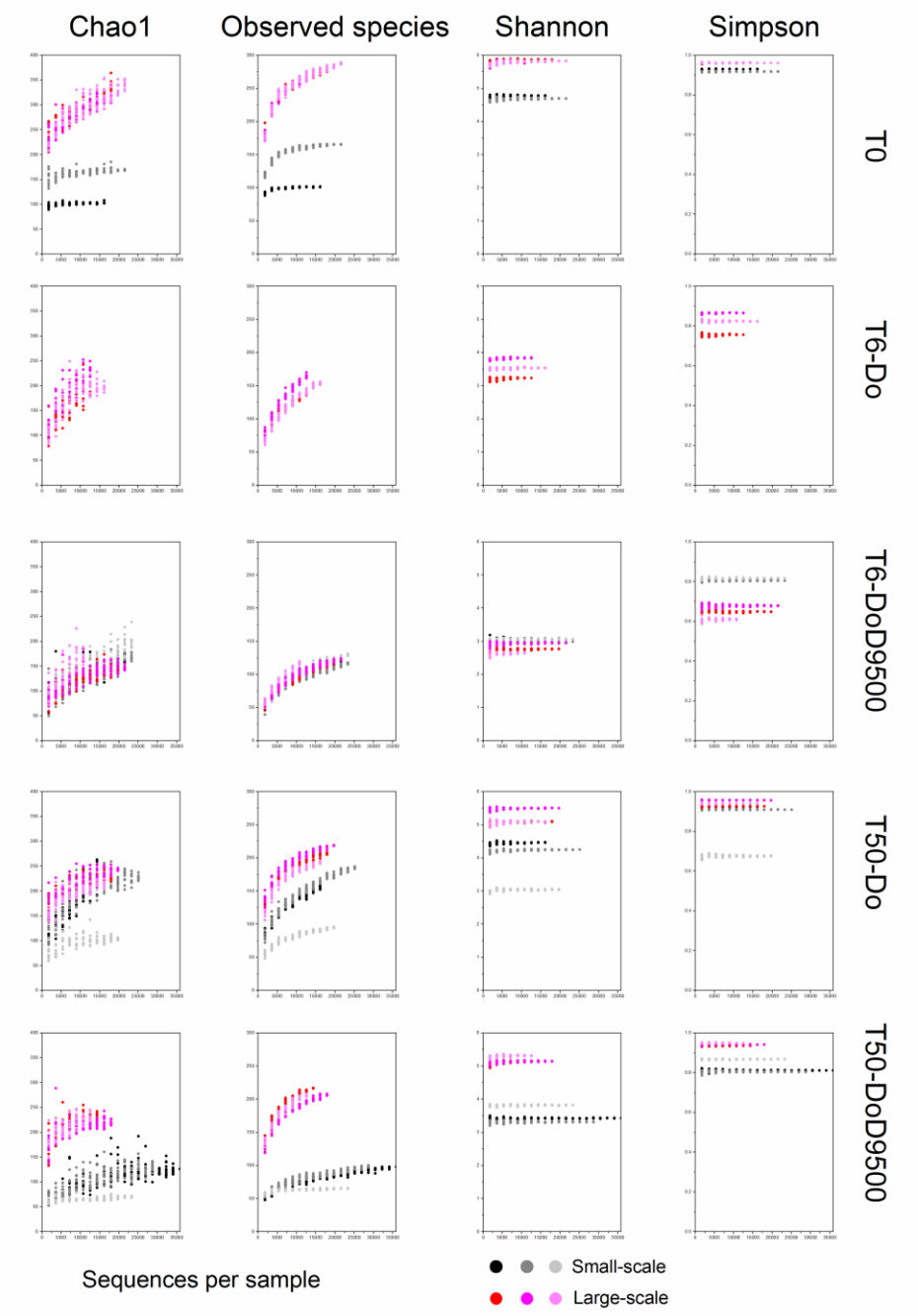

Figure 4.4 Rarefaction curves of the sequencing data in each microcosm.

The beta diversity analysis (i.e., PCoA, principal-coordinate analysis for Bray Curtis dissimilarity matrix) showed that microbial populations become less and less similar to the initial community over time (Figure 4.5). This finding is well-aligned with that reported by Schreiber et al. (2019), in which the incubation time is identified as an essential factor in shaping community composition. In the early stage, dilbit plus dispersant communities are more dissimilar to the initial community than dilbit-only communities (Figure 4.5), similar to what was reported by Tremblay et al. (2019) for small-scale crude oil microcosms. In the late-stage microcosms, microbial communities of both treatments gradually clustered together except for those in small-scale microcosms amended with dilbit plus dispersant (Figure 4.5). Both alpha and beta diversity analyses showed that late-stage large-scale microcosms were more similar, suggesting that dispersant application in the marine environment would have only a short-term effect on microbial communities after a dilbit spill.

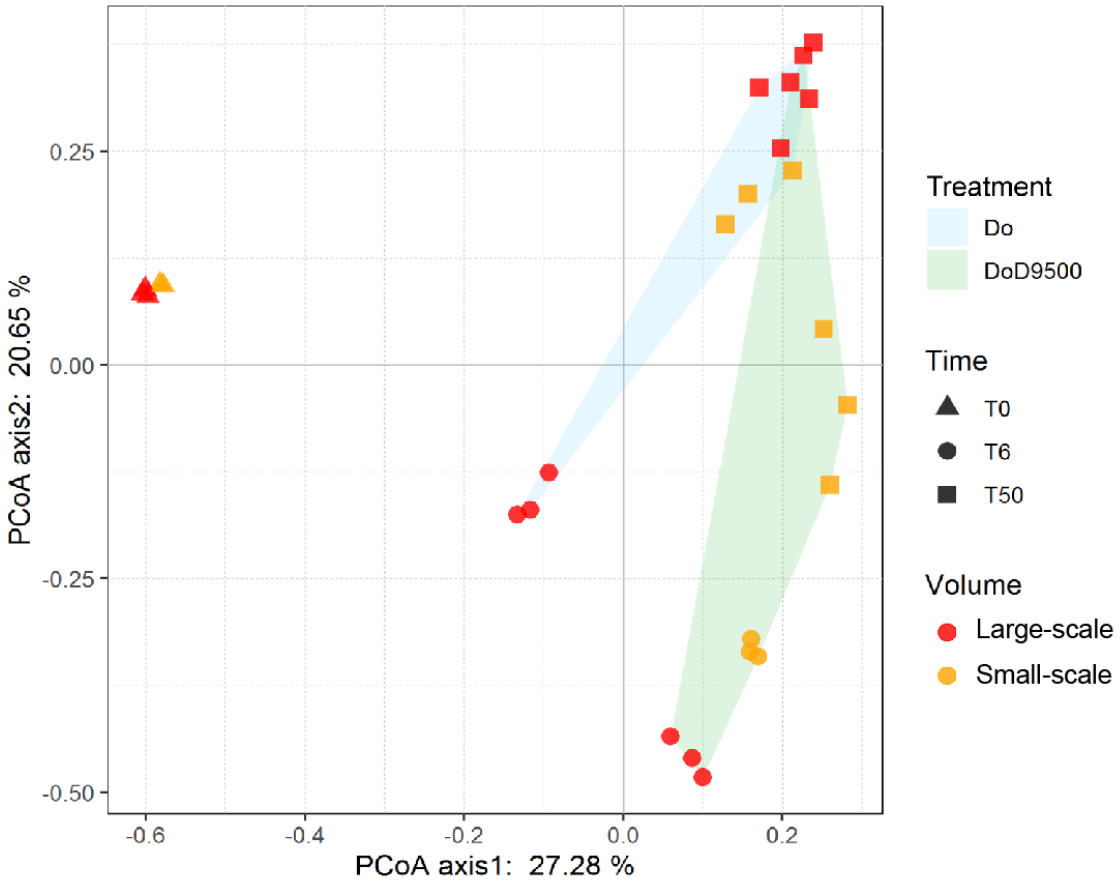

Figure 4.5 Beta diversity analysis using PCoA analysis.

In this figure, Do: dilbit-only treatment; DoD9500: dilbit plus dispersant treatment; T0: the microbial community of the initial seawater; T6 and T50: microbial communities in the early stage (6 days) and late stage (50 days); Large-scale: 1500 mL microcosms; Small-scale: 250 mL microcosms.

The microbial taxa at the class level showed that the initial seawater (T0) was dominated by the phylum of *Proteobacteria* (*Gammaproteobacteria* and *Alphaproteobacteria* classes) and *Bacteroidetes* (*Flavobacteriia* class) (Figure 4.6). *Proteobacteria,* especially *Gammaproteobacteria* were stimulated in the early stage, while *Alphaproteobacteria* were promoted in the late stage in both scale microcosms, regardless of dispersant addition (Figure 4.6). The class *Gammaproteobacteria* contains many important members and diversity of hydrocarbonoclastic bacteria involved in oil degradation (Sierra-Garcia et al., 2020), and *Alphaproteobacteria* persist more in PAH contaminated sites (Kuppusamy et al., 2016). In the late stage, the abundance of microbial classes (e.g., *Verrucomicrobiae*, *Betaproteobacteria*, *Cytophagia*, *Woesearchaeota*, *Planctomycetacia*, *Phycisphaerae*), which were rare or even undetectable (< 1%) in the initial seawater, were stimulated in large-scale microcosms of both treatments (Figure 4.6). However, these classes were not significantly enriched in the small-scale microcosms. Besides, in the early-stage microcosms amended with dilbit plus dispersant, the similarity between replicates representing the percentage of shared OTUs displayed similar values in both large (46%) and small (49%) scale microcosms (Figure 4.7). This may be because dispersant was deterministic in shaping the early-stage community composition regardless of the microcosm scale. In contrast, in the late stage, the similarity decreased for small-

scale microcosms (36%) but increased for large-scale microcosms (69%) (Figure 4.7). Our small-scale microcosms displayed a similar trend as the previous study using 100 mL microcosms (Schreiber et al., 2019) that showed the community similarity decreased over time. The increased similarity observed in our late-stage large-scale microcosms of both treatments indicates that increased population size may decrease the effects of stochastic elimination on community assembly after long-term incubation.

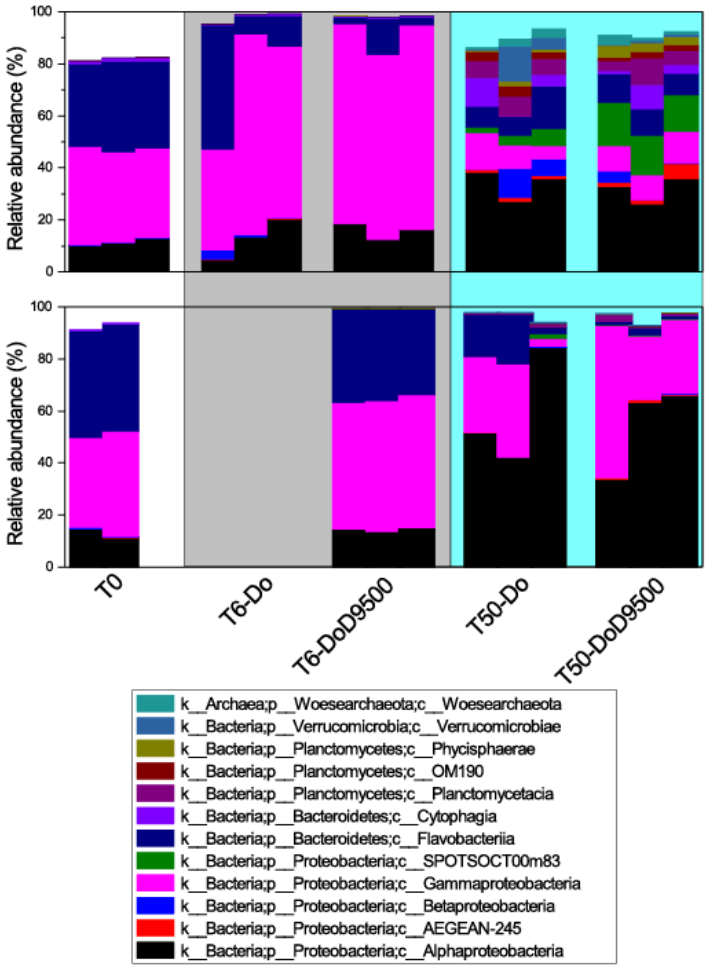

Figure 4.6 Microbial community taxa at the class level. Top: large-scale microcosms; bottom: small-scale microcosms.

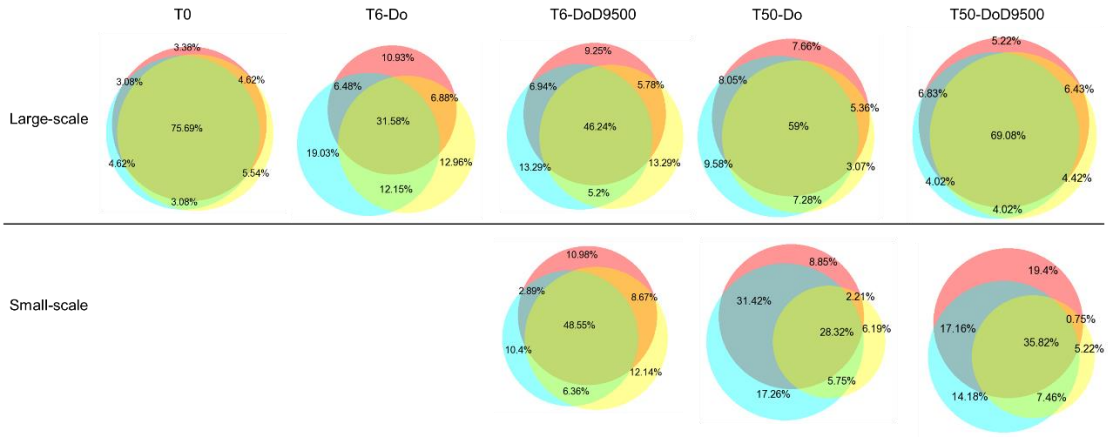

Figure 4.7 Venn diagram showing the percentage of shared Operational Taxonomic Units (OTUs) between replicates of each treatment based on 16S rRNA gene amplicon sequencing.

In this figure, the three colours represent the three replicates under each treatment. The area of the circle represents the amount of observed OTUs in specific microcosm. The overlap of the three circles represents the percentage of shared OUTs.

In the large-scale microcosms, the early-stage microbial community at the family level (Figure 4.8) showed that the order of *Alteromonadales*, specifically the *Alteromonadaceae* family, made up the highest relative abundance in the bacterial communities of microcosms amended with dilbit plus dispersant. In contrast, the communities in oil-only microcosms showed an enrichment of the orders *Oceanospirillales* (dominated by the families *Oceanospirillaceae* and *Alcanivoracaceae*), *Thiotrichales* (dominated by *Piscirickettsiaceae*), and *Rhodobacterales* (dominated by *Rhodobacteraceae*) compared to communities in the initial seawater. Moreover, the families *Cryomorphaceae* and *Thiotrichaceae* showed a decreased relative abundance in the microcosms of both treatments. The decreased abundance was possibly due to aromatics in the dilbit. The *Cryomorphaceae* family has been reported to be inhibited entirely in the presence of pyrene and phenanthrene (Rodrigues et al., 2018), and there is no evidence showing *Thiotrichaceae* can tolerate or degrade aromatics.

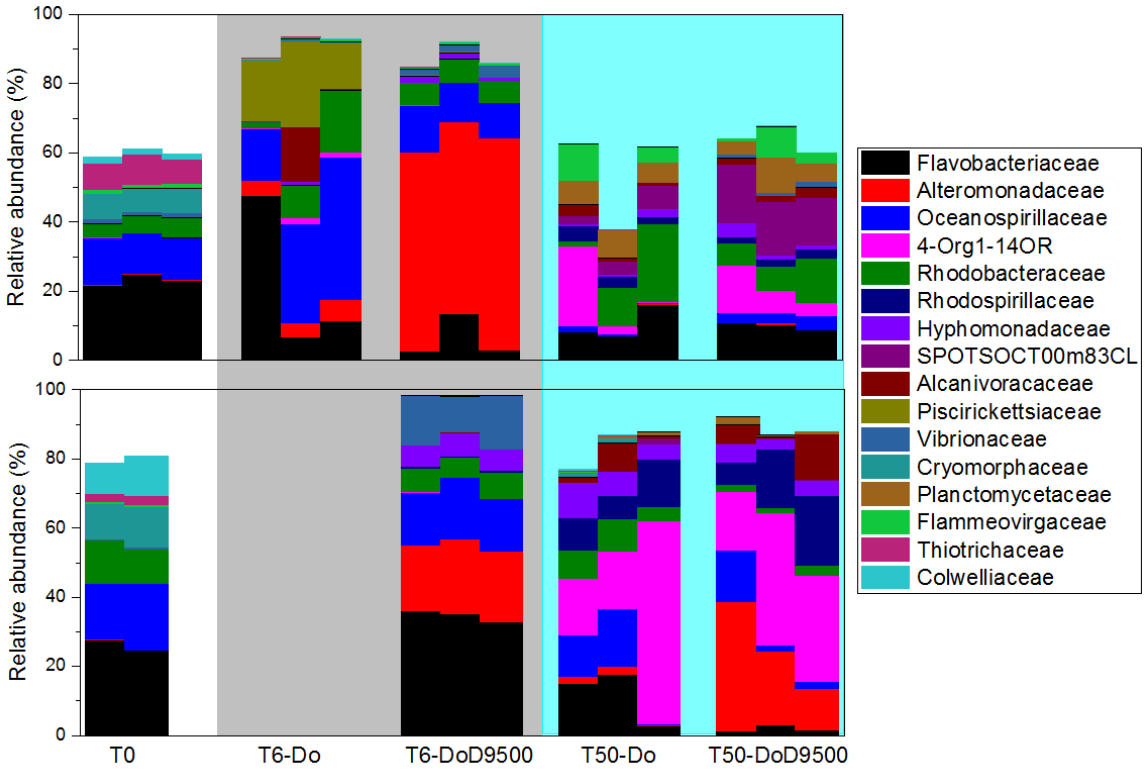

Figure 4.8 Microbial community taxa at the family level. Top: large-scale; bottom: small-scale.

4.3.2 Microbial functions and activities towards dilbit degradation using the contig-based shotgun metagenomic approach

To obtain a broad overview of metabolic functions and activities for the degradation of dilbit-only and chemically dispersed dilbit, large-scale microcosms were analyzed by contig-based shotgun metagenomic and metatranscriptomic sequencing. All the genes were annotated based on the KEGG database to reveal relevant microbial functions. PCoA analysis, based on assembled contigs, confirmed the results of 16S rRNA gene amplicon sequencing. In detail, dilbit plus dispersant communities were significantly dissimilar to dilbit-only ones in the early stage but clustered together in the late stage (Figure 4.9). Taxonomic profiles at the species level showed that in the early-stage dilbit-only microcosms, species belonging to the genera *Methylophaga*, *Marinobacterium*, *Alcanivorax*, *Phaeobacter*, and *Cycloclasticus* were mostly enriched (Figure 4.10). The inclusion of dispersants resulted in the enrichment of *Alteromonas* species, and there was a substantial increase in species related to *Alteromonas australica*. Tremblay et al. (2019) also showed that *Alteromonas* was the dispersant-associated genus in the early stage. In the late stage, similar taxonomic profiles were observed in both treatments, mostly with species belonging to *Alphaproteobacteria* (Figure 4.10).

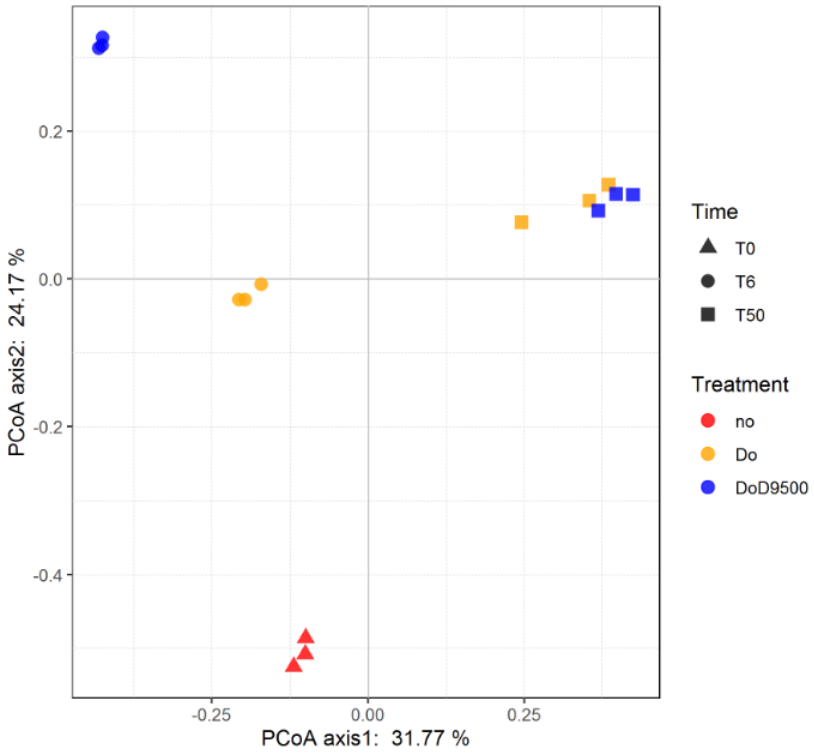

Figure 4.9 PCoA analysis based on assembled contigs using the metagenomic data in the large-scale microcosms.

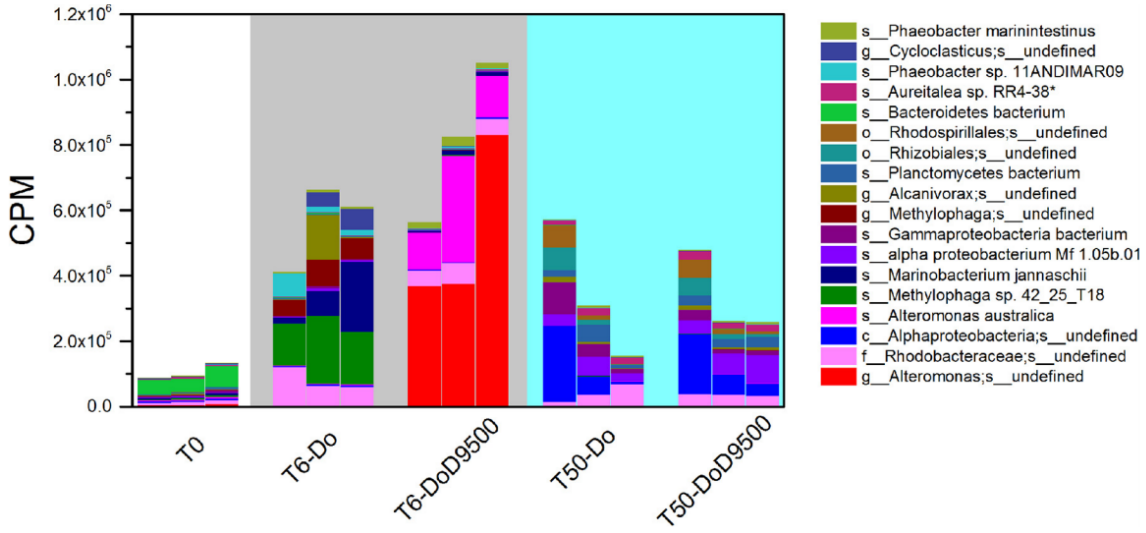

Figure 4.10 Metagenomic analysis showing the dominant microbial taxa at the species level using the contig-based approach in the large-scale microcosms.

Notably, microbial communities in both treatments appeared to strongly enrich pathways related to carbohydrate, energy, lipid, nucleotide, amino acid, cofactors and vitamins, and xenobiotics metabolism; genetic information processing related to translation, replication, and repair; environmental information processing related to membrane transport, signal transduction; as well as cellular processes related to cellular community, cell motility and drug resistance over time (Figure 4.11). Metatranscriptomic data showed that with dispersant, microbial communities further enriched the transcripts of these metabolic functions in the early stage compared with the dilbit-only microcosms (Figure 4.12). This indicated that the presence of dispersant with dilbit might facilitate certain metabolic activities for using dispersant components or the relatively bioavailable dispersed dilbit (Schreiber et al., 2019).

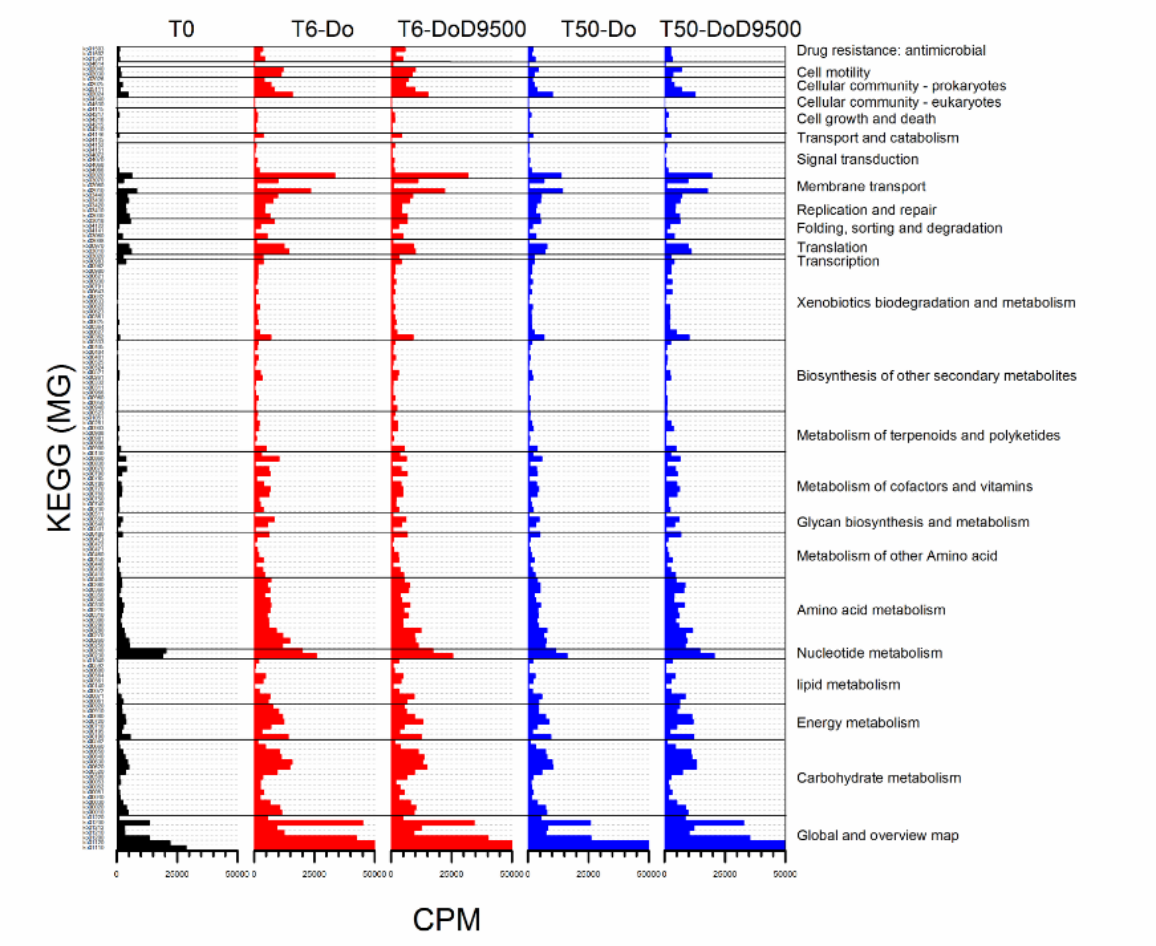

Figure 4.11 Metagenomic analysis showing the overview of microbial metabolic functions in large-scale microcosms.

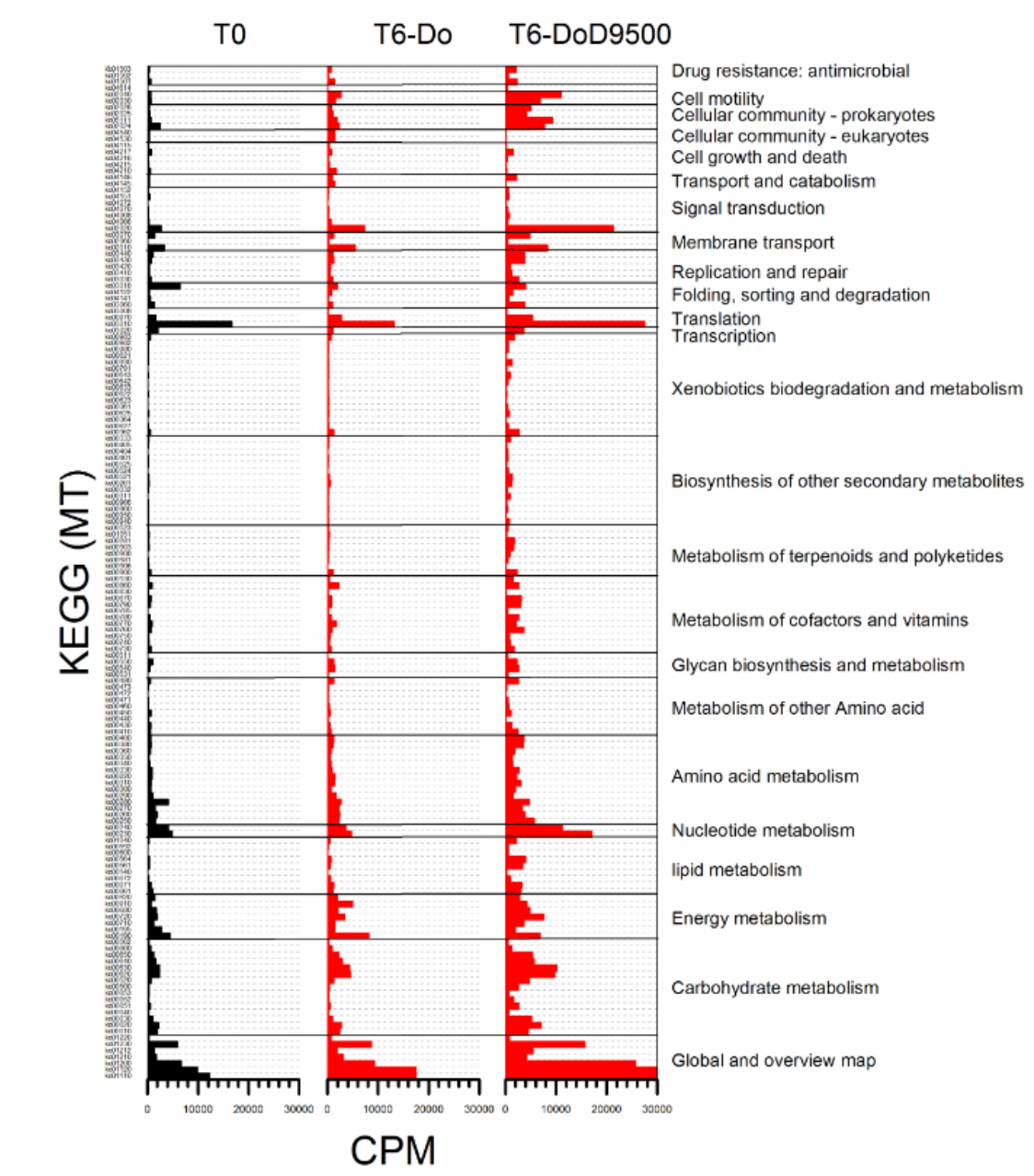

Figure 4.12 Metatranscriptomic analysis showing the overview of microbial metabolic activity in large-scale microcosms.

The abundance and expression levels of genes involved in the access to and uptake of hydrocarbons were further analyzed. “Accession” means bacterial chemotaxis and surface-active agents secretion to make them easily obtain the hydrocarbons, while the “uptake” means the transportation and degradation of the hydrocarbons. Bacterial chemotaxis (ko02030) that mediates bacterial affinity and motility in response to gradients of chemical substrates, and secretion systems (ko03070) that influence extracellular surface-active compounds (i.e., biosurfactants) for bioavailability of oils, are both described as upstream pathways for hydrocarbon degradation (Tremblay et al., 2019). The metagenomic data showed enrichment of bacterial methyl-accepting (mcp) chemotaxis in both treatments compared to the initial seawater in the early stage (Figure 4.13). However, the abundance decreased in the late stage. The abundance of genes for the type II and sec-SRP secretion systems was enriched over time, while *virB* series genes for the type IV secretion system decreased in the late stage (Figure 4.13). The type IV secretion system has been described as being responsible for the horizontal gene transfer of toxin resistance genes (Sgro et al., 2019), disclosing that these genes may play a role in the early-stage microbial survival and proliferation mechanisms towards dilbit-only or chemically dispersed dilbit. We propose that both the chemotaxis and type IV general secretion systems are the primary induced strategies for sensing and accessing dilbit in the short term. The

sustained high abundance of Type II and sec-SRP secretion systems over time indicate their involvement in the relatively complex chemical components that remained for the long term (i.e., 50 days). The metatranscriptomic data also showed that dispersant addition increased the transcripts of the associated microbial accessing genes compared with the dilbit-only communities in the early stage (Figure 4.13), which was in accordance with the findings of Tremblay et al. (2019).

Genes involved in alkane and aromatic degradation pathways were also analyzed. Alkanes are initially oxidized through alkane 1-monooxygenase (AlkB) to alcohols, which are further oxidized to aldehydes and then fatty acids, which enter the beta-oxidation pathway (Rojo, 2009). The corresponding genes (as shown in Materials and Methods) in the KEGG pathway for the degradation of both fatty acids (ko00071) and aromatic compounds (ko01220) are then integrated and summarized. Generally, dispersant addition suppressed the abundance of genes for aromatics degradation in the early stage compared with the dilbit-only communities. Due to the similarly shaped communities for the degradation of residual aromatics (as shown in chemical analysis), communities of both treatments showed increased gene abundance for aromatics degradation in the late stage (Figure 4.13). The metatranscriptomic data further indicated that, in the early stage, dispersant addition depressed the expression of most aromatic degrading genes (Figure

4.13). In contrast, the abundance and expression of genes like *pcaD* (k01055), *catC* (k03464), and *catA* (k03381), which are responsible for the degradation of the toxic intermediate catechol, were enriched (Ghosal et al., 2016). These findings suggest that dispersant addition may depress the degradation of aromatics.

Microbial contributions towards dilbit biodegradation in the early stage showed that multiple species were present in the dilbit-only microcosms, while *Alteromonas* was the most dominant contributor when dispersant was added (Figure 4.14). In dilbit-only communities, many genera dominated by *Methylophage*, carry the genes coding for the accessing system. The *Methylophage* (15.4%) and *Marinobacterium* (14.1%) account for the high transcripts for chemotaxis, while *Alcanivorax* (13.2%) and *Marinobacterium* (12.7%) had a high expression in the secretion system. The degradation genes were identified within a diverse community, and their expression was primarily associated with *Alcanivorax* (15.3%) and *Marinobacterium* (12.1%) for alkane degradation and *Cycloclasticus* (62.9%) for aromatics degradation. These genera are widely reported for the degradation of alkanes and aromatics in previous studies (Gregson et al., 2019; Kasai et al., 2002; Neufeld et al., 2007; Park & Park, 2018a; Wang et al., 2018a). Interestingly, the genes coding for the accessing system were rarely detected and expressed in *Cycloclasticus* (Fig. 5B). This suggests that *Cycloclasticus* may not have an affinity for LMW aromatics, which

have higher solubility and bioavailability in the aqueous phase (Cao et al., 2020b). In contrast, in the dilbit plus dispersant microcosms, *Alteromonas* was the predominant genus, possessing and expressing the accessing and degrading genes in the early stage. It has been reported that coordinated microbial degradation (i.e., multiple microbes involved in the biodegradation) can achieve a higher degradation efficiency towards aromatics compared to a single taxon (Chen et al., 2019; Dombrowski et al., 2016; Zhang et al., 2019). Since dispersant application suppressed microbial richness and diversity and primarily enriched *Alteromonas*, the early-stage degradation of aromatics may be inhibited.

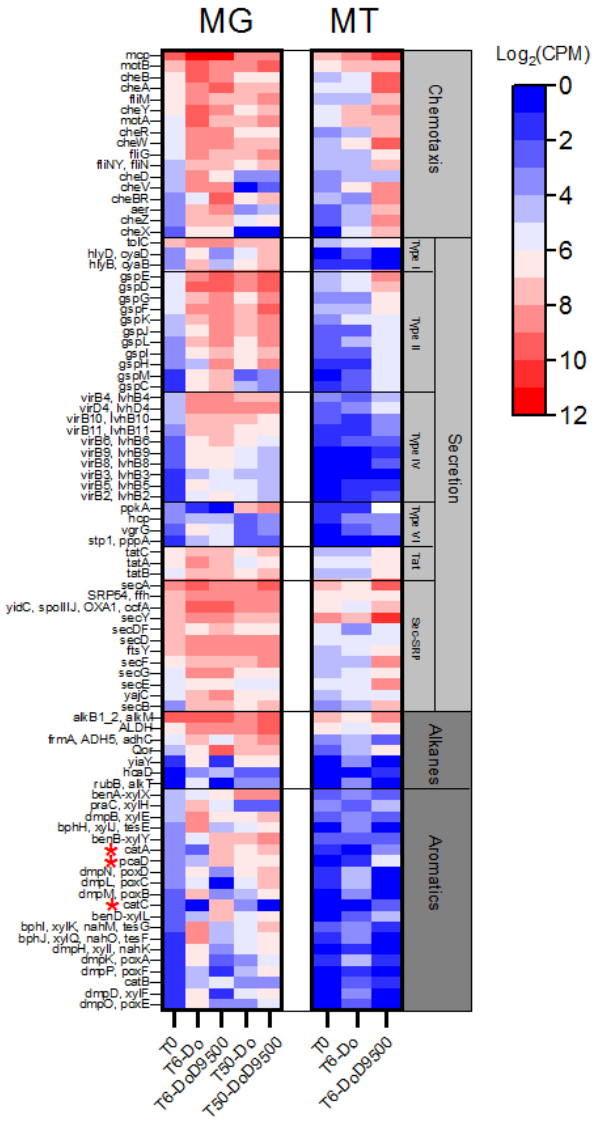

Figure 4.13 The abundance and expression of corresponding genes for microbial access and degradation pathways. Genes are plotted with abundance $Log_2CPM > 0$.

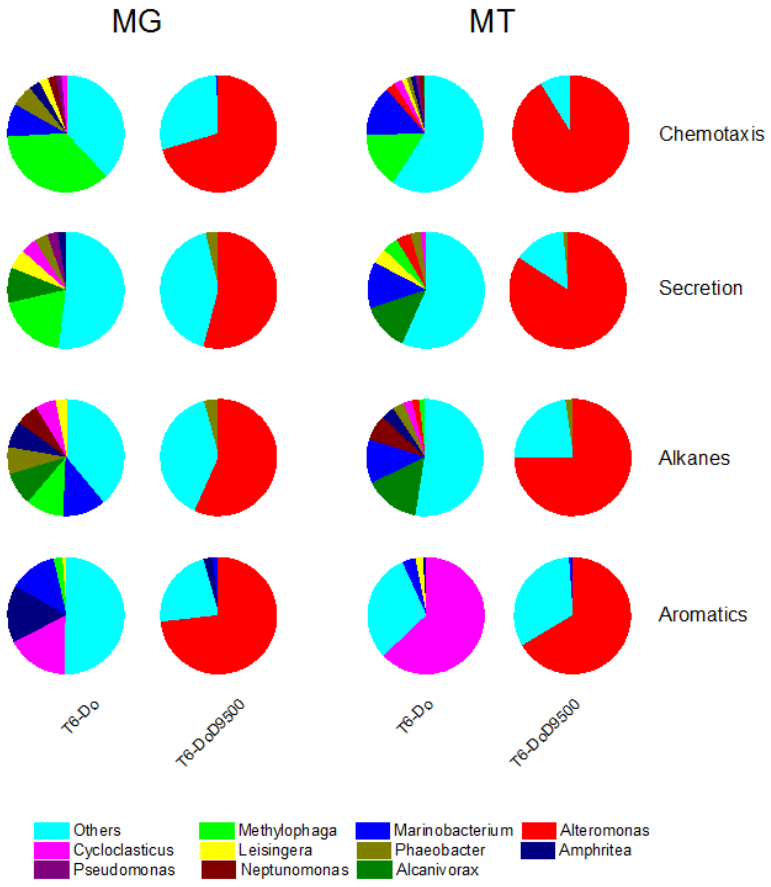

Figure 4.14 The dominant contributors (higher than 1%) toward the functions and activities for dilbit and chemically dispersed dilbit biodegradation.

4.3.3 Chemical analysis of percentage loss of *n*-alkanes and aromatics in abiotic and biotic microcosms

Chemical analysis was further applied to reveal the loss of n-alkanes and aromatics and changes of specific dispersant components in the abiotic and biotic microcosms. Our GC-MS results proved a similar abiotic loss of n-alkanes and aromatics in the dilbit-only and dilbit plus dispersant microcosms. Due to evaporation, nearly 41-42% of n-alkanes and 2-3% of aromatics were lost in the early stage, and the ratios reached 65-70% and 21-23%, respectively, in the late stage (Figure 4. 15). Obviously, the biotic microcosms could cause much higher removal of these hydrocarbons over time, showing that biodegradation played an indispensable role in dilbit removal (Figure 4.15). However, dispersant addition was found to have different effects on the loss of n-alkanes and aromatics over time. For n-alkanes, dispersant addition did not cause obvious changes compared to the dilbit-only microcosms, with nearly 69-77% and 90-92% lost in the early stage and late stage, respectively (Figure 4.15). In contrast, dispersant addition dropped the percentage loss of aromatics from 61% to 33% and 80% to 62% in the early stage and late stage, respectively (Figure 4.15). These results confirmed our observations from the metagenomic and metatranscriptomic analysis that dispersant addition exerted limited impacts on the removal of n-alkanes but inhibited the degradation of aromatics, especially in the early stage.

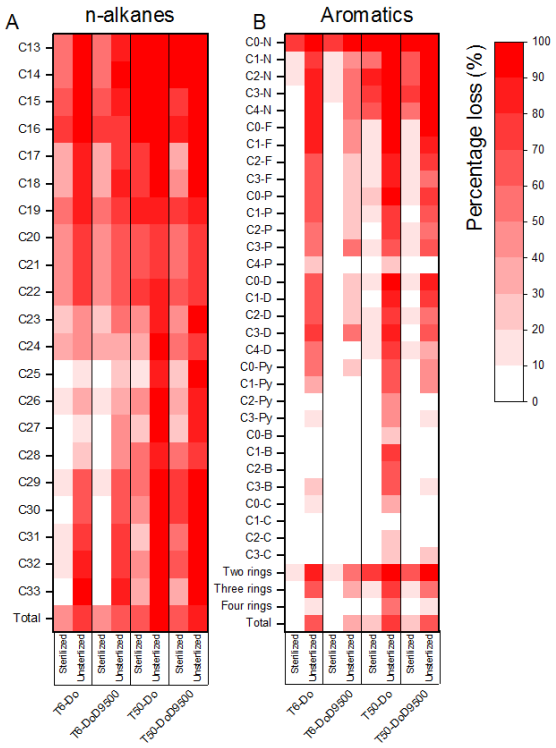

Figure 4.15 Chemical analysis showing percentage loss of (A) n-alkanes; (B) aromatics after 6 days and 50 days incubation of both treatments in abiotic and biotic microcosms.

In this figure, C13 - C33: n-alkanes with corresponding carbon atoms; C0-N, C1-N, C2-N, C3-N, and C4-N: naphthalene and its alkylated homologs; C0-F, C1-F, C2-F, and C3-F: fluorene and its alkylated homologs; C0-P, C1-P, C2-P, C3-P, and C4-P: phenanthrene and its alkylated homologs; C0-D, C1-D, C2-D, C3-D, and C4-D: dibenzothiophene and its alkylated homologs; C0-Py, C1-Py, C2-Py, and C3-Py: pyrene and its alkylated homologs; C0-B, C1-B, C2-B, and C3-B: benzonaphthothiophene and its alkylated homologs; C0-C, C1-C, C2-C, and C3-C: chrysene and its alkylated homologs.

It has been well known that LMW components, such as the short-chain n-alkanes, two-rings naphthalene, and its alkylated homologs, were more easily degraded. Our study further verified the degradation of multiple-ring aromatics like fluorene, pyrene, and dibenzothiophenes and their alkylated homologs in the early stage (Figure 4.15). These results were different from those reported by Schreiber et al. (2019), who used 150 ppm dilbit in their study. It is believed that lower oil concentrations could be more rapidly biodegraded in the marine environment than higher concentrations. Due to the lower initial concentration of dilbit (30 ppm) applied in our study, these multiple-ring aromatics may serve as carbon or energy sources after the depletion of *n*-alkanes and LMW aromatics.

We also observed that the peaks of dispersant components disappeared in the early-stage biotic microcosms (Figure 4.16). The finding is in alignment with Gofstein et al. (2020), who proved that Corexit 9500A could be biodegraded rapidly, with a concentration dropped to below the limit of detection (LOD) within 5 days. In addition, we further estimated cell density using the extractable DNA concentration. It showed that dispersant addition strongly enriched cell density in the early stage (Figure 4.17). Since the presence of dispersant in dilbit decreased the hydrocarbon utilization but enriched cell density in the early stage, we suggest that dispersant components could be primarily utilized for competing with microbial degradation of dilbit.

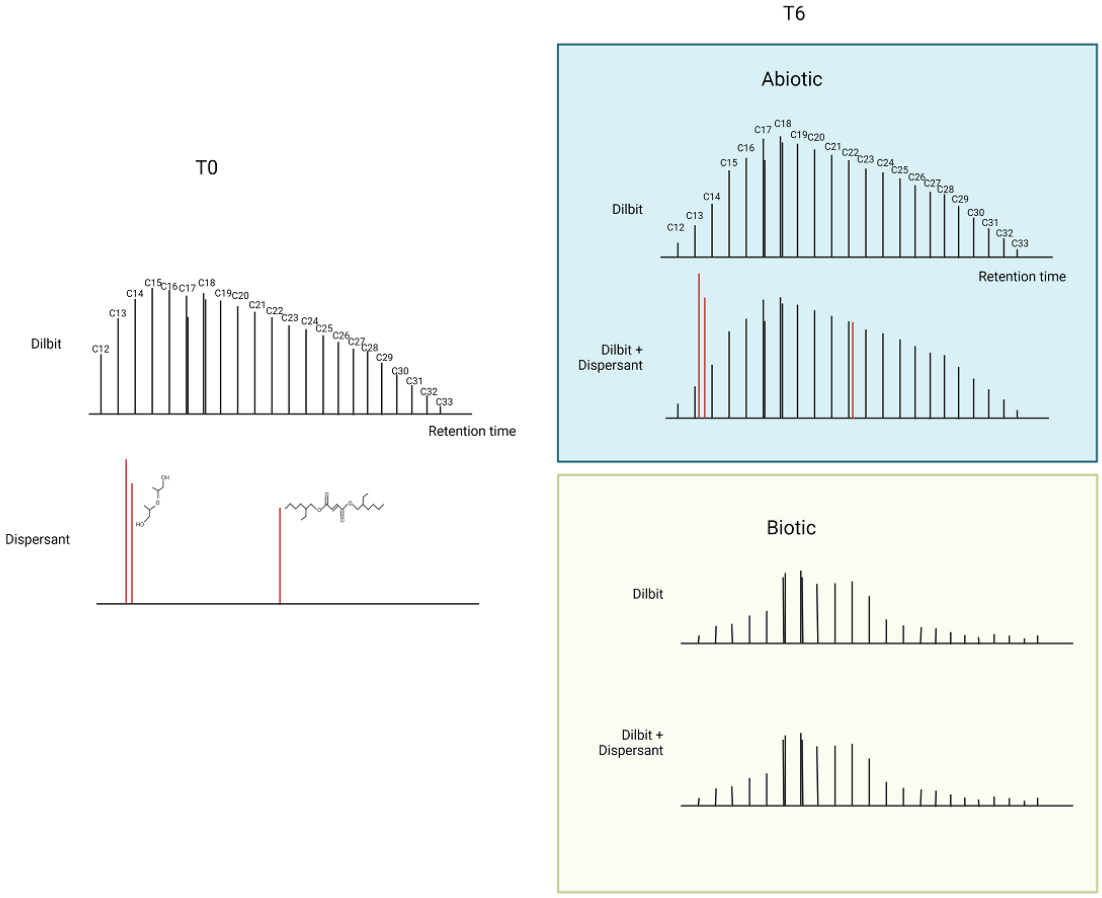

Figure 4.16 The scheme of GC-MS chromatograms showing the initial dilbit and dispersant and the early-stage abiotic and biotic microcosms.

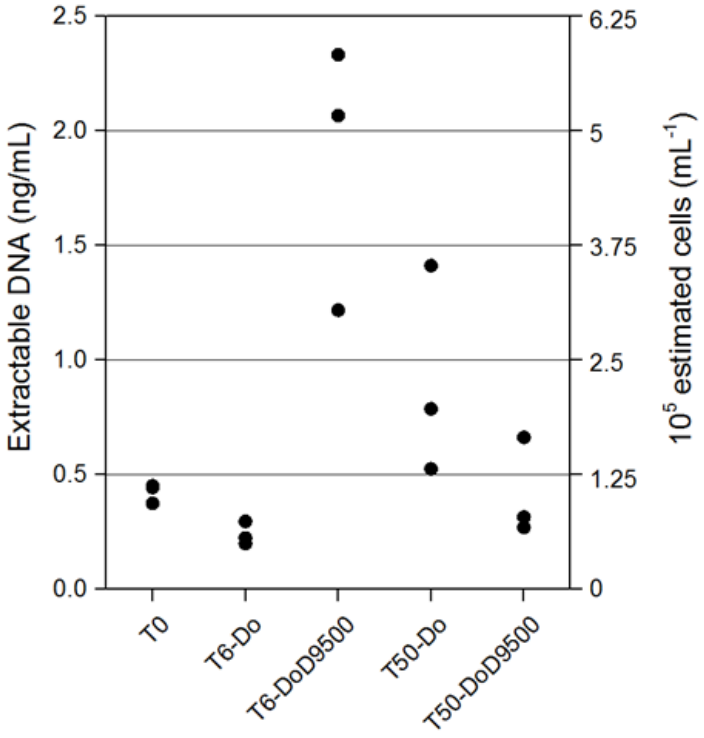

Figure 4.17 Estimation of cell density per milliliter of seawater using the extractable DNA concentration in the large-scale microcosms.

4.3.4 Dispersant application inducing microbial antioxidation in the early stage

In our large-scale microcosms, the presence of dispersant in dilbit would depress microbial community richness and diversity, and dispersant components can be primarily degraded for enriching cell density in the early stage. Apart from that, dispersant addition can also increase aquatic exposure to xenobiotics, including aromatics, to induce the overproduction of reactive oxygen species (ROS), causing potential inhibition to microorganisms (Rahsepar et al., 2016).

To answer whether dispersant application could cause the inhibition effects in our large-scale microcosms with the low dilbit concentration, we applied a binning-centric approach to evaluate dominated bacterial responses. Based on a total of 62,437 assembled contigs, 3,850 contigs were binned to generate 39 metagenomic bins, representing an integration rate of 6.17%. The heatmap (Figure 4.18) presents the relative abundances of 2-*Thiotrichales* (*Methylophaga* sp. 42_25_T18), 16-*Oceanospirillales* (*Marinobacterium jannaschii*), and bin-16 belonging to *Gammaproteobacteria* dominated the dilbit-only microcosms. In contrast, 1-*Alteromonadales* and 7-*Alteromonadales* (*Alteromonas australica*), which belong to the *Alteromonas* genus, were dominant in microcosms with added dispersant in the early stage. In the late stage, microbial communities became more diverse, with bin-14 and bin-6 showing the dominance of *Proteobacteria*. All these highly

abundant MAGs were rare (< 1%) in the initial seawater, indicating that these hydrocarbonoclastic bacteria can quickly respond and grow after a dilbit spill. However, based on the metagenomic binning approach, some important species for the degradation of alkanes (e.g., *Alcanivorax*) and aromatics (e.g., *Cycloclasticus*) were missing.

Microbial antioxidation can be utilized for evaluating microbial responses to ROS. The mechanisms were recently reported in an anaerobic system based on the recovered MAGs (Wu et al., 2021). However, there is little information on the microbial antioxidation response towards naturally and chemically dispersed dilbit in a microbial community. We thus employed a metatranscriptomic-based MAGs approach to elucidate microbial antioxidation potential in response to the dilbit and dispersant application. We focused on antioxidant enzymes consisting of superoxide dismutase (SOD), catalase (CAT), glutathione peroxidase (GPx), glutathione reductase (GR), and glutathione S-transferases (GST) that can directly catalyze the conjugation of xenobiotics through glutathione (GSH) for detoxification. Increased concentrations of xenobiotics can induce high concentrations of superoxide, which will be degraded by SOD to generate hydrogen peroxide (H_2O_2). There are two mechanisms for the removal of H_2O_2. The first one is directly through CAT, and the second one is via the GSH redox reaction. We found that the dilbit-only communities did not increase the transcripts of these genes compared to the initial seawater,

while dispersant addition particularly enriched the transcripts of the *GST*, *SOD*, and *CAT* genes (Fig. 7). Transcripts of these genes were primarily increased from the two *Alteromonas* species, indicating that *Alteromonas* species may directly conjugate xenobiotics and quench the induced ROS mainly via the first mechanism to address the short-term exposure to chemically dispersed dilbit.

It is well established that the expression of hydrocarbon-degrading genes will upregulate the microbial antioxidant enzymes (Mohapatra & Phale, 2021; Nikel et al., 2016). In our study, the expression of alkanes and aromatics degrading genes were highly expressed in both the dilbit-only and dilbit plus dispersant microcosms (Figure 4.13). However, the expression of antioxidation genes was not stimulated in the dilbit-only microcosms as that in the dilbit plus dispersant ones (Figure 4.19). It was also reported that inefficient aromatics degradation or the presence of toxic compounds would generate more ROS to enhance the expression of antioxidation genes (Mohapatra & Phale, 2021). These indicated that the increased toxicity effects rather than the increased expression of hydrocarbon-degrading genes might account for the stimulated antioxidation processes.

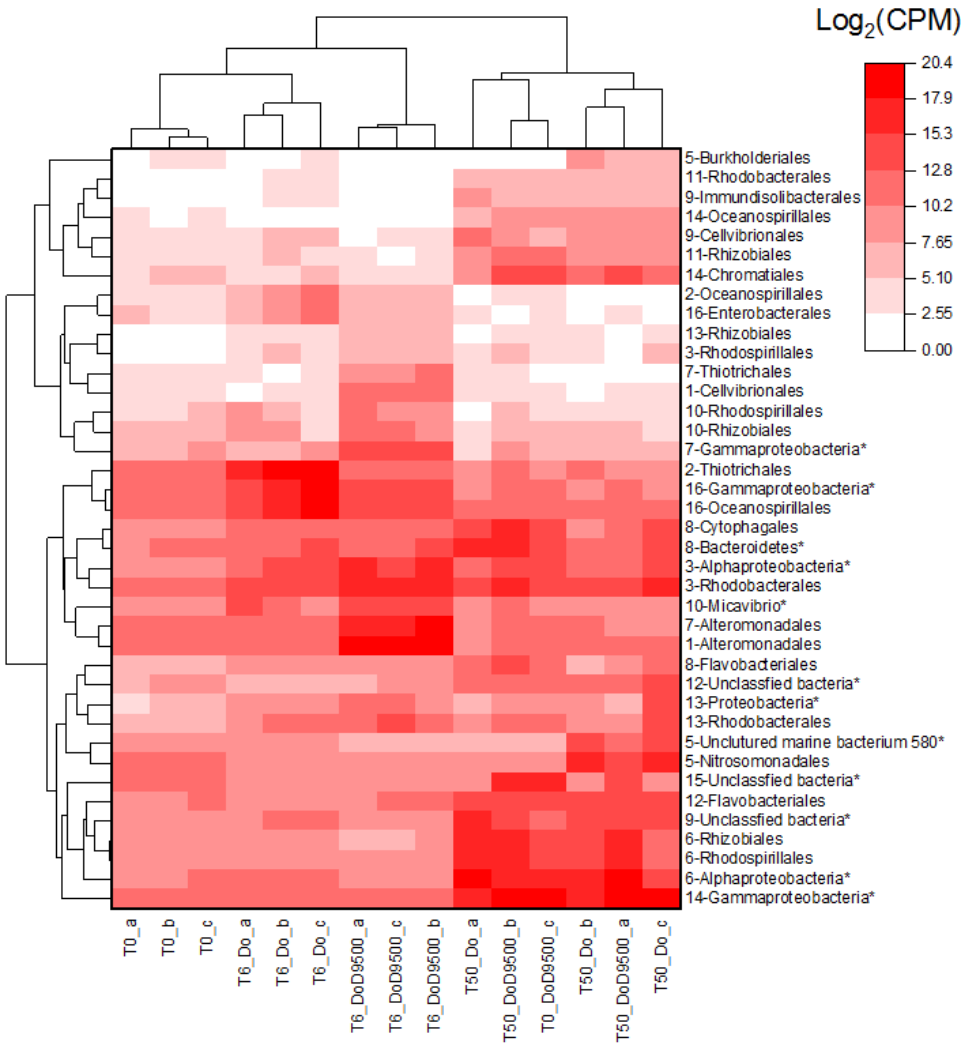

Figure 4.18 Heatmap showing the abundance of each metagenomic bin in the large-scale microcosms.

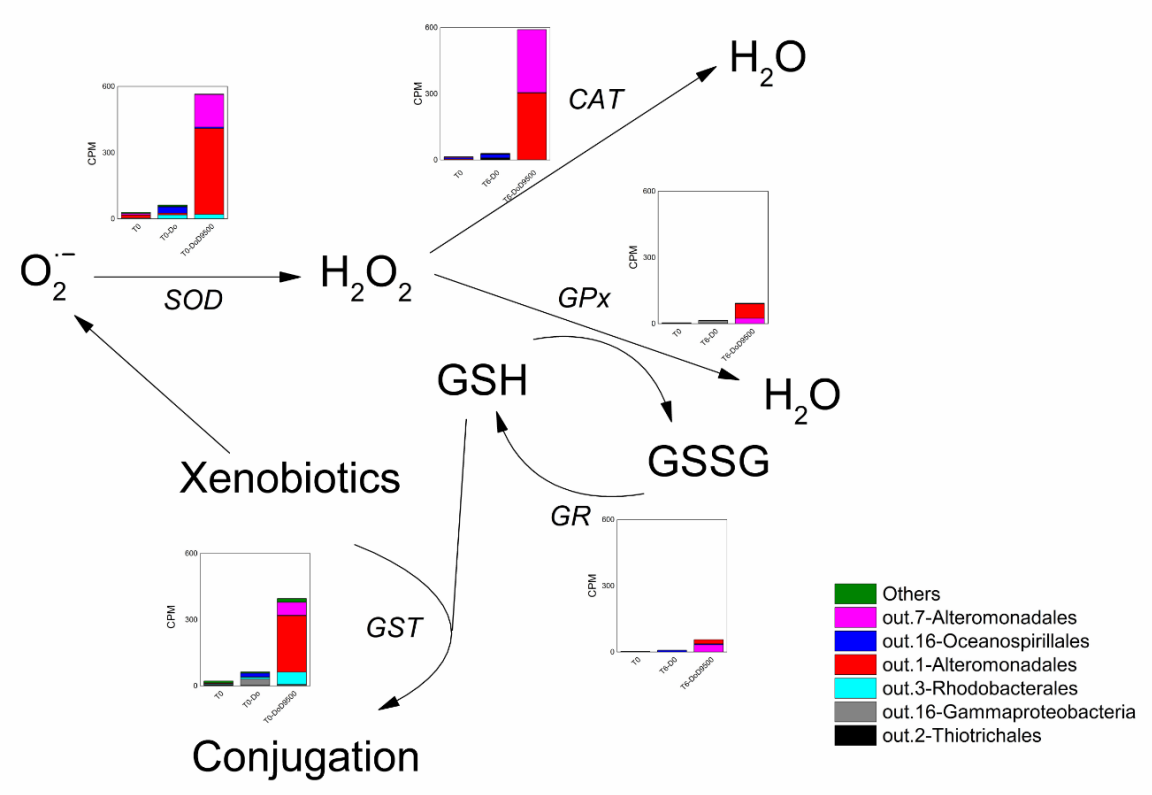

Figure 4.19 Microbial antioxidation mechanism of dominated MAGs in the early-stage large-scale microcosms based on the shotgun metatranscriptomic analysis.

4.3.5 Evaluation of the chemical dispersant as a dilbit spill treating agent

Dispersant application was previously reported to enhance microbial degradation activity towards oils with a large proportion of alkanes and limited aromatics in marine microcosms (Techtmann et al., 2017; Tremblay et al., 2017). However, as there is a large proportion of aromatics in dilbit (Figure 4.20), our microcosm results showed that dispersant addition inhibited the degradation of aromatics in the early stage. Based on all these chemical and biological analyses in this study, we suggest that in the early stage, the presence of dispersant in dilbit would (1) depress microbial richness and diversity, (2) compete for the utilization of hydrocarbons in dilbit, and (3) induce potential toxicity.

In our microcosm study, we used a higher DOR (1:10, vol/vol). A DOR of 1:20 or lower (i.e., 1:100) is the typical target ratio in an oil spill response, while for extremely heavy oils, it can be increased to 1:10 to enhance effectiveness (McFarlin et al., 2014). Due to the high viscosity of dilbit, the dispersant Corexit 9500A showed limited effectiveness below a DOR of 1:20 (Figure 4.20). It could only achieve 7.5% effectiveness after a 200 min retention time as many dispersed oil droplets tended to resurface (Figure 4.20). Fortunately, under the DOR ratio of 1:10, it showed high dispersion effectiveness (41.7%). Hence, a DOR of 1:10 could be more applicable in a dilbit spill response. Efficiently dispersed dilbit can significantly increase early-stage concentrations of xenobiotics like

aromatics in the aqueous phase. Although under the high DOR, our marine microcosms still demonstrated strong dilbit attenuation ability. In the early stage, specific species from the *Alteromonas* genus increased and degraded both n-alkanes and aromatics.

The goal of dispersant application is to rapidly emulsify the spilled oil slicks, leading to decreased deposition on the shorelines and producing smaller oil droplets that are more readily attacked by the microbial degraders. As marine environments do have a large dilution capacity, the short-term adverse effects of dispersant application on aromatics degradation would be alleviated to some extent. Furthermore, in the late stage, our microcosms showed similar community composition and metabolic functions irrespective of dispersant addition. The transformation of the remaining HMW compounds may be within the capabilities of the post-oil communities that contain higher microbial diversity and species richness.

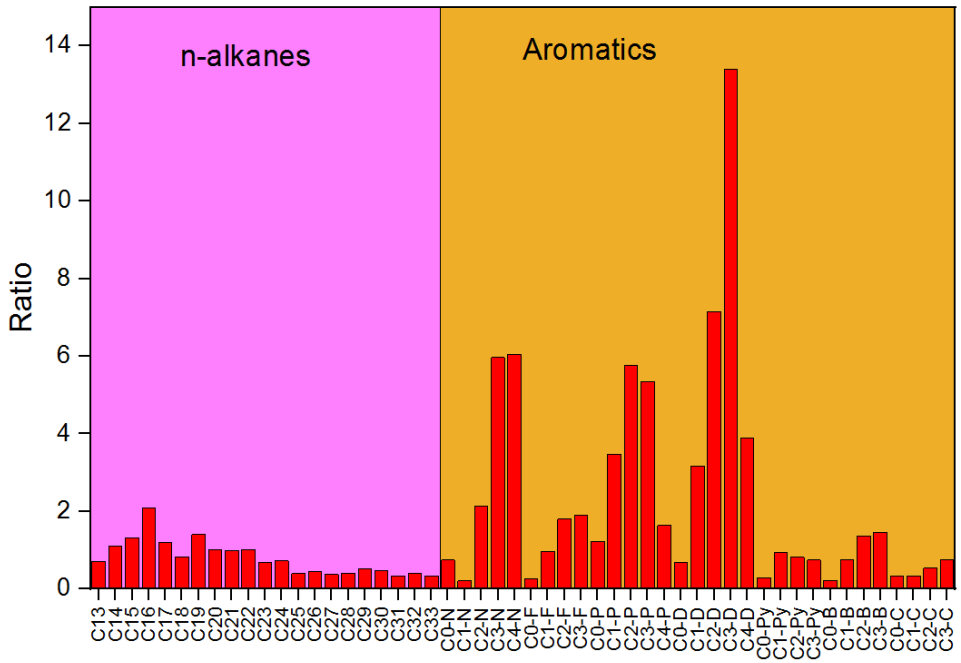

Figure 4.20 The ratios of peak areas of hydrocarbon components to the biomarker 30ab-hopane of the dilbit.

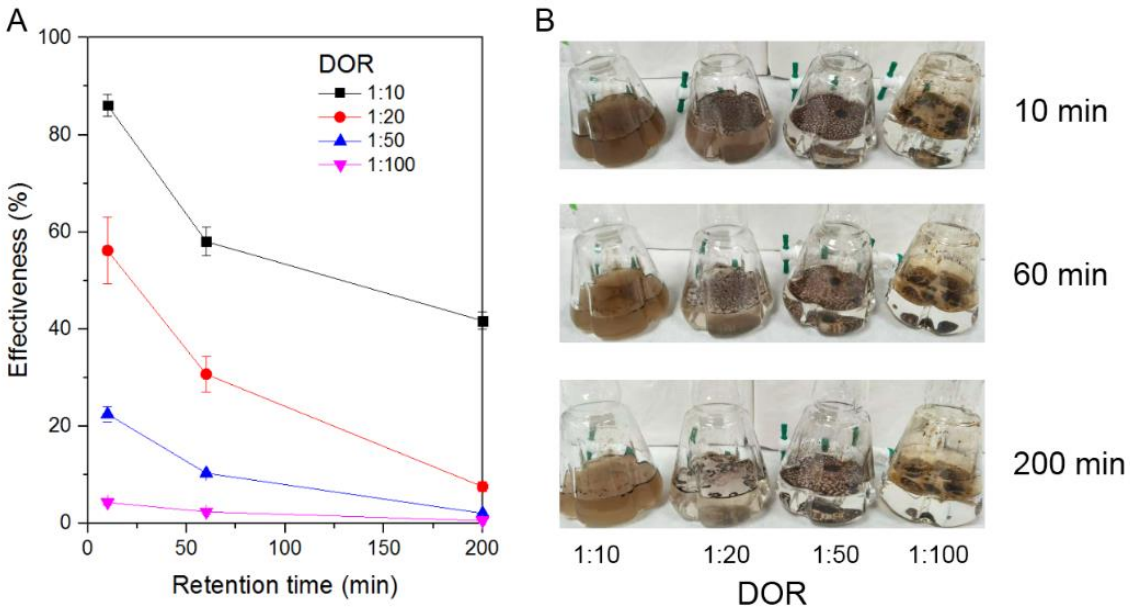

Figure 4.21 DOR affecting the dispersion effectiveness. (A) Dispersion effectiveness under different retention times (10, 60, and 200 min). (B) Images showing the performances of different DOR affecting oil dispersion.

4.4 Summary

In this study, we employed microcosms to study the effects of a marine dilbit spill and dispersant application on microbial community dynamics over time. In summary, our study demonstrated that increasing the microcosm scale could produce more reproducible microbial communities during a simulated marine dilbit spill. The hydrocarbonoclastic bacteria initially present at a low abundance in the seawater responded rapidly and increased their activity for dilbit degradation. The presence of dispersant in dilbit had different effects over time. In the early stage, dispersant addition inhibited dilbit degradation mainly because of (1) decreased microbial richness and diversity and predominantly enriched *Alteromonas* for degrading both alkanes and aromatics, (2) microbial utilization of dispersant components, competing for the degradation of dilbit, and (3) the induced potential toxicity. In the late stage, the inhibition effects could be relieved, and microbial communities showed similar compositions and metabolic functions regardless of dispersant addition. Although it is challenging to mimic a natural marine environment in laboratory microcosms, results generated from our large-scale microcosms without nutrient addition using low dilbit concentrations could increase our understanding of the microbial roles in natural attenuation and help evaluate the impact of a chemical dispersant as a dilbit spill treating agent.

CHAPTER 5 MAGNETIC NANOPARTICLES DECORATED BACTERIA FOR RESPONDING TO HEAVY CRUDE OIL POLLUTION[4]

[4] This chapter is generated based on and expanded from the following paper:

Cao, Y., Zhang, B., Zhu, Z., Rostami, M., Dong, G., Ling, J., Lee, K., Greer, C., & Chen, B. (2021). Access-dispersion-recovery strategy for enhanced mitigation of heavy crude oil pollution using magnetic nanoparticles decorated bacteria. *Bioresource Technology*, 125404. DOI: 10.1016/j.biortech.2021.125404

Roles: Cao designed and conducted the study under the guidance of Dr. Baiyu Zhang and Dr. Bing Chen and acted as the first author of the manuscript. Zhu and Rostami did the synthesis of nanoparticles. Other coauthors did the review and editing. Most contents of this paper were written by Cao and further polished by the other co-authors.

5.1 Introduction

Increasing global energy demands draw our sights into the production and usage of heavy crude oils, urging the need for effective heavy crude oil spill preparedness and responses (Nduagu & Gates, 2015). Unlike conventional light crude oil, heavy crude oil possesses a high viscosity and density, contains high contents of recalcitrant asphaltene and resin, and can cause catastrophic damage when spilled into the environment (Santos et al., 2014). The commonly used physically and chemically remediating practices are not conspicuously effective (Davoodi et al., 2020).

Biodegradation is an effective and environmentally friendly alternative for spilled oil mitigation (Ahmadi et al., 2020b). However, research on the biodegradation of heavy crude oil is limited. The highly viscous and dense heavy crude oils could easily stick to the surrounding environments, such as clogging the pipelines (Martínez-Palou et al., 2011) and rock pores (Adams, 2014), and precipitating and attaching to the sediments (Agarwal & Liu, 2015), limiting their bioavailability to oil-degrading bacteria. Besides, the dominant HMW aromatics, resins, and asphaltenes components in heavy crude oils are resistant to biodegradation. A previous study showed that only 19-29% of resins and 10-18% of asphaltenes could be removed after 45 days of biodegradation (Wang et al., 2018b). It is thus quite difficult to apply traditional biodegradation methodologies to heavy crude oil

mitigation.

Increasing the bioavailability of heavy crude oil to oil-degrading bacteria and recovering these unbiodegradable components can enhance the removal of heavy crude oil pollutions. Typically, some oil-degrading bacteria with stochastic access to crude oils can secrete surface-active agents (e.g., biosurfactants) to enhance oil bioavailability. The LMW components can thus be utilized and biodegraded. Improving initial bacterial abundance towards heavy crude oil may enhance oil biodegradation through accelerating oil bioavailability. In addition, oil weathering processes (e.g., evaporation and biodegradation) leave these recalcitrant components in oils with increased abundance and result in suspended pellets, including oil-bacteria aggregates (Lavania et al., 2012). Recovery of these recalcitrant compounds can significantly increase the total oil removal efficiency but receives limited investigations.

The two processes, namely enhancing initial bacterial abundance towards heavy crude oil and recovering the oil-bacteria aggregates, can be achieved by developing artificially manipulated oil-degrading bacteria. Recently, the modification of bacteria for behavior manipulation in given environments has become a research hot spot. Such attempts have been made from two-dimensional chemical immobilization to three-dimensional magnetically oriented motion. With Fe_3O_4 magnetic nanoparticles decorated on the bacteria,

navigated cell movements can be achieved by applying different magnetic fields, enabling manipulating microbial growth conditions and magnetic recovery. The magnetic nanoparticles decorated bacteria (MNPB) have been successfully manipulated for desired metabolic reactions like synthesizing bacterial biopolymers (Park et al., 2012), enhancing bio-desulfurization (Ansari et al., 2009), and recovering bacterial cells for fermenting menaquinone (Ebrahiminezhad et al., 2016). These studies indicated a great potential of applying specific MNPB to enhance the removal of heavy crude oil through orientating the bacterial movement towards the attached oil layer and a follow-up recovery of sticky oil-bacteria aggregates.

This study thus proposed an access-dispersion-recovery strategy for the first time to tackle the in-depth investigation of heavy crude oil mitigation, as shown in Figure 5.1. The MNPB was developed based on previously screened oil-degrading and biosurfactant-producing species *Rhodococcus erythropolis* (*R. erythropolis*) strain P6-4P (Cai et al., 2014). These oriented MNPB can stimulate oil dispersion and enable residue recovery in a magnetically controlled manner. The designed MNPB and novel bio-mitigating strategy can expand biodegradation applicability for heavy crude oil pollution.

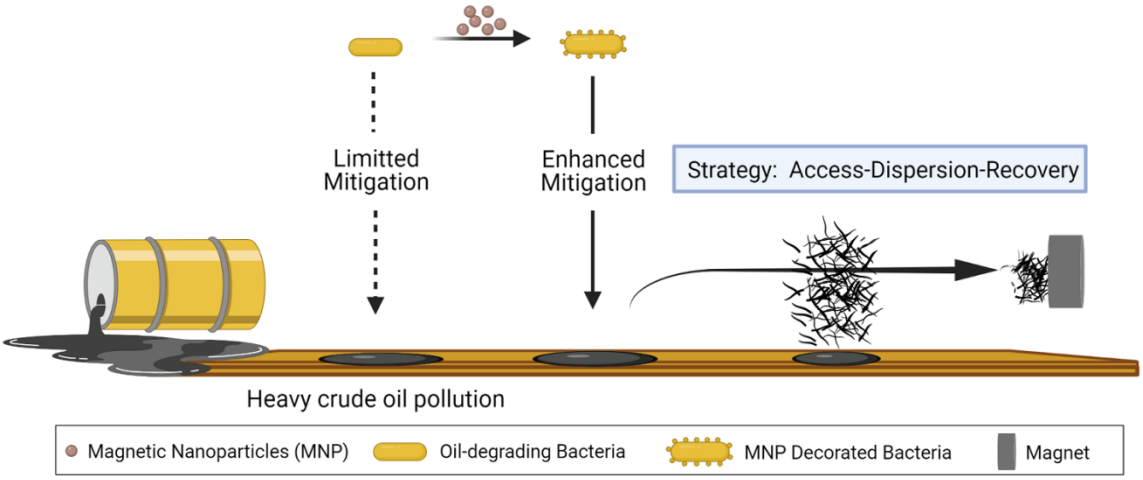

Figure 5.1 Schematic graph of the access-dispersion-recovery strategy

5.2 Materials and Methods

5.2.1 Nanoparticle synthesis, silica coating, and aldehyde functionalization

Synthesis of Fe_3O_4 magnetic nanoparticles and silica coating was performed following the procedures Ranjan et al. (2018) reported. Fe_3O_4 magnetic nanoparticles were synthesized based on modified coprecipitation methods. A mole ratio of Fe^{2+}/Fe^{3+} = 1:1.75 was chosen, with 1.5868 g $FeCl_2 \cdot 4H_2O$ and 3.7842 g $FeCl_3 \cdot 6H_2O$ dissolved in 160 ml distilled and degassed water. The mixed solution was stirred under N_2 atmosphere in order to prevent oxidation at 80 °C for 1 h at a stirring rate of 600 rpm. Then, 20 mL ammonium solution (25%) was injected into the mixture quickly, stirred vigorously (1000 rpm) under N_2 for another 1 h, and then cooled to room temperature. The black precipitated particles were washed three times with water and two times with ethanol and separated by magnetic decantation. Finally, the prepared MNPs were dried under vacuum at room temperature.

Silica coating was performed on the surface of Fe_3O_4 nanoparticles to obtain MNP@Si. Briefly, 1 g of Fe_3O_4 nanoparticles obtained in the previous step was mixed with 40 mL of ethanol, 6 mL of distilled and degassed water, and 2 mL of ammonium solution (25%). This mixture was homogenized by ultrasonic vibration in the water bath for 30 min at room temperature. Then, 1.5 mL of tetraethyl orthosilicate (TEOS) was injected into the mixture dropwise under vigorous stirring using a mechanical stirrer and N_2 flow for at least 12 hours.

After the reaction, the dark brown silica-coated particles were precipitated and washed with water and ethanol and separated by a magnet, and then dried under a vacuum.

The MNP@Si was obtained for aldehyde functionalization (Park et al., 2012). Briefly, 100 mg MNP@Si was dispersed into 10 mL ethanol by ultrasonication and then added to 100 μL triethoxysilylbutyraldehyde (Gelest Inc, Morrisville, USA) for 10 h. The aldehyde functionalized MNP@Si was collected by centrifugation at 10,000 rpm for 10 min and then vacuum dried. The X-ray diffraction spectroscopy (XRD), transmission electron microscope (TEM), and Fourier-transform infrared spectroscopy (FTIR) were applied to validate the synthesis.

5.2.2 Strain and nanoparticles decoration

R. erythropolis strain P6-4P was previously isolated from oily contaminated sediment samples (Cai et al., 2021). The Minimal Salt Medium (MSM), containing NaCl, 15 g; $(NH_4)_2SO_4$, 10 g; KH_2PO_4, 3.4 g; $K_2HPO_4 \cdot 3H_2O$, 4.4 g; $MgSO_4 \cdot 7H_2O$, 1.02 g; $FeSO_4 \cdot 7H_2O$, 0.00028 g and trace element ($ZnSO_4$, 0.29 g; $CaCl_2$, 0.24 g; $CuSO_4$, 0.25 g; $MnSO_4$, 0.17 g) per liter distilled water, was applied to biodegradation experiment (Cao et al., 2020b). Glucose (4 g/L) was added for bacterial enrichment. All incubations were performed at room temperature (~22 °C).

After overnight bacterial enrichment, cells were harvested by centrifugation at 6,000

rpm for 10 min. The cell pellets were washed three times and diluted to an optical density (OD) value at 600 nm of ~1.0 in MSM for decoration. Each portion of the harvested cells were decorated with aldehyde functionalized MNP@Si at different concentrations (i.e., 0, 60, 120, 180, 240, 300, 420 mg/L) in 50 mL Erlenmeyer flasks with 15 mL MSM. The aldehyde functionalized MNP@Si was added with continuous shaking at 200 rpm for one hour.

The MNPB was subsequently collected by applying an external magnetic field and characterized using scanning electron microscopy (SEM) and energy-dispersive X-ray spectroscopy (EDS). The sample was prepared following the method described by Cai et al. (2019). Briefly, bacterial cells were fixed overnight in 2% (vol/vol) glutaraldehyde prepared in a 50 mM potassium phosphate buffer. The fixed cells were washed three times with phosphate buffer and dehydrated using an increasing gradient of acetone in distilled water (30%, 50%, 70%, 80%, and 90%, respectively) for 10 min each and finally in 100% acetone for 30 min and air-dried. The specimens were sputter-coated with gold using a fine auto coater and visualized using SEM. The coating process and the SEM visualization were conducted in the Micro Analysis Facility (MAF IIC) of Memorial University.

5.2.3 Calculation of decoration ratio

Cells that failed the decoration process and remained in the aqueous phase were

quantified by directly measuring the OD value. The decoration ratio represents the percentage of aldehyde functionalized MNP@Si decorated cells and was calculated as follows:

$$\text{Decoration ratio} = \frac{\text{OD}_{\text{initial}} - \text{OD}_{\text{after recovery}}}{\text{OD}_{\text{initial}}}$$

Where $\text{OD}_{\text{initial}}$ means the initial bacterial OD value at 600 nm; $\text{OD}_{\text{after recovery}}$ represents the OD value in the aqueous phase after recovery.

5.2.4 Biodegradation experiment

The heavy crude oil used in this study was provided by Fisheries and Oceans Canada, with an API gravity around ten. To simulate an immobilized oil residue, 15 μL of heavy crude oil was preheated at 50°C to make it homogeneous and then spread on the bottom of a 50 mL Erlenmeyer flask to form a layer with a circular diameter of 2 cm using a professional pipette (GILSON MICROMAN E). The heavy crude oil coated in each flask was then weathered overnight. Its high viscosity resulted in a strong attachment of the heavy crude oil to the bottom of the flask. The biodegradation experiment was conducted by adding 15 mL of MSM containing identical amounts (OD600 value of 1) of fresh bacteria or MNPB under continuous shaking at 75 rpm for 14 days. For MNPB, a magnetic field was applied initially under the bottom of the flask for 10 min to attract the bacterial movement towards the simulated oil attachment and then withdrew. Considering that

Fe_3O_4@Si has limited catalytic effects on organics degradation (Li et al., 2016a), no comparisons were made using pure Fe_3O_4@Si in this study. Flasks with the same settings but without adding bacteria were prepared and operated as control runs.

5.2.5 Characterization and recovery of suspended pellets

Suspended pellets were transferred to a glass slide with a pipet and observed directly by a Leica DM2500M optical microscope (Leica Microsystems, Buffalo Grove, IL, USA). The recovery of suspended pellets was conducted by attaching a magnet to the flask wall under continuous shaking at 75 rpm for one hour. The MSM, after recovery, was carefully transferred to another clean flask and extracted three times using 10 mL of DCM.

5.2.6 Measurement of oil concentrations and components

A UV-VIS spectrophotometer (Thermo Fisher, GENESYS 10S) was used to determine the total oil concentration, including all the components dissolved in DCM. Measurements were done at the absorption wavelengths of 340, 370, and 400 nm (Yang et al., 2021).

GC-MS characterization was performed to detect alkanes and specific aromatics following a previously developed methodology (Cao et al., 2020b). Briefly, an Agilent 7890A instrument equipped with a DB-5MS column fused silica capillary column was used to differentiate hydrocarbon contents. The MS detection was conducted in the electron ionization mode with 70 eV and the ion source temperature was set at 300 °C. C30 17β(H)

21β(H) - hopane was used as an internal standard. Alkylated aromatics were identified at their specific m/z value, retention time, and chromatograms. The biodegradation and recovery efficiency of these components was calculated by referring to the internal standard.

5.2.7 Statistical analysis

All experiments were conducted in triplicate for quality control. The error bar represented each standard deviation from the means of the independent experiment. Statistical difference was evaluated using the One-way ANOVA analysis (n = 3) with $P < 0.05$ (*) as significant.

5.3 Results and Discussion

5.3.1 Development of nanoparticles decorated bacteria

The successful synthesis of MNP was validated using XRD (Deng et al., 2005). The TEM image showed that the size of MNP is nearly 10-20 nm (Figure 5.2). However, the pure MNP was very unstable and tended to agglomerate and host potential toxicity (Gawande et al., 2015). Silica coating and aldehyde functionalization were applied to facilitate their decoration onto bacterial surfaces. The FTIR analysis showed a vibrational band at 540 cm^{-1}, which is attributed to the Fe-O bond vibration (Ahmadi et al., 2020a). The successful synthesis of desired MNP@Si was confirmed by the vibration mode of the Si-O bond observed at 1062 cm^{-1} (Wang et al., 2011). The IR peaks at 2978 cm^{-1} and 1750

cm^{-1} represent C-H and C=O stretching, respectively, confirming the presence of aldehyde groups in functionalized MNP@Si (Park et al., 2012) (Figure 5.3).

The decoration ratio was then evaluated, and the results showed that 180 mg/L aldehyde functionalized MNP@Si could decorate up to 91% of bacterial cells (Figure 5.4). Since higher doses could not further enhance the decoration ratio, a concentration of 180 mg/L was selected for bacterial decoration. The SEM image and EDS analysis showed a successful decoration of MNP (Figure 5.5). Compared with pure bacteria (PB), MNP decoration did not affect the cell morphology. The decorated cells were then magnetically collected and considered as the MNPB for biodegradation experiments.

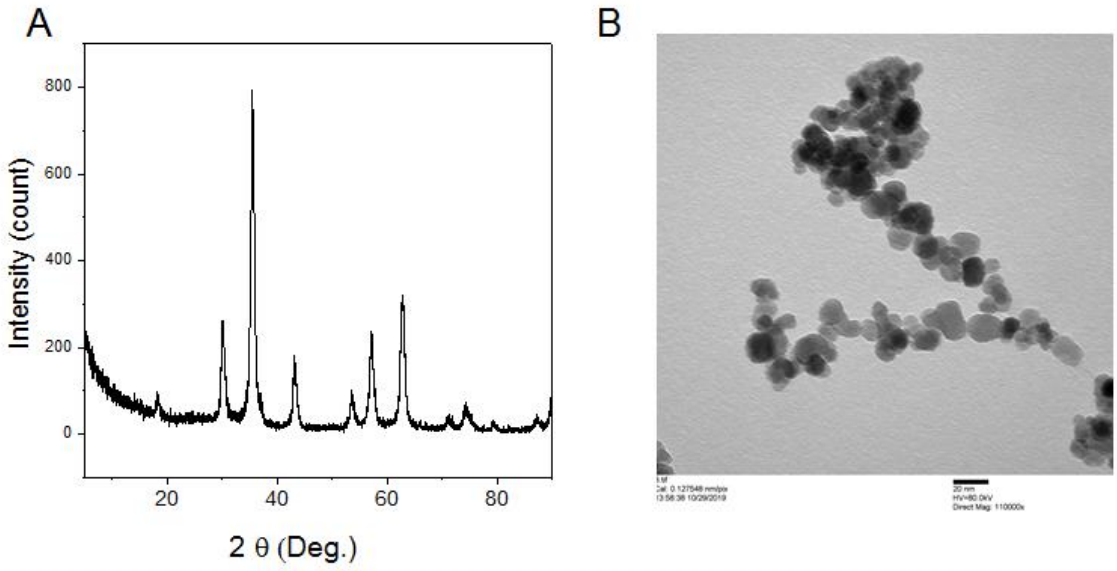

Figure 5.2 (A) XRD pattern and (B) TEM image of synthesized Fe_3O_4 nanoparticles.

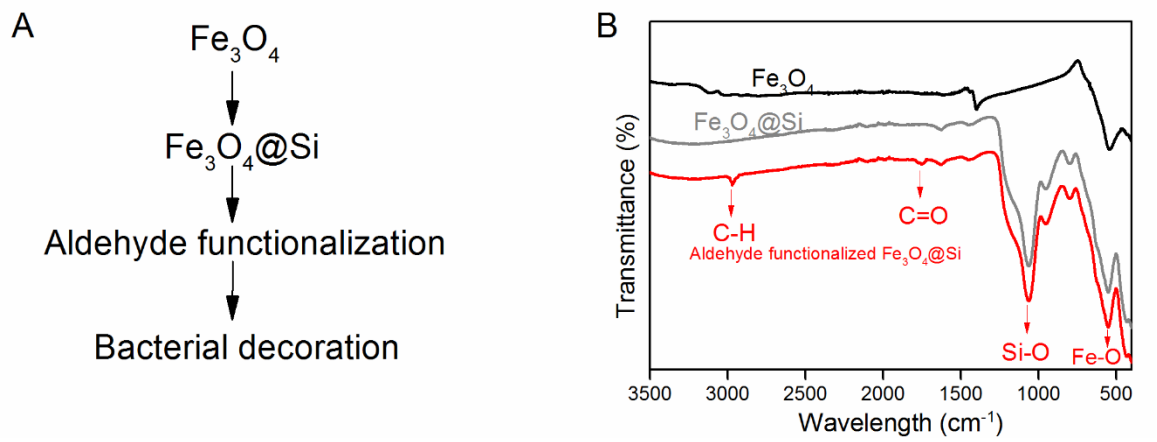

Figure 5.3 Synthesis of MNPB. (A) bacterial decoration steps; (B) FTIR patterns of Fe_3O_4 nanoparticles, Fe_3O_4@Si, and aldehyde functioned Fe_3O_4@Si.

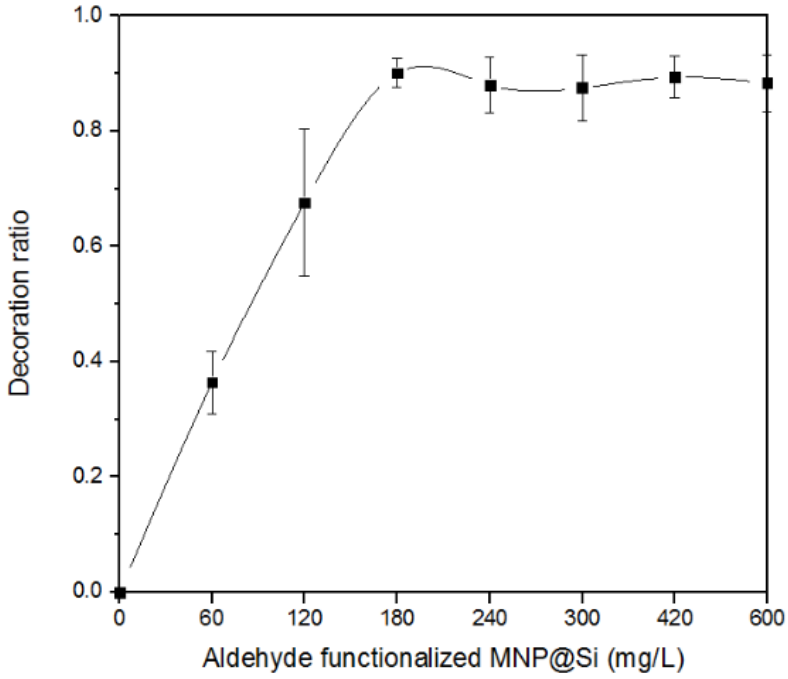

Figure 5.4 Bacterial decoration ratio using different concentrations of nanoparticles.

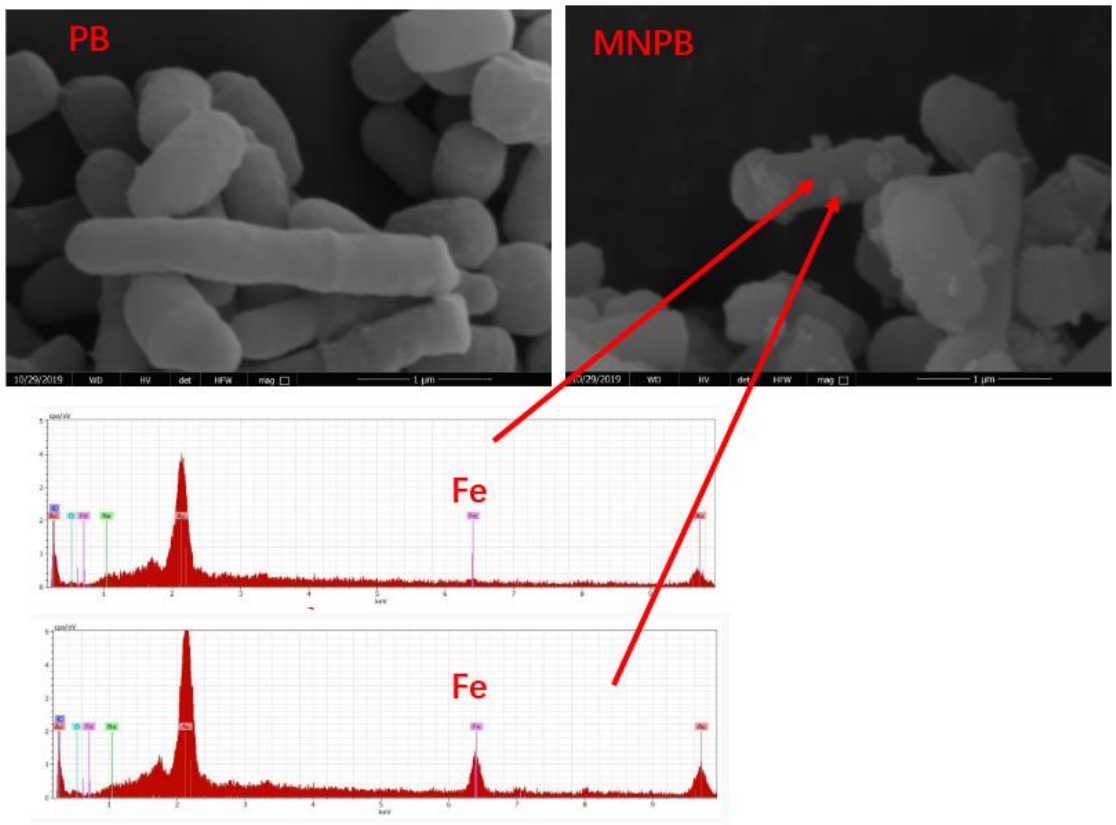

Figure 5.5 SEM images of PB and MNPB (top) and EDS pattern of the point towards cell surface and decorated particles (bottom).

5.3.2 The access-dispersion-recovery strategy for facilitating HCO mitigation

An attached oil layer was simulated by spreading 15 μL of HCO on the bottom of a 50 mL flask. The stability of the attached oil could be found in control runs without bacterial addition within 14 days. The steps of access, dispersion, and recovery processes were elaborated in Figure 5.6, including (1) magnetic attracting the MNPB to the oil layer; (2) oil dispersion with suspended pellets formed; (3) recovery of the suspended pellets using a magnet.

When a magnetic field was applied near the oil layer, a rapid and oriented microbial movement towards the oil layer was observed in the MNPB runs (Figure 5.6). The break-up and dispersion of the oil attachment occurred during the biodegradation, with suspended pellets formed. It may be because plenty of MNPB accessed the hydrophobic oil layer to secrete biosurfactants for oil dispersion (Zhu et al., 2016). These pellets were then directly examined by optical microscopy. Results revealed amounts of MNPB attached to the pellet, forming oil-bacteria aggregates (Figure 5.7).

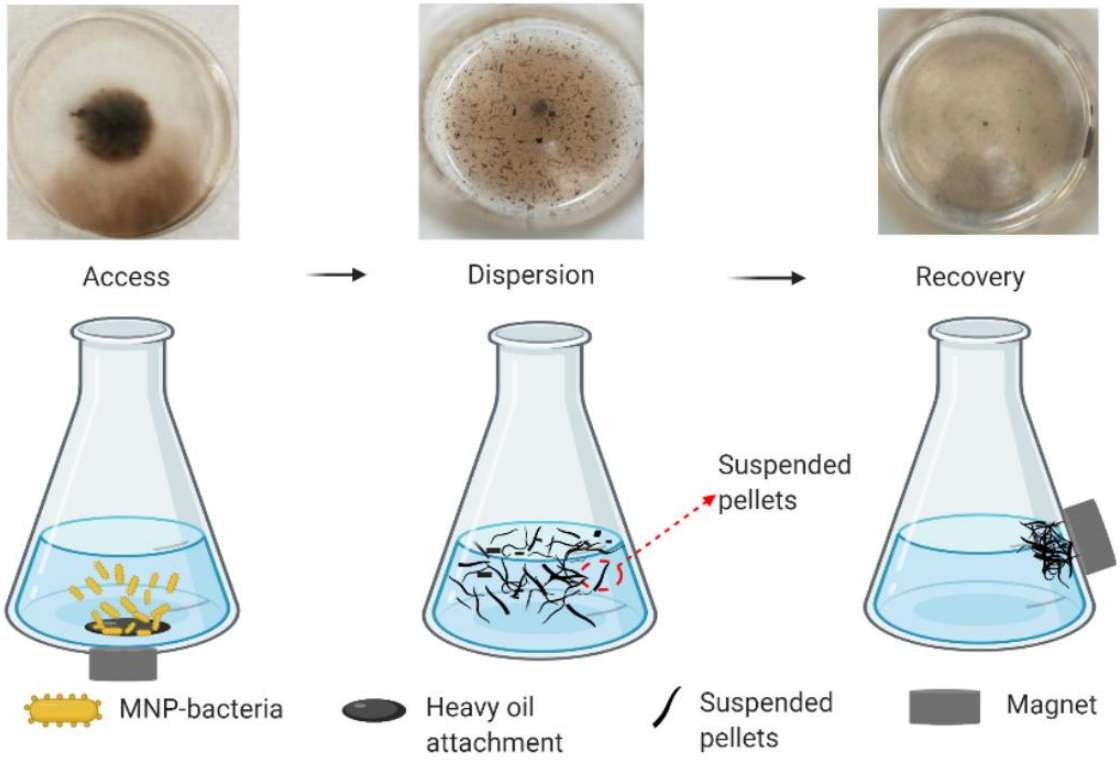

Figure 5.6 The images of the access-dispersion-recovery process.

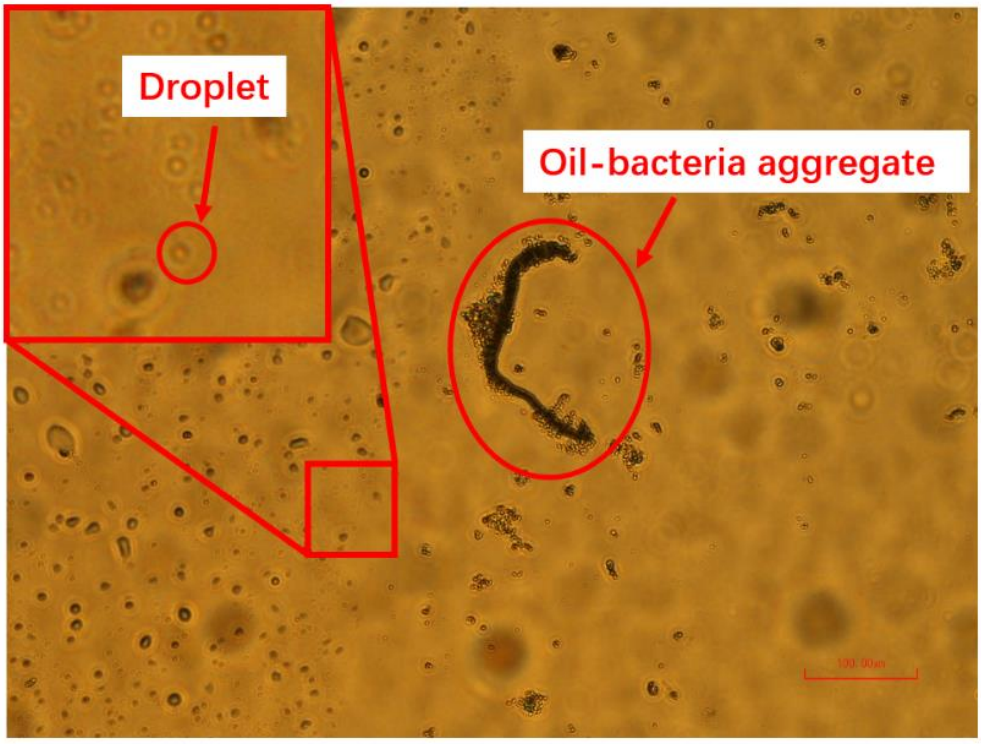

Figure 5.7 Optical image showing oil-bacteria aggregates after 14 days incubation.

Attached with MNPB, some pellets could be magnetically oriented and exhibit the character for magnetic recovery. It may be because that MNPB enhanced their cell surface hydrophobicity to stick to the pellets, forming oil-bacteria aggregates (Li et al., 2015). Then, the removal efficiency was estimated by measuring the total oil concentrations of the whole medium. It showed that the MNPB with recovery (MNPB-R) could lead to 62% removal of heavy crude oil (Figure 5.8). In comparison, the oil removal rate was 2.9% for the MNPB without recovery and undetectable for the PB (Figure 5.8). Due to the low proportion of LMW components in the HCO, biodegradation itself may have limited effects on the removal while the recovery process plays a critical role.

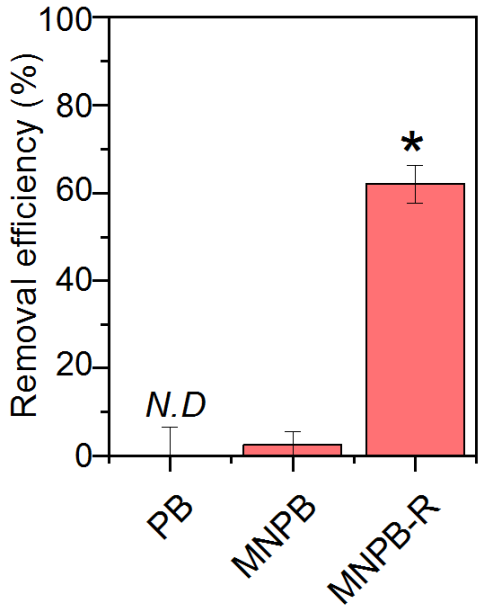

Figure 5.8 Total removal efficiency determined by UV-VIS spectrophotometer. "*" indicates significantly different.

5.3.3 Enhanced removal of HMW aromatics by magnetic recovery

Biodegradation usually occurs on LMW alkanes and aromatics, which show relatively higher bioavailability. GC-MS analysis was further applied to study residual oils in PB, MNPB, and MNPB-R runs. Results showed no significant peaks of alkanes in control runs (Figure 5.9), indicating no alkanes in the heavy crude oil. Only LMW aromatics, such as bicyclic benzothiophene and naphthalene and their alkylated methyl homologs, were biodegraded by PB within 14 days. These LMW aromatics were more susceptible to being treated due to their higher solubility in the aqueous phase and relatively unstable structures (González-Gaya et al., 2019). The MNPB can further enhance their removal, even for the alkylated homologs and tricyclic fluorene (Figure 5.9). It may be because of the oriented microbial access towards the heavy crude oil attachment that stimulated oil-bacteria interactions. Simultaneously, the increased MNPB towards the oil layer may enhance the secretion of biosurfactants for oil dispersion (Cao et al., 2020b). However, biodegradation towards relative HMW aromatics was undetectable within 14 days due to their stable chemical structures. Despite the fact that the biodegradation by MNPB was only confined to the LMW aromatics, the oriented bacteria accessing can induce significant oil dispersion and facilitate downstream recovery.

The MNPB-R could remove HMW aromatics and their alkylated homologs, while the

remaining LMW aromatics were not significantly changed compared with the non-recovery runs (Figure 5.9). Generally, the recovery efficiency increased along with the increased numbers of aromatic rings and alkylates. The highest removal efficiency was achieved for alkylated chrysenes (43-52%) (Figure 5.9). HMW aromatics and their alkylated homologs have much higher hydrophobicity (Cao et al., 2020b; González-Gaya et al., 2019). The high solubility of LMW compounds in the medium could prevent their recovery. On the contrary, by comparing the oil concentrations between the MNPB and MNPB-R treatments, we found that the HMW aromatics tended to be entrained into or absorbed by the oil-bacteria aggregates. The enhanced removal of HMW aromatics via recovery can expand the feasibility of the identified strategy, as the remaining LMW aromatics and decreased HMW aromatics are relatively easy to be weathered in the environments.

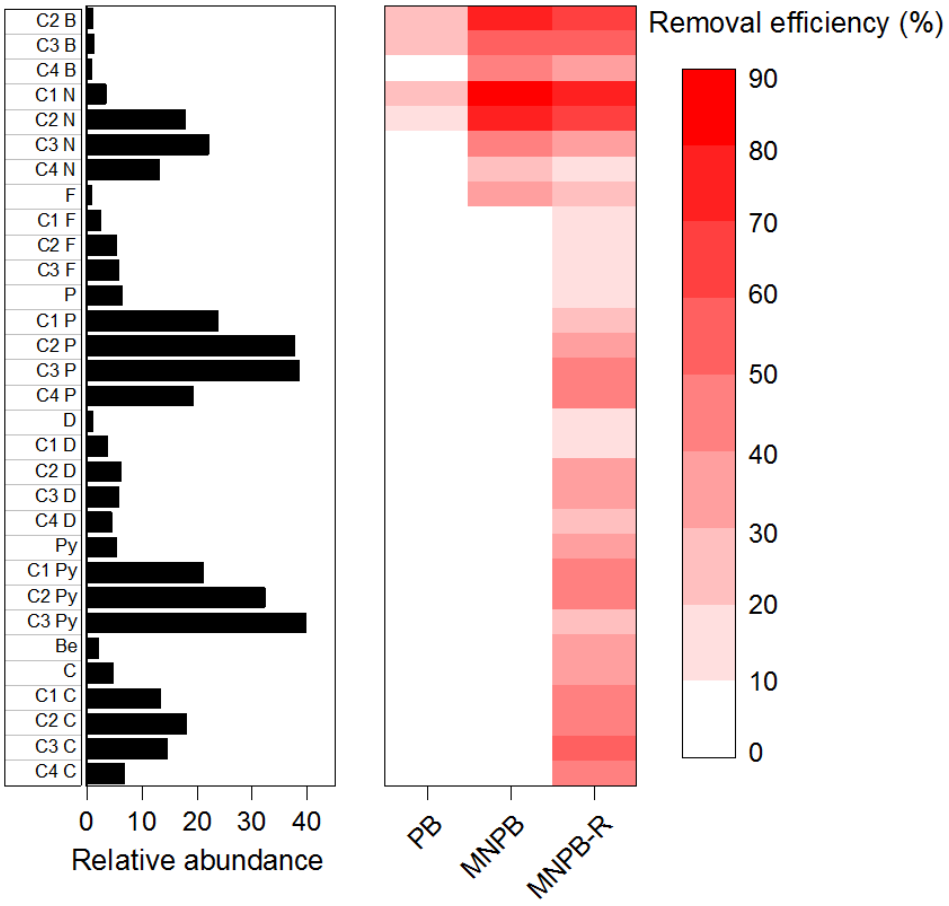

Figure 5.9 GC-MS measurements of the removal of each oil component.

In this figure, Left: relative abundance of aromatics and their alkylated homologs towards the biomarker 30ab hopane of the control runs without bacteria added. B: benzothiophenes, N: naphthalene, F: fluorene, P: phenanthrene; D: dibenzothiophene, Py: pyrene, Be: benz(a)anthracene, C: chrysene. Right: removal efficiency of each component.

5.3.4 Feasibility of MNPB for environmental applications

Through using MNPB for targeted removal of the simulated heavy crude oil attachment, we demonstrated that biodegradation efficiency was increased for these LMW aromatics, and the recovery process also functioned for these HMW aromatics. Since the recovery process could partially remove the HMW aromatics and oil-bacteria aggregates that are recalcitrant for biodegradation, the proposed strategy was beneficial for remediating heavy crude oil pollution.

However, in the field studies, it would be difficult to recover all the used MNP and augmented bacteria. The remaining MNP may affect ecosystems. For example, He et al. (2011) demonstrated that the addition of magnetic nanoparticles would change the microbial community structures and associated enzymatic activities; Malhotra et al. (2020) showed the toxicity of the MNP on cells. To properly apply these nanoparticles to environmental remediation, various magnetic-based nanocomposites with high specific areas and saturation magnetization have been introduced (Malhotra et al., 2020). In addition, optimization of the applied magnetic field may further enhance recovery efficiency and relieve potential adverse effects.

The efficiency of bioaugmentation depends on the activity of the introduced exogenous bacteria. On the one hand, most of the exogenous bacteria may not survive under specific

environmental conditions, and they may be outcompeted by the indigenous microbes. On the other hand, the exogenous bacteria may compete with the indigenous microbes and affect the community structures. Hence, the application of the MNPB should consider the local conditions.

Furthermore, in this study, we simulated a heavy crude oil attachment on the surface of the glass. In the natural environment, the attachments may occur on diverse materials, such as sediments, pipelines, and some other marine instruments. It is thus necessary to evaluate the effectiveness of various HCO attachments to expand the feasibility of the access-dispersion-recovery strategy,

5.4 Summary

In this study, we demonstrated a new access-dispersion-recovery strategy for mitigation of heavy crude oil pollution using MNPB developed from oil-degrading and biosurfactant-producing species. The magnetic orientation can trigger MNPB to access a simulated heavy crude oil layer to stimulate degrading LMW aromatics (e.g., benzothiophenes and naphthalenes), forming oil-bacteria aggregates for recovery. Up to 62% of oils can be recovered using this strategy after 14 days of incubation. Further, HMW aromatics can also be recovered because they were entrained in oil-bacteria aggregates. These findings expand the feasibility of biodegradation as a response to heavy crude oil pollution. To advance its applicability, future research could focus on the optimization of magnetic fields and the evaluation of the effectiveness of various heavy crude oil pollution scenarios.

CHAPTER 6 BIODEGRADATION OF ALKANES AND POLYHYDROXYBUTYRATE PLASTICS BY ALCANIVORAX SPECIES ISOLATED FROM THE NORTH ATLANTIC OCEAN[5]

[5] This chapter is generated based on and expanded from the following papers:

Cao, Y., Zhang, B., Zhu, Z., Cai, Q., Liu, B., Dong, G., Lee, K., Greer, C., & Chen, B. (2022). Biodegradation of alkanes and polyhydroxybutyrate plastics by *Alcanivorax* species isolated from North Atlantic: Importance of the ocean hydrocarbon cycles. *(Under revision in Environmental Pollution)*

Roles: Cao designed and conducted the study under the guidance of Dr. Baiyu Zhang and Dr. Bing Chen and acted as the first author of the manuscript. Zhu, Cai, and Liu helped with the methods. Other co-authors did the review and editing. Most contents of this paper were written by Cao and further polished by the other co-authors.

Cao, Y., Yu, M., Dong, G., Chen, B., & Zhang, B. (2020). Digital PCR as an emerging tool for monitoring of microbial biodegradation. *Molecules*, 25(3), 706. DOI: 10.3390/molecules25030706

Roles: Cao did the review under the guidance of Dr. Baiyu Zhang and Dr. Bing Chen and acted as the first author of the manuscript. Yu and Dong helped with the literature search. Most contents of this paper were written by Cao and further polished by the other co-authors.

6.1 Introduction

Marine oil spills can cause catastrophic impacts on ecosystems and human health. Biodegradation by indigenous hydrocarbon-degrading bacteria is a natural process that has mitigated oil spills in the marine environment (Martin et al., 2020). These hydrocarbon-degrading bacteria could derive carbon and energy through degrading petroleum hydrocarbons (Cao et al., 2022a).

In addition, the ocean is the ultimate pool of plastic wastes (Samalens et al., 2022). Seawater was reported to have high contents of plastic-based carbons (e.g., homogenized plastics in the North Pacific Gyre surface waters were reported to have 83% carbon by mass) (Stubbins et al., 2021; Zhu et al., 2020a). The abusive and improper disposal of plastics, which have incredibly high durability for even millions of years, have led to severe marine pollution (Bank et al., 2021). This concern has promoted studies to understand the potential capacity of hydrocarbon-degrading bacteria also to degrade plastics. Recently, bioplastics have been widely developed to replace conventionally petroleum-based formulations (Manfra et al., 2021; Rosenboom et al., 2022). However, not all bioplastics can be considered a panacea for dealing with plastic pollution, as there has been evidence for their environmental persistence. Nevertheless, one currently available bioplastic, i.e.,

polyhydroxybutyrate (PHB) plastic, has drawn much market attention as it has demonstrated a relatively fast degradation rate (Meereboer et al., 2020).

In terms of hydrocarbon and plastic degradation, attention has been given to obligate hydrocarbonoclastic bacteria under the genus *Alcanivorax* (Muriel-Millán et al., 2021). After oil spills, *Alcanivorax* would bloom and account for the high proportions of the associated microbial communities to degrade alkanes (Cao et al., 2022b). Also, in the plastic-polluted seawaters, *Alcanivorax* dominated in the plastisphere, a new ecosystem that hosts microbial communities on the surface of plastics (Wright et al., 2021), for the utilization of petroleum-based plastics such as low-density polyethylene (PE) (Delacuvellerie et al., 2019), polyethylene terephthalate (PET) (Hou et al., 2021), and polypropylene (PP) (Delacuvellerie et al., 2022). Furthermore, it was demonstrated that *Alcanivorax* could release specific esterase with a robust capacity for initiating biodegradation of bioplastics, such as PHB, poly(hydroxybutyrate-co-valerate) (PHBV), poly(ethylene succinate) (PES), polybutylene succinate (PBS), and polycaprolactone (PCL) (Zadjelovic et al., 2020).

Oil exploration, transportation, and spill events usually occur in the North Atlantic Ocean, which also acts as the most intense ocean carbon sink for 30% of the global ocean's CO_2 removal (Bates & Johnson, 2020). The magnitude and vulnerability of the North

Atlantic sink make it a "sentinel region" (Couldrey et al., 2019; DeVries et al., 2019). Based on the National Center for Biotechnology Information (NCBI) database, till now, there have been 15 kinds of *Alcanivorax* species recorded worldwide, including *A. borkumensis*, *A. dieselolei*, *A. gelatiniphagus*, *A. hongdengensis*, *A. indicus*, *A. jadensis*, *A. marinus*, *A. mobilis*, *A. nanhaiticus*, *A. pacificus*, *A. profundi*, *A. profundimaris*, *A. sediminis*, *A. venustensis*, *A. xenomutans*. However, there have been no reports about *Alcanivorax* species isolated from the North Atlantic to show the capability of degrading alkanes and plastics.

The capability of *Alcanivorax* for degrading alkanes and plastics, and its high abundance in plastic and/or oil contaminated sites, highlighted its importance for mitigating marine oil spills and plastic wastes. Apart from this, *Alcanivorax* was also recognized as an essential alkane-degrader that participated in the recently discovered cryptic ocean hydrocarbon cycles that include the short- and long-term cycles in the global oceans (Love et al., 2021). The short-term cycle occurs over a few days and starts from the CO_2 capture and conversion to hydrocarbons (dominated by *n*-pentadecane) via cyanobacterial photosynthesis. In contrast, the long-term cycle takes over a long period since it takes millions of years to convert marine organic matter to crude oil in sediments via diagenesis and catagenesis (McGenity et al., 2021). The ocean hydrocarbon cycles are linked with

cyanobacterial CO_2 capture, hydrocarbon production, and biodegradation to release CO_2 (Lea-Smith et al., 2015). The adaptation and ability of *Alcanivorax* to assimilate plastics indicated that the ocean has already developed ecosystem resilience to the impacts of plastics. The exploration of marine resilience to new plastic pollution necessitates the characterization and investigation of the eco-phycological responses of specific/representative *Alcanivorax* species to degrade alkanes and bioplastics.

In this study, we isolated a new *Alcanivorax* species named *Alcanivorax* sp. N3-2A, from the North Atlantic Canada firstly. We did the whole-genome sequencing (WGS) of this species and demonstrated its ability to adapt to cold temperatures. We found it harbors three types of alkane 1-monooxygenases (AlkB) and one PHB depolymerase (PhaZ) that acted as the first step for degrading alkanes and plastics. We further studied its physiological responses, including the growth profiling, modification of membrane composition, PhaZ activity, and the expression of three alkB genes when grown on alkanes and PHB plastics. At last, we highlighted the influence of *Alcanivorax* tied to the ocean hydrocarbon cycles on the remediation of plastics and the potential importance of plastics input affecting the ocean hydrocarbon cycles.

6.2 Materials and Methods

6.2.1 Isolation of the *Alcanivorax* species from the North Atlantic region

The species was isolated from oil-contaminated coastal sediment in the vicinity of a refinery company on the southeast coast of Newfoundland (Placentia Bay, 54.0ºE, 48.8ºN), Canada. Before isolation, the collected sample was enriched with Mineral Salt Medium (MSM): one liter of distilled water composed of NaCl, 15 g; $(NH_4)_2SO_4$, 10 g; $FeSO_4 \cdot 7H_2O$, 0.00028 g; KH_2PO_4, 3.4 g; $K_2HPO_4 \cdot 3H_2O$, 4.4 g; $MgSO_4 \cdot 7H_2O$, 1.02 g and trace element ($ZnSO_4$, 0.29 g; $CaCl_2$, 0.24 g; $CuSO_4$, 0.25 g; $MnSO_4$, 0.17 g). Clear diesel fuel (1%, v/v) was used as the sole carbon source. The obtained isolate was maintained on marine broth 2216 (Difco #279110) with a supplementary of 1% sodium pyruvate (PY, Sigma-Aldrich) at 28 ºC.

6.2.2 Identification of the species using whole-genome sequencing

The isolate was cultivated in the marine broth 2216 with the supplementary of 1% sodium pyruvate at 28 ºC for five days. The genomic DNA preparation and sequencing were described as previously reported (Cai et al., 2017a). Briefly, the DNA was extracted following Qiagen DNeasy Blood & Tissue Kit. Shotgun WGS was performed at the Donnelly Sequencing Center at the University of Toronto (Toronto, Canada) using an Illumina MiSeq 2500 with a 300-cycle MiSeq kit V2. Gene annotation was performed by

using the NCBI Prokaryotic Genome Annotation Pipeline. The sequence of the whole genome was deposited under the GenBank accession no. CP022307 to CP022309.

Sequences of *16S rRNA* gene, three AlkB (AlkB1, AlkB2, and AlkB3), and one PhaZ were obtained from the GenBank database. The gene sequence similarity was determined using the Basic Local Alignment Search Tool (BLAST). Phylogenetic trees and distances were calculated using the software package MEGA-X (Molecular Evolutionary Genetics Analysis) after the alignment of sequences with CLUSTALX. Distances were calculated using the Kimura two-parameter model. Trees were reconstructed using the neighbor-joining method with the use of 'default settings', and the bootstrap values were calculated based on 1000 replications. Average nucleotide identity (ANI) was calculated using the OrthoANIu algorithm (https://www.ezbiocloud.net/tools/ani) (Yoon et al., 2017).

6.2.3 Microbial growth and surface tension of the culture media

The liquid culture was prepared in 250 mL flasks filled with 50 mL MSM containing a carbon source and incubated with washed bacterial cells (1 mL, OD600 of 0.1). One milliliter of individual n-alkane (from C12 to C18, Sigma-Aldrich), 0.5 g/L PHB powder (poly[(R)-3-hydroxybutyric acid], #81329, Sigma-Aldrich), and sodium pyruvate (Sigma-Aldrich) were used as individual carbon source. The C18 was pre-heated in solid state at room temperature (~22 ^{o}C). MSM added with bacteria, but without the external carbon

sources, was used as the blank. All flasks were shaken at 150 rpm at 28 ºC for 10 days. Since clumps were formed by insoluble PHB powder, cell growth was estimated by measuring the total protein contents. Briefly, cells were harvested by centrifuging 10 mL of the well-mixed medium at 10,000 rpm for 10 min. One milliliter of 2% sodium dodecyl sulfate (SDS) lysis buffer (50 mM Tris-HCl buffer with 2% SDS, pH = 8) was added to the cells at room temperature for 1 h. The samples were sonicated for 1 min and centrifuged to obtain the soluble proteins, which were measured using the Pierce BCA Protein Assay Kit.

The cell-free medium was used for testing the surface tension via Du Nouy Ring method, as previously reported (Cai et al., 2019).

6.2.4 Phospholipid-derived fatty acids (PLFA) profiling

PLFA was carried out using the cells after 10 days of incubation. Briefly, cells were harvested and washed three times using the MSM. The washed cells were saponified under a water bath (100 ºC, 60 mins) to liberate fatty acids. Methylation was then conducted under 80 ºC for 10 mins. Finally, the methylated fatty acids (fatty acid methyl esters, FAMEs) were extracted and measured using a GC-MS system. An Agilent 7890A gas chromatography equipped with a DB-5MS column fused silica capillary column was used to differentiate FAMEs. The column temperature was programmed from 50 °C to 120 °C at a rate of 10 °C min^{-1}, and then to 280 °C at a rate of 3 °C min^{-1}. Individual compounds

were identified from their mass spectra and retention times with the standard spectra. The detailed protocol can be found from our previous study (Cai et al., 2017c). Quantization of each component was conducted with the m/z of 74 (Fan et al., 2017). Fatty acids are designated by the total number of carbon atoms to the number of double bonds (e.g., C12:0 represents the 12-carbon alkanoic acid).

6.2.5 Extracellular PhaZ activity measurement when grown on C15, PHB, and PY

The crude PhaZ activity of the cell-free medium on day ten was measured using a previously developed colorimetric method (Gowda & Shivakumar, 2015). Briefly, the assay was carried out in a 2.5 mL system by adding 0.5 mL of cell-free medium to a 2 mL reaction mixture (50 mM Tris, 200 μg of PHB, and 2 mM $CaCl_2$) and incubated at 55 °C for 1 h. One unit of PhaZ activity is defined as the amount of enzyme required to decrease the absorbance of 650 nm by 1.0 per hour.

6.2.6 Expression of three *alkB* genes when grown on C15, PHB, and PY

The expression of three *alkB* genes was quantified using a digital PCR (dPCR) system (QuantStudio 3D dPCR system, Applied Biosystems). Microbial growth on PY was set as the control. The chip-based dPCR hinges on the partition and distribution of template analytes into 20,000 individually amplified wells at a limiting dilution, for performing the absolute quantification without the requirements for endogenous references and calibration

(Cao et al., 2020a). The scheme of the workflow for dPCR analysis, including preparation, partitioning, amplification, and analysis, was shown in Figure 6.1.

Cells grown under C15, PHB, and PY were harvested from 10 mL of medium after ten days of incubation. The RNA was extracted using the Qiagen RNeasy Micro Kit. The reverse transcription was performed using the High-Capacity RNA-to-cDNA™ Kit (Applied Biosystems). Primers were designed for targeting the fragments of each gene via Primer Express 3.0.1 software (Table 6.1 and Table 6.2). Validation of each amplified fragment was performed using agarose gel electrophoresis (Figure 6.2). For the dPCR analysis, the PCR reaction (14.5μL) mixtures containing 7.25μL QuantStudio™ 3D PCR Master Mix V2, 2μL cDNA, 0.5 μL forward primer, 0.5μL reverse primer, 1.45μL SYBR green dye (20X in TE buffer), and 2μL DNase/RNase-Free water. The non-template control was performed using DNase/RNase-Free water to replace cDNA. The chips were loaded and sealed using a QuantStudio 3D chip loader (Applied Biosystem). The dPCR amplification reactions were performed in a ProFlex Flat thermal cycler (Applied Biosystem) with an initial denaturation at 96 °C for 10 min, followed by 39 cycles of 2 mins at 60 °C, 30 s at 98 °C, and 2 mins at 60 °C, and hold at 10 °C. Chips were read using a QuantStudio 3D Instrument and analyzed via the QuantStudio 3D AnalysisSuite Cloud Software. The *16S rRNA* gene was used as the housekeeping gene.

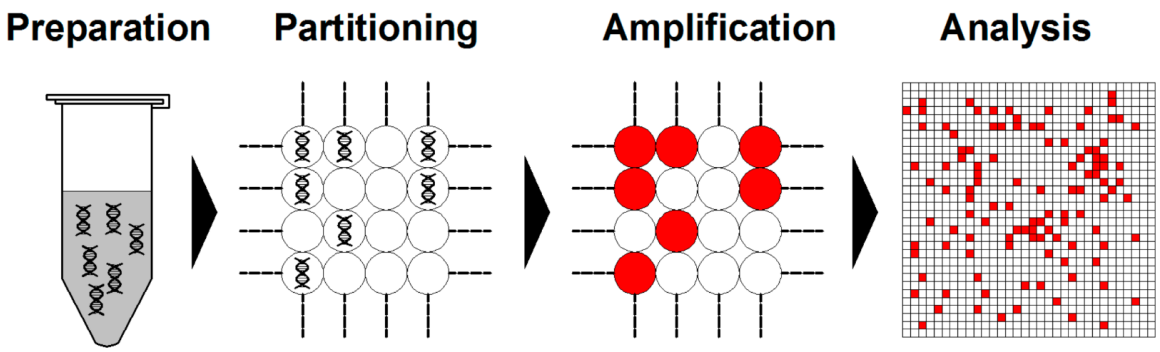

Figure 6.1 Scheme of dPCR workflow.

Table 6.1 Gene sequences of *alkB1*, *alkB2*, *alkB3*, and *16S rRNA* genes.

***alkB1* gene sequence (plasmid 2 and chromosome, 1215 bp):**
tcatttatgcgctacggtatcggctgattcagaaccagccacaccaaatttacgctcatagaattcacgcttacccgtctggatct
gaatctggtcgagatctcctttcgcccattccaccacccggtggtccatcatcgagcgaaaccatgagggaaacattgcggcc
agaaacattccagggtaacccgaaggtaaggacggcaggtctttgaaatcgcgaagcgactggtaggacctcgtaggatgg
gcgtgatggtcggaatgtcgttgcaaatgaaacagaatcaggttcgacataatatggttcgagttccaggagtggtacggttgc
tgacgctcgtaacgtccatccggcatcttcttacgcagcaggccataatgctcaatatagttcgcgctggtcagctgccaccag
ccgaaggccatctgaatgggcaagaagatcagcattaacggaccaaaaaacgccagcaatgtggcatagagtacaactgtt
agaagcatgggctgaagaacttcgttatccagactccagacacttttgccacatcggttgaggcgctgtccctccaacgcccat
gcccgcttgaaagcaccgggaatttcacgcagtgaaaacgagtagatggactcacccatgcgggatgtcgccgggtccatc
ggcgtagccacatcacggtgatgcccccttattgtgctcaatgaagaaatgaccatatccgaccacggcgaggacaagcttgg
ccatccaacggtcaaacgtttctttttttatggccgagttcgtggcctgtgttcagagccaggccattgatgatacccagggaaaa
ggccagtgcgaggaactcgaaaacattcatcgaatgcgtggccacccaccagcaactgacaatcagggatgcgtagtgaat
aggaacggtcaagtaggtcagcacccgatagtaacgatcctgttcaagccgaggcacagccgactcaggggggtttgaaaa
atcttctccgaacatggcatccatcaagggaactgcgccataccaaaagattaacaccaacccgtaccagatgctccatccag
tctgggataccaaataaaggccaataagaggcgtcgctggccacagcacagaaagaacccacagatggcgtttcctgtcca
cataaccctcggtatcaggatctttctgtggagactccgttaaaacattttccggcat
***alkB2* gene sequence (chromosome, 1149 bp):**

atgtttgcgaccatgcgttccgataccatgctgaaaataaaaaaatgggggtatctggggttttgggccctggtgttgccgttgc

tgccgttcagtgccctggtgggccgtgacaccggtactcaggactactgggcgtggttcctgtatttcgtggtgtttggcatcat

tccgttgctggattatctgatcggcaaggacccttccaacccggacgagcaggtccaggtgccctcgctgagcggcgagcg

gctgtacaccttctttctgtttctgatgggctttgtctggttcggcgcgctgttttacgccggctgggtgttcgtcaataacagctatt

cctggttcggcgcgctgggctggatcgtctccatcggcaccgtgggcggcattatcgccatcaatctgggccatgagttcgtg

cataaggatgcgaagctggaaaactggatgggcggcctgttgctcgcatcggtgacctacgccggcttcaaggtggagcac

gtgcgcggccaccacgtgcatgtctccacccccggggacgcgtcctcctcgcggtatgatcagagtgtgtatcagtttttgcc

gcgcgcctttaagcacaacttcctgaatgcctggaagctggaaaagcagtacctggagcgcaagggtaaaaagaacctgag

cgccgccaatgagctgatctggtggtacgctatttccgccctgttcacgctcgcctttggcctcgcgttcggctggatgggcgt

gttgttcttcctggcccagagtttcgtggctgcctttaccctggaagtgatcaactacatcgagcattacggtttgcaccggcgc

gtcaacgacaaaggccgctatgagcgggtcacgccggcgcacagctggaactccaactatctgttgaccaacctggccctg

tttcagctgcagcgccacagcgatcaccacgcctacgccaaacgccgctaccaggtgctgcggcattacgaggagagccc

gcaattgccgggcggctacgcggccatgtacgtcctggccctggttccgcccttgtggaagcggattatgaacccgcgcgtg

gaggcctattacgaaggtgaattggatcaactgttccgcgatggtcgccgcgttaacaacatcgtctga

***alkB3* gene sequence (chromosome, 1203 bp):**

ttatccctctgcgaccttcggcggcgcgtcgccgtattgaatgccgtacttgcggatcaacgtgtcccgcttggcggggtcga

agttgatgttgcgggcgtcgttgccggcgtgttcgagcaggcgtttgtccatgatccggtaccacagaggcggaaaatagctg

accaggaacatgccgaagtaaccgttgggcagttccggcagattctcgaaatggcgcaagctctggtagcgccgggtcggg

tgggcgtggtgatcggagtggcgctgcaggtggaaggtggcccagtttgagaacatgtggttgctgttccagctgtggtagg

gctgggtgcgctcgtagcggccgttggcgcgcctgtggcgcagcaggccatagtgctcgatgtagttggccgaggtcagtt

ggaacgcccccagaacgcggtgccgagaatatagggcagcaggccgatgccgaacacggcgagcacggtgccccag

gccacggcggtgatgatcgccggctggatgatctcgttttccagggaccacaccgatttgccctgaccattgaggcggtctttc

tccaggcgccaggcacgcttggcggcgcccggcagctcgcgcagggcgaatttccagatgctttcgcccatccgtgacga

agcggggtcttccggggtggccacgtccttgtggtggcccttgttgtgttcaataaagaaatgcccataggcgcacggcgcc

agcacgaacttggccagccagcgctcgcccttgcctttcttatggcccagctcatggcccaggttgatgcccacgccgcagg

tgccgccaatcagatagaccatcgccagcaccccgtgccagggcagatcctgggtgcccacgaaccaggcgccatagaac

caggcgccccagatcagcggcaccagcgcgtagagaatccagcggtagtaagggtcgtcctcaagctggggcaccacct

cttccggcgggttgctggtgtcttcgccgatcagcatgtccagcaccggcacggtcagatagtagaacgccagcggcagcc

acagggtcagggcattgccggtggcgaaatacagcgccggcccggcgaacacaatggcgggcacgaacagcgaggaa

aaccatagacgccgtttacggtcccgataaacgaccccggaggggccgatgaaaacgcctgccttgctcat

***16S rRNA* gene sequence (chromosome, 1542 bp):**

gaactgaagagtttgatcatggctcagattgaacgctggcggcaggcttaacacatgcaagtcgagcggtaacaggggtag

cttgctacccgctgacgagcggcggacgggtgagtaacacgtgggaatttacccatctgtgggggacaacccggggaaac

ccgggctaataccgcatacgccctacgggggaaagcaggggatcttcggaccttgcgcagatggatgagcccgcgtcgga

ttagctagttggtagggtaaaggcctaccaaggcgacgatccgtagctggtctgagaggatgaccagccacaccgggactg

agacacggcccggactcctacgggaggcagcagtggggaatcttggacaatgggggcaaccctgatccagccatgccgc

gtgtgtgaagaaggccttcgggttgtaaagcactttcagtagggaggaaggctttgggctaataccctggagtacttgacgtta

cctacagaagaagcaccggctaatttcgtgccagcagccgcggtaatacgaaaggtgcaagcgttaatcggaattactgggc

gtaaagcgcgcgtaggcggtgtgttaagtcggatgtgaaagcccagggctcaaccttggaactgcatccgatactggcacg

ctagagtgcagtagagggaggtggaatttccggtgtagcggtgaaatgcgtagagatcggaaggaacaccagtggcgaag

gcggcctcctggactgacactgacgctgaggtgcgaaagcgtggggagcaaacaggattagataccctggtagtccacgc

cgtaaacgatgtctactagccgttggggtccttagtgactttggtggcgcagctaacgcgataagtagaccgcctggggagta

cggccgcaaggttaaaactcaaatgaattgacgggggcccgcacaagcggtggagcatgtggtttaattcgatgcaacgcg

aagaaccttaccaggtcttgacatcctcggaatttggcggagacgccttagtgccttcgggagccgagtgacaggtgctgcat

ggctgtcgtcagctcgtgtcgtgagatgttgggttaagtcccgtaacgagcgcaacccttgtccctagttgccagcacttcggg

tgggaactctagggagactgccggtgacaaaccggaggaaggtggggacgacgtcaagtcatcatggcccttacgacctg

ggctacacacgtgctacaatggctggtacagagggttgcgaagtcgcgaggcgaagctaatcccttaaagccagtcgtagtc

cggattggagtctgcaactcgactccatgaagtcggaatcgctagtaatcgcggatcagaatgccgcggtgaatacgttcccg

ggccttgtacacaccgcccgtcacaccatgggagtggattgcaccagaagtggctagtttaaccttcgggagaacggtcacc

acggtgtggttcatgactggggtgaagtcgtaacaaggtagccgtaggggaacctgcggctggatcacctccttaa

Table 6.2 Primers designed and used.

Name	Primer sequences (5'to 3')	Length (bp)	Reference
*alkB1*_F	AGGTCAGCACCCGATAGT	190	This study
*alkB1*_R	CCAGCGACGCCTCTTA		
*alkB2*_F	TTCTGATGGGCTTTGTCTGG	213	This study
*alkB2*_R	CGTAGGTCACCGATGCGAG		
*alkB3*_F	GCCGAGGTCAGTTGGAAC	242	This study
*alkB3*_R	GGCGAAAGCATCTGGAAAT		
*16S*_F	CCTACGGGAGGCAGCAG	194	(Shah & Wang, 2019)
*16S*_R	ATTACCGCGGCTGCTGG		

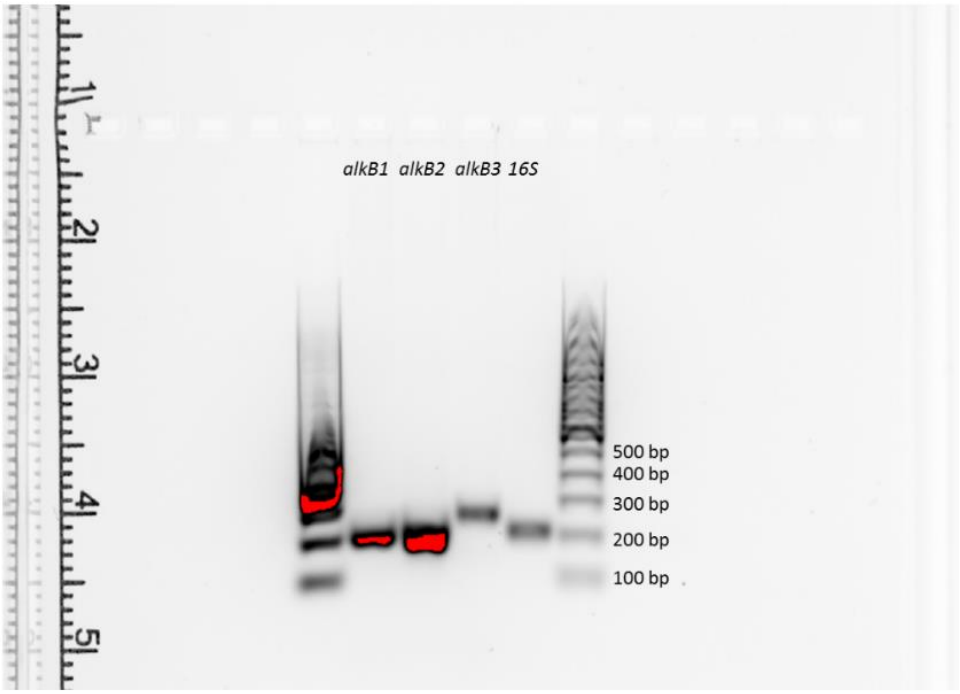

Figure 6.2 Validation of dPCR targeted fragments of genes by agarose gel electrophoresis.

6.2.7 Statistical analysis

All experiments were conducted in triplicate. The dPCR analyses were conducted in triplicate and following the Digital Minimum Information for Publication of Quantitative Digital PCR Experiments (dMIQE) Guidelines (Huggett et al., 2013). The differences between data were evaluated using the One-way ANOVA analysis ($n = 3$) with $P < 0.05$ (*) as a significant difference and $P < 0.001$ (**) as a very significant difference.

6.3 Results and Discussion

6.3.1 Characterization of the *Alcanivorax* species isolated from North Atlantic

The *16S rRNA* gene phylogenetic affiliation further showed that *Alcanivorax* sp. N3-2A clusters together with other *Alcanivorax* species and is closely related to *A. mobilis* MT13131 (100% similarity) (Figure 6.3). The ANI of the similarity index between the two whole genomes was further calculated, showing a 98.47% OrthoANIu value (Figure 6.3). It means that *Alcanivorax* sp. N3-2A belongs to the *A. mobilis* species. Differently, *A. mobilis* MT13131 was screened from deep-sea sediment (nearly 2800m) recovered from the Indian Ocean (49.5°E, 37.9°S) (Yang et al., 2018), while *Alcanivorax* sp. N3-2A was isolated from cold shallow-sea sediments (nearly 10m) in North Atlantic waters off the coast of Canada (54.0ºE, 48.8ºN).

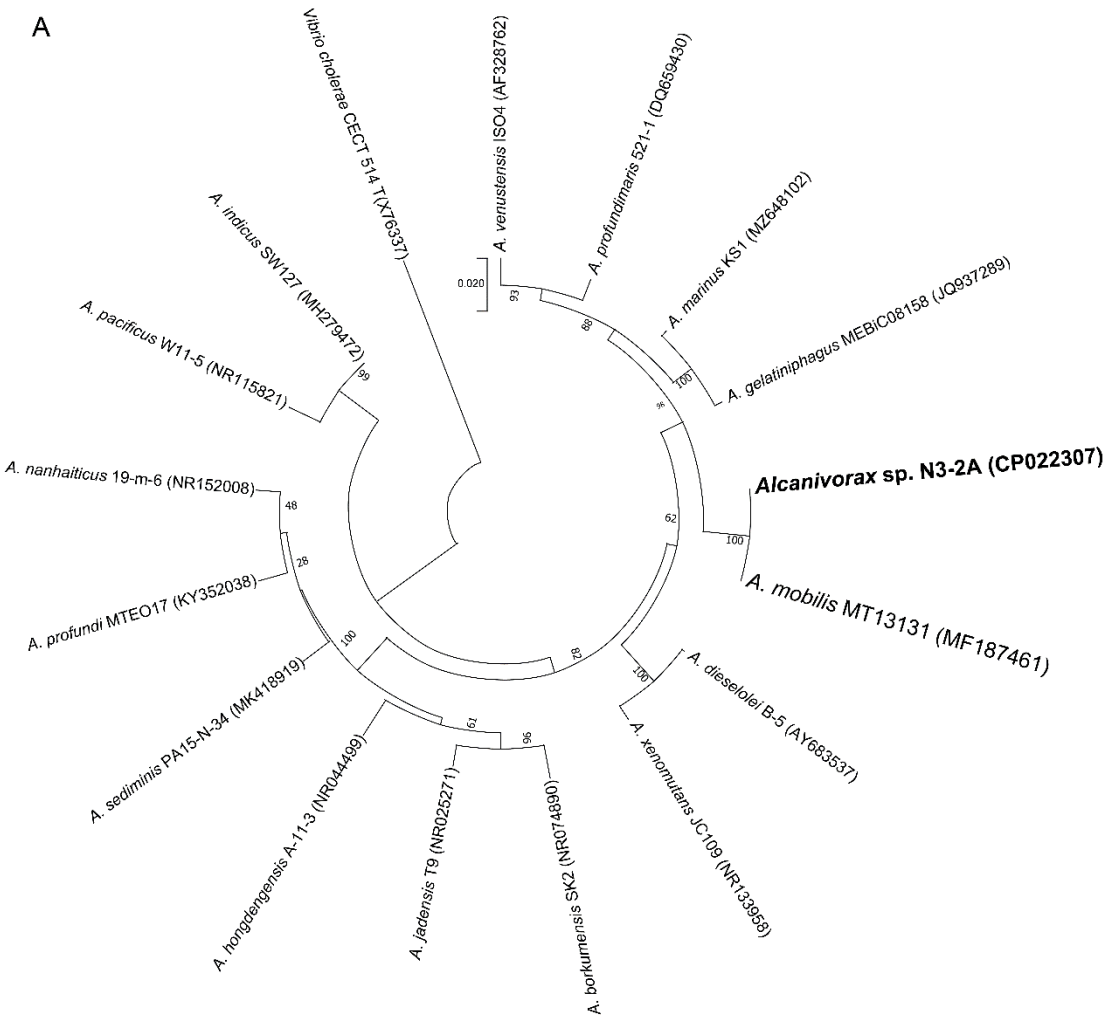

B

Strain	Genome length (bp)	Average aligned length (bp)	Coverage (%)	ANI value (%)
Alcanivorax sp. N3-2A	4,746,060	2,857,873	60.22	98.47
Alcanivorax mobilis MT13131	4,053,480		70.50	

Figure 6.3 (A) Phylogenetic tree based on 16S rRNA sequence of the *Alcanivorax* species. (B) Comparison of the genomes between *Alcanivorax* sp. N3-2A and *Alcanivorax mobilis* MT13131.

A chromosome type replicon (4,305,015 bp), with a G+C content of 63.02%, made of 210 contigs/scaffolds, was obtained for *Alcanivorax* sp. N3-2A, which harbors 4,162 coding sequences, including 3,309 proteins with identified functions. Three rRNA operons and 47 tRNAs were also annotated. Two plasmids with the size of 427,202 bp and 15,963 bp, respectively, contain a total of 407 coding sequences. The G+C contents of the two plasmids are 63.43% and 55.11%, respectively. As expected, diverse oxygenases, dehydrogenases, and cytochromes involved in the aerobic hydrocarbon biodegradation pathway were found in the genome, both in the chromosome and the plasmids, explaining the ability of the strain to degrade hydrocarbons. Several lipopolysaccharides and polysaccharide biosynthesis and export genes are presented in the chromosome, linking to the power of the strain to produce biosurfactants. In addition, we demonstrated its survival under the temperature range of 0 – 37 °C due to the existence of cold-shock proteins in the genome. It indicated its psychrotolerant capacity to adapt to cold environments. The spatial distribution (present in both northern and southern hemispheres) and temperature adaptivity of *A. mobilis* demonstrated here speak to its prevalence and evolution.

The AlkB played the first step in assimilating alkanes (Cao et al., 2022b). Three homologs of AlkB (i.e., AlkB1, AlkB2, and AlkB3) in the chromosome and one AlkB1 in a plasmid were detected in *Alcanivorax* sp. N3-2A. The presence of AlkB1 in both plasmid

and chromosome is unique among reported *Alcanivorax* species. The amino acid sequences of the AlkB homologs are much different and grouped in three distinct phylogenetic branches (Figure 6.4), suggesting their disparate functions for degrading various carbon sources. The AlkB1 was closely related to *Alcanivorax* sp. DSM 26295 and *Marinobacter*, while AlkB2 and AlkB3 were closely related to them in the chromosome of *A. mobilis* MT13131, whose genomics harbors only two types of AlkB homologs. Interestingly, the alkane-hydrolase (CDD: 239589), a type of integral-membrane di-iron enzyme that shares a requirement for iron and oxygen for activity, is included in the AlkB2 and AlkB3 but not in AlkB1 (Figure 6.5). These showed the differences between AlkB1 to AlkB2 and AlkB3.

It was reported that the biodegradation of PHB started from converting polymers to monomers via PhaZ (Zadjelovic et al., 2020). The amino acid sequences of depolymerase PhaZ in *Alcanivorax* sp. N3-2A was grouped in the phylogenetic branches of other *Alcanivorax* species and closely related to *A. mobilis* MT13131 (100% similarity) (Figure 6.6). Besides, α/β hydrolase domain (position 42-246, CDD: 328752) is included in the PhaZ (Figure 6.5), similar to that of the esterase characterized in the *Alcanivorax* sp. 24 for bioplastics (e.g., PHB, PHBC, PES, PBS, and PLC) degradation (Zadjelovic et al., 2020).

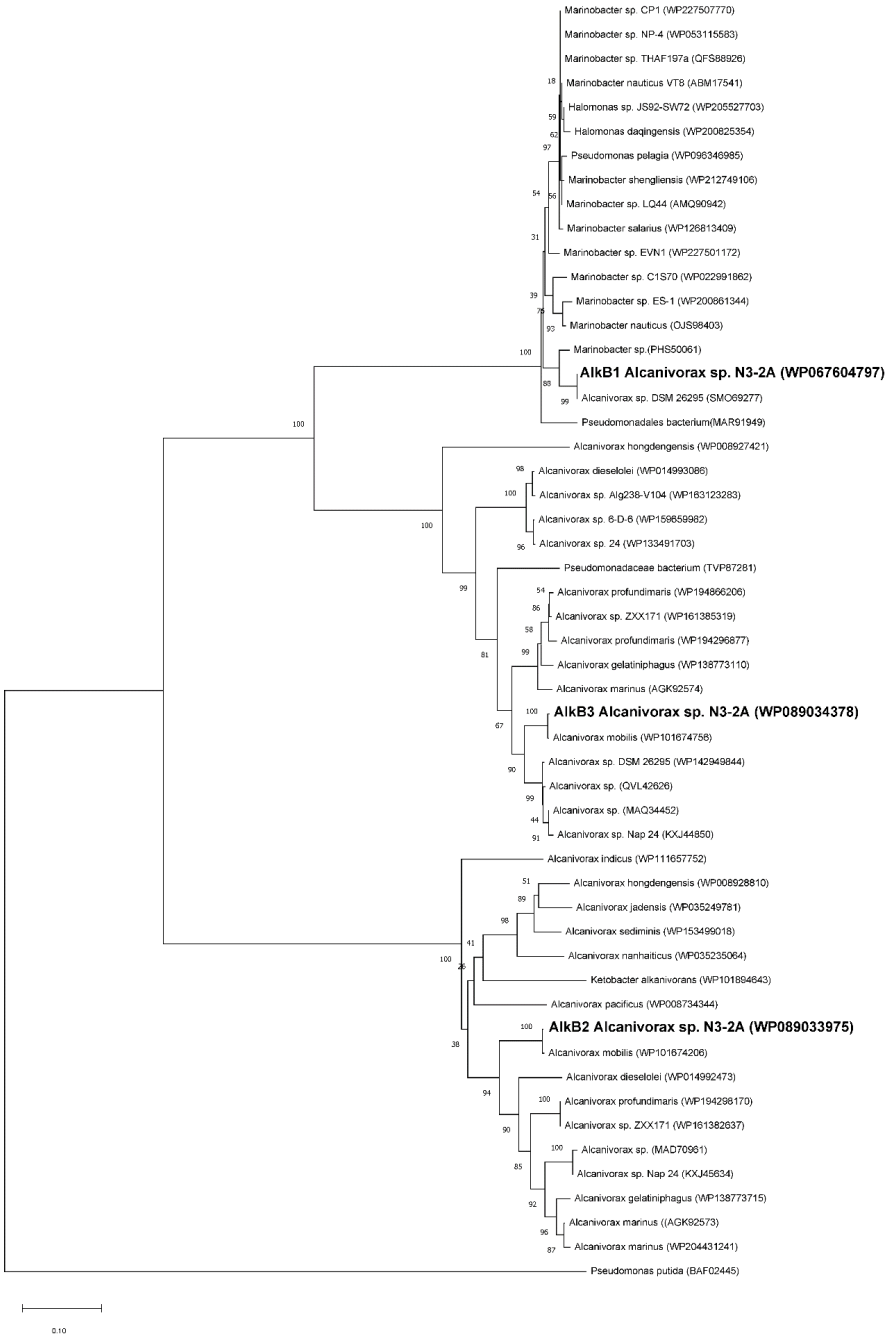

Figure 6.4 AlkB tree of the three homologs (amino acid sequence) present in *Alcanivorax* sp. N3-2A

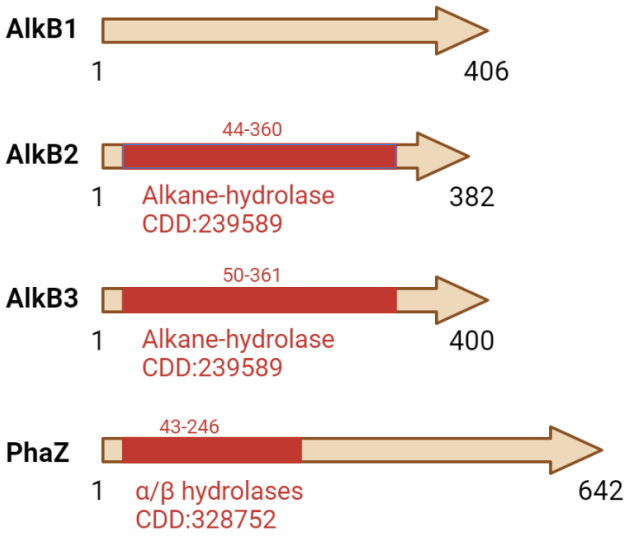

Figure 6.5 Scheme showing the protein domains and genomic context of AlkB1, AlkB2, AlkB3, and PhaZ enzymes.

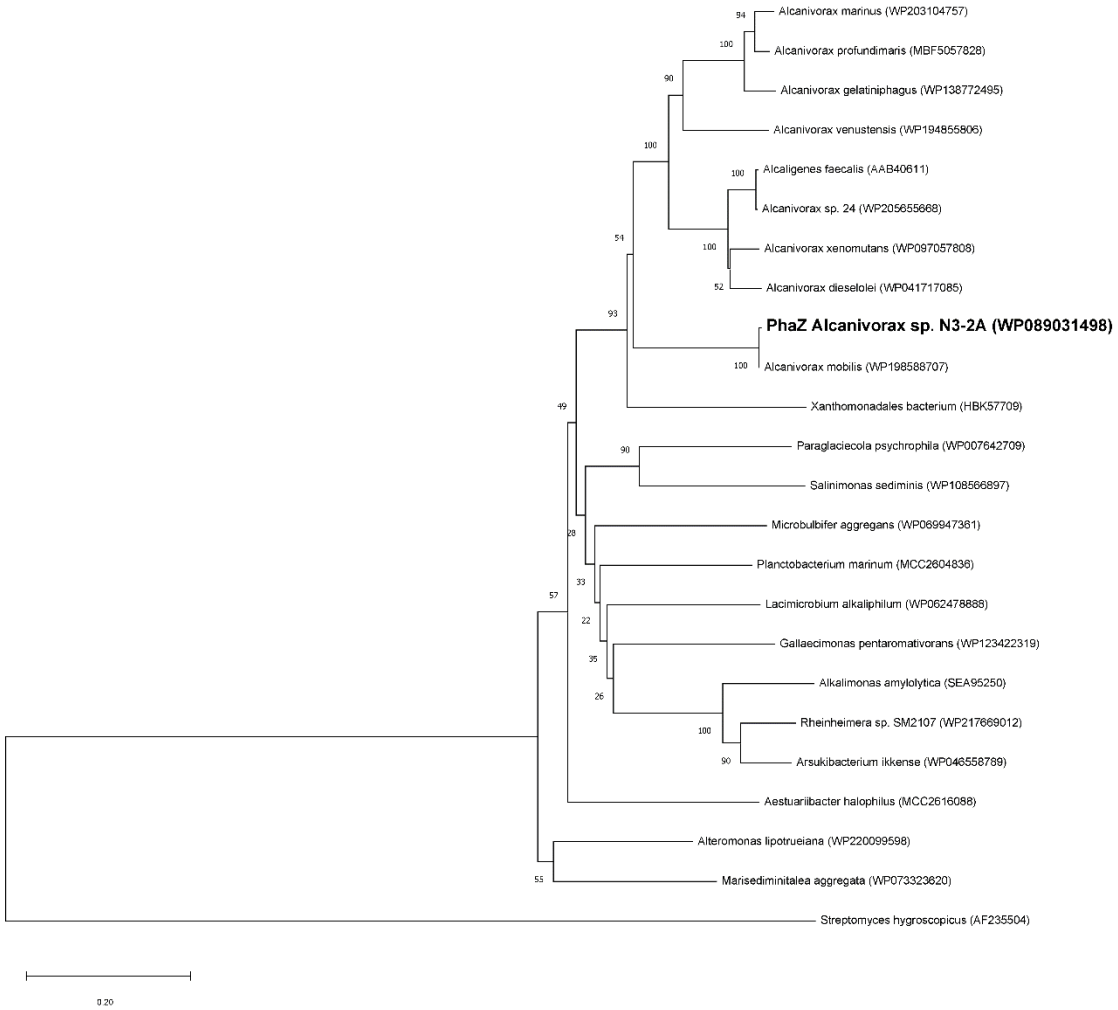

Figure 6.6 PhaZ tree of the PHB depolymerase (amino acid sequence) present in *Alcanivorax* sp. N3-2A.

6.3.2 C15 and PHB served as preferential carbon sources for promoting microbial growth

The bacterial growth was estimated by measuring the total protein contents when grown on individual n-alkane (C12 - C18), PHB, and PY. It showed that PY promoted more cell growth than PHB and alkanes after 10-day cultivation, with 750, 360, and 73 - 333 μg/mL detected, respectively (Figure 6.7). For different n-alkanes, microbial utilization of C15, C12, and C17 could stimulate more cell abundance than the utilization of other alkanes (73 - 122 μg/mL), with total protein reaching up to 333, 260, and 206 μg/mL, respectively (Figure 6.7). It is not surprising because PY is more labile than n-alkanes and PHB for promoting cell growth (Radwan et al., 2019). However, PY can also serve as the easily utilizable carbon source in the marine environment for other heterotrophic bacteria (Radwan et al., 2019), which may explain the lack of reports of *Alcanivorax* being enriched by PY. *Alcanivorax* sp. N3-2A had a higher enrichment when grown on C15 than other n-alkanes, indicating the evolution of *Alcanivorax* makes it more easily to assimilate C15, which has a broader distribution in the marine environments than other hydrocarbons as it is the primary hydrocarbon that cyanobacteria produced (Lea-Smith et al., 2015).

Oil-degrading microbes would secrete surface-active agents (e.g., biosurfactants) to increase oil bioavailability for biodegradation (Cao et al., 2020c). The surface tension of

the cell-free culture medium could indirectly reflect microbial biosurfactant production (Cai et al., 2019). Though *Alcanivorax* sp. N3-2A could decrease surface tension when utilizing all these carbon sources; it released more biosurfactants when grown on C12 - C17 than C18, PHB, and PY (Figure 6.7). The lowest surface tension was achieved when growing on C15 (43.3 mN/m). Compared with the solid phase (C18 and PHB) and soluble (PY) carbon sources, utilization of liquid n-alkanes (C12 - C17) was found to strongly correlate with enhanced microbial biosurfactant production, which facilitates oil bioavailability in the water phase.

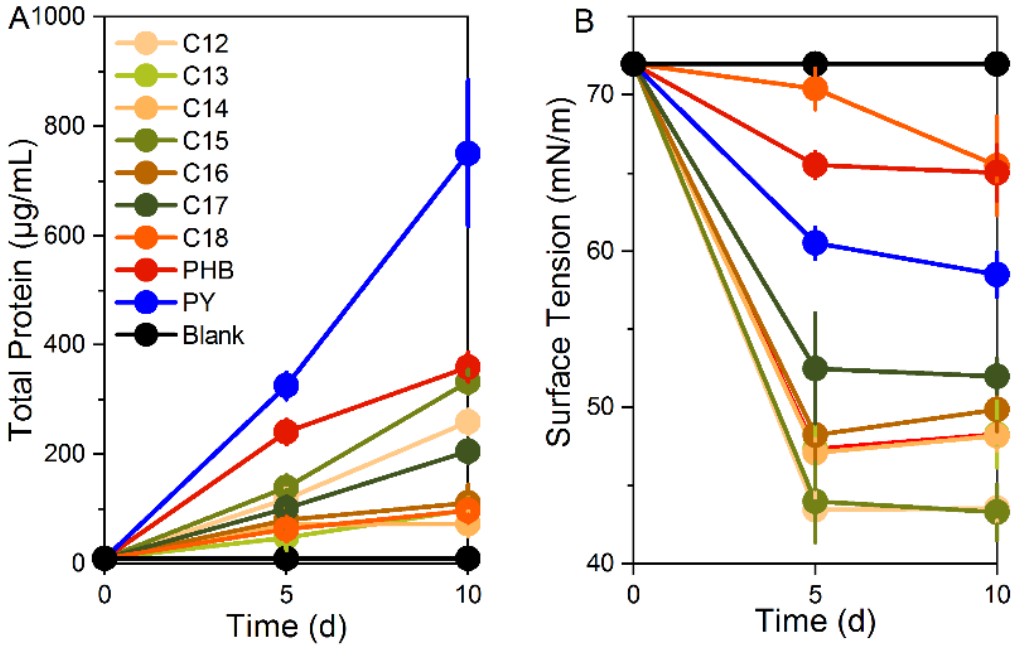

Figure 6.7 (A) Bacterial growth and (B) the surface tension of the cell-free culture media when grown on different n-alkanes (C12 - C18), PHB, and PY.

6.3.3 Microbial growth on C15 and PHB induced different membrane fatty acid compositions

To degrade different carbon sources, *Alcanivorax* not only incorporates but also to modifies fatty intermediates (Konieczna et al., 2018). The utilization of alkanes is directly associated with the synthesis of fatty acids, which further leads to beta-oxidation pathways (Cao et al., 2022b). Generally, saturated fatty acids are the primary fatty acids in the cell membrane, in which C16:0 is the primary fatty acid, while C13:0 and C14:0 are rarely detected when utilizing different carbons sources (Figure 6.8). This result is in accordance with related *Alcanivorax* strains, such as *A. mobilis* MT13131 (Yang et al., 2018), *A. marinus* LMG 24621 (Lai et al., 2013), *A. gelatiniphagus* JCM 18425 (Kwon et al., 2015), *A. venustensis* DSM 13974 (Fernández-Martínez et al., 2003), *A. xenomutans* KCTC 23751 (Rahul et al., 2014), and *A. dieselolei* DSM 16502 (Liu & Shao, 2005).

Interestingly, when grown on odd-numbered n-alkanes (i.e., C13, C15, and C17), the membrane fatty acids showed more complex results. When grown on C13, the fatty acids are mainly composed of C16:0 (42%), and then C17:0 (20.3%) and C15:0 (10.2%); when grown on C15, the fatty acids are mainly composed of C15:0 (42.9%), and then C16:0 (20.2%) and C17:0 (19.9%); when grown on C17, the fatty acids are mainly composed of C17:0 (39.9%), and then C16:0 (24.1%) and C15:0 (14.9%) (Figure 6.8). Besides, when

grown on *n*-alkanes except for C13 and C14, the increase of specific carbon-numbered fatty acids correlated with the use of corresponding *n*-alkanes. It indicates that assimilation of C13 and C14 in the cell membrane is relatively tricky for *Alcanivorax* sp. N3-2A (Figure 6.8). The PLFA analyses together with bacterial growth profiling implied the deficiency of *Alcanivorax* sp. N3-2A for the utilization of C13 and C14. Such results are different from the *A. borkumensis* SK2, which showed a strong capacity for using C13 and C14 for bacterial growth (Naether et al., 2013).

Alcanivorax species would modify the membrane lipid composition to incorporate n-alkanes with different chain lengths (Naether et al., 2013). However, such a process was not clarified for the assimilation of plastics. When PHB served as the sole carbon source, only even-numbered fatty acids dominated by C16:0 (nearly 65%) were detected (Figure 6.8). The non-metric multidimensional scaling (nMDS, Bray-Curtis is used as dissimilarity matrix) analysis showed that the membrane fatty acid patterns clustered together when grown on PHB, even-numbered n-alkanes, and PY (Figure 6.8). The utilization of odd-numbered n-alkanes drove the membrane fatty acids quite different from the utilization of PHB. *Alcanivorax* species may exert different eco-physiological responses to assimilate PHB and odd-numbered n-alkanes in the marine environment.

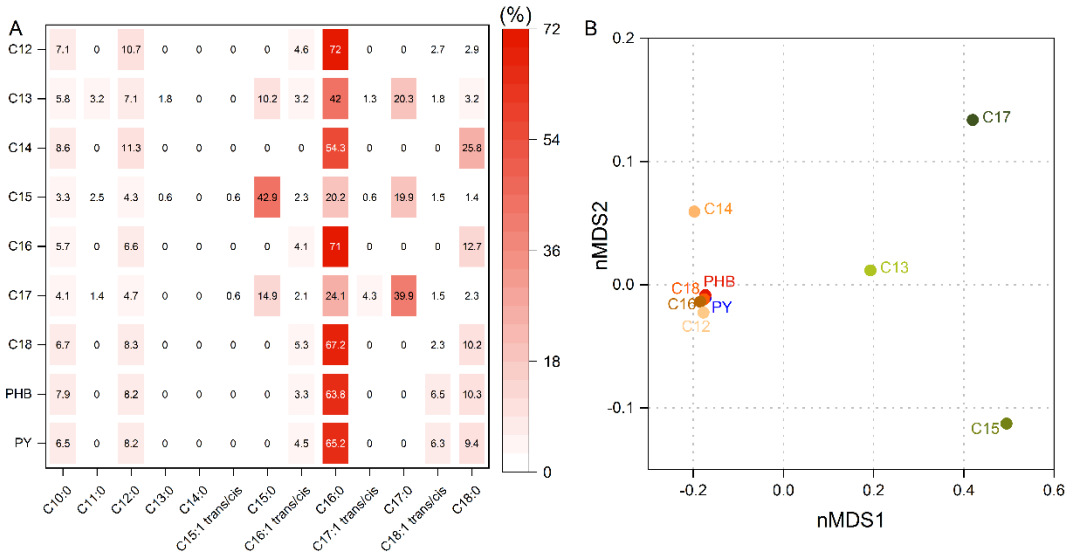

Figure 6.8 (A) PLFA profiling showing the membrane fatty acid patterns and (B) nMDS analysis of *Alcanivorax* sp. N3-2A when grown on different n-alkanes (C12 - C18), PHB, and PY.

6.3.4. Responses of PhaZ activity and *alkB* genes expression when grown on C15 and PHB

The utilization of plastics by *Alcanivorax* was initiated by the PhaZ to convert plastics to monomers (Zadjelovic et al., 2020). In contrast, biodegradation of alkanes started with AlkB to convert alkanes to corresponding alcohols, which were then transformed to fatty acids and entered the tricarboxylic acid cycle (TCA) for respiration (Park & Park, 2018a). To further illustrate the bacterial responses, we evaluated the PhaZ activity and expression of three *alkB* genes when grown on PHB and C15. It is not surprising that the utilization of PHB will induce the highest detectable PhaZ activity (0.08 U/mL) (Figure 6.9) to initiate the depolymerase of PHB. In contrast, when grown on C15, the PhaZ activity was rarely detected (Figure 6.9). Interestingly, we found that when PY served as the sole carbon source, the medium still had a certain PhaZ activity (0.04 U/mL) (Figure 6.9).

The transcription of *16S rRNA* gene showed that the active prokaryotes were similar when grown on C15 and PHB, and significantly lower than grown on PY (Figure 6.9). It was in line with the results of growth profiling (Figure 6.3) and further verified that C15 and PHB could serve as similar carbon sources for enriching cells. The expression pattern of three *alkB* genes in *Alcanivorax* sp. N3-2A unveiled through RT-dPCR absolutely quantification (Figure 6.10 – 6.12) showed that *alkB1* gene had the highest expression level

when grown on C15, while *alkB2 and alkB3* genes were highly expressed when PHB served as the sole carbon source (Figure 6.9). It seems that the *alkB1* gene was majorly responsible for the degradation of alkane and may serve as an optimizing indicator for hydrocarbon pollution surveillance. Further, the *alkB2* and *alkB3* have a similar expression pattern to different carbon sources (Figure 6.9). These results confirmed that *alkB1* is different from *alkB2* and *alkB3* based on genetic sequencing information (Figure 6.4) and expression patterns when using different carbon sources.

In addition, only *alkB1* gene in *Alcanivorax* sp. N3-2A was upregulated when grown on C15 than PY (Figure 6.9). Differently, a previous study showed two *alkB* genes in the strain *A. borkumensis* SK2 were both upregulated when grown on alkanes than grown on PY (Sabirova et al., 2011). It implied the diversity of feedback of AlkB during utilizing alkanes.

Pioneer studies also demonstrated that AlkB in *Pseudomonas aeruginosa* E7 was directly involved in the PE degradation (Jeon & Kim, 2015). However, the metagenomic analyses showed that alkane degradation pathway was not detected during biodegradation of specific plastics like PP and PE by *Alcanivorax* (Delacuvellerie et al., 2022). Our study, based on revealing the expression of different *alkB* genes of the newly screened *Alcanivorax* sp. N3-2A, indicated that *alkB2* and *alkB3*, rather than *alkB1*, may potentially

be responsible for the degradation of PHB (Figure 6.9). Such results confirmed that the utilization of PHB by *Alcanivorax* in the marine environment may be through the alkane biodegradation pathway, while the three AlkB have different contributions. The differences in the substrate preference of AlkB enzymes may be associated with the presence of bulky amino acids lining the substrate-binding pocket (Van Beilen et al., 2005). Through evaluating the expression patterns of *alkB* genes and PhaZ activities in the media, we confirmed that *Alcanivorax* sp. N3- 2A exerted different eco-physiological behaviors for the utilization of alkanes and PHB in the marine environment.

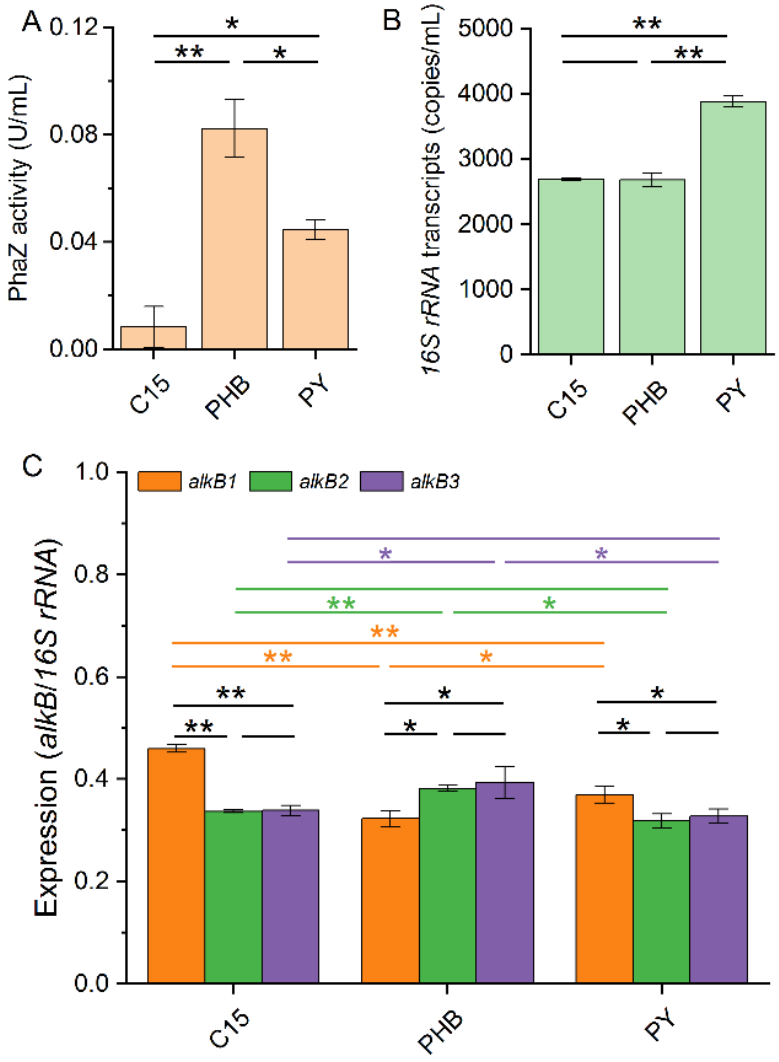

Figure 6.9 (A) PhaZ activity, (B) *16S rRNA* gene transcripts, and (C) expression of three *alkB* genes of *Alcanivorax* sp. N3-2A when grown on C15, PHB, and PY.

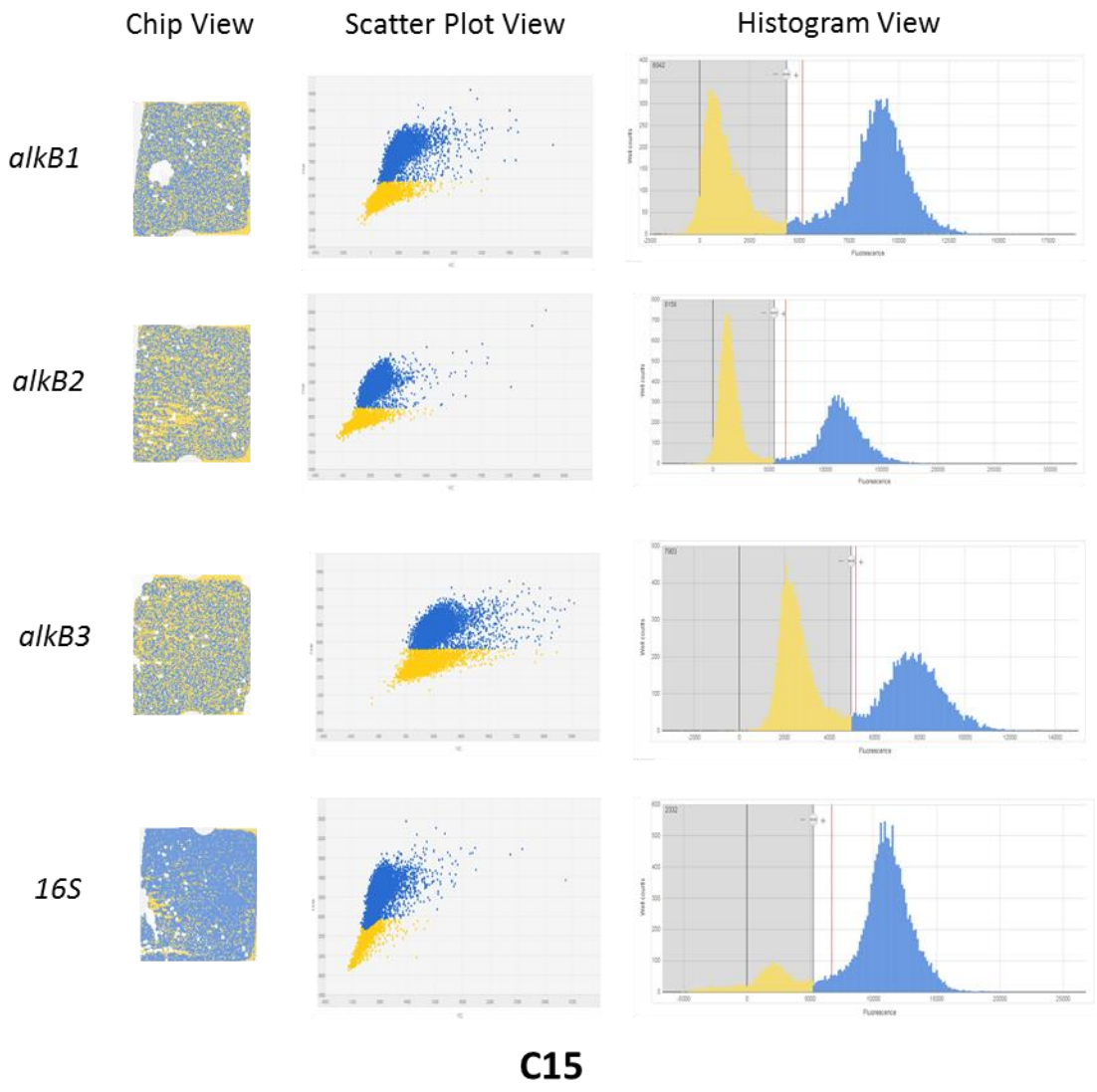

Figure 6.10 The dPCR analysis of alkB1, alkB2, alkB3, and 16S rRNA gene transcripts when grown on C15.

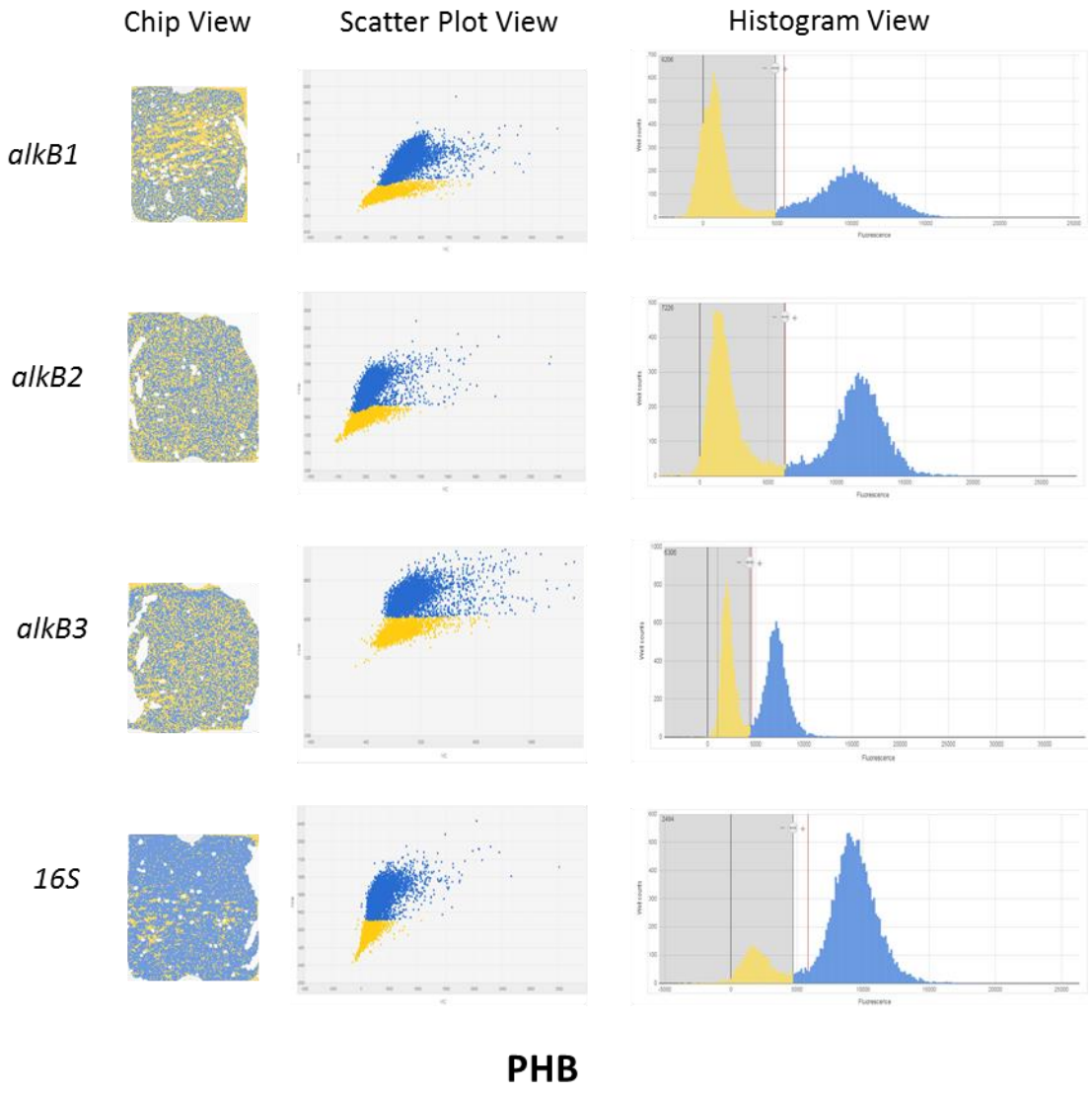

Figure 6.11 The dPCR analysis of *alkB1*, *alkB2*, *alkB3*, and *16S rRNA* gene transcripts when grown on PHB.

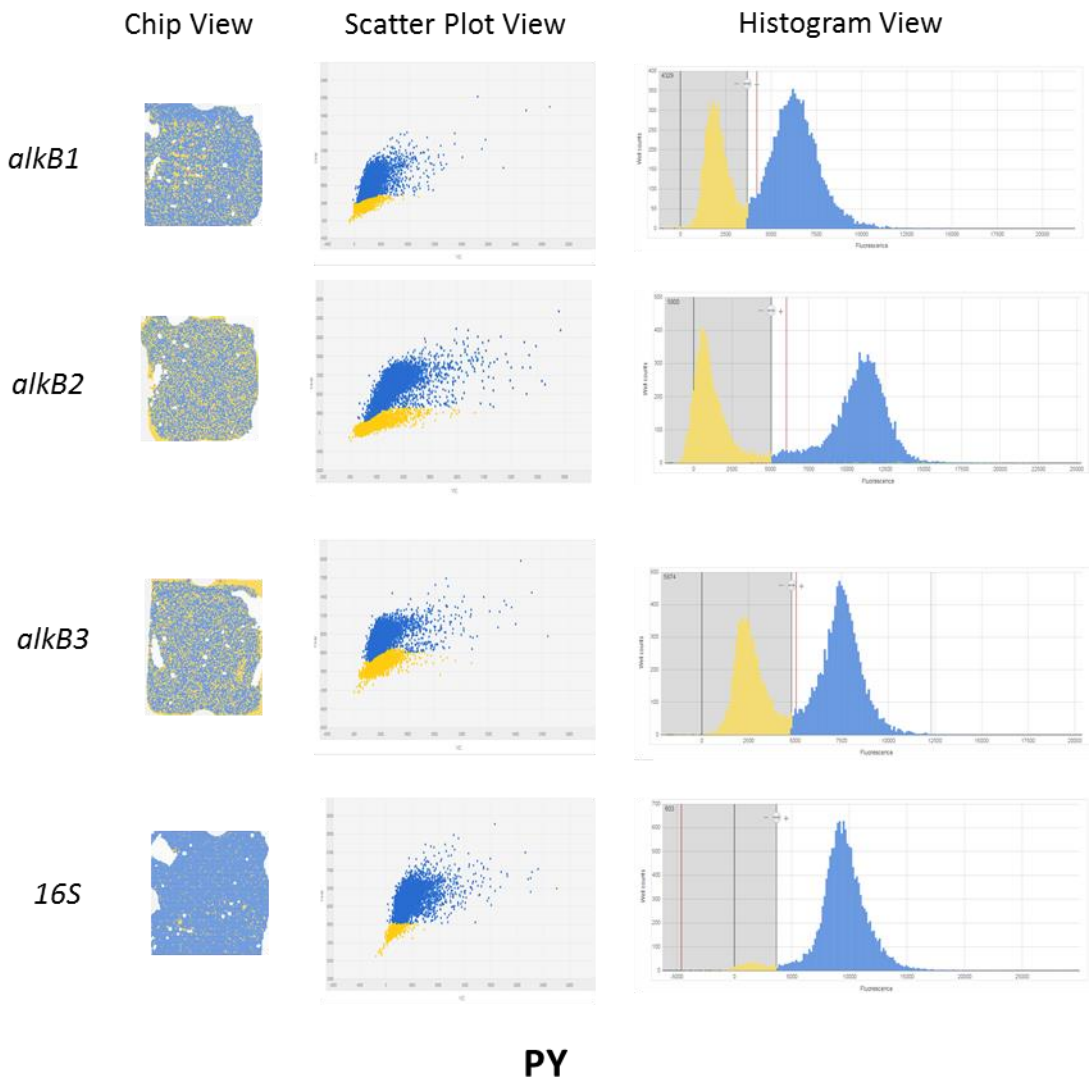

Figure 6.12 The dPCR analysis of *alkB1*, *alkB2*, *alkB3*, and *16S rRNA* gene transcripts when grown on PY.

6.3.5 Environmental implications

Marine oil spills and seeps (0.47 and 8.3 million tonnes of petroleum annually), together with cyanobacteria-released hydrocarbons (possibly 100 more times than petroleum sources), are the primary sources of marine hydrocarbons (Lea-Smith et al., 2015; McGenity et al., 2021). The extensive field study discovered cryptic marine hydrocarbon cycles are linked to hydrocarbon-degrading bacteria for removing both cyanobacteria-released alkanes and crude oils (Love et al., 2021). The released crude oils from seeps or spills in the long-term cycle contain thousands of different hydrocarbons dominated by *n*-alkanes (40–60%) (Cao et al., 2021b). Among these hydrocarbons, saturates are the most susceptible to being biodegraded. It indicates that specialist alkane-degrading bacteria, which normally degrade cyanobacteria-released alkanes, could respond quickly and expand populations to use these carbon sources to mitigate the potentially catastrophic marine oil spill issues.

Comparatively, annually, at least 14 million tonnes of plastic end up in the ocean, making up 80% of all marine debris found from surface waters to deep-sea sediments (Geng et al., 2019). The observed distribution of *Alcanivorax* in the plastisphere across multiple studies and environments (Wright et al., 2021) highlighted their importance in the plastic transformation processes. The capacity of utilizing these polymers implied that the

emerging plastics could serve as the desired carbon niches for the growth of *Alcanivorax*, in addition to the utilization of the cyanobacteria released C15.

In the pristine seawaters, *Alcanivorax* was always outcompeted by other heterotrophs and made up the rare biome in the pristine seawaters since it can only metabolize a couple of simple organics (e.g., acetate and pyruvate) in addition to alkanes (Naether et al., 2013). After hydrocarbons input (i.e., oil spills and increased cyanobacterial production of C15), *Alcanivorax* would bloom and account for the high proportions of the associated microbial communities to degrade alkanes and accumulate intracellular polymer-based carbon reservoirs (Zadjelovic et al., 2020). In this study, we showed that *Alcanivorax* species seldomly released PhaZ during bacterial growth on alkanes (Figure 6.9). It indicated that *Alcanivorax* would primarily synthesize intracellular polymers-based carbon reservoirs rather than degrading them. Differently, when grown on PY, it may simultaneously induce the storage and degradation of intracellular polymers. Degradation of PHB initiates the release of the highest level of PhaZ, indicating that *Alcanivorax* might entirely transform its physiological responses for degrading the polymers and rarely store them.

The ocean hydrocarbon cycles are of great importance since they are related to the mitigation of spilled hydrocarbons in the marine environment and CO_2 capture and release that affect global warming. *Alcanivorax* tied to the cycles could also respond to degrade the

plastic wastes. On the one hand, since the level and rate of hydrocarbons input linked to the cycles is massive and has been there long before the new anthropogenic plastics input (Stubbins et al., 2021), existing processes related to the activity of important oil-degrading bacteria, especially *Alcanivorax* in the ocean hydrocarbon cycles may aid in the ecosystem resilience to the impact of plastics. On the other hand, with the growth of marine plastic input, the migration and transformation of plastics may have a potential influence on hydrocarbon biodegradation in the marine environment. The enriched *Alcanivorax* abundance via utilizing plastics may enhance alkanes degradation; on the contrary, degradation of plastics may compete for the utilization of alkanes. The carbon balance among the CO_2 capture, hydrocarbon production, as well as the plastics and hydrocarbon biodegradation for emitting CO_2 should be calculated in the future.

The adaptation and ability of *Alcanivorax* to assimilate different carbon sources are critical to the ocean hydrocarbon cycles, as well as to the bioremediation of oil-polluted and even plastic-polluted marine environments. This study highlighted that *Alcanivorax* exhibited significantly different physiological strategies to degrade C15 and PHB. For the degradation of C15, sufficient biosurfactants were produced to enhance its bioavailability; in contrast, for the degradation of PHB, PhaZ showed high activity to potentially convert plastics to monomers (Figure 6.13). For incorporating C15 and PHB, the membrane lipid

composition and three AlkBs responded differently. Modifying the fatty acid or synthesizing them *de nove* is energy-consuming (Naether et al., 2013). To realize desired growth, *Alcanivorax* may not waste energy degrading different types of carbon sources. These indicated that the degradation of plastics and alkanes in the marine environment depends on which carbon source will be acquired by *Alcanivorax* first. The depletion of a specific carbon source may alter its physiological strategy and transform to the alternative metabolic mode tailed to utilize other carbon sources, which needs further investigation.

The AlkB was identified for involving in the biodegradation of PHB and alkanes, whereas different AlkB in the same species had various performances. In the *Alcanivorax*. sp. N3-2A, the *alkB1* gene was downregulated, while *alkB2* and *alkB3* genes were upregulated when grown on PHB than C15 (Figure 6.9). The biodegradation of plastics in the marine environment may also depend on the alkane biodegradation pathways (Delacuvellerie et al., 2022). It further indicated that AlkB had a potentially vast degradation capacity for metabolizing diverse organic contaminants.

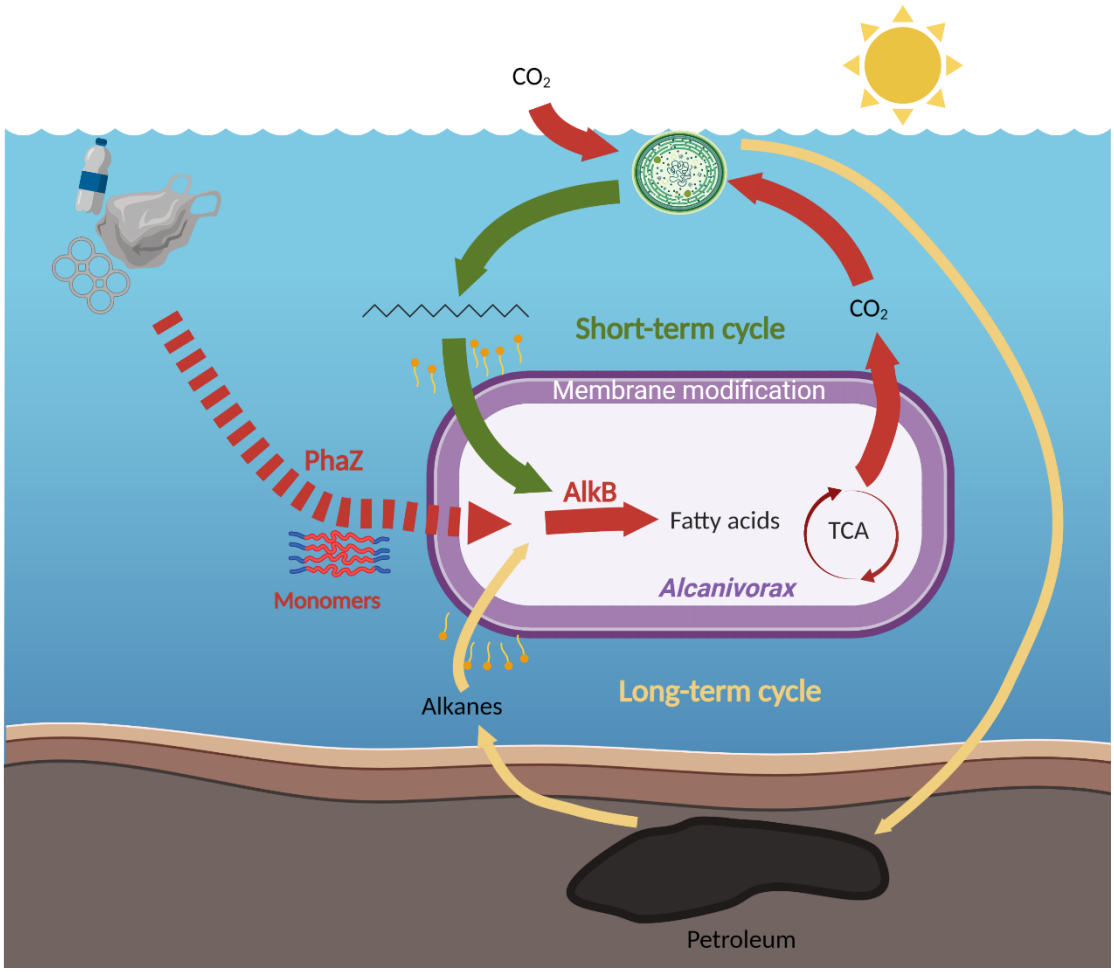

Figure 6.13 Scheme showing the importance of the current ocean hydrocarbon cycles for mitigation of plastics.

6.4 Summary

In summary, we isolated a new *Alcanivorax* species, named *Alcanivorax* sp. N3-2A, from the cold Northern Atlantic region for the first time. We identified that PHB could highly enrich *Alcanivorax* amounts and further verified the potentially critical role of *Alcanivorax* in mitigating plastic wastes and hydrocarbon pollution in the marine environment. We also showed that the physiological strategies of *Alcanivorax* grown on C15 and PHB were different, indicating the vast environmental adaptability of *Alcanivorax* for utilizing these carbon sources. It highlighted that *Alcanivorax* involved in ocean hydrocarbon cycles has already been primed for the mitigation of new plastic-based carbons. This study also raised discussions regarding the potential rewired ocean hydrocarbon cycles to mediate CO_2 capture and hydrocarbon removal due to the growth of plastic input.

CHAPTER 7 CONCLUSIONS AND RECOMMENDATIONS

7.1 Conclusions

The microbially mediated natural attenuation process in the marine environment determines the biotransformation fate of spilled oils. Various kinds of environmental factors, oil spill response options, and spilled oil types lead to more complicated microbial behaviors. This thesis reveals the effects of salinity, dispersant application, and oil property on microbial responses to oil biodegradation.

For salinity effects on crude oil biodegradation, we examined a model halotolerant oil-degrading bacterium *Exiguobacterium* sp. N4-1P for responding to conventional ANS crude oil biodegradation. We found that salinity can mediate microbial growth between oil and water phases by regulating cell surface hydrophobicity (CSH). High CSH observed under low salinities (0 - 5 g/L NaCl) led to high biosurfactant productivity for degrading hydrophobic compounds such as long-chain alkanes. In contrast, low CSH under high salinities (50 - 70 g/L NaCl) led to low biosurfactant productivity for degrading hydrophilic compounds such as LMW naphthalene. Further, we evaluated the dispersant effects on the responses of *Exiguobacterium* sp. N4-1P to degrade ANS under different salinities. We found that dispersant addition can relieve the biodegradation barriers caused by high salinities. Through applying the advanced structural causal model (SCM), we also concluded that the positive effects of dispersant addition on oil biodegradation were mainly

due to the enrichment of cell abundance. These findings could benefit our understanding of sophisticated microbial eco-physiological responses for salinity-mediated biodegradation of crude oil and chemically dispersed oil.

We also evaluated dispersant effects on the biodegradation of unconventional heavy crude oils. We took dilbit as an example due to its increased marine transportation and spill risks. We performed realistic microcosm studies (using a low dilbit concentration without nutrient addition) to evaluate the effects of marine dilbit spill and dispersant application on microbial community dynamics over time. We evaluated the impacts of the microcosm scale and found that increasing the scale is beneficial for reducing community stochasticity, especially in the late stage of biodegradation. We observed that dispersant application suppressed aromatics biodegradation in the early stage (6 days) whereas exerting insignificant effects in the late stage (50 days), from both substance removal and metagenomic/metatranscriptomic perspectives. We further found that *Alteromonas* species are vital for the early-stage chemically dispersed oil biodegradation and clarified their degradation and antioxidation mechanisms. These findings could help us understand microcosm studies and microbial roles for biodegrading dilbit and chemically dispersed dilbit in the marine environment.

To further understand oil properties on oil biodegradation, we developed magnetic

nanoparticles decorated bacteria (MNPB) using an oil-degrading and biosurfactant-producing species for responding to heavy crude oil pollution. We proposed an access-dispersion-recovery strategy for enhanced mitigation of a simulated heavy crude oil attachment. We found that magnetic orientation can trigger MNPB to access the heavy crude oil layer to stimulate degrading LMW aromatics and form oil-bacteria aggregates for recovery. The magnetic recovery could remove up to 62% of heavy crude oil. Besides, HMW aromatics could also be recovered mainly because they were entrained in oil-bacteria aggregates. We believe this exploration not only helps us understand the property of heavy crude oil affecting its removal but also develops a new heavy crude oil bio-mitigation tool.

Apart from that, we isolated a new *Alcanivorax* species from the North Atlantic. *Alcanivorax* is a well-known obligate alkane-degrader, and recently, it was also reported to degrade plastics. Since seawater was reported to have high contents of plastic-based carbon, the plastic input may affect the biodegradation of oils. We evaluated the responses of the newly isolated *Alcanivorax* for degrading individual alkanes (C12 - C18) and PHB plastic (one of the emerging bioplastics that may capture the future plastics market). We found that C15 (the main alkane in the marine environment due to cyanobacterial production other than oil spills) and PHB could serve as preferential carbon sources for promoting growth. However, the cell membrane composition and associated enzymatic activities were

completely different when grown on C15 and PHB. Given that *Alcanivorax* is a well-recognized alkane-degrader that participates in the ocean hydrocarbon cycles that link with marine cyanobacterial CO_2 capture and hydrocarbon production and removal, our discovery supports that the existing biogeochemical processes may add to the marine ecosystem resilience to the impacts of plastics.

7.2 Research Contributions

This thesis can be summarized and highlighted by the following contributions:

(1) The mechanisms of microbial eco-physiological responses to salinity-mediated crude oil biodegradation were unveiled. In addition, dispersant effects on oil biodegradation under diverse salinities were quantitively estimated. These findings could help us understand the complicated biodegradation of oil and chemically dispersed oils under diverse salinities and benefit decision-making for adopting chemical dispersants under diverse saline environments.

(2) Microbial community responses towards naturally and chemically dispersed dilbit over time were comprehensively evaluated in realistic large-scale (1,500 mL) microcosms without nutrient addition using a low dilbit concentration (30 ppm). The microcosm scale effects on microbial community evaluation were highlighted. The short-term inhibiting but the long-term minimal effects of dispersant application on

microbially mediated natural attenuation of potential marine dilbit spills were uncovered.

(3) The MNPB was successfully developed, and the access-dispersion-recovery strategy was identified for enhanced mitigation of a simulated heavy crude oil polluted scenario. This study not only benefits our understanding of the biodegradation of unconventional heavy crude oil but also generates a promising tool for bio-mitigation of potential heavy crude oil pollution.

(4) Responses of a newly isolated *Alcanivorax* species, named *Alcanivorax* sp. N3-2A, isolated from the North Atlantic for the degradation of alkanes and PHB plastics, were explored. The robust capacity of *Alcanivorax* for utilizing C15 and PHB was demonstrated. This study further highlighted that the ocean might be more resilient than we think (as is the case for oil spills) due to the natural biogeochemical process (i.e., ocean hydrocarbon cycles).

7.3 Recommendations for Future Research

(1) The microbial eco-physiological strategies for salinity-mediated naturally and chemically dispersed oil were elucidated in Chapters 2 and 3 using the model halotolerant species *Exiguobacterium* sp. N3-2A. However, the responses were not discovered using transcriptomics and metabolomics, which could provide insights at

the molecular level. In addition, in real marine environments, the microbial interactions also affect their behaviors for oil biodegradation. Exploration of microbial community responses towards oil biodegradation and dispersant application under diverse salinities could further uncover the salinity effects on the microbially mediated natural attenuation process.

(2) Regarding unconventional dilbit biodegradation, microcosm scale effects were evaluated. Interpreting the dispersant effects on oil biodegradation via microcosms is challenging; it is still recommended that dispersant evaluation in large-scale systems and even through field trials would be more realistic after a marine oil spill response. Further, investigations on the biodegradation of these unconventional heavy crude oils under diverse environmental conditions (e.g., temperature, wave energy, the existence of sea ices, etc.) could be conducted to advance our understanding of the complicated biodegradation processes of unconventional oils.

(3) Heavy crude oil pollution could be mitigated using the MNPB. To expand the feasibility of this tool, the optimization of magnetic field and MNP development, as well as the applications of this tool for tackling different oil pollution scenarios, should be further conducted. In addition, the impacts of MNPB on the marine environment need to be evaluated before the adoption of the new tool. The eco-

toxicology of MNPB on specific organisms and ecosystems should be comprehensively assessed.

(4) The *Alcanivorax* species were identified for degrading alkanes and plastics. However, there are two questions: (i) how does *Alcanivorax* utilize alkanes and plastics when they are co-existed? (ii) Will the plastic input affect the marine hydrocarbon cycles? To help answer these questions, simulated co-culture micro-ecosystems with indigenous cyanobacteria and *Alcanivorax* can be built and tested.

7.4 Publications

Peer-reviewed journal publications

(1) **Cao, Y.**, Zhang, B., Greer, C., Lee, K., Cai, Q., Song, X., Tremblay, J., Zhu, Z., Dong, G., & Chen, B. (2022). Metagenomic and metatranscriptomic responses of chemical dispersant application during a marine dilbit spill. *Applied and Environmental Microbiology*, 88(5). DOI: 10.1128/aem.02151-21

(2) **Cao, Y.**, Kang, Q., Zhang, B., Zhu, Z., Dong, G., Cai, Q., & Chen, B. (2022). Machine learning-aided causal inference for unraveling chemical dispersant and salinity effects on crude oil biodegradation. *Bioresource Technology*, 345, 126468. DOI: 10.1016/j.biortech.2021.126468

(3) **Cao, Y.**, Zhang, B., Zhu, Z., Rostami, M., Dong, G., Ling, J., Lee, K., Greer, C., & Chen, B. (2021). Access-dispersion-recovery Strategy for Enhanced Mitigation of Heavy Crude Oil Pollution Using Magnetic Nanoparticles Decorated Bacteria. *Bioresource Technology*, 125404. DOI: 10.1016/j.biortech.2021.125404

(4) **Cao, Y.**, Zhang, B., Zhu, Z., Xin, X., Wu, H., & Chen, B. (2021). Microfluidic based whole-cell biosensors for simultaneously on-site monitoring of multiple environmental contaminants. *Frontiers in Bioengineering and Biotechnology*, 9, 178. DOI: 10.3389/fbioe.2021.622108

(5) **Cao, Y.**, Zhang, B., Zhu, Z., Song, X., Cai, Q., Chen, B., Dong, G., & Ye, X. (2020). Microbial eco-physiological strategies for salinity-mediated crude oil biodegradation. *Science of the Total Environment*, 727, 138723. DOI: 10.1016/j.scitotenv.2020.138723

(6) **Cao, Y.**, Yu, M., Dong, G., Chen, B., & Zhang, B. (2020). Digital PCR as an emerging tool for monitoring of microbial biodegradation. *Molecules*, 25(3), 706. DOI: 10.3390/molecules25030706

(7) **Cao, Y.,** Li, Q., Xia, P., Wei, L., Guo, N., Li, J., & Wang, S. (2017). AraBAD based toolkit for gene expression and metabolic robustness improvement in *Synechococcus elongatus*. *Scientific Reports*, 7, 18059. DOI: s41598-017-17035-4

(8) Song, X., Zhang, B., **Cao, Y.**, Liu, B., & Chen, B. (2022). Shrimp-waste based dispersant as oil spill treating agent: biodegradation of dispersant and dispersed oil. *Journal of Hazardous Materials*, 439, 129617. DOI: 10.1016/j.jhazmat.2022.129617

(9) Zhu, Z., Merlin, F., Yang, M., Lee, K., Chen, B., Liu, B., **Cao, Y.**, Song, X., Ye, X., Li, Q., Greer, C., Boufadel, M., Isaacman, L., & Zhang, B. (2022). Recent advances in chemical and biological degradation of spilled oil: A review of dispersants application in the marine environment. *Journal of Hazardous Materials*. DOI: 10.1016/j.jhazmat.2022.129260

(10) Yu, M., Zhu, Z., Chen, B., **Cao, Y.**, & Zhang, B. (2022). Bioherder generated by

Rhodococcus erythropolis as marine oil spill treating agent. *Frontiers in Microbiology*. DOI: 10.3389/fmicb.2022.860458

(11) Dong, G., Chen, B., Liu, B., Hounjet, L. J., **Cao, Y.**, Stoyanov, S. R., Yang, M., & Zhang, B. (2022). Advanced oxidation processes in microreactors for water and wastewater treatment: development, challenges, and opportunities. *Water Research*, 211, 118047. DOI: 10.1016/j.watres.2022.118047

(12) Tan, L., **Cao, Y.**, Li, J., Xia, P., & Wang, S. (2022). Transcriptomics and metabolomics of engineered *Synechococcus elongatus* during photomixotrophic growth. *Microbial Cell Factories*, 21, 31. DOI: 10.1186/s12934-022-01760-1

(13) Zhu, Z., Song, X., **Cao, Y.**, Chen, B., Lee, K., & Zhang, B. (2022). Recent advancement in the development of new dispersants as oil spill treating agents. *Current Opinion in Chemical Engineering*, 36, 100770. DOI: 10.1016/j.coche.2021.100770

(14) Zhu, Z., Zhang, B., Cai, Q., **Cao, Y.**, Ling, J., Lee, K., & Chen, B. (2021). A critical review on the environmental application of lipopeptide micelles. *Bioresource Technology*, 339, 125602. DOI: 10.1016/j.biortech.2021.125602

Journal papers under revision

(1) **Cao, Y.**, Zhang, B., Cai, Q., Zhu, Z., Liu, B., Dong, G., Greer, C., Lee, K., & Chen, B.

(2022). Biodegradation of alkanes and polyhydroxybutyrate plastics by *Alcanivorax* species isolated from North Atlantic: Importance of the ocean hydrocarbon cycles. (*Under revision in Environmental Pollution*)

REFERENCES

Abou-Khalil, C., Prince, R.C., Greer, C.W., Lee, K., Boufadel, M.C. 2022. Bioremediation of petroleum hydrocarbons in the upper parts of sandy beaches. *Environmental Science & Technology*. DOI: 10.1021/acs.est.2c01338

Abou Khalil, C., Fortin, N., Prince, R.C., Greer, C.W., Lee, K., Boufadel, M.C. 2021. Crude oil biodegradation in upper and supratidal seashores. *Journal of Hazardous Materials*, **416**, 125919.

Abou Khalil, C., Prince, V.L., Prince, R.C., Greer, C.W., Lee, K., Zhang, B., Boufadel, M.C. 2020. Occurrence and biodegradation of hydrocarbons at high salinities. *Science of the Total Environment*, 143165.

Adam, M. 2016. Biodegradation of marine crude oil pollution using a salt-tolerant bacterial consortium isolated from Bohai Bay, China. *Marine Pollution Bulletin*, **105**(1), 43-50.

Adams, J.J. 2014. Asphaltene adsorption, a literature review. *Energy & Fuels*, **28**(5), 2831-2856.

Agarwal, A., Liu, Y. 2015. Remediation technologies for oil-contaminated sediments. *Marine Pollution Bulletin*, **101**(2), 483-490.

Ahmadi, E., Shokri, B., Mesdaghinia, A., Nabizadeh, R., Khani, M.R., Yousefzadeh, S., Salehi, M., Yaghmaeian, K. 2020a. Synergistic effects of α-Fe_2O_3-TiO_2 and

$Na_2S_2O_8$ on the performance of a non-thermal plasma reactor as a novel catalytic oxidation process for dimethyl phthalate degradation. *Separation and Purification Technology*, **250**, 117185.

Ahmadi, E., Yousefzadeh, S., Mokammel, A., Miri, M., Ansari, M., Arfaeinia, H., Badi, M.Y., Ghaffari, H.R., Rezaei, S., Mahvi, A.H. 2020b. Kinetic study and performance evaluation of an integrated two-phase fixed-film baffled bioreactor for bioenergy recovery from wastewater and bio-wasted sludge. *Renewable and Sustainable Energy Reviews*, **121**, 109674.

Ansari, F., Grigoriev, P., Libor, S., Tothill, I.E., Ramsden, J.J. 2009. DBT degradation enhancement by decorating Rhodococcus erythropolis IGST8 with magnetic Fe3O4 nanoparticles. *Biotechnology and Bioengineering*, **102**(5), 1505-1512.

Ashoori, S., Sharifi, M., Masoumi, M., Salehi, M.M. 2017. The relationship between SARA fractions and crude oil stability. *Egyptian Journal of Petroleum*, **26**(1), 209-213.

Azinfar, B., Zirrahi, M., Hassanzadeh, H., Abedi, J. 2018. Characterization of heavy crude oils and residues using combined Gel Permeation Chromatography and simulated distillation. *Fuel*, **233**, 885-893.

Bank, M.S., Swarzenski, P.W., Duarte, C.M., Rillig, M.C., Koelmans, A.A., Metian, M., Wright, S., Provencher, J.F., Sanden, M., Jordaan, A. 2021. Global plastic pollution

observation system to aid policy. *Environmental Science & Technology*, **55**(12), 7770-7775.

Bates, N.R., Johnson, R.J. 2020. Acceleration of ocean warming, salinification, deoxygenation and acidification in the surface subtropical North Atlantic Ocean. *Communications Earth & Environment*, **1**(1), 1-12.

Beyer, J., Trannum, H.C., Bakke, T., Hodson, P.V., Collier, T.K. 2016. Environmental effects of the Deepwater Horizon oil spill: A review. *Marine Pollution Bulletin*, **110**(1), 28-51.

Bianco, F., Race, M., Papirio, S., Esposito, G. 2020. Removal of polycyclic aromatic hydrocarbons during anaerobic biostimulation of marine sediments. *Science of The Total Environment*, **709**, 136141.

Boutron, O., Paugam, C., Luna-Laurent, E., Chauvelon, P., Sous, D., Rey, V., Meulé, S., Chérain, Y., Cheiron, A., Migne, E. 2021. Hydro-saline dynamics of a shallow mediterranean coastal lagoon: Complementary information from short and long term monitoring. *Journal of Marine Science and Engineering*, **9**(7), 701.

Brown, D.G. 2007. Relationship between micellar and hemi-micellar processes and the bioavailability of surfactant-solubilized hydrophobic organic compounds. *Environmental Science & Technology*, **41**(4), 1194-1199.

Butcher, B., Huang, V.S., Robinson, C., Reffin, J., Sgaier, S.K., Charles, G., Quadrianto, N. 2021. Causal datasheet for datasets: An evaluation guide for real-world data analysis and data collection design using bayesian networks. *Frontiers in Artificial Intelligence*, **4**, 18.

Cai, Q., Ye, X., Chen, B., Zhang, B. 2017a. Complete genome sequence of *Exiguobacterium* sp. strain N4-1P, a psychrophilic bioemulsifier producer isolated from a cold marine environment in north atlantic Canada. *Genome Announcements*, **5**(44), e01248-17.

Cai, Q., Ye, X., Chen, B., Zhang, B. 2017b. Complete genome sequence of *Exiguobacterium* sp. strain N4-1P, a psychrophilic bioemulsifier producer isolated from a cold marine environment in North Atlantic Canada. *Genome Announcements*, **5**(44), e01248-17.

Cai, Q., Zhang, B., Chen, B., Zhu, Z., Lin, W., Cao, T. 2014. Screening of biosurfactant producers from petroleum hydrocarbon contaminated sources in cold marine environments. *Marine Pollution Bulletin*, **86**(1-2), 402-410.

Cai, Q., Zhang, B., Chen, B., Zhu, Z., Zhao, Y. 2017c. A novel bioemulsifier produced by *Exiguobacterium* sp. strain N4-1P isolated from petroleum hydrocarbon contaminated coastal sediment. *RSC Advances*, **7**(68), 42699-42708.

Cai, Q., Zhu, Z., Chen, B., Lee, K., Nedwed, T.J., Greer, C., Zhang, B. 2021. A cross-comparison of biosurfactants as marine oil spill dispersants: Governing factors, synergetic effects and fates. *Journal of Hazardous Materials*, 126122.

Cai, Q., Zhu, Z., Chen, B., Zhang, B. 2019. Oil-in-water emulsion breaking marine bacteria for demulsifying oily wastewater. *Water Research*, **149**, 292-301.

Campo, P., Venosa, A.D., Suidan, M.T. 2013. Biodegradability of Corexit 9500 and dispersed South Louisiana crude oil at 5 and 25°C. *Environmental Science & Technology*, **47**(4), 1960-1967.

Cao, Y., Kang, Q., Zhang, B., Zhu, Z., Dong, G., Cai, Q., Lee, K., Chen, B. 2022a. Machine learning-aided causal inference for unraveling chemical dispersant and salinity effects on crude oil biodegradation. *Bioresource Technology*, **345**, 126468.

Cao, Y., Yu, M., Dong, G., Chen, B., Zhang, B. 2020a. Digital PCR as an emerging tool for monitoring of microbial biodegradation. *Molecules*, **25**(3), 706.

Cao, Y., Zhang, B., Greer, C.W., Lee, K., Cai, Q., Song, X., Tremblay, J., Zhu, Z., Dong, G., Chen, B. 2022b. Metagenomic and metatranscriptomic responses of chemical dispersant application during a marine dilbit spill. *Applied And Environmental Microbiology*, aem. 02151-21.

Cao, Y., Zhang, B., Zhu, Z., Rostami, M., Dong, G., Ling, J., Lee, K., Greer, C.W., Chen,

B. 2021a. Access-dispersion-recovery strategy for enhanced mitigation of heavy crude oil pollution using magnetic nanoparticles decorated bacteria. *Bioresource Technology*, 125404.

Cao, Y., Zhang, B., Zhu, Z., Song, X., Cai, Q., Chen, B., Dong, G., Ye, X. 2020b. Microbial eco-physiological strategies for salinity-mediated crude oil biodegradation. *Science of The Total Environment*, 138723.

Carriger, J.F., Barron, M.G., Newman, M.C. 2016. Bayesian networks improve causal environmental assessments for evidence-based policy. *Environmental Science & Technology*, **50**(24), 13195-13205.

Chandrasekar, S., Sorial, G.A., Weaver, J.W. 2006. Dispersant effectiveness on oil spills–impact of salinity. *ICES Journal of Marine Science*, **63**(8), 1418-1430.

Chapman, H., Purnell, K., Law, R.J., Kirby, M.F. 2007. The use of chemical dispersants to combat oil spills at sea: A review of practice and research needs in Europe. *Marine Pollution Bulletin*, **54**(7), 827-838.

Chen, Y. 2021. Development of an oil spill model adaptable to exposure and submergence conversion of tidal flats: A case study in the Changjiang Estuary. *Marine Pollution Bulletin*, **171**, 112715.

Chen, Y., Zhang, G., Liu, H., Qu, J. 2019. Confining free radicals in close vicinity to

contaminants enables ultrafast fenton-like processes in the interspacing of MOS_2 membranes. *Angewandte Chemie International Edition*, **58**(24), 8134-8138.

Chernozhukov, V., Chetverikov, D., Demirer, M., Duflo, E., Hansen, C., Newey, W. 2017. Double/debiased/neyman machine learning of treatment effects. *American Economic Review*, **107**(5), 261-65.

Couldrey, M.P., Oliver, K.I., Yool, A., Halloran, P.R., Achterberg, E.P. 2019. Drivers of 21 st Century carbon cycle variability in the North Atlantic Ocean. *Biogeosciences Discussions*, 1-33.

Díaz, M.P., Boyd, K.G., Grigson, S.J., Burgess, J.G. 2002. Biodegradation of crude oil across a wide range of salinities by an extremely halotolerant bacterial consortium MPD - M, immobilized onto polypropylene fibers. *Biotechnology and Bioengineering*, **79**(2), 145-153.

Dahal, R.H., Chaudhary, D.K., Kim, J. 2017. *Acinetobacter halotolerans* sp. nov., a novel halotolerant, alkalitolerant, and hydrocarbon degrading bacterium, isolated from soil. *Archives of microbiology*, **199**(5), 701-710.

Davoodi, S.M., Miri, S., Taheran, M., Brar, S.K., Galvez-Cloutier, R., Martel, R. 2020. Bioremediation of unconventional oil contaminated ecosystems under natural and assisted conditions: A review. *Environmental Science & Technology*, **54**(4), 2054-

2067.

Delacuvellerie, A., Cyriaque, V., Gobert, S., Benali, S., Wattiez, R. 2019. The plastisphere in marine ecosystem hosts potential specific microbial degraders including Alcanivorax borkumensis as a key player for the low-density polyethylene degradation. *Journal of Hazardous Materials*, **380**, 120899.

Delacuvellerie, A., Géron, A., Gobert, S., Wattiez, R. 2022. New insights into the functioning and structure of the PE and PP plastispheres from the Mediterranean Sea. *Environmental Pollution*, **295**, 118678.

DeLorenzo, M., Eckmann, C., Chung, K., Key, P., Fulton, M. 2016. Effects of salinity on oil dispersant toxicity in the grass shrimp, Palaemonetes pugio. *Ecotoxicology and Environmental Safety*, **134**, 256-263.

Deng, Y.-H., Wang, C.-C., Hu, J.-H., Yang, W.-L., Fu, S.-K. 2005. Investigation of formation of silica-coated magnetite nanoparticles via sol–gel approach. *Colloids and Surfaces A: Physicochemical and Engineering Aspects*, **262**(1-3), 87-93.

DeVries, T., Le Quéré, C., Andrews, O., Berthet, S., Hauck, J., Ilyina, T., Landschützer, P., Lenton, A., Lima, I.D., Nowicki, M. 2019. Decadal trends in the ocean carbon sink. *Proceedings of the National Academy of Sciences*, **116**(24), 11646-11651.

Dhaka, A., Chattopadhyay, P. 2021. A review on physical remediation techniques for

treatment of marine oil spills. *Journal of Environmental Management*, **288**, 112428.

Dombrowski, N., Donaho, J.A., Gutierrez, T., Seitz, K.W., Teske, A.P., Baker, B.J. 2016. Reconstructing metabolic pathways of hydrocarbon-degrading bacteria from the Deepwater Horizon oil spill. *Nature Microbiology*, **1**(7), 1-7.

Duarte, C.M., Røstad, A., Michoud, G., Barozzi, A., Merlino, G., Delgado-Huertas, A., Hession, B.C., Mallon, F.L., Afifi, A.M., Daffonchio, D. 2020. Discovery of Afifi, the shallowest and southernmost brine pool reported in the Red Sea. *Scientific Reports*, **10**(1), 1-17.

Dubinsky, E.A., Conrad, M.E., Chakraborty, R., Bill, M., Borglin, S.E., Hollibaugh, J.T., Mason, O.U., M. Piceno, Y., Reid, F.C., Stringfellow, W.T. 2013. Succession of hydrocarbon-degrading bacteria in the aftermath of the Deepwater Horizon oil spill in the Gulf of Mexico. *Environmental Science & Technology*, **47**(19), 10860-10867.

Ebrahiminezhad, A., Varma, V., Yang, S., Berenjian, A. 2016. Magnetic immobilization of Bacillus subtilis natto cells for menaquinone-7 fermentation. *Applied Microbiology and Biotechnology*, **100**(1), 173-180.

Eke, C.D., Anifowose, B., Van De Wiel, M.J., Lawler, D., Knaapen, M.A. 2021. Numerical Modelling of Oil Spill Transport in Tide-Dominated Estuaries: A Case Study of Humber Estuary, UK. *Journal of Marine Science and Engineering*, **9**(9), 1034.

Fan, F., Zhang, B., Morrill, P.L. 2017. Phospholipid fatty acid (PLFA) analysis for profiling microbial communities in offshore produced water. *Marine pollution bulletin*, **122**(1-2), 194-206.

Fathepure, B.Z. 2014. Recent studies in microbial degradation of petroleum hydrocarbons in hypersaline environments. *Frontiers in microbiology*, **5**, 173.

Fernández-Martínez, J., Pujalte, M.J., García-Martínez, J., Mata, M., Garay, E., Rodríguez-Valera, F. 2003. Description of Alcanivorax venustensis sp. nov. and reclassification of Fundibacter jadensis DSM 12178T (Bruns and Berthe-Corti 1999) as Alcanivorax jadensis comb. nov., members of the emended genus Alcanivorax. *International journal of systematic and evolutionary microbiology*, **53**(1), 331-338.

Ferrarin, C., Bajo, M., Bellafiore, D., Cucco, A., De Pascalis, F., Ghezzo, M., Umgiesser, G. 2014. Toward homogenization of Mediterranean lagoons and their loss of hydrodiversity. *Geophysical Research Letters*, **41**(16), 5935-5941.

Fingas, M., Wang, Z., Fieldhouse, B., Smith, P. 2003. Chemical Characteristics of an Oil and the Relationship to Dispersant Effectiveness. *Proceedings of the 26th Arctic and Marine Oil Spill Program (AMOP) Technical Seminar*. pp. 679-730.

Foster, D.J., Syrgkanis, V. 2019. Orthogonal statistical learning. *arXiv preprint arXiv:1901.09036*.

Fowler, S., Readman, J., Oregioni, B., Villeneuve, J.-P., McKay, K. 1993. Petroleum hydrocarbons and trace metals in nearshore Gulf sediments and biota before and after the 1991 war: an assessment of temporal and spatial trends. *Marine Pollution Bulletin*, **27**, 171-182.

Gao, W., Cui, Z., Li, Q., Xu, G., Jia, X., Zheng, L. 2013. Marinobacter nanhaiticus sp. nov., polycyclic aromatic hydrocarbon-degrading bacterium isolated from the sediment of the South China Sea. *Antonie Van Leeuwenhoek*, **103**(3), 485-491.

Gawande, M.B., Monga, Y., Zboril, R., Sharma, R. 2015. Silica-decorated magnetic nanocomposites for catalytic applications. *Coordination Chemistry Reviews*, **288**, 118-143.

Geng, X., Boufadel, M.C., Jackson, N.L. 2016. Evidence of salt accumulation in beach intertidal zone due to evaporation. *Scientific Reports*, **6**(1), 1-5.

Geng, Y., Sarkis, J., Bleischwitz, R. 2019. How to globalize the circular economy, Nature Publishing Group.

Ghosal, D., Ghosh, S., Dutta, T.K., Ahn, Y. 2016. Current state of knowledge in microbial degradation of polycyclic aromatic hydrocarbons (PAHs): A review. *Frontiers in Microbiology*, **7**, 1369.

Glymour, C., Zhang, K., Spirtes, P. 2019. Review of causal discovery methods based on

graphical models. *Frontiers in Genetics*, **10**, 524.

Gofstein, T.R., Perkins, M., Field, J., Leigh, M.B. 2020. The interactive effects of crude oil and Corexit 9500 on their biodegradation in Arctic seawater. *Applied and Environmental Microbiology*, **86**(21), e01194-20.

González-Gaya, B., Martínez-Varela, A., Vila-Costa, M., Casal, P., Cerro-Gálvez, E., Berrojalbiz, N., Lundin, D., Vidal, M., Mompeán, C., Bode, A. 2019. Biodegradation as an important sink of aromatic hydrocarbons in the oceans. *Nature Geoscience*, **12**(2), 119-125.

Gowda, U., Shivakumar, S. 2015. Poly (-β-hydroxybutyrate)(PHB) depolymerase PHAZ Pen from Penicillium expansum: purification, characterization and kinetic studies. *3 Biotech*, **5**(6), 901-909.

Gregson, B.H., Metodieva, G., Metodiev, M.V., McKew, B.A. 2019. Differential protein expression during growth on linear versus branched alkanes in the obligate marine hydrocarbon‐degrading bacterium *Alcanivorax borkumensis* SK2T. *Environmental Microbiology*, **21**(7), 2347-2359.

Gros, J., Reddy, C.M., Aeppli, C., Nelson, R.K., Carmichael, C.A., Arey, J.S. 2014. Resolving biodegradation patterns of persistent saturated hydrocarbons in weathered oil samples from the Deepwater Horizon disaster. *Environmental Science*

& Technology, **48**(3), 1628-1637.

Hall-Stoodley, L., Costerton, J.W., Stoodley, P. 2004. Bacterial biofilms: from the natural environment to infectious diseases. *Nature Reviews Microbiology*, **2**(2), 95.

Haritash, A., Kaushik, C. 2009. Biodegradation aspects of polycyclic aromatic hydrocarbons (PAHs): a review. *Journal of Hazardous Materials*, **169**(1-3), 1-15.

Hart, D.J., Vreeland, R.H. 1988. Changes in the hydrophobic-hydrophilic cell surface character of Halomonas elongata in response to NaCl. *Journal of Bacteriology*, **170**(1), 132-135.

Hazen, T.C., Prince, R.C., Mahmoudi, N. 2016. Marine oil biodegradation, ACS Publications.

He, S., Feng, Y., Ren, H., Zhang, Y., Gu, N., Lin, X. 2011. The impact of iron oxide magnetic nanoparticles on the soil bacterial community. *Journal of Soils and Sediments*, **11**(8), 1408-1417.

Hou, D., Hong, M., Wang, K., Yan, H., Wang, Y., Dong, P., Li, D., Liu, K., Zhou, Z., Zhang, D. 2021. Prokaryotic community succession and assembly on different types of microplastics in a mariculture cage. *Environmental Pollution*, **268**, 115756.

Huang, H., Bowler, B.F., Oldenburg, T.B., Larter, S.R. 2004. The effect of biodegradation on polycyclic aromatic hydrocarbons in reservoired oils from the Liaohe basin, NE

China. *Organic geochemistry*, **35**(11-12), 1619-1634.

Huang, X., Wang, J., Ma, C., Ma, L., Qiao, C. 2019. Diversity analysis of microbial communities and biodegradation performance of two halotolerant and thermotolerant *Bacillus licheniformis* strains in oilfield-produced wastewater. *International Biodeterioration & Biodegradation*, **137**, 30-41.

Huggett, J.F., Foy, C.A., Benes, V., Emslie, K., Garson, J.A., Haynes, R., Hellemans, J., Kubista, M., Mueller, R.D., Nolan, T. 2013. The Digital MIQE Guidelines: M inimum I nformation for Publication of Q uantitative Digital PCR E xperiments. *Clinical Chemistry*, **59**(6), 892-902.

Hyatt, D., Chen, G.-L., LoCascio, P.F., Land, M.L., Larimer, F.W., Hauser, L.J. 2010. Prodigal: prokaryotic gene recognition and translation initiation site identification. *BMC Bioinformatics*, **11**(1), 119.

Ilyin, S., Arinina, M., Polyakova, M.Y., Kulichikhin, V., Malkin, A.Y. 2016. Rheological comparison of light and heavy crude oils. *Fuel*, **186**, 157-167.

Imbens, G.W., Rubin, D.B. 2015. *Causal inference in statistics, social, and biomedical sciences*. Cambridge University Press.

Jeon, H.J., Kim, M.N. 2015. Functional analysis of alkane hydroxylase system derived from Pseudomonas aeruginosa E7 for low molecular weight polyethylene

biodegradation. *International Biodeterioration & Biodegradation*, **103**, 141-146.

Johannessen, S.C., Greer, C.W., Hannah, C.G., King, T.L., Lee, K., Pawlowicz, R., Wright, C.A. 2020. Fate of diluted bitumen spilled in the coastal waters of British Columbia, Canada. *Marine Pollution Bulletin*, **150**, 110691.

Judea, P. 2010. An introduction to causal inference. *The International Journal of Biostatistics*, **6**(2), 1-62.

Jurelevicius, D., Alvarez, V.M., Marques, J.M., de Sousa Lima, L.R.F., de Almeida Dias, F., Seldin, L. 2013. Bacterial community response to petroleum hydrocarbon amendments in freshwater, marine, and hypersaline water-containing microcosms. *Applied and Environmental Microbiology*, **79**(19), 5927-5935.

Kang, D.D., Li, F., Kirton, E., Thomas, A., Egan, R., An, H., Wang, Z. 2019. MetaBAT 2: an adaptive binning algorithm for robust and efficient genome reconstruction from metagenome assemblies. *PeerJ*, **7**, e7359.

Kang, Q., Song, X., Xin, X., Chen, B., Chen, Y., Ye, X., Zhang, B. 2021. Machine learning-aided causal inference framework for environmental data analysis: A COVID-19 case study. *Environmental Science & Technology*. DOI: 10.1021/acs.est.1c02204.

Kasai, Y., Kishira, H., Harayama, S. 2002. Bacteria belonging to the genus *Cycloclasticus* play a primary role in the degradation of aromatic hydrocarbons released in a marine

environment. *Applied and Environmental Microbiology*, **68**(11), 5625-5633.

Kasana, R.C., Pandey, C. 2018. *Exiguobacterium*: an overview of a versatile genus with potential in industry and agriculture. *Critical Reviews in Biotechnology*, **38**(1), 141-156.

Ke, C.-Y., Lu, G.-M., Wei, Y.-L., Sun, W.-J., Hui, J.-F., Zheng, X.-Y., Zhang, Q.-Z., Zhang, X.-L. 2019. Biodegradation of crude oil by *Chelatococcus daeguensis* HB-4 and its potential for microbial enhanced oil recovery (MEOR) in heavy oil reservoirs. *Bioresource Technology*, **287**, 121442.

Kimes, N.E., Callaghan, A.V., Suflita, J.M., Morris, P.J. 2014. Microbial transformation of the Deepwater Horizon oil spill—past, present, and future perspectives. *Frontiers in Microbiology*, **5**, 603.

King, G., Kostka, J., Hazen, T., Sobecky, P. 2015a. Microbial responses to the Deepwater Horizon oil spill: from coastal wetlands to the deep sea. *Annual Review of Marine Science*, **7**, 377-401.

King, T.L., Robinson, B., McIntyre, C., Toole, P., Ryan, S., Saleh, F., Boufadel, M.C., Lee, K. 2015b. Fate of surface spills of Cold Lake blend diluted bitumen treated with dispersant and mineral fines in a wave tank. *Environmental Engineering Science*, **32**(3), 250-261.

Kleindienst, S., Paul, J.H., Joye, S.B. 2015a. Using dispersants after oil spills: impacts on the composition and activity of microbial communities. *Nature Reviews Microbiology*, **13**(6), 388-396.

Kleindienst, S., Seidel, M., Ziervogel, K., Grim, S., Loftis, K., Harrison, S., Malkin, S.Y., Perkins, M.J., Field, J., Sogin, M.L. 2015b. Chemical dispersants can suppress the activity of natural oil-degrading microorganisms. *Proceedings of the National Academy of Sciences*, **112**(48), 14900-14905.

Konieczna, M., Olzog, M., Naether, D.J., Chrzanowski, Ł., Heipieper, H.J. 2018. Membrane fatty acid composition and cell surface hydrophobicity of marine hydrocarbonoclastic *Alcanivorax borkumensis* SK2 grown on diesel, biodiesel and rapeseed oil as carbon sources. *Molecules*, **23**(6), 1432.

Kostianoy, A., Litovchenko, K., Lavrova, O., Mityagina, M., Bocharova, T., Lebedev, S., Stanichny, S., Soloviev, D., Sirota, A., Pichuzhkina, O. 2006. Operational Satellite Monitoring of Oil Spill Pollution in the Southeastern Baltic Sea: 18 Months Experience. *Environmental Research, Engineering & Management*, **38**(4).

Kuhl, A.J., Nyman, J.A., Kaller, M.D., Green, C.C. 2013. Dispersant and salinity effects on weathering and acute toxicity of South Louisiana crude oil. *Environmental Toxicology and Chemistry*, **32**(11), 2611-2620.

Kujawinski, E.B., Reddy, C.M., Rodgers, R.P., Thrash, J.C., Valentine, D.L., White, H.K. 2020. The first decade of scientific insights from the Deepwater Horizon oil release. *Nature Reviews Earth & Environment*, 1-14.

Kumar, M., Leon, V., De Sisto Materano, A., Ilzins, O.A. 2006. Enhancement of oil degradation by co-culture of hydrocarbon degrading and biosurfactant producing bacteria. *Polish Journal of Microbiology*, **55**(2), 139-146.

Kuppusamy, S., Thavamani, P., Megharaj, M., Venkateswarlu, K., Lee, Y.B., Naidu, R. 2016. Pyrosequencing analysis of bacterial diversity in soils contaminated long-term with PAHs and heavy metals: implications to bioremediation. *Journal of Hazardous Materials*, **317**, 169-179.

Kwon, K.K., Oh, J.H., Yang, S.-H., Seo, H.-S., Lee, J.-H. 2015. *Alcanivorax gelatiniphagus* sp. nov., a marine bacterium isolated from tidal flat sediments enriched with crude oil. *International Journal of Systematic and Evolutionary Microbiology*, **65**(Pt_7), 2204-2208.

Lai, Q., Wang, J., Gu, L., Zheng, T., Shao, Z. 2013. *Alcanivorax marinus* sp. nov., isolated from deep-sea water. *International Journal of Systematic and Evolutionary Microbiology*, **63**(Pt_12), 4428-4432.

Lannuzel, D., Tedesco, L., Van Leeuwe, M., Campbell, K., Flores, H., Delille, B., Miller,

L., Stefels, J., Assmy, P., Bowman, J. 2020. The future of Arctic sea-ice biogeochemistry and ice-associated ecosystems. *Nature Climate Change*, **10**(11), 983-992.

Lanzon, J.B., Brown, D.G. 2013. Partitioning of phenanthrene into surfactant hemi-micelles on the bacterial cell surface and implications for surfactant-enhanced biodegradation. *Water Research*, **47**(13), 4612-4620.

Lavania, M., Cheema, S., Sarma, P.M., Mandal, A.K., Lal, B. 2012. Biodegradation of asphalt by *Garciaella petrolearia* TERIG02 for viscosity reduction of heavy oil. *Biodegradation*, **23**(1), 15-24.

Le Magrex-Debar, E., Lemoine, J., Gellé, M.-P., Jacquelin, L.-F., Choisy, C. 2000. Evaluation of biohazards in dehydrated biofilms on foodstuff packaging. *International Journal of Food Microbiology*, **55**(1-3), 239-243.

Lea-Smith, D.J., Biller, S.J., Davey, M.P., Cotton, C.A., Sepulveda, B.M.P., Turchyn, A.V., Scanlan, D.J., Smith, A.G., Chisholm, S.W., Howe, C.J. 2015. Contribution of cyanobacterial alkane production to the ocean hydrocarbon cycle. *Proceedings of the National Academy of Sciences*, **112**(44), 13591-13596.

Lee, K., Nedwed, T., Prince, R.C., Palandro, D. 2013. Lab tests on the biodegradation of chemically dispersed oil should consider the rapid dilution that occurs at sea.

Marine Pollution Bulletin, **73**(1), 314-318.

Lewis, A., Prince, R.C. 2018. Integrating dispersants in oil spill response in Arctic and other icy environments. *Environmental Science & Technology*, **52**(11), 6098-6112.

Li, C., Sun, J., Chen, D., Han, G., Yu, S., Kang, S., Mei, L. 2016a. Ag-decorated Fe3O4@ SiO2 nanorods: synthesis, characterization, and applications in degradation of organic dyes. *Journal of Nanomaterials*, **2016**.

Li, D., Luo, R., Liu, C.-M., Leung, C.-M., Ting, H.-F., Sadakane, K., Yamashita, H., Lam, T.-W. 2016b. MEGAHIT v1. 0: a fast and scalable metagenome assembler driven by advanced methodologies and community practices. *Methods*, **102**, 3-11.

Li, F., Zhu, L., Wang, L., Zhan, Y. 2015. Gene expression of an arthrobacter in surfactant-enhanced biodegradation of a hydrophobic organic compound. *Environmental Science & Technology*, **49**(6), 3698-3704.

Li, H., Durbin, R. 2009. Fast and accurate short read alignment with Burrows–Wheeler transform. *Bioinformatics*, **25**(14), 1754-1760.

Li, P., Cai, Q., Lin, W., Chen, B., Zhang, B. 2016c. Offshore oil spill response practices and emerging challenges. *Marine Pollution Bulletin*, **110**(1), 6-27.

Liu, C., Shao, Z. 2005. Alcanivorax dieselolei sp. nov., a novel alkane-degrading bacterium isolated from sea water and deep-sea sediment. *International Journal of Systematic*

and Evolutionary Microbiology, **55**(3), 1181-1186.

Liu, Y., Du, Q., Wang, Q., Yu, H., Liu, J., Tian, Y., Chang, C., Lei, J. 2017. Causal inference between bioavailability of heavy metals and environmental factors in a large-scale region. *Environmental Pollution*, **226**, 370-378.

Liu, Y., Zhao, Y. 2019. Effect of simple carbon source on degradation performance of long-chain alkane degrading bacteria. *International Core Journal of Engineering*, 5(7), 221-226.

Love, C.R., Arrington, E.C., Gosselin, K.M., Reddy, C.M., Van Mooy, B.A., Nelson, R.K., Valentine, D.L. 2021. Microbial production and consumption of hydrocarbons in the global ocean. *Nature Microbiology*, **6**(4), 489-498.

Malhotra, N., Lee, J.-S., Liman, R.A.D., Ruallo, J.M.S., Villaflores, O.B., Ger, T.-R., Hsiao, C.-D. 2020. Potential toxicity of iron oxide magnetic nanoparticles: A review. *Molecules*, **25**(14), 3159.

Manfra, L., Marengo, V., Libralato, G., Costantini, M., De Falco, F., Cocca, M. 2021. Biodegradable polymers: A real opportunity to solve marine plastic pollution? *Journal of Hazardous Materials*, **416**, 125763.

Margesin, R., Schinner, F. 2001. Potential of halotolerant and halophilic microorganisms for biotechnology. *Extremophiles*, **5**(2), 73-83.

Markus, K.A. 2021. Causal effects and counterfactual conditionals: contrasting Rubin, Lewis and Pearl. *Economics & Philosophy*, 1-21.

Martínez-Palou, R., de Lourdes Mosqueira, M., Zapata-Rendón, B., Mar-Juárez, E., Bernal-Huicochea, C., de la Cruz Clavel-López, J., Aburto, J. 2011. Transportation of heavy and extra-heavy crude oil by pipeline: A review. *Journal of Petroleum Science and Engineering*, **75**(3-4), 274-282.

Martin, C.W., Lewis, K.A., McDonald, A.M., Spearman, T.P., Alford, S.B., Christian, R.C., Valentine, J.F. 2020. Disturbance-driven changes to northern Gulf of Mexico nekton communities following the Deepwater Horizon oil spill. *Marine Pollution Bulletin*, **155**, 111098.

McFarlin, K.M., Prince, R.C., Perkins, R., Leigh, M.B. 2014. Biodegradation of dispersed oil in arctic seawater at -1°C. *PloS One*, **9**(1), e84297.

McGenity, T., Gramain, A. 2010. Cultivation of halophilic hydrocarbon degraders. *Handbook of Hydrocarbon and Lipid Microbiology*, 3847-3854.

McGenity, T.J., McKew, B.A., Lea-Smith, D.J. 2021. Cryptic microbial hydrocarbon cycling. *Nature Microbiology*, **6**(4), 419-420.

Meereboer, K.W., Misra, M., Mohanty, A.K. 2020. Review of recent advances in the biodegradability of polyhydroxyalkanoate (PHA) bioplastics and their composites.

Green Chemistry, **22**(17), 5519-5558.

Meier, W.N., Hovelsrud, G.K., Van Oort, B.E., Key, J.R., Kovacs, K.M., Michel, C., Haas, C., Granskog, M.A., Gerland, S., Perovich, D.K. 2014. Arctic sea ice in transformation: A review of recent observed changes and impacts on biology and human activity. *Reviews of Geophysics*, **52**(3), 185-217.

Merlin, F., Zhu, Z., Yang, M., Chen, B., Lee, K., Boufadel, M.C., Isaacman, L., Zhang, B. 2021. Dispersants as marine oil spill treating agents: a review on mesoscale tests and field trials. *Environmental Systems Research*, **10**(1), 1-19.

Mille, G., Almallah, M., Bianchi, M., Van Wambeke, F., Bertrand, J. 1991. Effect of salinity on petroleum biodegradation. *Fresenius' journal of analytical chemistry*, **339**(10), 788-791.

Mohapatra, B., Phale, P.S. 2021. Microbial degradation of naphthalene and substituted naphthalenes: metabolic diversity and genomic insight for bioremediation. *Frontiers in Bioengineering and Biotechnology*, **9**, 144.

Mukherji, S., Jagadevan, S., Mohapatra, G., Vijay, A. 2004. Biodegradation of diesel oil by an Arabian Sea sediment culture isolated from the vicinity of an oil field. *Bioresource Technology*, **95**(3), 281-286.

Mundy, C., Meiners, K.M. 2021. Ecology of Arctic Sea Ice. *Arctic Ecology*, 261-288.

Muriel-Millán, L.F., Millán-López, S., Pardo-López, L. 2021. Biotechnological applications of marine bacteria in bioremediation of environments polluted with hydrocarbons and plastics. *Applied Microbiology and Biotechnology*, **105**(19), 7171-7185.

Naether, D.J., Slawtschew, S., Stasik, S., Engel, M., Olzog, M., Wick, L.Y., Timmis, K.N., Heipieper, H.J. 2013. Adaptation of the hydrocarbonoclastic bacterium *Alcanivorax borkumensis* SK2 to alkanes and toxic organic compounds: a physiological and transcriptomic approach. *Applied and Environmental Microbiology*, **79**(14), 4282-4293.

Nduagu, E.I., Gates, I.D. 2015. Unconventional heavy oil growth and global greenhouse gas emissions. *Environmental Science & Technology*, **49**(14), 8824-8832.

Neufeld, J.D., Schäfer, H., Cox, M.J., Boden, R., McDonald, I.R., Murrell, J.C. 2007. Stable-isotope probing implicates *Methylophaga* spp and novel *Gammaproteobacteria* in marine methanol and methylamine metabolism. *The ISME Journal*, **1**(6), 480-491.

Nguyen, U.T., Lincoln, S.A., Juarez, A.G.V., Schedler, M., Macalady, J.L., Müller, R., Freeman, K.H. 2018. The influence of pressure on crude oil biodegradation in shallow and deep Gulf of Mexico sediments. *PloS One*, **13**(7), e0199784.

Nikel, P.I., Pérez-Pantoja, D., de Lorenzo, V. 2016. Pyridine nucleotide transhydrogenases enable redox balance of Pseudomonas putida during biodegradation of aromatic compounds. *Environmental Microbiology*, **18**(10), 3565-3582.

Noirungsee, N., Hackbusch, S., Viamonte, J., Bubenheim, P., Liese, A., Müller, R. 2020. Influence of oil, dispersant, and pressure on microbial communities from the Gulf of Mexico. *Scientific Reports*, **10**(1), 1-9.

Ortmann, A.C., Cobanli, S.E., Wohlgeschaffen, G., Thamer, P., McIntyre, C., Mason, J., King, T.L. 2019. Inorganic nutrients have a significant, but minimal, impact on a coastal microbial community's response to fresh diluted bitumen. *Marine Pollution Bulletin*, **139**, 381-389.

Ospina-Forero, L., Castañeda, G., Guerrero, O.A. 2020. Estimating networks of sustainable development goals. *Information & Management*, 103342.

Overholt, W.A., Marks, K.P., Romero, I.C., Hollander, D.J., Snell, T.W., Kostka, J.E. 2016. Hydrocarbon-degrading bacteria exhibit a species-specific response to dispersed oil while moderating ecotoxicity. *Applied and Environmental Microbiology*, **82**(2), 518-527.

Péquin, B., Cai, Q., Lee, K., Greer, C.W. 2022. Natural attenuation of oil in marine environments: A review. *Marine Pollution Bulletin*, **176**, 113464.

Pagaling, E., Vassileva, K., Mills, C.G., Bush, T., Blythe, R.A., Schwarz‐Linek, J., Strathdee, F., Allen, R.J., Free, A. 2017. Assembly of microbial communities in replicate nutrient‐cycling model ecosystems follows divergent trajectories, leading to alternate stable states. *Environmental Microbiology*, **19**(8), 3374-3386.

Park, C., Park, W. 2018a. Survival and energy producing strategies of alkane degraders under extreme conditions and their biotechnological potential. *Frontiers in Microbiology*, **9**, 1081.

Park, M., Park, S., Hyun, J. 2012. Use of magnetic nanoparticles to manipulate the metabolic environment of bacteria for controlled biopolymer synthesis. *ACS Applied Materials & Interfaces*, **4**(10), 5114-5117.

Patel, V.K., Srivastava, R., Sharma, A., Srivastava, A.K., Singh, S., Srivastava, A.K., Kashyap, P.L., Chakdar, H., Pandiyan, K., Kalra, A. 2018. Halotolerant Exiguobacterium profundum PHM11 tolerate salinity by accumulating L-Proline and fine-tuning gene expression profiles of related metabolic pathways. *Frontiers in Microbiology*, **9**, 423.

Pearl, J., Mackenzie, D. 2018. *The book of why: the new science of cause and effect*. Basic books.

Perfumo, A., Smyth, T., Marchant, R., Banat, I. 2010. Production and roles of biosurfactants

and bioemulsifiers in accessing hydrophobic substrates. *Handbook of Hydrocarbon and Lipid Microbiology*, 1501-1512.

Pi, Y., Chen, B., Bao, M., Fan, F., Cai, Q., Ze, L., Zhang, B. 2017. Microbial degradation of four crude oil by biosurfactant producing strain *Rhodococcus* sp. *Bioresource Technology*, **232**, 263-269.

Prince, R.C. 2015. Oil spill dispersants: boon or bane? *Environmental Science & Technology*, **49**(11), 6376-6384.

Prince, R.C., Butler, J.D. 2014. A protocol for assessing the effectiveness of oil spill dispersants in stimulating the biodegradation of oil. *Environmental Science and Pollution Research*, **21**(16), 9506-9510.

Prince, R.C., McFarlin, K.M., Butler, J.D., Febbo, E.J., Wang, F.C., Nedwed, T.J. 2013. The primary biodegradation of dispersed crude oil in the sea. *Chemosphere*, **90**(2), 521-526.

Prosperi, M., Guo, Y., Sperrin, M., Koopman, J.S., Min, J.S., He, X., Rich, S., Wang, M., Buchan, I.E., Bian, J. 2020. Causal inference and counterfactual prediction in machine learning for actionable healthcare. *Nature Machine Intelligence*, **2**(7), 369-375.

Quammen, M.L., Onuf, C.P. 1993. Laguna Madre: seagrass changes continue decades after

salinity reduction. *Estuaries*, **16**(2), 302-310.

Radović, J.R., Romero, I.C., Oldenburg, T.B., Larter, S.R., Tunnell, J.W. 2020. 40 years of weathering of coastal oil residues in the Southern Gulf of Mexico. in: *Deep Oil Spills*, Springer, pp. 328-340.

Radwan, S.S., Khanafer, M.M., Al-Awadhi, H.A. 2019. Ability of the so-called obligate hydrocarbonoclastic bacteria to utilize nonhydrocarbon substrates thus enhancing their activities despite their misleading name. *BMC Microbiology*, **19**(1), 1-12.

Rahsepar, S., Smit, M.P., Murk, A.J., Rijnaarts, H.H., Langenhoff, A.A. 2016. Chemical dispersants: oil biodegradation friend or foe? *Marine Pollution Bulletin*, **108**(1-2), 113-119.

Rahul, K., Sasikala, C., Tushar, L., Debadrita, R., Ramana, C.V. 2014. Alcanivorax xenomutans sp. nov., a hydrocarbonoclastic bacterium isolated from a shrimp cultivation pond. *International Journal of Systematic and Evolutionary Microbiology*, **64**(Pt_10), 3553-3558.

Rajendran, S., Vethamony, P., Sadooni, F.N., Al-Kuwari, H.A.-S., Al-Khayat, J.A., Seegobin, V.O., Govil, H., Nasir, S. 2021. Detection of Wakashio oil spill off Mauritius using Sentinel-1 and 2 data: Capability of sensors, image transformation methods and mapping. *Environmental Pollution*, **274**, 116618.

Rakhmatullin, I., Efimov, S., Tyurin, V., Gafurov, M., Al-Muntaser, A., Varfolomeev, M., Klochkov, V. 2020. Qualitative and quantitative analysis of heavy crude oil samples and their SARA fractions with 13C nuclear magnetic resonance. *Processes*, **8**(8), 995.

Ranjan, B., Pillai, S., Permaul, K., Singh, S. 2018. A novel strategy for the efficient removal of toxic cyanate by the combinatorial use of recombinant enzymes immobilized on aminosilane modified magnetic nanoparticles. *Bioresource Technology*, **253**, 105-111.

Remonsellez, F., Castro-Severyn, J., Aguilar Espinosa, P.M., Fortt, J., Salinas, C., Barahona, S., León, J., Pardo-Esté, C., Fuentes, B., Areche, C. 2018. Characterization and salt response in recurrent halotolerant *Exiguobacterium* sp. SH31 isolated from sediments of Salar de Huasco, Chilean Altiplano. *Frontiers in Microbiology*, **9**, 2228.

Rezić, T., Presečki, A.V., Kurtanjek, Ž. 2021. New approach to the evaluation of lignocellulose derived by-products impact on lytic-polysaccharide monooxygenase activity by using molecular descriptor structural causality model. *Bioresource Technology*, 125990.

Riis, V., Kleinsteuber, S., Babel, W. 2003. Influence of high salinities on the degradation of

diesel fuel by bacterial consortia. *Canadian Journal of Microbiology*, **49**(11), 713-721.

Roberts, M.F. 2005a. Organic compatible solutes of halotolerant and halophilic microorganisms. *Saline Systems*, **1**(1), 5.

Roberts, M.F. 2005b. Organic compatible solutes of halotolerant and halophilic microorganisms. *Saline systems*, **1**(1), 1-30.

Robinson, M.D., McCarthy, D.J., Smyth, G.K. 2010. edgeR: a Bioconductor package for differential expression analysis of digital gene expression data. *Bioinformatics*, **26**(1), 139-140.

Rodrigues, E.M., Morais, D.K., Pylro, V.S., Redmile-Gordon, M., de Oliveira, J.A., Roesch, L.F.W., Cesar, D.E., Tótola, M.R. 2018. Aliphatic hydrocarbon enhances phenanthrene degradation by autochthonous prokaryotic communities from a pristine seawater. *Microbial Ecology*, **75**(3), 688-700.

Rognes, T., Flouri, T., Nichols, B., Quince, C., Mahé, F. 2016. VSEARCH: a versatile open source tool for metagenomics. *PeerJ*, **4**, e2584.

Rohrer, J.M. 2018. Thinking clearly about correlations and causation: Graphical causal models for observational data. *Advances in Methods and Practices in Psychological Science*, **1**(1), 27-42.

Rojo, F. 2009. Degradation of alkanes by bacteria. *Environmental Microbiology*, **11**(10), 2477-2490.

Rosenboom, J.-G., Langer, R., Traverso, G. 2022. Bioplastics for a circular economy. *Nature Reviews Materials*, 1-21.

Rubin, D.B. 1974. Estimating causal effects of treatments in randomized and nonrandomized studies. *Journal of Educational Psychology*, **66**(5), 688.

Rughöft, S., Jehmlich, N., Gutierrez, T., Kleindienst, S. 2021. Comparative proteomics of *Marinobacter* sp. tt1 reveals Corexit impacts on hydrocarbon metabolism, chemotactic motility, and biofilm formation. *Microorganisms*, **9**(1), 3.

Sabirova, J.S., Becker, A., Lünsdorf, H., Nicaud, J.-M., Timmis, K.N., Golyshin, P.N. 2011. Transcriptional profiling of the marine oil-degrading bacterium *Alcanivorax borkumensis* during growth on n-alkanes. *FEMS Microbiology Letters*, **319**(2), 160-168.

Sakdapetsiri, C., Kaokhum, N., Pinyakong, O. 2021. Biodegradation of crude oil by immobilized *Exiguobacterium* sp. AO-11 and shelf life evaluation. *Scientific Reports*, **11**(1), 1-13.

Salcedo, D.L., Soto, L.A., Estradas-Romero, A., Botello, A.V. 2017. Interannual variability of soft-bottom macrobenthic communities of the NW Gulf of Mexico in relationship

to the Deepwater Horizon oil spill. *Marine Pollution Bulletin*, **114**(2), 987-994.

Samalens, F., Thomas, M., Claverie, M., Castejon, N., Zhang, Y., Blanc, S., Fernandes, S. 2022. Progresses and future prospects in biodegradation of marine biopolymers and emerging biopolymer-based materials for sustainable marine ecosystems. *Green Chemistry*.

Santos, R.G.d., Loh, W., Bannwart, A., Trevisan, O. 2014. An overview of heavy oil properties and its recovery and transportation methods. *Brazilian Journal of Chemical Engineering*, **31**(3), 571-590.

Satpute, S.K., Banat, I.M., Dhakephalkar, P.K., Banpurkar, A.G., Chopade, B.A. 2010. Biosurfactants, bioemulsifiers and exopolysaccharides from marine microorganisms. *Biotechnology Advances*, **28**(4), 436-450.

Schmidt, M., Al-Farawati, R., Botz, R. 2015. Geochemical classification of brine-filled Red Sea deeps. in: *The Red Sea*, Springer, pp. 219-233.

Schmidt, T.S., Van Metre, P.C., Carlisle, D.M. 2018. Linking the agricultural landscape of the Midwest to stream health with structural equation modeling. *Environmental Science & Technology*, **53**(1), 452-462.

Schreiber, L., Fortin, N., Tremblay, J., Wasserscheid, J., Elias, M., Mason, J., Sanschagrin, S., Cobanli, S., King, T., Lee, K. 2019. Potential for microbially mediated natural

attenuation of diluted bitumen on the coast of British Columbia (Canada). *Applied and Environmental Microbiology*, **85**(10), e00086-19.

Schreiber, L., Fortin, N., Tremblay, J., Wasserscheid, J., Sanschagrin, S., Mason, J., Wright, C.A., Spear, D., Johannessen, S.C., Robinson, B. 2021. In situ microcosms deployed at the coast of British Columbia (Canada) to study dilbit weathering and associated microbial communities under marine conditions. *FEMS Microbiology Ecology*, **97**(7), fiab082.

Sgro, G.G., Oka, G.U., Souza, D.P., Cenens, W., Bayer-Santos, E., Matsuyama, B.Y., Bueno, N.F., Dos Santos, T.R., Alvarez-Martinez, C.E., Salinas, R.K. 2019. Bacteria-killing type IV secretion systems. *Frontiers in Microbiology*, **10**, 1078.

Shah, P., Wang, Z.-W. 2019. Using digital polymerase chain reaction to characterize microbial communities in wetland mesocosm soils under different vegetation and seasonal nutrient loadings. *Science of The Total Environment*, **689**, 269-277.

Shao, Z., Wang, W. 2013. Enzymes and genes involved in aerobic alkane degradation. *Frontiers in Microbiology*, **4**, 116.

Sharma, A., Kiciman, E. 2020. DoWhy: An end-to-end library for causal inference. *arXiv preprint arXiv:2011.04216*.

Shetaia, Y.M., Mohamed, T.M., Farahat, L.A., ElMekawy, A. 2016. Potential

biodegradation of crude petroleum oil by newly isolated halotolerant microbial strains from polluted Red Sea area. *Marine Pollution Bulletin*, **111**(1-2), 435-442.

Si-Zhong, Y., Hui-Jun, J., Zhi, W., Rui-Xia, H., Yan-Jun, J., Xiu-Mei, L., Shao-Peng, Y. 2009. Bioremediation of oil spills in cold environments: a review. *Pedosphere*, **19**(3), 371-381.

Sierra-Garcia, I.N., Belgini, D.R., Torres-Ballesteros, A., Paez-Espino, D., Capilla, R., Neto, E.V.S., Gray, N., de Oliveira, V.M. 2020. In depth metagenomic analysis in contrasting oil wells reveals syntrophic bacterial and archaeal associations for oil biodegradation in petroleum reservoirs. *Science of the Total Environment*, **715**, 136646.

Singh, A.K., Sherry, A., Gray, N.D., Jones, D.M., Bowler, B.F., Head, I.M. 2014. Kinetic parameters for nutrient enhanced crude oil biodegradation in intertidal marine sediments. *Frontiers in Microbiology*, **5**, 160.

Sleep, S., Laurenzi, I.J., Bergerson, J.A., MacLean, H.L. 2018. Evaluation of variability in greenhouse gas intensity of Canadian oil sands surface mining and upgrading operations. *Environmental Science & Technology*, **52**(20), 11941-11951.

Sokol, E., Kozmenko, O., Smirnov, S., Sokol, I., Novikova, S., Tomilenko, A., Kokh, S., Ryazanova, T., Reutsky, V., Bul'bak, T. 2014. Geochemical assessment of

hydrocarbon migration phenomena: Case studies from the south-western margin of the Dead Sea Basin. *Journal of Asian Earth Sciences*, **93**, 211-228.

Song, X., Zhang, B., Chen, B., Cai, Q. 2016. Use of sesquiterpanes, steranes, and terpanes for forensic fingerprinting of chemically dispersed oil. *Water, Air, & Soil Pollution*, **227**(8), 281.

Song, X., Zhang, B., Chen, B., Lye, L., Li, X. 2018. Aliphatic and aromatic biomarkers for fingerprinting of weathered chemically dispersed oil. *Environmental Science and Pollution Research*, **25**(16), 15702-15714.

Stanford, L.A., Kim, S., Klein, G.C., Smith, D.F., Rodgers, R.P., Marshall, A.G. 2007. Identification of water-soluble heavy crude oil organic-acids, bases, and neutrals by electrospray ionization and field desorption ionization Fourier transform ion cyclotron resonance mass spectrometry. *Environmental Science & Technology*, **41**(8), 2696-2702.

Stout, S.A., Payne, J.R., Emsbo-Mattingly, S.D., Baker, G. 2016. Weathering of field-collected floating and stranded Macondo oils during and shortly after the Deepwater Horizon oil spill. *Marine Pollution Bulletin*, **105**(1), 7-22.

Stubbins, A., Law, K.L., Muñoz, S.E., Bianchi, T.S., Zhu, L. 2021. Plastics in the Earth system. *Science*, **373**(6550), 51-55.

Tansel, B., Lee, M., Berbakov, J., Tansel, D.Z., Koklonis, U. 2014. Dispersion of Louisiana crude oil in salt water environment by Corexit 9500A in the presence of natural coastal materials. *Estuarine, Coastal and Shelf Science*, **143**, 58-64.

Taylor, E., Reimer, D. 2008. Oil persistence on beaches in Prince William Sound–A review of SCAT surveys conducted from 1989 to 2002. *Marine Pollution Bulletin*, **56**(3), 458-474.

Techtmann, S.M., Zhuang, M., Campo, P., Holder, E., Elk, M., Hazen, T.C., Conmy, R., Santo Domingo, J.W. 2017. Corexit 9500 enhances oil biodegradation and changes active bacterial community structure of oil-enriched microcosms. *Applied and Environmental Microbiology*, **83**(10).

Thavasi, R., Banat, I.M. 2010. Biosurfactants and bioemulsifiers from marine sources. *Biosurfactants*, 125.

Timmis, K.N., McGenity, T., Van Der Meer, J.R., de Lorenzo, V. 2010. *Handbook of Hydrocarbon and Lipid Microbiology*. Springer Berlin.

Tremblay, J., Fortin, N., Elias, M., Wasserscheid, J., King, T.L., Lee, K., Greer, C.W. 2019. Metagenomic and metatranscriptomic responses of natural oil degrading bacteria in the presence of dispersants. *Environmental Microbiology*, **21**(7), 2307-2319.

Tremblay, J., Yergeau, E. 2019. Systematic processing of ribosomal RNA gene amplicon

sequencing data. *GigaScience*, **8**(12), giz146.

Tremblay, J., Yergeau, E., Fortin, N., Cobanli, S., Elias, M., King, T.L., Lee, K., Greer, C.W. 2017. Chemical dispersants enhance the activity of oil-and gas condensate-degrading marine bacteria. *The ISME Journal*, **11**(12), 2793-2808.

Turner, R.E., Rabalais, N.N., Overton, E.B., Meyer, B.M., McClenachan, G., Swenson, E.M., Besonen, M., Parsons, M.L., Zingre, J. 2019. Oiling of the continental shelf and coastal marshes over eight years after the 2010 Deepwater Horizon oil spill. *Environmental Pollution*, **252**, 1367-1376.

Van Beilen, J.B., Smits, T.H., Roos, F.F., Brunner, T., Balada, S.B., Röthlisberger, M., Witholt, B. 2005. Identification of an amino acid position that determines the substrate range of integral membrane alkane hydroxylases. *Journal of Bacteriology*, **187**(1), 85-91.

Varjani, S., Upasani, V.N. 2019. Evaluation of rhamnolipid production by a halotolerant novel strain of Pseudomonas aeruginosa. *Bioresource Technology*, 121577.

Varjani, S.J. 2017. Microbial degradation of petroleum hydrocarbons. *Bioresource Technology*, **223**, 277-286.

Varjani, S.J., Rana, D.P., Jain, A.K., Bateja, S., Upasani, V.N. 2015. Synergistic ex-situ biodegradation of crude oil by halotolerant bacterial consortium of indigenous

strains isolated from on shore sites of Gujarat, India. *International Biodeterioration & Biodegradation*, **103**, 116-124.

Vaughan, P.P., Wilson, T., Kamerman, R., Hagy, M.E., McKenna, A., Chen, H., Jeffrey, W.H. 2016. Photochemical changes in water accommodated fractions of MC252 and surrogate oil created during solar exposure as determined by FT-ICR MS. *Marine Pollution Bulletin*, **104**(1-2), 262-268.

Venosa, A., Suidan, M., King, D., Wrenn, B. 1997. Use of hopane as a conservative biomarker for monitoring the bioremediation effectiveness of crude oil contaminating a sandy beach. *Journal of Industrial Microbiology and Biotechnology*, **18**(2-3), 131-139.

Venosa, A.D., King, D.W., Sorial, G.A. 2002. The baffled flask test for dispersant effectiveness: a round robin evaluation of reproducibility and repeatability. *Spill Science & Technology Bulletin*, **7**(5-6), 299-308.

Vishnivetskaya, T.A., Kathariou, S., Tiedje, J.M. 2009. The Exiguobacterium genus: biodiversity and biogeography. *Extremophiles*, **13**(3), 541-555.

Wang, L., Sun, Y., Wang, J., Wang, J., Yu, A., Zhang, H., Song, D. 2011. Preparation of surface plasmon resonance biosensor based on magnetic core/shell Fe_3O_4/SiO_2 and $Fe_3O_4/Ag/SiO_2$ nanoparticles. *Colloids and Surfaces B: Biointerfaces*, **84**(2), 484-

490.

Wang, W., Shao, Z. 2012. Diversity of flavin-binding monooxygenase genes (almA) in marine bacteria capable of degradation long-chain alkanes. *FEMS Microbiology Ecology*, **80**(3), 523-533.

Wang, W., Wang, L., Shao, Z. 2018a. Polycyclic aromatic hydrocarbon (PAH) degradation pathways of the obligate marine PAH degrader *Cycloclasticus* sp. strain P1. *Applied and Environmental Microbiology*, **84**(21).

Wang, X., Cai, T., Wen, W., Zhang, Z. 2018b. Effect of biosurfactant on biodegradation of heteroatom compounds in heavy oil. *Fuel*, **230**, 418-429.

Wang, Y.-N., Cai, H., Chi, C.-Q., Lu, A.-H., Lin, X.-G., Jiang, Z.-F., Wu, X.-L. 2007. Halomonas shengliensis sp. nov., a moderately halophilic, denitrifying, crude-oil-utilizing bacterium. *International Journal of Systematic and Evolutionary Microbiology*, **57**(6), 1222-1226.

Wang, Z., Fingas, M., Sergy, G. 1994. Study of 22-year-old Arrow oil samples using biomarker compounds by GC/MS. *Environmental Science & Technology*, **28**(9), 1733-1746.

White III, R.A., Soles, S.A., Gavelis, G., Gosselin, E., Slater, G.F., Lim, D.S., Leander, B., Suttle, C.A. 2019. The complete genome and physiological analysis of the

eurythermal firmicute *Exiguobacterium chiriqhucha* strain rw2 isolated from a freshwater microbialite, widely adaptable to broad thermal, ph, and salinity ranges. *Frontiers in Microbiology*, **9**, 3189.

Wood, J.M. 2015. Bacterial responses to osmotic challenges. *The Journal of General Physiology*, **145**(5), 381-388.

Wright, R.J., Langille, M.G., Walker, T.R. 2021. Food or just a free ride? A meta-analysis reveals the global diversity of the Plastisphere. *The ISME Journal*, **15**(3), 789-806.

Wu, Z., Nguyen, D., Lam, T.Y., Zhuang, H., Shrestha, S., Raskin, L., Khanal, S.K., Lee, P.-H. 2021. Synergistic association between cytochrome bd-encoded Proteiniphilum and reactive oxygen species (ROS)-scavenging methanogens in microaerobic-anaerobic digestion of lignocellulosic biomass. *Water Research*, **190**, 116721.

Xue, J., Yu, Y., Bai, Y., Wang, L., Wu, Y. 2015. Marine oil-degrading microorganisms and biodegradation process of petroleum hydrocarbon in marine environments: a review. *Current Microbiology*, **71**(2), 220-228.

Yang, M., Chen, B., Xin, X., Song, X., Liu, J., Dong, G., Lee, K., Zhang, B. 2021. Interactions between microplastics and oil dispersion in the marine environment. *Journal of Hazardous Materials*, **403**, 123944.

Yang, S., Li, M., Lai, Q., Li, G., Shao, Z. 2018. Alcanivorax mobilis sp. nov., a new

hydrocarbon-degrading bacterium isolated from deep-sea sediment. *International Journal of Systematic and Evolutionary Microbiology*, **68**(5), 1639-1643.

Yoon, S.-H., Ha, S.-M., Lim, J., Kwon, S., Chun, J. 2017. A large-scale evaluation of algorithms to calculate average nucleotide identity. *Antonie Van Leeuwenhoek*, **110**(10), 1281-1286.

Yuan, C., Varfolomeev, M.A., Emelianov, D.A., Eskin, A.A., Nagrimanov, R.N., Kok, M.V., Afanasiev, I.S., Fedorchenko, G.D., Kopylova, E.V. 2018. Oxidation behavior of light crude oil and its SARA fractions characterized by TG and DSC techniques: differences and connections. *Energy & Fuels*, **32**(1), 801-808.

Zadjelovic, V., Chhun, A., Quareshy, M., Silvano, E., Hernandez-Fernaud, J.R., Aguilo-Ferretjans, M.M., Bosch, R., Dorador, C., Gibson, M.I., Christie-Oleza, J.A. 2020. Beyond oil degradation: enzymatic potential of *Alcanivorax* to degrade natural and synthetic polyesters. *Environmental Microbiology*, **22**(4), 1356-1369.

Zermeno-Motante, M.I., Nieto-Delgado, C., Cannon, F.S., Cash, C.C., Wunz, C.C. 2016. Chemical modeling for precipitation from hypersaline hydrofracturing brines. *Water Research*, **103**, 233-244.

Zhang, S., Hu, Z., Wang, H. 2019. Metagenomic analysis exhibited the co-metabolism of polycyclic aromatic hydrocarbons by bacterial community from estuarine sediment.

Environment International, **129**, 308-319.

Zheng, C., He, J., Wang, Y., Wang, M., Huang, Z. 2011. Hydrocarbon degradation and bioemulsifier production by thermophilic *Geobacillus pallidus* strains. *Bioresource technology*, **102**(19), 9155-9161.

Zhou, J., Ning, D. 2017. Stochastic community assembly: does it matter in microbial ecology? *Microbiology and Molecular Biology Reviews*, **81**(4), e00002-17.

Zhu, L., Zhao, S., Bittar, T.B., Stubbins, A., Li, D. 2020a. Photochemical dissolution of buoyant microplastics to dissolved organic carbon: rates and microbial impacts. *Journal of Hazardous Materials*, **383**, 121065.

Zhu, Z., Zhang, B., Cai, Q., Cao, Y., Ling, J., Lee, K., Chen, B. 2021. A critical review on the environmental application of lipopeptide micelles. *Bioresource Technology*, 125602.

Zhu, Z., Zhang, B., Cai, Q., Ling, J., Lee, K., Chen, B. 2020b. Fish waste based lipopeptide production and the potential application as a bio-dispersant for oil spill control. *Frontiers in Bioengineering and Biotechnology*, **8**, 734.

Zhu, Z., Zhang, B., Chen, B., Cai, Q., Lin, W. 2016. Biosurfactant production by marine-originated bacteria *Bacillus subtilis* and its application for crude oil removal. *Water, Air, & Soil Pollution*, **227**(9), 1-14.

Zhu, Z., Zhang, B., Chen, B., Ling, J., Cai, Q., Husain, T. 2019. Fly ash based robust biocatalyst generation: a sustainable strategy towards enhanced green biosurfactant production and waste utilization. *RSC Advances*, **9**(35), 20216-20225.